KONINKLIJKE NEDERLANDSE AKADEMIE VAN WETENSCHAPPEN

PROCEEDINGS

SERIES B

PHYSICAL SCIENCES

64

VOLUME LXIV - No. 1

NORTH-HOLLAND PUBLISHING COMPANY - AMSTERDAM - 1961

JOURNAL DE PHYSIQUE
10, Rue Vauquelin
PARIS-V

20 MAI 1961

The complete Proceedings consist of three Series, viz.:

SERIES A: MATHEMATICAL SCIENCES

SERIES B: PHYSICAL SCIENCES

SERIES C: BIOLOGICAL AND MEDICAL SCIENCES

Articles for these Series cannot be accepted unless formally communicated for publication by one of the members of the Royal Neth. Academy of Sciences.

SILICON TETRACHLORIDE TREATED PAPER IN THE PAPER CHROMATOGRAPHY OF PHOSPHATIDES

IVa. ORIGIN OF THE GRADIENT AND FACTORS INFLUENCING THE COURSE OF THE GRADIENT CURVE

BY

H. G. BUNGENBERG DE JONG AND J. TH. HOOGEVEEN

(Communicated at the meeting of April 30, 1960)

1. *Introduction*

In Parts II and III of this series we have investigated the mechanism of the chromatography of egg phosphatides on non-impregnated paper and on $SiCl_4$-treated paper, using di-isobutylketone – acetic acid – H_2O (50:25:5) as mobile phase and the large slit-feeding apparatus as chromatographic device [1] [2].

We came to the conclusion that in both cases the mechanism must be considered to consist of adsorption chromatography combined with gradient elution. The sequence and degree of resolution of the components are different on the two papers, due to the adsorbent being different (cellulose; impregnated cellulose). The gradient curve for acetic acid is, however, practically the same for non-impregnated paper and for HCl-free $SiCl_4$-treated paper. For the aims expressed in the title we may, therefore, use both non-impregnated paper and $SiCl_4$-treated paper. We begin (section 3) with investigating the influence of the available air-space in the chromatographic device on the separation of spots on the course of the gradient curve. The results will allow us to draw some general conclusions whereby in principle the influence may be predicted of a number of other factors.

2. *Methods*

In the present study we use—when not stated otherwise—Schleicher and Schüll paper 2043*b* in sheets or strips which are cut in such a way that the direction of ascension of the mobile phase coincides with the direction of the smaller suction rate.

Part of the experiments are performed with non-impregnated paper, part with acid $SiCl_4$-treated paper of different age and neutralized $SiCl_4$-treated paper. In preparing the latter we follow the directions given in Part I [3].

The phosphatide preparation used throughout this investigation is the "Reference Mixture", a mixture of column fractions containing lecithin (L); cephalin (C); sphingomyelin (S); lysolecithin (LL) and lysocephalin (LC) in proportions suitable for chromatography [1]). By means of a self-filling capillary pipette (of about 5 mm^3

[1]) We thank Dr. G. J. M. HOOGHWINKEL for putting a solution of this reference mixture dissolved in chloroform-methanol (4:1) to our disposal.

M 14419
6667
B

capacity) the phosphatide solution (in ½ % or 1 % concentration) is brought up on the starting points. As chromatographic devices various types of apparatus are used especially constructed for our aims, which are described in the experimental sections.

Chromatography was performed in a dark room at 20° (when not stated otherwise) with di-isobutyl ketone—acetic acid—H_2O in the proportions of 50:25:5 or 40:25:5.

After drying the chromatogram is stained with the Acid Fuchsin–$UO_2(NO_3)_2$-0.01 N HCl staining solution described in former communications [4] [5]. After drying once more, the spots are circumlined with a pencil. The method used in determining the gradient in the mobile phase has been described in detail in Part III, and will not be repeated here [2].

In a few experiments *washed* $SiCl_4$*-treated paper* has been used. This kind of paper, not yet used in the preceding parts of this series, gives better chromatograms (smaller and better separated spots) than acid paper which has hung sufficiently long in the air to have lost practically all HCl.

Sheets of 17 × 28 cm are prepared as follows. We first prepare $SiCl_4$-treated paper (pulling the paper in 10 sec through a 2 % solution of $SiCl_4$ in CCl_4) then hang it 30 min in air and subsequently wash each sheet twice during 5 min with 250 ml distilled water. The sheets are then hung in air and can be used three days later. As far as we know it does not change its properties with time.

3. *Experiments with three chromatographic devices differing widely as to available air space*

a) Apparatus

In a previous communication it was observed that with the large slit-feeding apparatus (air space = 5.9 l) the spots lie farther apart on the chromatogram than with the small slit-feeding apparatus (air space = 0.66 l), though in both cases the front was allowed to ascend to the same height [6]. It was concluded that evaporation from the wetted strip may play a role in the chromatography.

From the above observation one should not conclude that increase of the air space leads to a larger mutual distance of the spots by virtue of the fact that in the large apparatus paper sheets of 17 cm width are used and in the small apparatus paper strips of only 4.5 cm width. At the same front height the evaporating surface of the wetted paper is in the large apparatus 3.8 times larger than in the small apparatus. As two factors are different (volume of the air space and area of the wetted paper), it remains unknown why the mutual distance of the spots on the chromatograms is different in the two kinds of apparatus.

Four our present aims we shall use three forms of apparatus with very different air spaces, in which equally broad strips (4 cm) are used. The front will be allowed to rise to the same height above the immersion line (21 cm) and with starting points on the same distance from the immersion line (4.5 cm). These devices will be called A, B and C, which letters will also be used in the figures and tables in this section. A short characterisation will now follow:

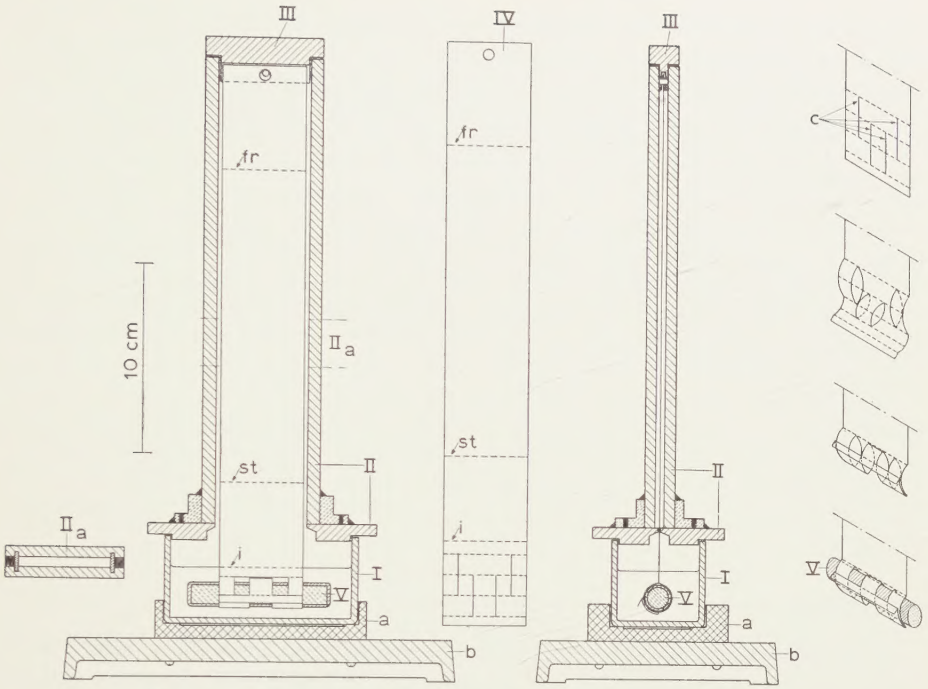

Fig. 1. Chromatographic apparatus with small air space.

A = apparatus given in fig. 1. Total air space as used in the experiments = 130 ml, of which 60 ml in the upper important part. Details are given below (see small print).

B = the small slit-feeding apparatus. described in a former publication [6]. It consists of a glass cylinder of 660 ml capacity, closed by a cork which bears the slit-feeding tube.

C = Erlemeyer flask of 4000 ml capacity, closed by cork bearing the slit-feeding tube of a small slit-feeding apparatus.

Apparatus A, consisting of three loose parts I, II and III, is placed with I in a wooden block *a* attached to an iron plate *b* (base of a support stand), to give the whole assemblage a firm stand.

Part I is a rectangular glass tray with 180 ml volume.

Part II consists of a plate of plate glass, provided with a slit (47 mm long and 0.8 mm wide) to which is attached the "house" of plate glass; inner dimensions of crosssection = 5 mm × 47 mm).

The total air space in this "house" from slit to upper end is only 60 ml. Part II, built up of plates and strips and blocks of glass is sealed together with "Devcon, wire resistant", (black in the figure) while care is taken that as little as possible of this cement stands in direct contact with the inner air space of the house [1]). Compare the crosssection II*a*.

[1]) In our first attemps to build an apparatus of type A, Part II and III were made wholy of Perspex. This material proved to be quite inadequate for our purposes, the inner surface of the "house" swelling and liquefying in the vapours of the mobile phase. As a result it was decided that the apparatus should be built of glass.

Part III is a glass piece, fitting loosely in the upper opening of Part II. It has a slit and a hole. The upper end of the paper strip IV with perforation hole is put in the slit so that the holes coincide, after which a short glass pin is put in the holes. Before fastening the strip, it has been provided with phosphatide spots on the starting points on line st and has been pushed with its upper end through the slit of the groundplate of Part II, until it comes out above the opening of the house. After fastening to Part III, the latter is placed into the opening of Part II.

To prevent that the paper strip makes contact with the walls of the glasshouse it must be provided with a weight V at its lower end. For this purpose the lower end of the strip has four incisions *c* as shown in the figure. By folding the paper as shown to the right in fig. 1, we can now push in the glass-tube V with sealed-in piece of iron rod (volume 10 ml; weight 53 g). After having controlled that the strip hangs stretched in the glasshouse of II, nowhere touching the walls, Part II is placed as a lid on Part I. The tray has been filled beforehand with so much of the mobile phase (100 ml), that after immersion of the weighted lower part of the strip, the meniscus coincides with the pencil line *i* on the paper. After the front has risen to the pencil line *fr*, Part II is lifted up and with a pair of scissors we cut off the lower part, lift up Part III with which the paperstrip is removed out of the glasshouse of Part II.

b) Particulars on the experiments

With the above apparatus A, B and C chromatograms have been made on non-impregnated paper, on practically HCl-free $SiCl_4$-treated paper and on neutralised paper, using as mobile phase di-isobutylketone – acetic acid – H_2O = 40:25:5 and allowing the front to rise 21 cm above the immersion line. With the two first-named papers and the same mobile phase chromatograms were made without applying the Reference mixture. They served for the determination of the acetic acid gradient in the mobile phase wetting the paper. On the strips pencil lines were drawn beforehand at 3; 6; 9; 12; 15; 18 and 21 cm above the immersion line. The front was allowed to ascend to the 21 cm line. Then the strip was rapidly cut with a pair of scissors along the pencil lines. We obtained seven zones in which we determined the mean acetic acid concentration of the mobile phase wetting the zone. The method is described in details in Part III of this series.

c) Results with non-impregnated paper

α) GRADIENT DETERMINATIONS

Two independent series of gradient determinations have been made, to get an idea of the possible errors. Compare Table I. As the analysed paper zones (3×4 cm) are much smaller here than in the gradient determinations in Part III (4.5×17) one would beforehand expect greater errors than in Part III (where an error of at least 1 weight percent acetic acid was present).

When we compare the results of the series a and b in the Table this is confirmed. We find here six times a difference of about 2 weight %, once of 3.5 % (C III) and once even of 6.1 % (B IV).

When for each series apart the data of Table I are plotted two figures are obtained which resemble one another much. Thus despite the errors the conclusion is not endangered that the descend of the gradient curve is steepest in apparatus A, less steep in apparatus B and still less steep in apparatus C.

TABLE I

Gradient determinations in non-impregnated paper

Zone	Mean acetic acid concentration (weight %) and in parentheses location of centre of zones (in % of fr_i) in two independent series of experiments a and b					
	Apparatus A		Apparatus B		Apparatus C	
	a	b	a	b	a	b
I	43.4 (7.0)	43.6 (7.2)	44.2 (7.1)	45.2 (7.0)	41.5 (7.3)	40.7 (6.9)
II	42.5 (21.3)	40.5 (21.5)	44.3 (21.6)	44.7 (21.0)	34.2 (21.9)	36.2 (21.1)
III	40.1 (35.8)	41.7 (35.5)	41.0 (36.2)	43.1 (35.4)	30.8 (36.4)	34.6 (35.6)
IV	42.5 (50.2)	42.4 (49.5)	31.9 (50.4)	38.0 (50.0)	30.4 (50.5)	30.7 (49.9)
V	— * (64.6)	26.8 (64.0)	24.2 (64.7)	26.3 (64.3)	26.3 (64.6)	28.3 (64.2)
VI	6.2 (79.0)	8.7 (78.5)	19.0 (79.0)	18.4 (78.6)	24.5 (78.6)	24.4 (78.5)
VII	0.7 (93.1)	0.8 (92.9)	17.3 (93.1)	18.4 (92.9)	24.1 (92.8)	24.7 (92.8)

* extract unreliable by leak of the flask.

β CHROMATOGRAMS

The chromatograms obtained from the "Reference Mixture" (5 mm^3 of a $\frac{1}{2}$ or a 1 % solution have been applied on the starting points) are given in fig. 2. The R_{f_i}-values [1]) of the spots are given in the next survey.

Apparatus	L + C	S	LL + LC
A	0.65	0.65	0.58
B	0.69^5	0.64^5	0.48
C	0.72^5	0.64^5	0.36^5

[1]) The notion R_{f_i} = distance base of the spot to immersion line (i) divided by fr_i = distance of front to immersion line, as a characteristic number for describing the position of a spot on a chromatogram, has been introduced in former publications [7] [1].

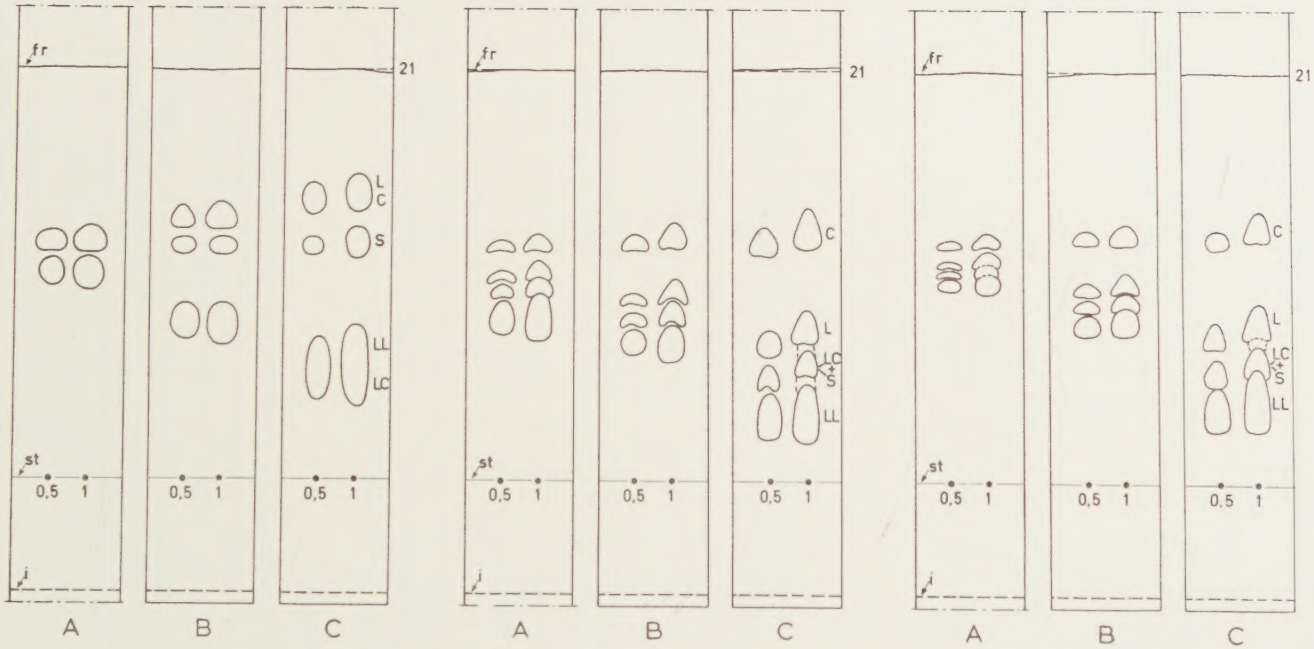

Figs. 2–4. Influence of air space in the chromatographic apparatus on chromatography of the Reference mixture on non-impregnated paper (fig. 2), on neutralized $SiCl_4$-treated paper (fig. 3) and on practically HCl-free $SiCl_4$-treated paper (fig. 4). A, B and C each time give the results obtained with the apparatus A, B and C.

γ) COMPARISON OF CHROMATOGRAMS AND GRADIENT CURVES

We read from Table I that in apparatus A (with the smallest air space), the gradient curve proceeds first nearly horizontally, and then descends very steeply. The corresponding chromatogram A in fig. 2 shows two spots only, which lie close together. The R_{f_i} values of these spots lie in the tract of % fr_i values where the steep descent of the gradient curve A is situated.

The gradient curve in apparatus B proceeds downwards much less steeply (see Table I) and the spreading of the spots on the chromatogram B in fig. 2 is greater now, besides we obtain already three spots.

With apparatus C, the slope of the gradient curve is still smaller (see Table I) and the spread of the three spots is still much greater than with apparatus B. Compare chromatogram C in fig. 2. Thus there is a very distinct correlation between spread of the spots and the slope of the gradient curve.

A further discussion of the results will follow in section 4.

d) Results with practically HCl-free $SiCl_4$-treated paper

α) *gradient determinations*

$SiCl_4$-treated paper was used after hanging 91 hrs in air. In this time span most of the HCl present in the paper directly after preparation evaporates. The very small quantity still present can be completely

TABLE II

Gradient determination in practically HCl-free $SiCl_4$-treated paper

Zone	Mean acetic acid concentration (weight %) and in parentheses location of centre of zones (in % of fr_i)		
	Apparatus A	Apparatus B	Apparatus C
I	41.7 (7.2)	43.5 (7.1)	37.2 (7.2)
II	41.3 (21.6)	42.8 (21.7)	32.5 (21.6)
III	41.9 (36.1)	40.7 (36.2)	31.2 (36.1)
IV	41.2 (50.5)	35.4 (50.2)	29.1 (50.2)
V	26.4 (64.8)	25.1 (64.2)	27.8 (63.7)
VI	8.4 (79.1)	19.9 (78.5)	24.0 (78.0)
VII	2.1 (93.1)	18.1 (92.9)	23.6 (92.7)

neglected, compared with the acetic acid present [1]). Thus the titrations of the extracts of the zones refer practically only to acetic acid.

The results of the gradient determinations are given in Table II.

β) Chromatograms

The chromatograms obtained from the Reference mixture are given in fig. 4. The R_{f_i}-values of the spots are given in the following survey:

Apparatus	C	L	LC + S	LL
A	0.66	0.62	0.60^5	0.58
B	0.67	0.57	0.54	0.49^5
C	0.66	0.47	0.40	0.32^5

γ) Comparison of Chromatograms and Gradient curves

We read from Table II that the apparatus with smallest air space (A) gives a gradient curve with very steep descending branch. The slope of the descent of the gradient curve is less in apparatus B and still smaller in apparatus C (with the largest air-space).

The chromatograms in fig. 4, show once more a similar correlation between slope of the gradient curve and separation of spots as was present with non-impregnated paper: the separation of spots is smallest when the slope of descending branch of the gradient is steepest. The separation increases as the slope of the gradient curve diminishes.

These results confirm the picture arrived to in Parts II and III of this series of the mechanism of the chromatography on $SiCl_4$-treated paper, namely adsorption chromatography combined with gradient elution.

Further particulars are discussed in section 4.

ε) Results with neutralized $SiCl_4$-treated paper

We found already in Part III, that in the determination of the acetic acid gradient difficulties arise by the NH_4Cl present in neutralized paper [2]. For this reason we have not made gradient determinations here. The chromatograms obtained are given in fig. 3. We see here in principle the same influence of the increase of the air-space in the chromatographic apparatus as in the case of non-impregnated paper (fig. 2) and $SiCl_4$-treated paper (fig. 4). With increase of the air-space the spread of the spots increases. So this is an indication that for neutralized papers too will hold that with increasing air-space the slope of the gradient curve diminishes.

Next survey gives the R_{f_i} value of the spots.

Apparatus	C	L	LC + S	LL
A	0.65	0.59	0.56	0.49
B	0.65	0.54^5	0.51	0.46
C	0.64	0.45	0.39	0.29^5

[1]) For decrease of HCl content with time see fig. 6 in Part III of this series [2].

4. *Origin of gradient and role of air space in the chromatographic apparatus*

a) Origin of gradient

We will start our discussion from the combined results of the three sets of gradient determinations given in the Tables I and II [1]). In Table III we give for each apparatus A, B and C the mean acetic acid concentration in the seven zones and the mean location of the centre of these zones expressed in % of fr_i (=distance front to immersion line). The data of the table have been plotted in fig. 5.

In this figure, three striking points draw our attention:

1. In the apparatus with the smallest air space (A), the gradient curve has a very steep descent, in the apparatus with larger (B) and very large air space (C) the descent is less and still less steep.
2. The gradient curves A, B and C intersect one another.
3. Taking into account the errors still present (though diminished by taking the mean of three sets of determination) it seems possible that the intersections points of the three gradient curves coincide.

Point 3, which suggests the existence of a turning point on the gradient curve will not be considered here in more detail.

Point 1 is important for the question of the origin of the gradient.

One could for instance suppose that when no air space was present in the chromatographic apparatus, the mobile phase would have up to the front everywhere the same composition as the mobile phase which is

TABLE III

Gradient determinations in Apparatus A, B and C (mean of the three series in Tables I and II)

Apparatus	Mean acetic acid concentration (weight %) in zones I–VII and in parentheses location of the centres of zones (in % of fr_i)*						
	I	II	III	IV	V	VI	VII
A	42.9	41.4	41.2	42.0	26.6	7.8	1.2
	(7.1)	(21.5)	(35.8)	(50.1)	(64.4)	(78.9)	(93.0)
B	44.3	43.9	41.6	35.1	25.2	19.1	17.9
	(7.1)	(21.4)	(35.9)	(50.2)	(64.4)	(78.7)	(93.0)
C	39.8	34.3	32.2	30.1	27.5	24.3	24.1
	(7.1)	(21.5)	(36.0)	(50.2)	(64.2)	(78.4)	(92.8)

* fr_i = distance front to immersion line.

[1]) In Part III of this series, it appeared that the gradient curves on non-impregnated paper and on HCl-free $SiCl_4$-treated paper run in the same apparatus did not differ more than the experimental error (1 or 2 weight % acetic acid). In the Tables I and II of the present communication, the experimental errors are greater (2, sometimes more than 2 weight %, see Table I), but the same differences also are found between the results in Table II and each of the series in Table I. To minimize the errors and to obtain, therefore, a better picture of the gradient curves in apparatus A, B and C, it is indicated to start from the means of the results in table I and II.

sucked up at the immersion line. When an air space is present a gradient could then arise by preferential evaporation of acetic acid from the upper part of the wetted strip, the lower end always being fed by the unaltered mobile phase.

When this supposition applied one would expect that this preferential loss of acetic acid would be greater as the available volume of the container is greater. This then would lead to an ever steeper gradient, so that at last the acetic acid concentration of the mobile phase in the upper part would become smaller.

When we consider fig. 5, we see that just the reverse actually occurs. With the largest air space the steepness of the acetic acid gradient curve is smallest, it increases in steepness as the available air space is smaller. There is every reason to suppose, that when an apparatus could be realised with air space zero, the descent of the gradient curve will be still steeper than is shown in apparatus A [1]).

In this case, the paper will behave as an adsorption column, which preferentially adsorbs acetic acid from the mobile phase.

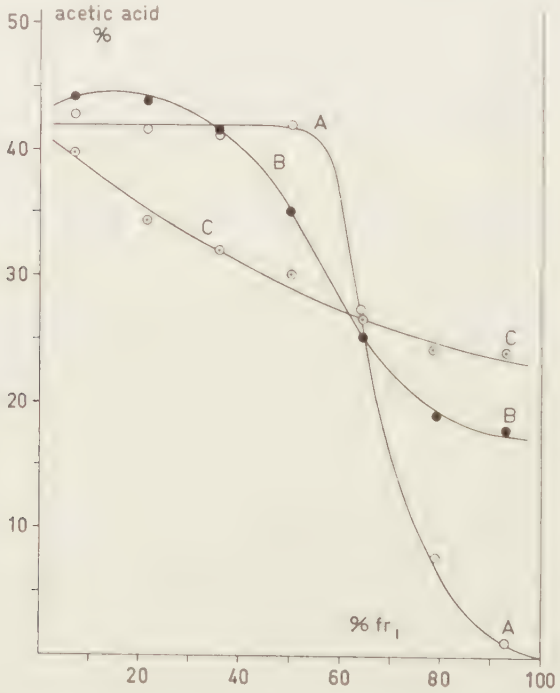

Fig. 5. Gradient curves obtained with apparatus A, B and C (mean of the three sets of gradient determinations in section 3).

[1]) Attempts have been made to realise chromatography in paper immersed in mercury, but because of undesired wetting effects of the paper by mercury (especially of $SiCl_4$-treated paper) and other complications, we have not succeeded in constructing an apparatus in which the air space approximates zero.

b) Role of the air space in the chromatographic apparatus

The partial vapour pressures of the components of the mobile phase will in the case considered above be very different at both sides of the small zone in which the very steep gradient is present. If there is no air space, no possibility for interchange will exist. As soon as an air space is present such an interchange becomes possible by diffusion through the air space. Thus acetic acid evaporating from the lower part of the paper may diffuse to the upper part of the paper and may be taken up by the mobile phase present there. Vice versa, di-isobutyl ketone evaporates from the upper part of the paper, diffuses (through the air space) in downward direction and is taken up by the liquid wetting the lower part of the paper. As a result the gradient curve for acetic acid will diminish in slope, whereby the new gradient curve will intersect the very steep original gradient curve (see point 2 in paragraph *a*).

We may further expect that more of the components can be transported through the air space as its volume increases not so much as a direct consequence of the enlarged volume itself, but because in general the area of the cross section of the air space perpendicular to the paper will be greater in a larger vessel. Thus with a larger volume of the container a gradient curve will be obtained with smaller slope. This is just what we found experimentally, compare in fig. 5 the curves A, B and C.

c) Resolution of spots on the chromatogram and air space in the chromatographic apparatus

In the preceding Part I and II of this series we came to the conclusion that the chromatography of phosphatides with di-isobutyl ketone – acetic acid – H_2O mixtures is to be considered as adsorption chromatography combined with gradient elution. For each spot a characteristic composition of the mobile phase would exist at which that spot is at its base eluted with maximal rate (compared to the rate of ascension of the front).

One must thus expect that when the slope of the gradient curve is diminished, the relative distance of the spots on the chromatograms will increase. This is just what has been found in section 3.

In fig. 6 we have plotted the R_{f_i}-values given in the surveys of section 3 for the three apparatuses A, B and C. We see that on the three kinds of papers used the mutual distance of the spots increases from A over B to C.

We first discuss the chromatograms on non-impregnated paper. In A the upper spot has not yet been dissolved in an S and L+C spot, this takes place in B and C.

An interesting point is that with increase of the volume the L+C spot moves in upward direction, the S spot remains on its place and the LL+LC spot moves downwards.

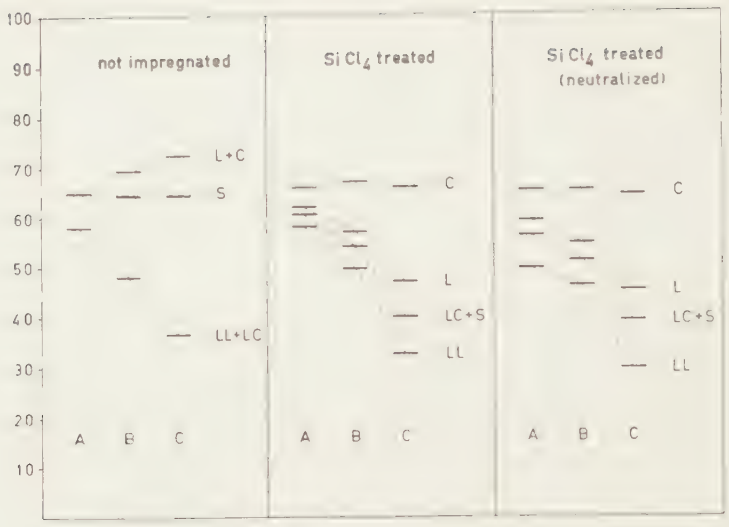

Fig. 6. R_{fi} values of the chromatograms of fig.s 2-4.

When we consider the gradient curves A, B and C in fig. 5, this becomes clear at once. The intersection of the three curves lies about at the same fr_i value namely at about 64 %. The R_{fi} value of the S spot has about the same value, namely 0.65 (A); 0.64^5 (B) and 0.64^5 (C). Hence the decrease of the slope of the gradient curve from apparatus A over B to C should not alter the position of the S spot on non-impregnated paper.

The L + C spot though not visibly separated must lie in A somewhat higher than $fr_i = 0.64$ and therefore will shift in upward direction with decrease of the slope of the gradient curve (A → B → C). For the LL + LC spot applies the reverse. In A its R_{fi}-value lies lower than 0.64; with decrease of the slope of the gradient curve (A → B → C) it should only move downward on the chromatogram.

Now turning to the $SiCl_4$-treated papers we find that here no spot moves upwards at increase of the volume of the chromatographic apparatus (see fig. 6). The upper spot, which here is C (cephalin) remains, however, in its place, the three other spots move downwards with decreasing slope of the gradient curve (A → B → C).

As C lies on both kinds of $SiCl_4$-treated paper at about the same R_{fi} value as S on non-impregnated paper, C must lie on or very near to the intersection point of the three gradient curves. Hence it will not move. The three lower spots of course must move downwards with increasing volume of the chromatographic apparatus.

d) Concluding remarks

The air space in a chromatographic apparatus is not an inert entity, but takes an essential part in the resolution of spots. This knowledge allows us to foresee, or at least to explain, the influence of a number of

other factors on chromatography, which will be investigated in the sections 6–10.

5. *The mechanism of elution and the sequence of spots on the chromatograms*

Already in paragraph a of section 4 we came to the conclusion that if no air space were present, the paper would behave as an adsorption column, which preferentially adsorbs acetic acid from the mobile phase. This sheds light to the mechanism of the resolution of the spots on the chromatograms. The elution process may be considered as an adsorption displacement by acetic acid from the mobile phase. The concentration of acetic acid in the mobile phase required for eluting a phosphatide spot at its base will be higher as the adsorption intensity of the phosphatide spot will be higher. Thus the lower a spot is situated on the chromatogram the stronger it is adsorbed. So the sequences for increasing adsorption intensity are:

$$L + C < S < LL + LC \text{ (non-impregnated papers)}$$

$$C < L < LC + S < LL \text{ ($SiCl_4$-treated papers)}$$

Taking into consideration that the phosphatides are adsorbed from a hydrophobic medium (di-isobutylketone) on a polar adsorbent (cellulose or silica-covered cellulose), they will be actively adsorbed by means of hydrophilic groups in their molecules. Small differences in lengths of the hydrocarbon chains should be relatively less important. So we have to consider the ampho-ion part of the molecule (cholinephosphate; colaminephosphate) and eventually present OH groups.

Non-impregnated paper – cellulose being a neutral substance – makes evidently practically no distinction between the ionized colamine group and the quaternary ammonium group of choline. This follows from the fact that L and C form a composite spot, equally so LL + LC. That the last-named spots lie so much lower on the chromatogram has two causes; first, they contain an OH group, and further one long hydrocarbon chain is no longer present. In sphingomyelin an OH group is present too, but it still possesses two long hydrocarbon chains. Thus compared to lecithin it should be adsorbed stronger, but not as strong as lysolecithin.

The above leads to the sequence of the three spots actually found in the chromatograms on non-impregnated paper:

$$\text{(upper)}\ \ (L + C) - S - (LL + LC)\ \ \text{(lower)}$$

On $SiCl_4$-treated paper the adsorbent is silica, which envelopes the cellulose fibres [2]. Silica being an acidic substance it does discriminate between the ionized primary amine group (of colamine) and quarternary ammoniumgroup (of choline). The affinity of the latter ionized group to

the adsorbent is evidently greater than the former [1]). The outcome is a resolution of the composite spots which we found on non-impregnated paper. Thus the L spot lies lower than the C spot, similarly the LL spot lower than the LC spot. For the rest the influence of the presence of an OH-group (sphingomyelin), and the influence of introduction of an OH group accompanied by loss of a long hydrocarbon chain (lyso products) remains the same.

The above explains the actually found sequence of the spots on $SiCl_4$-treated paper:

$$\text{(upper) } C-L-(LC+S)-LL \text{ (lower)}$$

The S and LC spots come so near to one another that they can only with difficulty be resolved; as a rule they form a composite spot.

6. *Comparison of ascending and descending chromatography by means of a slit-feeding apparatus*

a. Apparatus

The apparatus used is given in fig. 7. It consists of a glass-cylinder I (8.3 cm inner diameter and 29 cm high, volume about 1.6 l), and a plate of glass II, with two holes, in which with corks are fastened a glass rod with hook (*a*) and the filling tube (*b*) which gives entrance to the slit-feeding tube (*c*), having a slit 1.5 mm wide and 70 mm long. For ascending chromatography the filling tube (*b*) is slid downwards, and the paper strip is fastened to the hook of rod *a* by means of a perforation hole. The coverplate II is shifted to a position such that *a* coincides with the axis of cylinder I. The lower end of the strip dips 5 mm into the slit of the slit-tube.

For descending chromatography rod *a* is not used. The filling tube *b* is drawn up into the position as shown in the figure. At right angles to the middle of the slit-feeding tube a glass rod *d* is sealed, ending in a hook. The paper strip hangs on this hook by means of a perforation hole. It is stretched down by a glass rod *e* fastened in two slits in the free hanging end of the strip. The other end dips 5 mm into the slit-tube. The starting points lie 5 cm from the immersion line, that is 1.5 cm past the perforation hole. To make the ascending chromatography comparable here too the strip had a perforation hole, 1.5 cm below the starting line, while the distance of the starting line to the slit was also 5 cm.

b) Results

α) *Non-impregnated paper*

Fig. 8 gives two chromatograms on non-impregnated Schleicher and Schüll 2043b of $\frac{1}{2}$% spots (5 mm³) of the Reference mixture. As mobile phase was used di-isobutyl ketone – acetic acid – H_2O – 50:25:5 and the front was allowed to rise (or descend) to 22 cm from the immersion line. The time needed to reach this was in descending chromatography shorter (216 min) than in escending chromatography (256 min). It is observed

[1]) In former investigations it has already appeared that the affinity of quaternary ammoniumions to SiO_2 is greater than of the cations of primary amines. Compare in Colloid Science II, Elsevier, Amsterdam (1949) chapter IX, p. 304, fig. 29.

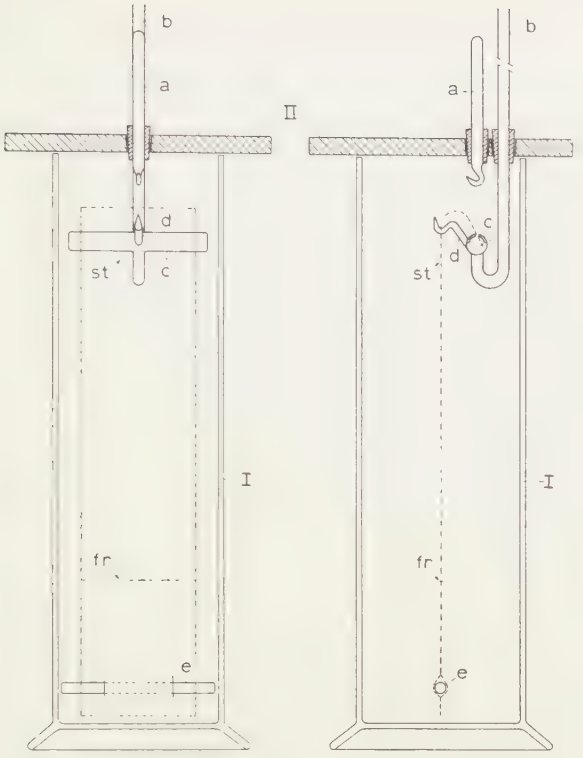

Fig. 7. Slit-feeding apparatus used to compare descending and ascending chromatography. For ascending chromatography the slit-feeding unit is lowered.

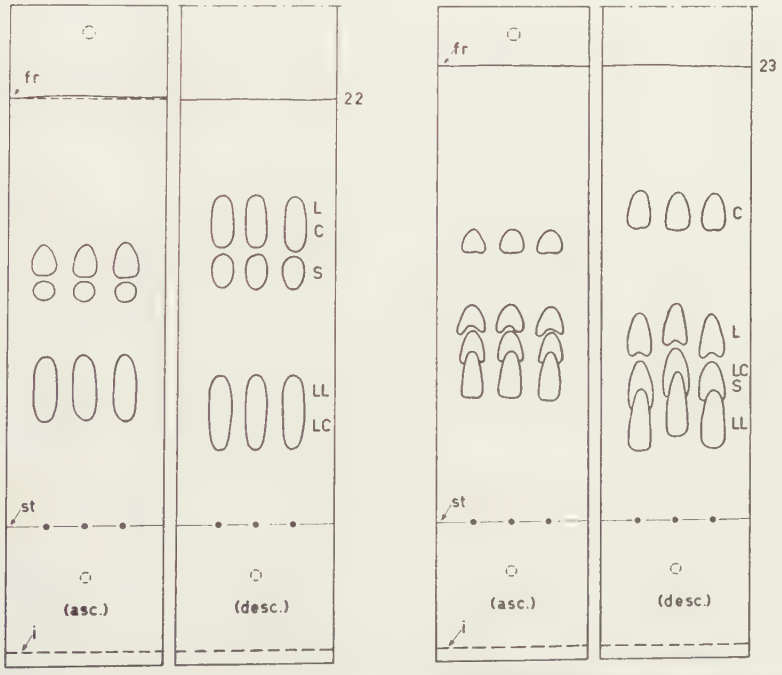

Figs. 8–9. Comparison of ascending (asc.) and descending (desc.) chromatography of the Reference mixture on non-impregnated paper (fig. 8) and on practically HCl-free $SiCl_4$-treated paper (fig. 9) respectively.

that with descending chromatography the three spots stand wider apart than with ascending chromatography. It must be concluded that with descending chromatography the gradient is less steep than with ascending chromatography.

β) HCl-free $SiCl_4$-treated paper

Here too Schleicher and Schüll 2043b is used, but now 12 days after preparation with 2 % $SiCl_4$ in CCl_4.

Fig. 9 gives the two chromatograms obtained. The results are similar to those obtained with non-impregnated paper: The four spots stand farther apart with descending chromatography, so the gradient is less steep here than with ascending chromatography.

The time necessary to reach the front line (23 cm from the immersion line) is shorter in descending chromatography (222 min.) than in ascending chromatography (282 min).

c. Discussion

In ascending chromatography the capillary forces move the front in a direction against gravity, in descending chromatography in the same direction as gravity. So there is no problem why the time for the front to reach a same distance from the immersion line is shorter in descending chromatography than in ascending chromatography.

If diffusion were the only means of transport through the vapour space, one would from the shorter time available expect that in descending chromatography the gradient curve is steeper than in ascending chromatography, that is the spots would stand nearer to one another.

As just the reverse is the case, there must be a second transport mechanism which in the case of descending chromatography is much more effective in lessening the slope of the gradient curve than in the case of ascending chromatography.

The wetted part of the paper strip will be covered on both sides by a layer of saturated vapour of the mobile phase. This layer is denser than the vapour in the container, and will move downward along the strip. Given this downward movement, there must be an upward movement in another place of the container. So a rotation in the vapour space at-both sides of the strip (or sheet in the case of a large slit-feeding apparatus) sets in, moving downwards along the strip and upwards along the glass walls of the container.

The direction of rotation is the same both in ascending chromatography as in descending chromatography, but the efficiency of transport of a given component of the mobile phase is different. Let us choose for our argument acetic acid. In ascending chromatography the rotation current in its downward movement takes up acetic acid mainly from the slit-side part of the wetted strip. This acetic acid taken up can be given off to the mobile phase at the front side of the wetted strip only after having

completed a half cycle in upward direction along the glass wall. Meanwhile it may have lost part of its acetic acid by diffusion. Thus the transport of acetic acid is not so efficient. In descending chromatography the reverse applies. Here the rotation current descending along the wetted strip takes up acetic acid from the slit side part of the strip and gives it off at the front side part of the strip while further descending. Here the transport of acetic acid is much more efficient. For the other main component of the mobile phase (di-isobutyl ketone) just the reverse holds, so that we obtain:

Transport of named component towards part of the strip	ascending chromatography	descending chromatography
acetic acid, towards frontside	less efficient	more efficient
di-isobutyl ketone, towards slitside	more efficient	less efficient

From the greater spread of the spots obtained with descending chromatography than with ascending chromatography we must conclude that the efficiency of the transport of acetic acid is a much more important factor in lessening the slope of the gradient curve than the efficiency of the transport of di-isobutylketone. We will not try to explain this in detail (possibly the lower boiling point of acetic acid plays a part). In any case the results show that we have in general (so also in ascending chromatography) to reckon with two transport mechanisms in the vapour space, namely diffusion and rotation.

From what follows below it is probable that in descending chromatography the rotation current has a labile character.

In our experience it is much more difficult in descending chromatography to obtain regular and reasonably reproducible chromatograms than in ascending chromatography. For no obvious reason, perturbations may very easily occur. We found often that the three spots on one row (especially the lower spots) stand on an oblique line, though the front was horizontal. In fig. 8 and 9 the best chromatograms have been reproduced. That in fig. 9 shows still an irregularity, the middle lower spot lying higher than the adjacent one. For routine work we therefore cannot recommend descending chromatography.

(To be continued)

SILICON TETRACHLORIDE TREATED PAPER IN THE PAPER CHROMATOGRAPHY OF PHOSPHATIDES

IVB. ORIGIN OF THE GRADIENT AND FACTORS INFLUENCING THE COURSE OF THE GRADIENT CURVE

BY

H. G. BUNGENBERG DE JONG AND J. TH. HOOGEVEEN

(Communicated at the meeting of April 30, 1960)

7. *Comparison of chromatograms run in the direction of smaller and larger ascension rate*

In Part I–III of this series and the preceding sections of the present Part we have always cut the Schleicher and Schüll 2043b in such a way that in running the chromatogram the mobile phase ascends in the direction of the smaller ascension rate. It was found empirically that in this way a somewhat greater separation of spots is obtained than when the chromatogram is run in the direction of the larger suction rate.

We give here some examples with $SiCl_4$-treated Ederol 208 paper (small slit-feeding apparatus, di-isobutyl ketone – acetid acid – H_2O = 50:25:5, ascension height of the front = 18 cm above the immersion line). This paper shows a marked difference in ascension rate into the two directions of the paper and the above-mentioned effect is clearly present here. Compare fig. 10 in which the pair A and B refers to acid $SiCl_4$-treated paper of 21 hr age, C and D to neutralized $SiCl_4$-treated paper and E and F to washed out $SiCl_4$-treated paper [1]).

In the survey below we give for each chromatogram the ascension time in minutes, the R_{f_i}-values (mean of $\frac{1}{2}$ % and 1 % R) of the upper spot (C) and the lower spot (LL). As a measure of separation we take the differences of the R_{f_i} values of the C and LL spot.

chromatogram	A	B	C	D	E	F
ascension time (min)	275	207	265	202	266	200
R_{f_i} of C spot	0.63^5	0.63	0.63	0.62^5	0.62^5	0.61^5
R_{f_i} of LL spot	0.35^5	0.38^5	0.35	0.38	0.38^5	0.39^5
separation	0.28	0.24^5	0.28	0.24^5	0.24	0.22
kind of paper	acid (21 hr age)		neutralized		washed out	

[1]) We have also compared two strips of acid $SiCl_4$-treated paper of $\frac{1}{2}$ hr. age. Here the distinct effect is not present. But as such newly prepared $SiCl_4$-treated paper rapidly loses HCl to the air, the difference in ascension time (more than 1 hour!) of the strips into the two directions, is no longer short compared to the ascension time. Hence the papers are no longer comparable.

Fig. 10. Comparison of chromatograms of the Reference mixture run in the direction of smaller and larger ascension rates. Arrows give the direction of larger ascension rate. A and B on $SiCl_4$-treated paper, 21 hours after preparation; C and D on neutralized paper; E and F on washed $SiCl_4$-treated paper (Ederol 208).

The results show the signs of a change in the slope of the gradient curve. As the R_{f_i} values of C for the two chromatograms belonging to each pair are within the errors equal, the turning point of the gradient curve lies at or very near to the C spot (as was also the case with $SiCl_4$-treated Schleicher and Schüll 2043b, compare fig. 6).

For that chromatogram of each pair on which the R_{f_i} value of the LL spot lies lower, the gradient curve must proceed with less slope.

A simple explanation offers itself from the distinct correlation between ascension time and separation in the above survey. For each pair the separation is greater as the ascension time is longer. With a longer ascension time there is more time available for transport through the vapour space, with as a result a greater decrease of the slope of the gradient curve, hence a greater separation of the spots.

In this simple explanation the anisotropy of the texture of the paper does not play a role itself. Whether this anisotropy may really be neglected must be left undecided here.

8. *Influence of stirring in the vapour space on chromatography*

a) Large slit-feeding apparatus with stirrers

The apparatus used in this section is given in fig. 11. It has practically the same dimensions as the large slit-feeding apparatus described in a former communication [6]. The manipulations and precautions to be

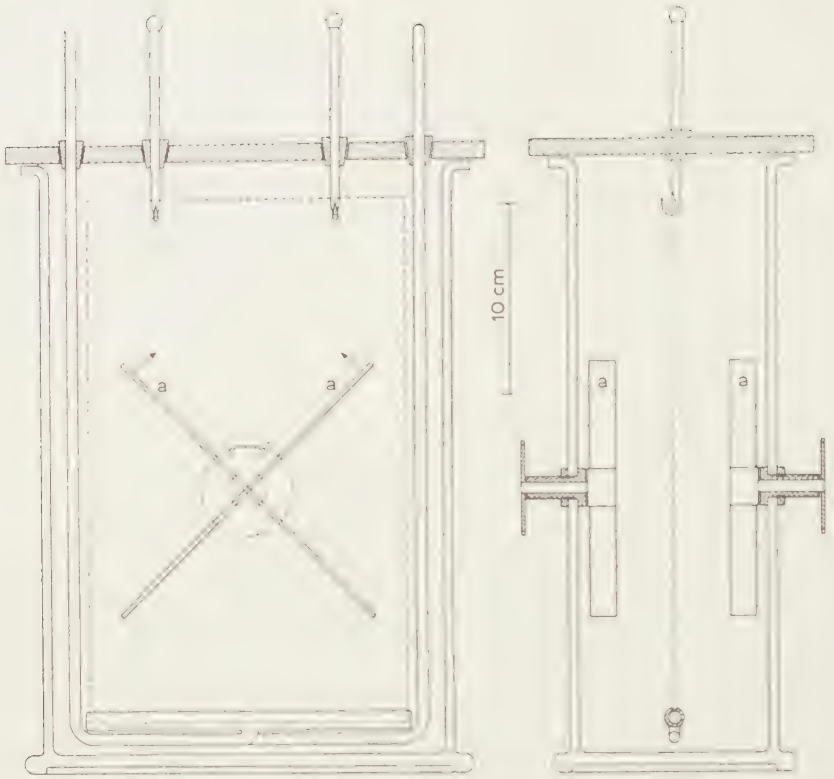

Fig. 11. Large slit-feeding apparatus with stirrers fastened in front and back wall of the glass-container.

taken are exactly the same. The apparatus only differs from the formerly described one by the possession of two stirrers a (glass strips 1.4×19 cm) fastened to an Akulon axis, turning on Akulon bearings, fastened in the front and back glass wall of the container. Each stirrer can be driven by a separate synchronic motor standing about 30 cm beside the chromatographic apparatus [1]). The synchronic motors are so placed that the two stirrers turn in opposite directions. Chain transmission ensures a constant speed of stirring. The stirrers make 50 revolutions per minute. After the paper sheet is brought in its place, the stirrers are set in motion. By viewing through the apparatus (with 4 Volt-incandescent lamp behind the back wall) one can make sure that the stirrers pass one another in an approximately vertical position. We now fill in the mobile phase and chromatography begins. Despite stirring the front rises horizontally out of the slit tube and remains practically horizontal during the experiment.

[1]) The synchronic motor should not stand too near the chromatographic apparatus, to avoid disturbances from radiation of the motor which becomes hand-warm while functioning.

So with the above apparatus we may compare chromatography without stirring (both stirrers are then placed vertically), with one stirrer turning, and with both turning.

b) Chromatography of the Reference mixture on non-impregnated paper with di-isobutyl ketone – actic acid – H_2O = 40:25:5 and 50:25:5 respectively

We have run with each mobile phase three chromatograms to a front height of 18 cm above the immersion line, one without stirring, one with only the front stirrer moving and the third with both stirrers moving. The chromatograms obtained with one stirrer turning and two stirrers turning hardly differed. It therefore may suffice to give in the figures 12 and 13 only the chromatograms obtained without stirring and with two stirrers turning.

One observes a great influence of stirring; the spots lie much farther apart than without stirring. The next survey gives the R_{f_i} values of the three spots.

Mobile phase	stirrers turning	L + C	S	LL + LC
40:25:5	–	0.69	0.63[5]	0.42
	1	0.70	0.63	0.32
	2	0.72	0.63[5]	0.31
50:25:5	–	0.67	0.62	0.40
	1	0.60	0.52[5]	0.21
	2	0.61	0.52	0.19[5]

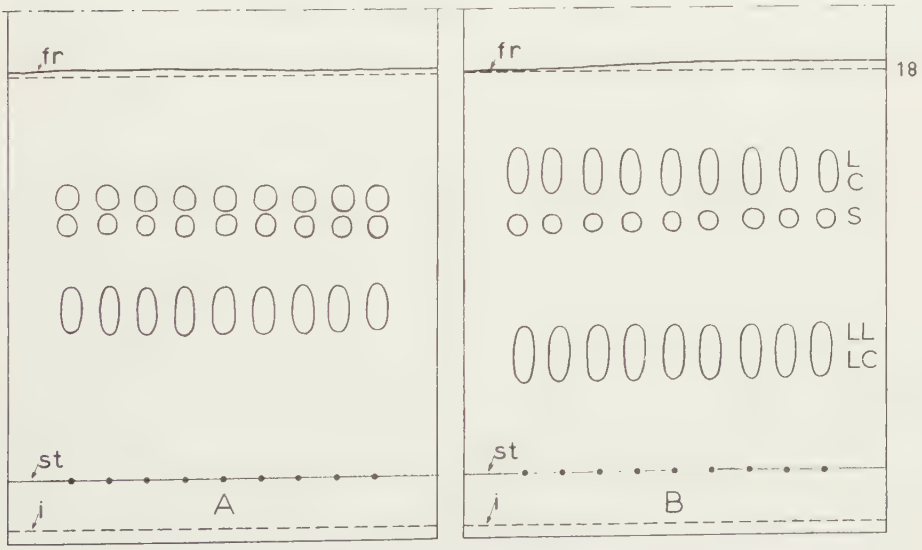

Fig. 12. Influence of stirring on chromatography of the Reference mixture with di-isobutyl ketone—acetic acid—H_2O = 40:25:5 on non-impregnated paper. A stirrers at rest, B the two stirrers turning.

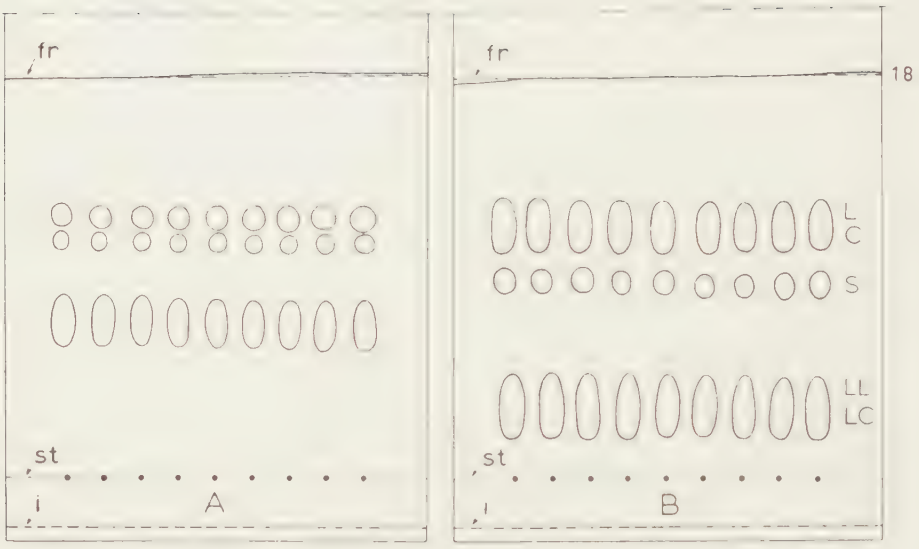

Fig. 13. Influence of stirring on chromatography of the Reference mixture with di-isobutyl ketone—acetic acid—H_2O = 50:25:5 on non-impregnated paper. A stirrers at rest, B the two stirrers turning.

c) Chromatography of the Reference mixture on washed $SiCl_4$-treated paper with di-isobutyl ketone – acetic acid – H_2O = 50:25:5

The chromatograms (front height 18 cm above the immersion line) are given in fig. 14. The R_{f_i}-values of base and upper margin of the spots are given in the next survey.

The results are in principle the same as in the preceding paragraph: With stirring a greater mutual distance of the spots is obtained than without stirring.

stirrers turning	C	L	LC + S	LL
	0.61	0.49	0.42	0.33
2	0.59	0.37	0.26	0.16

d) Discussion

In section 4 the greater spread of the spots which is obtained by increasing the volume of the chromatographic container (see section 3) has been discussed. It was assumed that the greater space allowed a more effective transport by diffusion of acetic acid evaporated from the lower part of the wetted paper and taken up by the higher part of the wetted paper, similarly of di-isobutyl ketone in the reverse direction. Thus the gradient curve becomes less steep and as a consequence the distance of the spots on the chromatogram increases with increasing volume of the container.

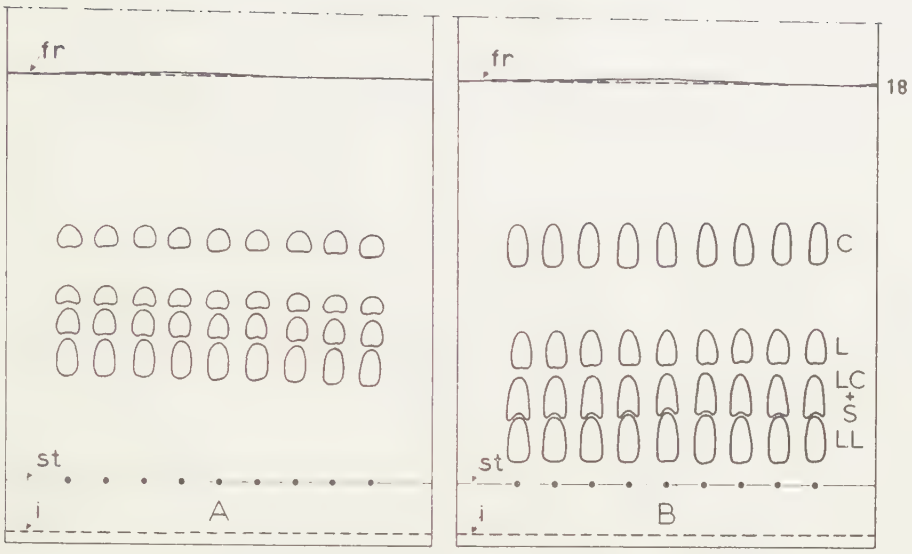

Fig. 14. Influence of stirring on chromatography of the Reference mixture with di-isobutyl ketone—acetic acid—H_2O = 50:25:5 on washed $SiCl_4$-treated paper. A stirrers at rest; B the two stirrers turning.

Accordingly, in an apparatus with vapour space, diffusion is the limiting factor in the chain of events (evaporation – transport through the vapour space by diffusion – condensation) which will determine the degree of diminished slope of the gradient curve compared to the very steep slope in an apparatus without air space (though such an apparatus could not be realized).

The slow transport through the vapour space which takes place in a container without stirring is probably not only due to diffusion. In section 7 we have obtained indications that a slow transport by convection in the vapour space also plays a role.

So it must be expected that a greater decrease of the slope of the gradient curve will occur with stirring than without stirring because diffusion and rotation as limiting factors are cancelled out by stirring. Consequently the spots will stand further apart with stirring than without stirring. This is indeed what has been found in this section. Compare figs. 12, 13 and 14.

Before we may safely accept the above given explanations we shall check in the next section that indeed the gradient curve proceeds with smaller slope while stirring in the vapour space, than without stirring.

9. *Influence of stirring in the vapour space on the gradient curve*

a) Chromatograms

For the experiments in this section $SiCl_4$-treated paper has been used, which has been exposed sufficiently long to the air (90 hours or longer) to have lost practically all HCl.

Two chromatograms on paper sheets 17×28 cm have been run with di-isobutyl ketone–acetic acid–H_2O = 50:25:5, allowing the front to rise to 22.5 cm above the immersion line, the one without stirring in the vapour space, the second with the two stirrers turning. The chromatograms are given in fig. 15.

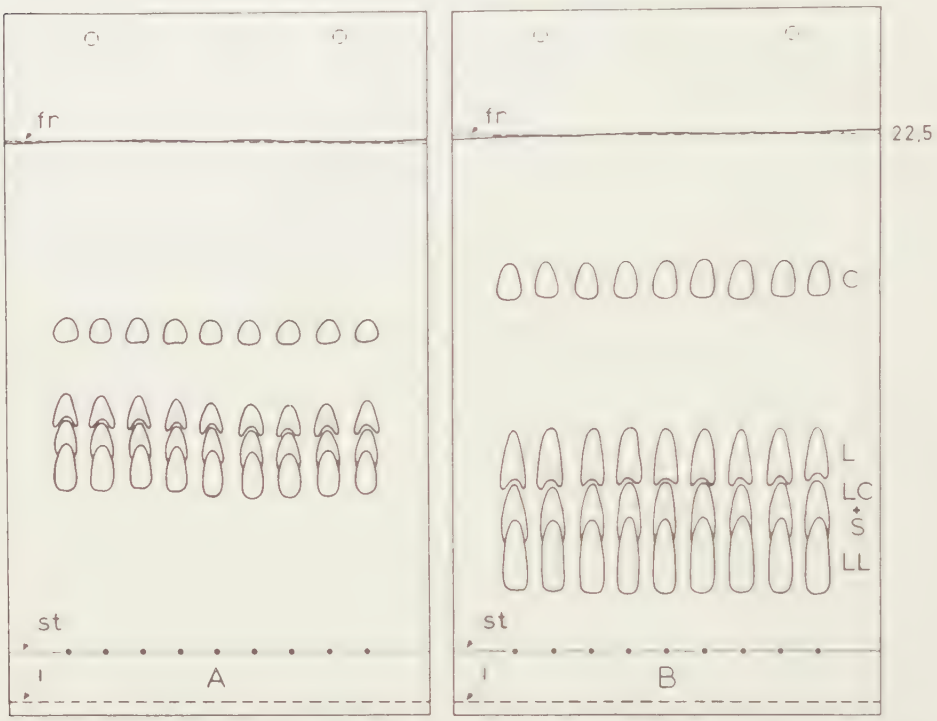

Fig. 15. Influence of stirring on chromatography of the reference mixture with di-isobutyl ketone—acetic acid—H_2O = 50:25:5 on old $SiCl_4$-treated paper (practically HCl-free). A stirrers at rest; B the two stirrers turning.

The following survey gives the R_{f_i} values:

	C	L	LC + S	LL
without stirring	0.64	0.48	0.43	0.37
with stirring	0.71	0.38	0.28[5]	0.19

b) Gradient determinations

For these determinations we used paper sheets, on which besides the immersion line and the future front line (22.5 cm above the immersion line) were drawn further horizontal pencil lines on 4.5 cm mutual distance. After rise of the front to the front line, the paper was cut rapidly into five zones, each of 17×4.5 cm, which were analysed as given in detail in Part III of this series [2]. The immersion zone (17×0.5 cm) is of course cut off and disregarded.

The results have been given in Table IV. The data of the table have been used in fig. 16 to draw the gradient curves.

TABLE IV

Influence of stirring in the vapour space on the acetic acid gradient in practically HCl-free $SiCl_4$-treated paper

Without stirring				Stirring with two stirrers turning			
position of zone; % of fr_i	wet strip –dry strip mg	acetic acid mg	acetic acid %	position of zone; % of fr_i	wet strip –dry strip mg	acetic acid mg	acetic acid %
0 – 19.9	811	311	38^3	0 – 19.7	782	252	32^2
19.9– 40.2	746	249	33^4	19.7– 39.5	711	206	29^0
40.2– 60.2	686	174	25^4	39.5– 60.1	736	202	27^4
60.2– 80.3	533	112	21^0	60.1– 80.0	614	170	27^7
80.3–100	313	64	20^4	80.0–100	380	114	30^0

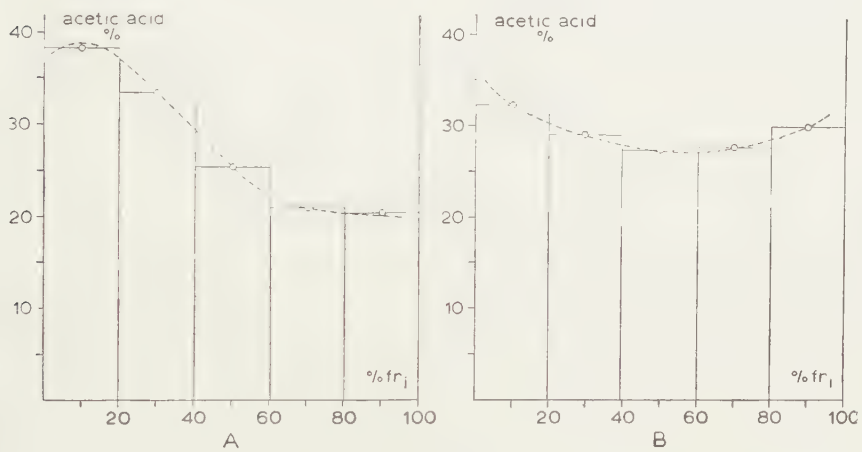

Fig. 16. Influence of stirring on the acetic acid gradient in the mobile phase wetting the paper (same mobile phase, ascension height of the front and kind of $SiCl_4$-treated paper as in fig. 15). A without stirring; B with two stirrers turning.

c) Discussion

α) *Change in slope of the gradient curve as a result of stirring in the vapour space*

When we first consider the chromatograms given in fig. 15, one sees that with the paper used a similar strong effect of stirring on the spread of spots is present, as we met in the preceding section.

It has been argued in preceding sections that the great influence of stirring in the vapour space must be due to an elimination of diffusion and rotation as limiting factors as a result of which the gradient curve should proceed less steeply.

The gradient determinations in this section confirm this argument.

The gradient curve has indeed a much smaller slope than without stirring.

A peculiarity is that the transport through the vapour space has been so efficacious that the gradient curve with stirring proceeds nearly horizontally to the right of the intersection point with the gradient curve without stirring, or even (when this is no experimental error) goes here through a flat minimum. Compare fig. 16, B.

That this remarkable shape of the gradient curve may arise, must be due to the fact that the liquid wetting the paper decreases strongly from immersion line to front (see columns 2 and 6 in Table IV). When (as a result of stirring) the vapour in the whole vapour space has nearly the same composition, the acetic acid concentration may increase with greater rate just in the last zone below the front, where the least amount of liquid is present.

β) Position of R_{fi}*-values on the two gradient curves*

The results in the preceding parts II and III of this series led to a picture of the mechanism of the chromatography, namely adsorption-chromatography combined with gradient elution. The base of a spot should lie at a particular composition of the mobile phase (as an approximate measure of which we take the acetic acid concentration) where it is eluted, while higher up the phosphatide is readsorbed.

When by external means we are able to change the gradient curve, it should appear that the R_{fi} values of the spots lie on the gradient curves at equal acetic acid concentration.

In section 3 we found that the slope of the gradient curve decreases with increase of the volume of the chromatographic apparatus. The gradient determinations in this case, however, are subject to great experimental errors (the zones analysed being only $4 \times 3\frac{1}{2}$ cm) to allow a control of the above discussed position of the R_{fi} values on the gradient curves.

It would seem that we are here in a more favourable condition. The error will be less since the zones analysed are $17 \times 4\frac{1}{2}$ cm, and gradient curves do not proceed so steeply).

In fig. 17, we have redrawn from fig. 16 the gradient curve without stirring (left diagram) and with stirring (right diagram). On each curve, points have been indicated with abscissa corresponding to the R_{fi} values given in the survey of paragraph a).

We see that in the case of points LL, LC+S and L the spots on the chromatograms are situated within experimental error at the same acetic acid concentrations. Compare the three horizontal broken lines which pass the points on the two gradient curves at distances of at most one weight % acetic acid (the experimental error).

It is not possible to draw such a horizontal line through the C-spots. Must we conclude that the mechanism proposed in Parts II and III of this series for chromatography without stirring, only holds for LL,

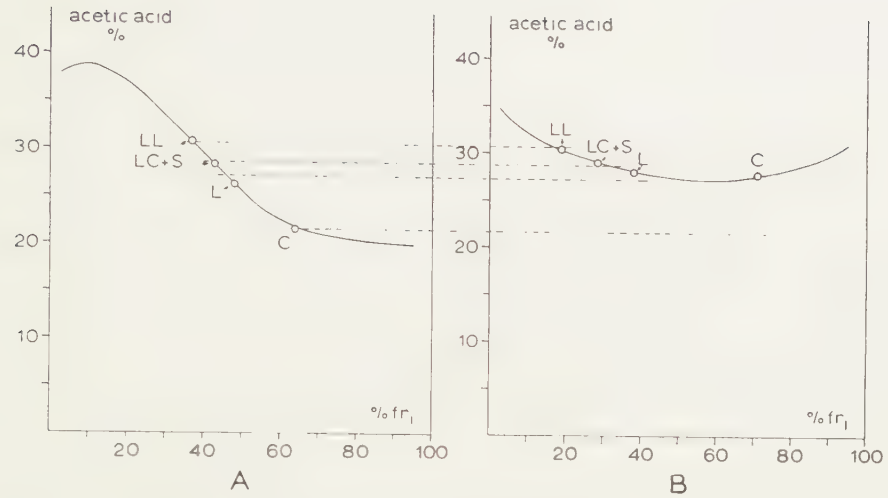

Fig. 17. Position of the R_{f_1}-values of the spots on the two gradient curves of fig. 16. A without stirring; B with two stirrers turning.

LC+S and L, but does not apply for C? This conclusion is not valid, for with stirring the gradient curve has its deepest point at an acetic acid concentration which lies higher than the elution concentration of C (given by the point on the left gradient curve). Hence with stirring the C spot on the chromatogram is no longer adsorbed on the paper, but moves in an eluted state.

Here the question arises as to the mechanism in which chromatography of the C spot occurs in the case of stirring. Another question also arises: should we regard the mechanism of chromatography with stirring of the other spots (LL, LC+L) still as adsorption chromatography combined with gradient elution?

We shall not go into these questions here. They will be dealt with experimentally in the next following part of this series.

10. *Influence of temperature*

a) Experimental

The experiments have been made on non-impregnated Ederol 208 paper in the large slit-feeding apparatus provided with stirrers (see fig. 11). At each temperature investigated (4°, 20°, 25° C) two chromatograms (ascension height of the front 18 cm) have been run with di-isobutyl ketone—acetic acid—H_2O = 40:25:5, of the Reference mixture (5 mm^3 $\frac{1}{2}$ % solution); one chromatogram without stirring, the second chromatogram with both stirrers turning. The chromatograms obtained are given in fig. 18 and fig. 19.

b) Results

The results of the experiments without stirring (fig. 18) show clearly that with increasing temperature the mutual distance of the three spots increases. Hence we conclude that with increasing temperature the slope of the acetic acid gradient

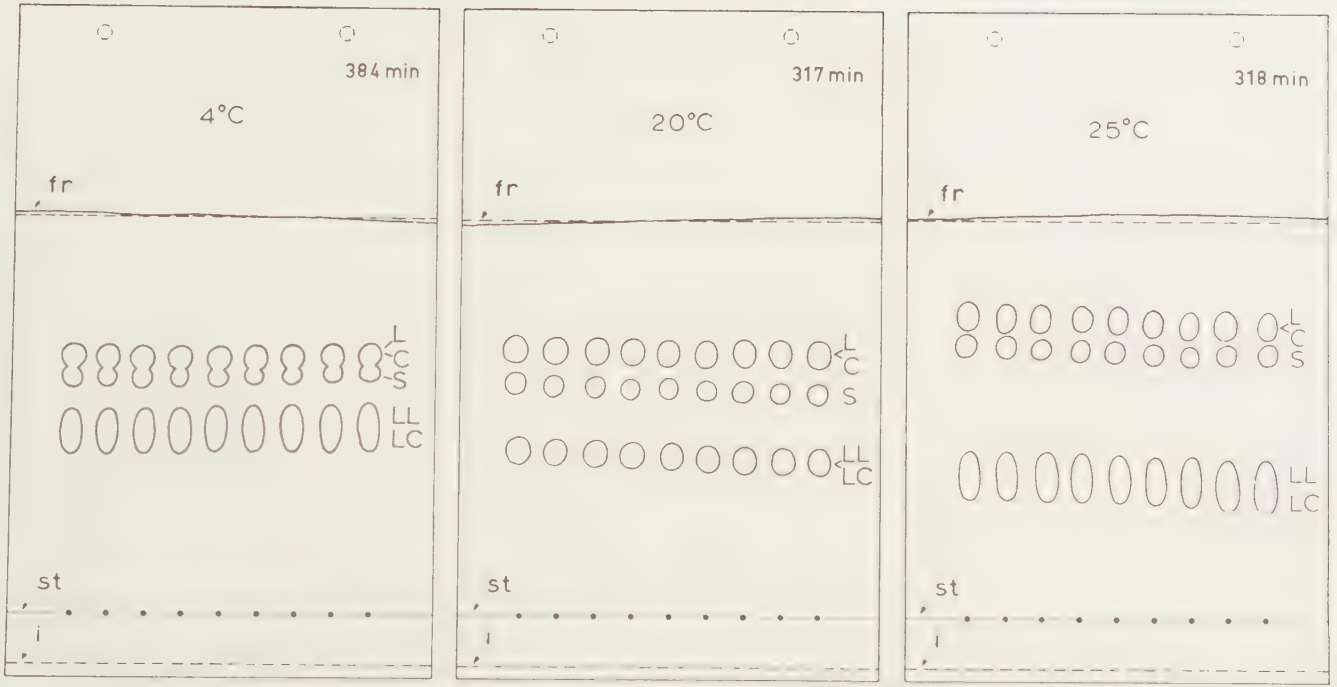

Fig. 18. Influence of temperature on the chromatography of the Reference mixture with di-isobutyl ketone—acetic acid—H_2O = 40:25:5 on non-impregnated Ederol 208 paper. The stirrers are at rest.

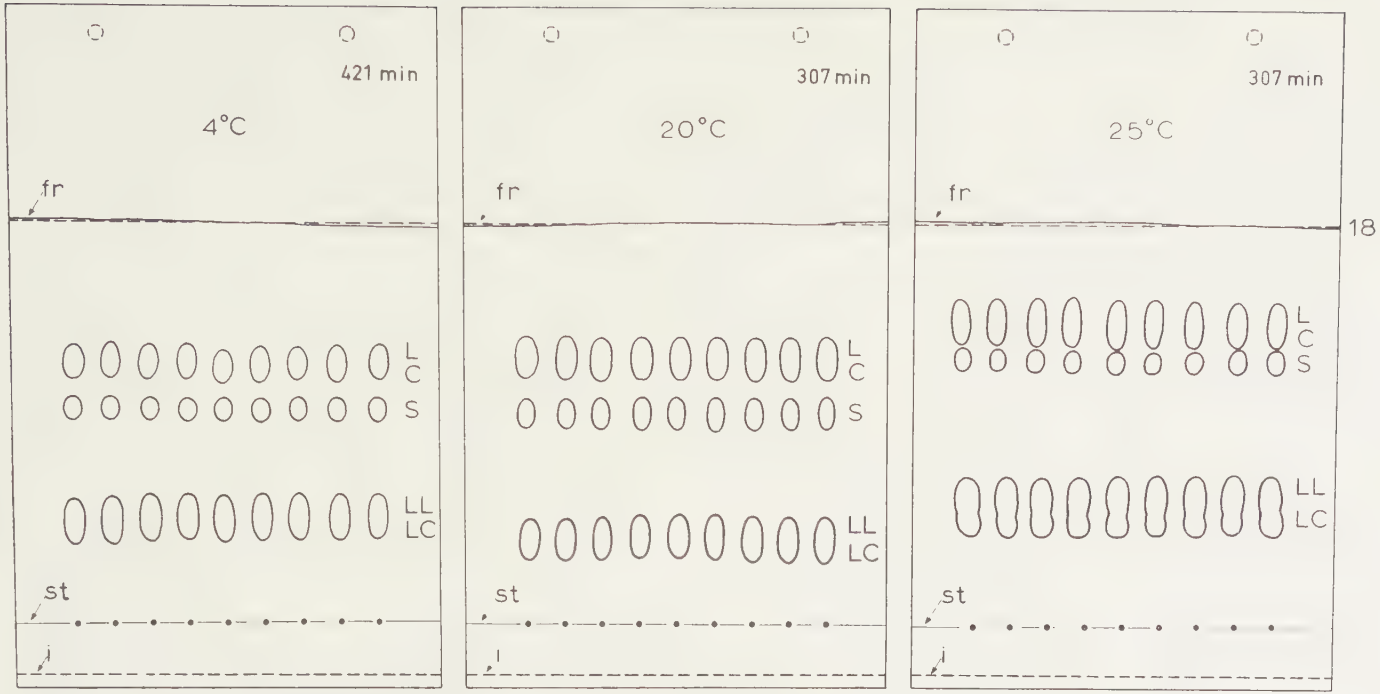

Fig. 19. Influence of temperature on the chromatography of the Reference mixture with di-isobutyl ketone—acetic acid—H_2O = 40:25:5 on non-impregnated Ederol 208 paper. The two stirrers turning.

decreases. A remarkable detail is that the separation of the two upper spots (L + C; S) which has taken place going from 4° to 20°, does not increase (even becomes less) going from 20° to 25°. Whereas the S-spot remains on its place from 4° to 20°, it shifts in upward direction going from 20° to 25°.

The results of the experiments with stirring (fig. 19) show in principle also an increase of spreading of the spots with increasing temperature, at least when the distance of the upper spot (L + C) to the lower spot (LL + LC) is considered.

The effect of increase of the temperature is less pronounced than in the experiments without stirring. This is plausible as with stirring the gradient already has a smaller slope and it cannot be made very much smaller by another factor.

In fig. 19 we see a similar detail as was mentioned above for the chromatograms obtained without stirring:

Going from 4° to 20° the S spot remains on its place, the L + C spot moves somewhat upwards and the LL + LC spot somewhat downwards. So these are signs of a regular decrease of the slope of the gradient.

Going from 20° to 25° all spots move in upward direction. It seems therefore that the gradient curve shifts in upward direction.

c) Discussion

α) *Complexity of the temperature influence*

When it is tried to argue which will be the influence of increased temperature on the mutual spreading of the spots, that is on the change in the gradient, we meet with the difficulty that so many factors are involved. We may divide them into four groups. For each factor we shall design in the survey below the influence of increased temperature with ↑ when the gradient by this factor alone would become less steep, that is the spreading of spots becomes greater. The sign ↓ will be used in the reverse case.

I. *Ascension time*

a) *surface tension* (driving force of ascension) decrease with temperature, hence by this factor alone the ascension will become slower and more time will be available for the transport mechanisms, so ↑.

b) *viscosity* (resistance for ascension) decreases with temperature hence available time for transport is shorter, so ↓.

II. *Partial vapour pressures*

c) *vapour pressure* increases with temperature, hence all other factors being constant, the amount transported through the vapour space is greater, hence ↑.

III. *Transport mechanisms*

d) *diffusion* in the vapour phase increases with temperature, so in the same time more transport, hence ↑.

e) *driving force of the rotation* will increase with temperature as the downward moving gas layer near the paper (section 6) will increase in density as a result of increased vapour tension. Hence more transport, so ↑.

f) *viscosity* of gases increases with temperature, hence slows down the convection by rotation in the vapour space. Hence less transport, so ↓.

IV. *Adsorption and elution*

In the above groups I, II and III it was assumed that in the range of temperature investigated, adsorption and elution are not affected by increase

of the temperature. When this is not true it is difficult to argue the effect of temperature on both and from this the influence the spreading of the spots is difficult to foresee, and this will not be tried here.

β) Temperature influence between 4° and 20°

When in fig. 18 the chromatograms at 4° and at 20° are compared, there is no indication that we must seriously take into account factors belonging to group IV of the above survey. The S spot remains practically on its place, as was also the case with non-impregnated Schleicher and Schüll paper and the same mobile phase (see fig. 6). Hence the turning point of the gradient remains on its place going from 4° to 20°. So we shall only consider the groups I, II and III of the above survey.

As to group I, it appears from the time in minutes written on each chromatogram, that from 4° to 20° the ascension time distinctly decreases, so the influence of temperature on factor *b* preponderated over that in *a*.

So when in the shorter time available a greater mutual distance of spots is obtained at 20° than at 4°, in the experiments without stirring (fig. 18) it follows that the net result of increased temperature on the factors mentioned in groups II and III is a distinct decrease of the slope of the gradient curve.

In the experiments with stirring (fig. 19) the slow transport mechanisms are removed. So the factors mentioned in group III need not to be considered for explaining the increase of mutual the distances of the spots. So group II remains, the increase of the partial vapour pressures with temperature.

In the experiments without stirring, the transport mechanisms are the limiting factors, which is evident from the great influence of stirring. It follows that the net effect of increasing temperature on factors *d*, *e* and *f* leads to a decrease of the slope of the gradient curve, and as factor *f* would in principle lead to the reverse result, the increased rate of diffusion (*d*) and of rotation of the vapour mass by factor *e*, preponderate.

Resuming we may say that without stirring the increased distance of the spots with increase of the temperature results from increase of vapour tension and of the increased rate of the transport mechanisms.

γ) Temperature influence between 20° and 25°

It is not so easy to explain the changes which take place in the chromatograms developed at temperatures from 20° to 25°. It seems likely that in this temperature interval factors involved in group IV can no longer be neglected, since there are signs that the gradient curve shifts in upward direction (compare paragraph *b*).

11. *Summary*

1. With specially constructed chromatographic apparatuses differing widely in available air space the resolution of the spots of the Reference mixture (C = cephalin, L = lecithin, LC and LL = their lysoproducts and S = sphingomyelin) has been investigated. Non-impregnated and $SiCl_4$-treated paper were used, with as a mobile phase di-isobutyl ketone – acetic acid – H_2O. The acetic acid gradient in the mobile phase wetting the paper has been investigated.

2. Resolution of spots is small with a very small available air space; the gradient curve in this case is very steep.

With increasing air space the resolution of spots increases and the slope of the gradient curve diminishes. The results support the conclusions

reached in Part III of this series, i.e. the location of a chromatographic spot indicates a particular acetic acid concentration on the gradient curve, at which the spot is eluted at its base with maximal rate.

3. In the not realizable case of an apparatus without air space, the gradient curve will consist of three parts; a horizontal part from immersion line to a certain fraction of the distance front to immersion line, an extremely steep descent and a second horizontal part up to the front and with acetic acid concentration zero. The origin of the gradient is attributed to adsorption of acetic acid to the paper. Elution of spots occurs by adsorption displacement. The sequence of the spots on non-impregnated paper and on $SiCl_4$-treated paper can be explained from this point of view.

4. The air space in a chromatographic apparatus allows acetic acid transport by diffusion through the vapour phase from the lower part of the wetted strip to the upper part. Similarly di-isobutyl ketone transport occurs from the upper part of the strip to the lower part. So the slope of the descending part of the gradient curve is lowered and as a consequence the mutual distance of the spots on the chromatogram increases. The effect is greater as diffusion is more effective, for instance in an apparatus with larger air-space.

5. With a specially constructed slit-feeding apparatus descending and ascending chromatography have been compared.

The results (greater separation of spots in descending chromatography) point to an additional transport mechanism in the vapour phase. A downward movement of the vapour occurs along the wetted strip and upward along the glass wall of the container. In descending chromatography the transport of acetic acid from the slit-side part to the frontside part of the wetted strip by means of this rotation current of the vapour is much more efficient than in ascending chromatography. Hence the slope of the gradient curve is smaller here than in ascending chromatography. In practice descending chromatography is not recommended. It is difficult to obtain acceptable and reproducible chromatograms.

6. The recognition that the vapour space in a chromatographic apparatus partly determines the degree of separation of spots allows to foresee, or helps to explain, the influence of other factors.

7. With a given chromatographic paper, separation is somewhat greater when the mobile phase ascends in the direction of the slower suction rate than in the direction of faster suction rate. The ascension time is longer in the first mentioned case, so here is more time for diminishing the slope of the gradient curve.

8. One should expect that stirring in the vapour space will increase the resolution of spots. Stirring will eliminate as a limiting factor the slow transport mechanisms in the vapour space (diffusion; rotation). Hence the slope of the gradient curve will be diminished in the case of stirring.

These expectations have been confirmed by means of a specially con-

structed, large slit-feeding apparatus, provided with stirrers. The experiments show indeed an increased resolution and a strongly dimished slope of the gradient curve.

An unforeseen but easily explained additional detail is that the gradient curve with stirring shows a shallow minimum, the implications of which have been discussed for the mechanism of chromatography with stirring.

9. It is difficult to predict the influence of temperature on the separation of spots in general. The net result will be composed of the effect of temperature on all partial processes involved in chromatography.

Without stirring the separation of spots increases in the range 4°–20°. It is argued that this is due to the preponderating influence of increased partial vapour tensions, increased rate of diffusion, and increased intensity of rotation.

10. With stirring the separation of spots also increases with temperature. The limiting transport mechanisms are eliminated by stirring so the effect must be due to the preponderating influence of increased partial vapour tensions.

11. Our experiments suggest that in the range 20°–25° the influence of temperature on adsorption and elution begins to become apparent.

Department of Medical Chemistry,
University of Leyden

REFERENCES

1. Bungenberg de Jong, H. G. and J. Th. Hoogeveen, these Proceedings, Series **B 63**, 228 (1960).
2. ———— and ————, these Proceedings, Series **B 63**, 383 (1960).
3. ———— and ————, these Proceedings, Series **B 63**, 190 (1960).
4. ———— and G. R. van Someren, these Proceedings, Series **B 62**, 150 (1959).
5. Hooghwinkel, G. J. M., J. Th. Hoogeveen, M. J. Lexmond and H. G. Bungenberg de Jong, these Proceedings, Series **B 62**, 222 (1959).
6. Bungenberg de Jong, H. G. and J. Th. Hoogeveen, these Proceedings, Series **B 63**, 1 (1960).
7. ———— and ————, these Proceedings, Series **B 63**, 15 (1960).

GRAPHITIC OXIDE

VI. SOME PHYSICO-CHEMICAL PROPERTIES

BY

J. H. DE BOER AND A. B. C. VAN DOORN

(Communicated at the meeting of September 24, 1960)

1. *Introduction*

In the preceding paper (communication V) [1] we discussed the swelling of graphitic oxide by the adsorption of water. From this discussion resulted the remark that perhaps the röntgenographically determined c-spacings might be wrong in so far as these spacings should not represent the actual situation and should only be average values.

In order to investigate this suggestion we determined the density of anhydrous graphitic oxide and of some water containing samples using benzene as imbibition liquid. For it is known that graphitic oxide does not swell in benzene and in this manner we can thus measure the changes in volume of graphitic oxide caused by the penetration of water between the hexagon layers.

Moreover we determined the density of anhydrous graphitic oxide in a number of other imbibition liquids.

The final conclusions from these experiments and from those described in the preceding paper will be discussed.

2. *The density of graphitic oxide in benzene*

The density of graphitic oxide was determined in a pycnometer (about 4 ml) in the following way. About 200 mg graphitic oxide were immersed by 1 ml of dry benzene and afterwards the sample was de-aerated by careful evacuation at a pressure of about 18 mm Hg. Thereupon the pycnometer was filled with benzene and placed in a thermostat at 25° C.

Figure 1 gives the change of the specific volume of graphitic oxide (V_s) in relation with the water content of the samples. It is seen that the specific volume reaches a minimum value at a water content of 4.2 %; afterwards the specific volume increases linearly with increasing water content.

As a matter of fact the specific volume is calculated per gram material, so the amount of graphitic oxide decreases with increasing water content. It is, however, much more convenient to relate the volume of 1.000 mg anhydrous graphitic oxide (V_s') plus the volume of the adsorbed water (V_a) with the water content. By way of example we recalculate two points of figure 1 in this manner:

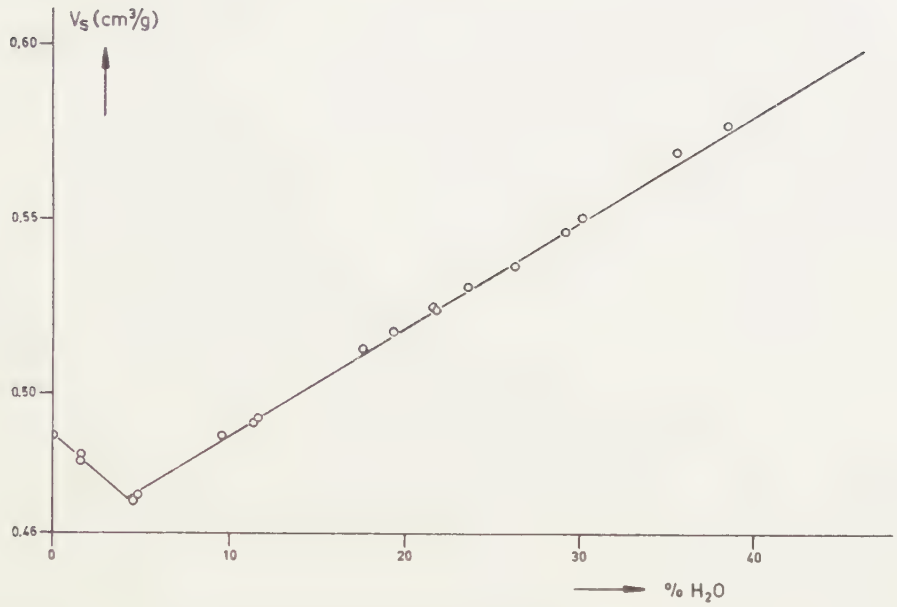

Fig. 1. V_s is specific volume in benzene of graphitic oxide containing known amounts of water. % H_2O has been calculated on anhydrous graphitic oxide.

One sample graphitic oxide contains 1.6 % H_2O (calculated on dry material) and the specific volume is 0.481 ml. One gram of this product thus contains 984.3 mg graphitic oxide and 15.7 mg H_2O. Thus 1,000 mg anhydrous graphitic oxide and 16.0 mg H_2O together have a volume of $\frac{1{,}016}{1{,}000} \times 0.481 = 0.489$ ml.

The second sample contains 4.3 % water and the specific volume is 0.468 ml. One gram of this sample consists of 958.8 mg anhydrous graphitic oxide and 41.2 mg water. Thus 1,000 mg anhydrous graphitic oxide plus 43 mg water together have a volume $\frac{1{,}000}{1{,}043} \times 0.468 = 0.488$ ml.

In this manner all experimental points of figure 1 are recalculated and are shown in figure 2 (curve A). We see now that graphitic oxide indeed is capable of adsorbing 4.2 % water without any swelling. There must thus be free space in the graphitic oxide lattice. In figure 2 is also drawn curve B which relates the water content with the sum of the volumes of 1,000 mg anhydric graphitic oxide (0.489) and of the amount of free water (density = 1), corresponding with the amount of adsorbed water.

The slope of curve B is not equal to that of the ascending part of curve A. However, this is caused by the fact that graphitic oxide, containing more than 10 % water, looses part of the water which is taken up by the dry benzene. This was experimentally verified in the following way. After the determination of the density of graphitic oxide, the upper layer of benzene was withdrawn with a pipette, and the water content and the density of this benzene were both determined. The

specific volume of the graphitic oxide was now again calculated, using the changed density of the benzene; moreover the water content of the graphitic oxide was corrected for the loss of water. This specific volume of graphitic oxide, calculated per 1,000 mg anhydrous material, is given in figure 2 by curve C. We see that curves B and C in this figure are completely parallel. We therefore must conclude that the density of the adsorbed water is indeed equal to 1.

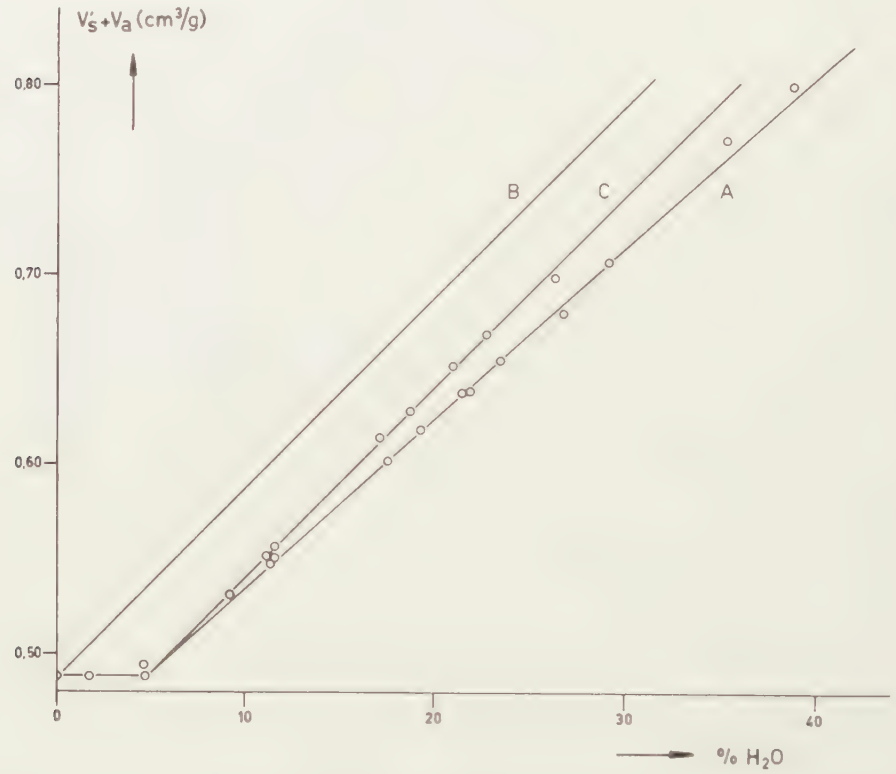

Fig. 2. $V_s' + V_a$ is volume of 1 gram of graphitic oxide plus the volume of the amount of water adsorbed. % H_2O has been calculated on anhydrous graphitic oxide.

3. *The density of graphitic oxide in several imbibition media*

The technique of these determinations is the same as already described in the preceding section.

Preliminary experiments were carried out with different graphitic oxides viz. 3H′, 6H′ and with 3X. No difference in specific volume between these samples was observed using water, benzene or methanol as imbibition liquid. Also in this respect the different graphitic oxides all show the same behaviour.

In table I are given the specific volumes of graphitic oxides in a number of imbibition media.

TABLE I

Imbibition medium	Specific volume ml/g
methanol	0.383
1–4 dioxane	0.399
ethanol	0.400
pyridine	0.412
water	0.423
nitrobenzene	0.446
helium (corrected)	0.465
reciprocal röntgen-density	0.466
benzene	0.488
carbontetrachloride	0.515

The specific volume of graphitic oxide in helium [1]) is 0.475 ml/g. It was recently shown [2] that the true specific volume of an adsorbent is best approximated by correcting the specific volume in helium for the distance to which the helium atoms approach the surface of the adsorbent. If we take for this distance the radius of the helium atom, calculated from the b-term of the Van der Waals equation, i.e. 1.3 Å, then this sterical correction has the value: $S \times 1.3 \times 10^{-8}$ ml. Here S is the outer surface of the adsorbent; in our case $S = 74.8$ m²/g, so the correction has a value of $74.8 \times 10^4 \times 1.3 \times 10^{-8} = 0.010$ ml/g. The corrected specific volume in helium becomes thus: $0.475 - 0.010 = 0.465$ ml/g. This value agrees very well with the reciprocal X-ray density, i.e. 0.466 ml/g. The latter was calculated as follows: one gram $C_7O_4H_2$, having a unit weight 150, contains $\frac{6.02 \times 10^{23}}{150}$ units $C_7O_4H_2$; the surface of one unit $C_7O_4H_2$, corresponding with 3.5 hexagons, is $3.5 \times 5.25 = 18.4$ Å² whereas the distance between two hexagon layers is 6.3 Å. Thus the calculated specific volume becomes:

$$\frac{6.02 \times 10^{23}}{150} \times 18.4 \times 6.3 \times 10^{-24} = 0.466 \text{ ml/g.}$$

The agreement between the calculated and the experimentally observed value (in helium) of the specific volume seems to indicate that graphitic oxide has retained the graphite character in the hexagon layers during the oxidation. On the other side this graphite character is improbable in view of the hydroaromatical character which we must assume in order to understand the flexibility of the hexagon layers. In a future paper we hope to return to this discrepancy.

The difference between the specific volume in water and in helium (corrected) is 0.042 ml. This is in perfect agreement with the fact (known from the röntgenographic investigation (communication V) [1] and shown above) that graphitic oxide can adsorb the first 4.2 % of water without

[1]) Our thanks may be expressed here to Mr. P. Zwietering who determined the specific volume of graphitic oxide in helium for us.

any swelling. This water, which penetrates into the lattice, is apparently taken up by free space between the hexagon layers. Gases, including He and liquids which do not penetrate into the lattice, cannot be taken up by this space.

Remarkable is furthermore the very low specific volume of graphitic oxide in methanol and in dioxane. The dioxane molecules, which are much larger than the water molecules, evidently fill a larger space between the hexagon layers than the water molecules. The reason of this fact is perhaps that the water molecules are adsorbed on specific centres. One could imagine that these specific centres are to be identified with the carbon-oxygen complexes.

4. *Discussion of the results*

There is a discrepancy between the X-ray data of the swelling in water (communication V [1]) and the specific volume data of the swelling in the present communication. According to the present data 4.2 % of water is taken up by graphitic oxide without any swelling, whilst any more water, taken up by swelling, adds its own volume (specific volume of this water being 1.0) to that of the graphitic oxide. The X-ray data agree with the lack of swelling by the first 4.2 % of water. From 4.2 % to about 16 % of water, however, X-ray data indicate only a linear swelling of the distance between hexagon layers from 6.3 Å to 6.8 Å. The absorption of 12 % of water, therefore, results only in an increase of this distance of 0.5 Å, whilst it should be 2.1 Å. This latter figure is, indeed, found on further swelling, as already indicated in communication V [1].

It has already been stated in communication V that 16.2 % of water corresponds with the so-called unimolecular layer of the B.E.T.-theory; it is the V_m value. This V_m value, however, is too small for a unimolecular layer of water molecules, covering the total surface of all hexagon layers. As already stated above these water molecules may be bound to specific, hydrophylic centres.

From the conclusion of the investigation of the oxidative properties of graphitic oxide (communication IV [3]) we know that the *bruto* formula $C_7O_4H_2$ can be written as:

$$\{C_7(=O)H\}O_3H \rightleftharpoons \{C_7(OH)\}O_3H$$

Furthermore it appeared that the hydrogen atom of the O_3H combination is bound to an oxygen atom in either an OH or an OOH group. In this discussion we will tentatively call this combination an "OH" group.

It seems justified to identify the V_m value of the water-sorption isotherm with that quantity of water required to hydrate all hydrophilic, say "OH", groups. The absorption of water may thus take place on two different groups viz. the enolic OH group and the above mentioned "OH" group. The swelling of graphitic oxide takes place moreover in

two steps. The first 4.2 % H_2O (i.e. 0.36 mol H_2O per unit $C_7O_4H_2$) are taken up without any swelling; afterwards the adsorption of water is accompanied by swelling. When 16.2 % H_2O is adsorbed (i.e. the V_m-value) there is exactly 1 mol H_2O more adsorbed since the first 4.2 % H_2O; for 16.2 % H_2O corresponds with 1.35 mol H_2O.

This, however, does not mean that really every "OH" group is hydrated, for the V_m-value corresponds with a statistical monolayer. As a matter of fact those "OH" groups which are situated near the edges of the lamellae are hydrated more easily than the "OH" groups in the middle of the lamellae. However, if the first "OH" groups (i.e. the most accessible) are hydrated, these hydrated "OH" groups can serve as second adsorption centres. This is the more probable if one keeps in mind that the attraction forces between the hexagon layers are essentially Van der Waals forces. These are, however, inversely proportional to r^3 if r is the distance between the layers. As this distance is increased by the adsorption of the water molecules, the energy required for the second molecule of water may be smaller. It is true the real adsorption energy will be smaller for the second molecule but the total adsorption energy (i.e. real adsorption energy minus swelling energy) may be more favourable than if the second water molecule penetrates further into the lattice in order to hydrate the "OH" groups lying further inwards. These same arguments hold for the adsorption in the third and higher layers.

A similar process of gradual penetration from the outside to the inside of the layer lattice is found with Mg-vermicullite. Walker [4] observed that the penetration of water causes an increase of the layer-distance from 11.6 Å to 13.8 Å. This increase starts from the outside and is followed by a second increase from 13.8 Å to 14.4 Å, even before the first increase has reached the centers of the platelets. The gradual swelling here proceeds in distinct steps, whilst in graphite oxide it proceeds continuously. This latter behaviour is caused by the great flexibility of the hexagon layers (see communication V [1]) in contrast to the rigidity of the layer of the Mg-vermicullite lattice. One may visualize that in the case of graphitic oxide the penetrating water causes the layers to bend, as is shown schematically in figure 3.

This process of bending of the lamellae proceeds so far until it is energetically more favourable for the water molecules to penetrate further into the lattice rather than to separate the layers more from each other.

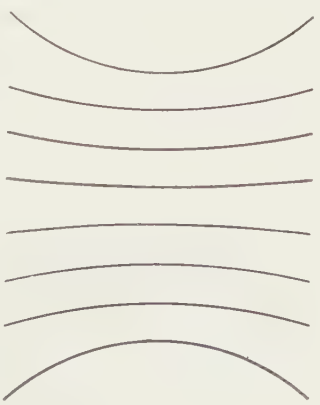

Fig. 3. The swelling of a particle of graphitic oxide by the uptake of water.

Schematically this process of swelling is given in figure 3. It is evident that we obtain a continuous spectrum of c-spacings. Röntgenographically we only determine an average of the mostly occurring c-spacings. The extreme values of the c-spacing, which occur only in relatively small quantities but which, however, correspond with a large part of the adsorbed water, are not determined röntgenographically and thus the c-spacing, determined in this manner, is too small.

This process of adsorbing and swelling goes on in the manner described till graphitic oxide has a water content of 16.2 %; because from this point onwards the swelling in the direction perpendicular to the laminae increases linearly with the water content, and one has to conclude that from this stage onwards swelling and further penetrating into the layer lattice proceed equally well. For the average increase of the c-spacing from 16.2 to 32.4 % H_2O (i.e. the forming of the second statistical layer of adsorbed water molecules) is 2.1 Å which is a value also found with the swelling of montmorillonite [5, 6].

The V_m-value from the water vapour isotherm is thus probably best identified with the number of hydrophilic centres in graphitic oxide. On these centres the water molecules are bound by localized adsorption. This explains the large difference between the "water-surface" and the theoretically calculated lamellar surface of graphitic oxide viz. 585.1 and 738.4 m^2 per gram respectively (see our preceding paper [1]).

From the density in helium and from the specific surface we can calculate the number of hexagon layers per crystallite of graphitic oxide. Suppose there are n particles per gram; the volume of 1 gram is: $n \times \pi r^2 h = 0.465 \times 10^{24}$ Å^3. The surface per gram is: $n \times 2\pi r^2 = 0.70 \times 10^{20}$ Å^2. From this it follows h = 130 Å corresponding with $\frac{130}{6.3}$ is about 20 hexagon layers.

Acknowledgements

One of the authors (A. v. D.) gratefully acknowledges the permission of the National Defence Research Council TNO to publish the results of this investigation. He also wishes to express his thanks to the Director of the Chemical Laboratory of this Council, Mr J. van Ormondt, for his constant interest in this study.

The authors are greatly indebted to Mr J. R. Reinsma for his valuable assistance in the experimental work.

LITERATURE

1. Boer, J. H. de and A. B. C. van Doorn, Proc. Kon. Ned. Akad. Wet. **B 61**, 242 (1958).
2. ——— and J. J. Steggerda, Proc. Kon. Ned. Akad. Wet. **B 61**, 317 (1958).
3. ——— and A. B. C. van Doorn, Proc. Kon. Ned. Akad. Wet. **B 61**, 160 (1958).
4. Walker, G. F., Nature **177**, 239 (1956).
5. Hendricks, S. B., *a.o.*, J.A.C.S. **62**, 1457 (1940).
6. Mooney, R. W., *a.o.*, ibid. **74**, 1371 (1952).

DICERORHINUS HEMITOECHUS FALC. IN THE NETHERLANDS

BY

H. LOOSE

(Communicated by Prof. I. M. VAN DER VLERK at the meeting of September 24, 1960)

During sand dredging operations in the Zwarte Water, near Westerveld (province of Overijssel), a rhinoceros skull was found in May '58.

It had the general form of Coelodonta antiquitatis, with some important differential characteristics. These all pointed to Dicerorhinus hemitoechus Falc., a species not yet recorded from the Netherlands.

Of this well preserved skull (a few, not very important, fragments and the mandible are missing) a summary description, followed by some general remarks on the species, is given here.

(See fig. 2–5). The nostrils extend farther backwards than in C. antiquitatis. While in that species the posterior border lies approximately between P^3 and P^4, in this skull the nostrils end above the posterior rim of P^4.

The rugosity of the nasal horn base is considerable. The frontal horn base is seen in lateral view by a slight curve of the frontals only.

While C. antiquitatis is known for its complete bony nasal septum, in this skull the bony septum is incomplete in the middle. There are traces of a cartilaginous part where the bony septum ends.

The zygomatic arch shows a double bend. The maxillar part extends in a straight line to the rear; the jugal turns up and backward at an angle of 30°; at the glenoïd fossa, the arch runs downward toward the median sagittal plane.

The articular plane on the anterior rim of the glenoid fossa is 11.5 cm wide, measured perpendicular to the m.s. plane. In two skulls of C. antiquitatis values of 9.5 and 10 cm were found.

Behind the fossa there is a well developed postglenoidal processus, forming the anterior rim of the auditory meatus (a triangle pointing downward with one angle), the paroccipital processus providing the posterior rim.

The parietals are deeply constricted by the cristae temporales (minimum width 3.4 cm; in skulls of C. antiquitatis 7.5–12 cm).

The occipital crest is not as wide as the base of the skull. This causes the occipital view of the skull to be a trapezium. In C. antiquitatis this part is a rectangle.

The occipital crest of this skull is 16.5 cm wide, in C. antiquitatis about 23 cm.

In the occipital crest of C. antiquitatis a median fossa is an exception, sometimes there is a median protuberance. The present skull has a marked median fossa.

The foramen magnum has the shape of an ellipse, with its shorter axis in the median sagittal plane. In C. antiquitatis the foramen is higher, with the shape of an ovoid or triangle. This is caused in part by a difference in the orientation of the foramen magnum. In the skull from the Zwarte Water the angle between the vertical axis of the foramen magnum and the roof of the mouth is 119°. In C. antiquitatis (ZEUNER, 1934, 19 ind.) the maximum was 107°, the median 95°, the minimum 83°.

In 1822 CUVIER described a rhinoceros skull *without* bony nasal septum under the name *Rh. leptorhinus*. DE CHRISTOL thought (an opinion entirely founded on reproductions of drawings of the type specimen) that a complete bony septum had been present. Therefore he described the skull without septum, found in 1835 near Montpellier (dép. Hérault), under the name *Rh. megarhinus*.

In 1846 OWEN described part of a skull from Clacton-on-Sea (Essex) *with* septum as identical with *Rh. leptorhinus Cuv.*, thereby endorsing the judgement of DE CHRISTOL. Finally FALCONER in 1860 created the species *Rh. hemitoechus* for the Clacton skull and some others with an incomplete bony septum, after showing the impossibility of maintaining the name *Rh. leptorhinus*, given by CUVIER to a skull *without* septum.

The species, described by JAGER originally in 1839 as *Rh. kirchbergensis* and subsequently in 1841 as *Rh. Merckii*, is rejected by FALCONER as founded on insufficient data (^{2}M, M^3, 1 lower molar) and provisionally identified as belonging to *Rh. megarhinus*.

Now confusion is complete. Only one species remains well defined, despite frequent changes in the name of the genus: *Coelodonta antiquitatis Blum*. Much has been published on the other pleistocene species in the century after FALCONER, with usually every author taking the opposite view of his predecessor.

In this battle of systematics, *Rh. leptorhinus* and *Rh. megarhinus* appear as rather vague and loosely defined names of doubtful value. Most of the heavy fighting has been (and in some countries still is) over the question: are *hemitoechus* and *kirchbergensis* separate species?

Complete, well preserved skulls are rare. The efforts to differentiate the species *D. etruscus hemitoechus kirchbergensis* are therefore mostly based on differences in dentition. The fact that this is extremely difficult for *D. hemitoechus* and *D. kirchbergensis* is no proof that these species are actually one. When the complete skulls are compared, all evidence is to the contrary [1]).

F. ZEUNER has shown [2]) a connection between anatomy of the skull

[1]) STAESCHE '41.

[2]) ZEUNER '34.

and ecology in the Rhinocerotidae. To this end certain standard measurements were treated statistically.

Owing to lack of material ZEUNER was unable to apply his method to *D. hemitoechus*. In the present publication. measurements according to ZEUNER (and an additional dimension) are given for 8 crania of *D. hemitoechus* (6 in the British Museum, Natural History, the skull from the Zwarte Water and the cranium from the Stuttgart Staatl. Museum für Naturkunde).

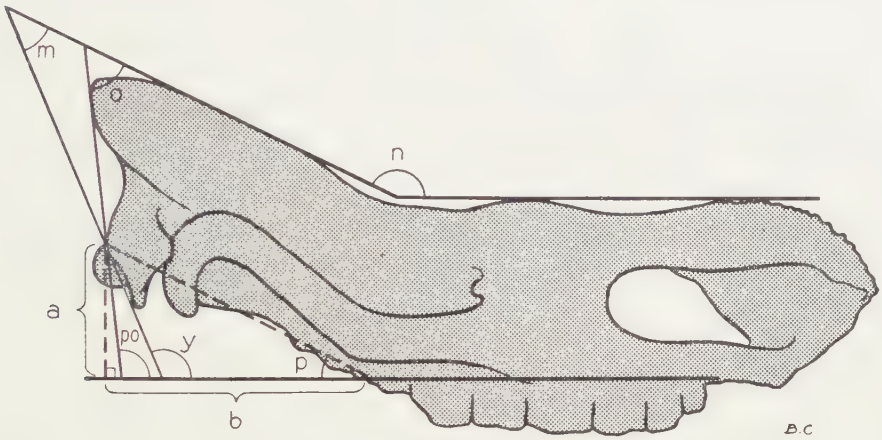

Fig. 1

Fig. 2. Leiden No. 93302 occipital view.

	Coelodonta antiquitatis Blum.					*D. hemitoechus Falc.*					*D. kirchbergensis Jäg.*				
	min.	med.	max.	arithm. mean	number of spec.	min.	med.	max.	arithm. mean	number of spec.	min.	med.	max.	arithm. mean	number of spec.
l	540	700	780		29	630	655	725	672	5	630	670	740		3
st	0	0	14	1	32	0	10	60	24	7	10	11	14	12	5
o	42	54	65	53	35	47	53	56	52	7	70	77.5	83	77	4
i	42	54	65	54	37	47	53	56	52	7	68	76	83	75	5
n	143	154	163	154	29	145	154	160	153	6	147	152	155	151	3
p	18	24.5	31	25	18	22		23.8		2	21	27	28	26	4
po	80	98	117	100	19	90		93		2	67	67	72	69	3
y	83	95	107	95	19	110	118	120	116.6	5	82	95.5	109	95.5	4
m	40	53	80	55	34	28	37	44	37	6	41	55	66	54	5
x	—14	—1.5	+27	+1	32	—21	—14	—9	—14.6	6	—42	—17.5	—13	—22.5	4
z	75	88	120	92.6	12	34	49	60	47.75	8					

The measurements for *Coelodonta* and *D. kirchbergensis* have been taken from Zeuner '34. At the ext right are the values for the skull from the Zwarte Water

Abbreviations

l, st and z have been measured in mm, all others in degrees. All measurements, except z, have been taken in the median sagittal plane. The m.s.p. is not mentioned in the definitions, to keep them as simple as possible. (See also fig. 1).

l Distance rhinion-basion (length from tip of nasals to lower margin of foramen magnum). As the development of the occipital crest varies for species, age and sex, the basal length of the skull has been taken as standard.

st Incision in the middle of the occipital crest.

o Angle between opisthion + occipital crest and the parietals.

i Angle between parietals and hindmost point of the occipitals.

n Angle between parietals and tangent of hornbases.

p

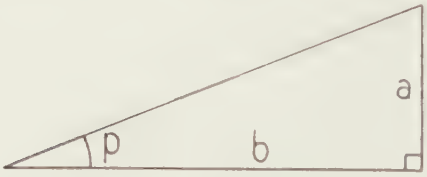

a = height opisthion-extended roof of mouth

b = distance aboral end of roof of mouth-intersection with a.

po Angle between opisthocranion + opisthion and roof of mouth (aborally extended).

y Angle between basion + opisthion and roof of mouth.

m Angle between basion + opisthion and parietals.

x x = m − o

z Minimal width between the cristae temporales.

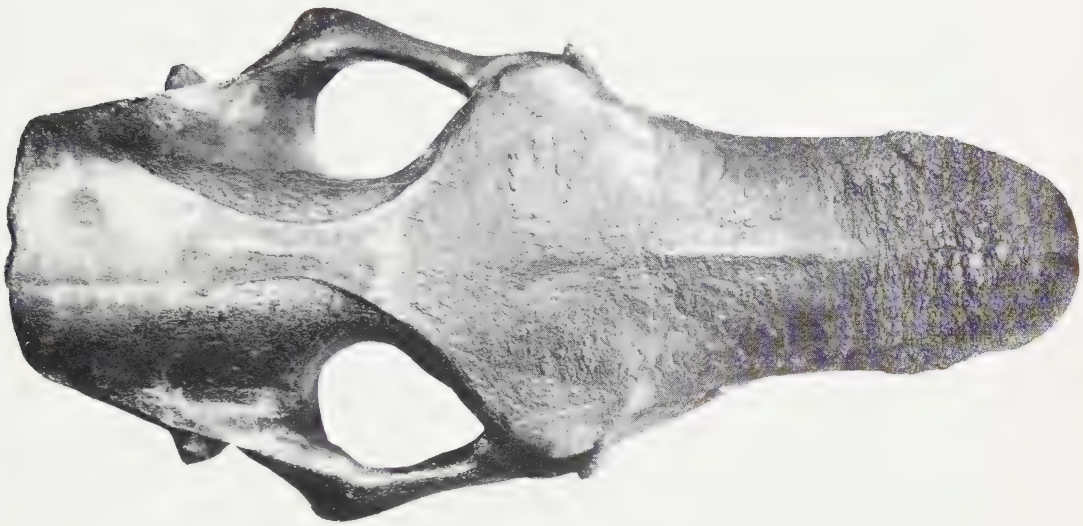

Fig. 3. Leiden No. 93302 vertical view.

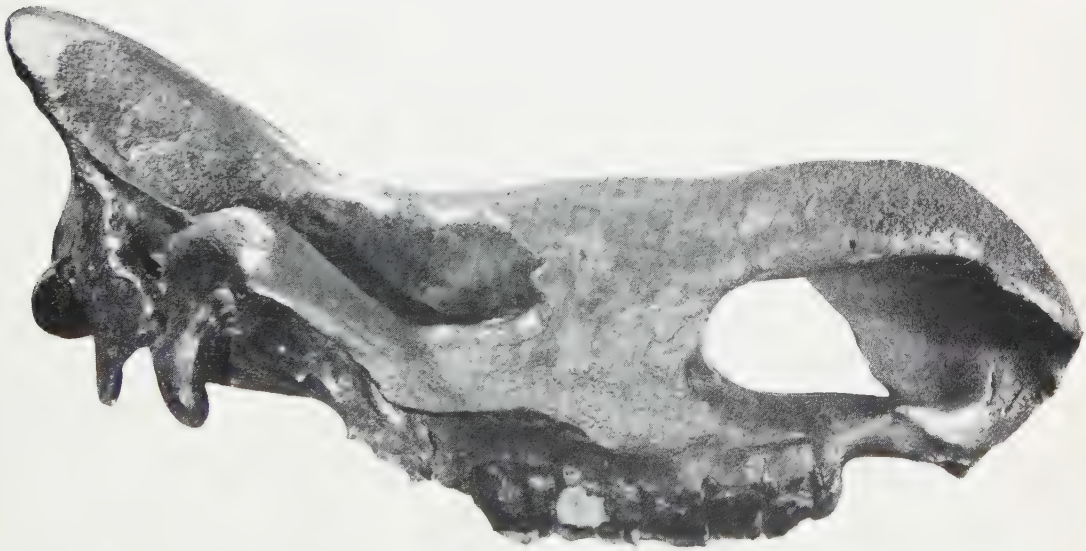

Fig. 4. Leiden No. 93302 lateral view.

Fig. 5. Leiden No. 93302 basal view.

l Of the 3 species *Coelodonta antiquitatis* is the largest. *D. kirchbergensis* is slightly larger than *D. hemitoechus*. This conclusion is confirmed by dental evidence given by STAESCHE '41.

st Mostly absent in *Coelodonta*, often replaced by a protuberance. No such protuberance has been found in the *hemitoechus* skulls examined. According to DUERST 1926, p. 143, protuberances and crests indicate tangential insertion of tendon on bone, incisions and fossae an insertion perpendicular to the bone.

o, i Always identical in *D. hemitoechus*. In *Coelodonta* and *D. kirchbergensis* irregularities in the relief of the occipitals sometimes occur.

n No significant differences between the three species.

y The angle y in *D. hemitoechus* was found to be considerable, even when no exact measurements were possible.

The figures for y are:	Leiden	93302	119
	Brit. Mus.	20013	120
		27836	—
		45205	110
		M5113	—
		40946	—
		45206	118
	Stuttgart	16938	116

STAESCHE '41 p. 115 had already seen the divergence of *y*. As he had only the Stuttgart skull at his disposal, he could not decide between a fortuitous aberration and a typical characteristic. The fact that in all skulls of *D. hemitoechus* the angle y was rather large, must decide for the latter.

D. hemitoechus and *Coelodonta antiquitatis* were animals of the open country, getting their food mainly by grazing, also by browsing on small shrubs. In *Coelodonta*, when grazing, the skull was held in a direct line with the cervical vertebrae, all pointing in a straight line to the ground (ZEUNER '34). A reconstruction of *D. hemitoechus* should correspond with the white rhino, *Ceratotherium simum Burch.*, holding its neck approximately horizontal when at rest, the head pointing to the ground.

m, x Because of the large values for y, m is small. This is seen even better with *x* (= m − o). ZEUNER has measured values between + 27 and − 14 for *Coelodonta*. In *D. hemitoechus* all measurements were negative.

z In *Coelodonta* z varies between 72 and 120, in *D. hemitoechus* between 34 and 60.

The material of the genus Dicerorhinus used in this study may not be very impressing in number. Yet a few conclusions are warranted.

If we disregard the form of the occiput and the dentition, the best characteristic of *Dicerorhinus hemitoechus Falc.* is y. Also, m would be useful, but m-max. is already slightly higher than m-min. for *Coelodonta* or *D. kirchbergensis*. Both m and y reflect the exceptional angle between foramen magnum and rest of the skull.

Acknowledgements

I am extremely thankful to:
the Director of the Rijksmuseum van Geologie en Mineralogie, Leiden, for entrusting me with the description of this new acquisition;
Dr A. J. Sutcliffe of the British Museum (Natural History) and Dr K. D. Adam of the Staatliche Museum für Naturkunde, Stuttgart, for their permission to study the Dicerorhinus skulls in their care;
the "Stichting Het Moolengraaff-fonds" for providing a part of the funds for this publication;
Mr B. F. M. Collet of the Rijksmuseum van Geologie for making the photographs and the drawings.

Rijksmuseum van Geologie en Mineralogie, Leiden

LITERATURE

Duerst, U., Vergleichende Untersuchungsmethoden am Skelett bei Säugern Abderhalden, Hdb. d. biol. Arbeitsmethoden VII, 2 Berlin u. Wien (1926).

Falconer, H., Palaeontological Memoirs II 1868.

Freudenberg, W., Die Säugetiere des älteren Quartärs von Mittel Europa etc. Geol. u. Pal. Abh. N.F. 12, 4/5.

Lydekker, R., Catalogue of fossil mammals in the British Museum (Nat. Hist.) III, 119-123 (1886).

Schroeder, H., Über Rhinoceros mercki und seine nord- und mittel-deutschen Fundstellen Abh. Preuss. Geol. Landesanstallt N.F. 124 (1930).

Staesche, K., Nashörner der Gattung Dicerorhinus aus dem Diluvium Württembergs Abh. Reichstelle für Bodenforschung N.F. 200 (1941).

Wust, E., Beiträge zur Kenntnis der diluvialen Nashörner Europas Centralbl. f. Min. etc. (1922).

Zeuner, F., Beziehung zwischen Schädelform und Lebensweise bei Nashörnern, Ber. der Naturf. Ges. zu Freiburg im Br. (1934).

ON THE TORSION OF A CYLINDRICAL BAR WITH SLITS

BY

J. B. ALBLAS [1])

(Communicated by Prof. C. J. BOUWKAMP at the meeting of October 29, 1960)

1. *Introduction*

The problem of the torsion of a cylindrical body, which was first investigated in 1855 by de SAINT–VENANT (ref. 1), has since attracted much attention. General methods for the evaluation of the torsional rigidity have been developed and an exact or approximate solution is known for a great number of cross-sections. It is remarkable that not much attention is paid to a class of interesting and important special problems, which arise if the cylindrical bar is weakened by one or more slits. Although some special cases of this kind have been treated, a general theory that bears practical results is not yet available. The energy method for the solution of torsion problems can of course be used here, but it does not suit this purpose very well.

The solutions which have been found for the special cases are nearly all obtained by means of some conformal mapping. FILON (ref. 2) has investigated the problem of the torsion of a cylinder of circular cross-section with one or two keyways. The boundaries of the keyways are confocal hyperbolas and he gives special attention to the case when the hyperbolas degenerate into straight lines. SHEPHERD (ref. 3) treats the problem of a circular shaft with one, two or four equal and evenly placed slits of any depth from the surface towards the axis. WIGGLESWORTH (ref. 4) has generalized one of the problems of Shepherd: the problem of the circular cross-section with two slits extending from the ends of a diameter to any depth along the diameter.

The first who has attacked the class of slit problems in a different way, viz. by means of an integral equation technique, is NOWACKI (ref. 5). Nowacki gives the solution for the special case of a rectangular cross-section. In general his integral equation is hard to solve.

It is the purpose of this paper to give a general method for the evaluation of the reduction in torsional rigidity. To this end we also start from an integral equation formulation as Nowacki does. We indicate a solution method for the singular integral equation(s), by reducing it (them) to Fredholm equation(s). But we denote special attention to a variational principle, which we derive from the integral equation(s), and from which

[1]) Technological University of Eindhoven.

we deduce directly an approximate value of the reduction in torsional rigidity. This principle is similar to RAYLEIGH's principle (ref. 6) or to LEVINE and SCHWINGER's principle (ref. 7) for diffraction problems.

In this method we assume that the problem is solved (or approximately solved) for the same cross-section with less or no slits. Using trial functions we derive from this solution an approximate value of the reduction factor. As we know the character of the singularity at the end of the slit and the value at the boundary, it is easy to find "physically reasonable" trial functions, which can be expected in many cases to give a good approximation without too much computation.

As an example we solve the integral equation for a complete radial slit in a circular cross-section. We compare the exact solution with the result which is obtained by the variational method. The agreement is very good.

2. *Mathematical formulation of the problem*

We consider a cylindrical bar with an arbitrary cross-section with one or more slits (cf. fig. 1). The only non-vanishing stresses can be derived from a stress function $F(x, y)$ according to

Fig. 1

$$\tau_{zx} = \alpha G \frac{\partial F}{\partial y}, \qquad \tau_{zy} = -\alpha G \frac{\partial F}{\partial x}, \tag{1}$$

where G is the shear modulus and α the twist per unit length. The function $F(x, y)$ satisfies

$$\Delta F = \frac{\partial^2 F}{\partial x^2} + \frac{\partial^2 F}{\partial y^2} = -2 \tag{2}$$

in the domain R of the cross-section, while on the boundary C_1 of R (including the slits), the boundary condition is

$$F = 0. \tag{3}$$

If we have solved the problem (2), (3) we find the torsional rigidity D by

$$D = 2G \iint_R F(x, y)\, \mathrm{d}x\, \mathrm{d}y. \tag{4}$$

There are several methods which can be tried to solve the problem (2), (3). One of them makes use of a Green's function formulation. If we know the solution $G(x, y;\ \xi, \eta)$ of

$$\Delta G = \frac{\partial^2 G}{\partial x^2} + \frac{\partial^2 G}{\partial y^2} = -2\pi\, \delta(x-\xi)\, \delta(y-\eta), \tag{5}$$

with the boundary condition

$$G = 0, \text{ along } C_1, \tag{6}$$

we find from Green's formula

$$\iint_R (G\Delta F - F\Delta G)\,dx\,dy = -2\iint_R G\,dx\,dy + 2\pi F(\xi,\eta) = \int_{C_1}\left(G\frac{\partial F}{\partial n} - F\frac{\partial G}{\partial n}\right)ds = 0,$$

from which we derive

$$F(\xi,\eta) = \frac{1}{\pi}\iint_R G(x,y;\,\xi,\eta)\,dx\,dy, \tag{7}$$

where n is the normal in the outward direction.

The formulation (5), (6) cannot be considered as a simplification of the problem (2), (3). If we replace the boundary condition (6) by

$$G = 0, \text{ along } C, \tag{8}$$

where C is the boundary of the domain R, excluding the slits (or including a smaller number of slits), the problem (5), (8) is obtained, which can more easily be solved. In the following we shall assume that the stress function solution ((2), (3)) of this problem is known. We now have

$$F(\xi,\eta) = \frac{1}{\pi}\iint_R G(x,y;\,\xi,\eta)\,dx\,dy + \frac{1}{2\pi}\int_L G\frac{\partial F}{\partial n}\,ds, \tag{9}$$

where L is the union of the disconnected arcs of the excluded slits and s is measured along the slits. Introducing the unknown function $S(s)$ by

$$S(s) = \left(\frac{\partial F}{\partial n}\right)_+ + \left(\frac{\partial F}{\partial n}\right)_-, \tag{10}$$

where the $+$ and $-$ signs denote the "upper" and "lower" sides of the arcs, we have from (9), (7),

$$F(\xi,\eta) = F_0(\xi,\eta) + \frac{1}{2\pi}\int_L G(x,y;\,\xi,\eta)\,S(s)\,ds, \tag{11}$$

where $F_0(\xi,\eta)$ is the stress function of the bar without slits (or with a smaller number of slits). If we denote by σ the pair of coordinates (ξ,η) on L, we find from (11) for $S(s)$ the integral equation

$$\int_L G(s,\sigma)\,S(s)\,ds = -2\pi F_0(\sigma), \qquad (\sigma \text{ on } L). \tag{12}$$

We remark that, in general, the formula (12) is an abbreviated notation for a system of integral equations.

With the help of (4) we find for the rigidity

$$D = D_0 + G\int_L F_0(s)\,S(s)\,ds, \tag{13}$$

where D_0 is the rigidity of the cross-section with a smaller number of slits. In the derivation of (13) the formula (7) has been used. For the reduction factor D_{red} we have from (13) the simple expression

$$D_{\text{red}} = -G\int_L F_0(s)\,S(s)\,ds. \tag{14}$$

The problem formulated in this way is divided into two simpler ones:
(a) the construction of the Green's function for the contour,
(b) the exact or approximate solution of the integral equation (12).

The construction of the Green's function for a simple contour can be reduced to the determination of a function which maps the domain D onto the unit circle. If, with the complex variable

$$z = x + iy, \tag{15}$$

this function is denoted by

$$\omega = f(z), \tag{16}$$

the Green's function becomes (ref. 8)

$$G(z, z_0) = -\log \left| \frac{f(z) - f(z_0)}{1 - \overline{f(z_0)}\, f(z)} \right|, \tag{17}$$

where the point $z = z_0$ is carried into the origin $\omega = 0$. We can always write

$$G(z, z_0) = -\log |z - z_0| + g(z, z_0), \tag{18}$$

where $g(z, z_0)$ is harmonic in R.
We also can write

$$G(z, z_0) = -\log (z - z_0) + h(z, z_0),$$

and with the help of this expression we can derive from (12) a singular integral equation, which can be reduced to a Fredholm integral equation of the second kind. We shall not develop this method here.

3. *The variational principle*

The main purpose of our considerations is the calculation of the reduction in torsional rigidity. Without solving the complete system of integral equations (12), it is possible to give an expression for this reduction which can be used for practical computations. We introduce the factor A by

$$A = \frac{-D_{\text{red}}}{G}, \tag{19}$$

and we have from (14) and (12)

$$A = \frac{\int_L F_0(s)\, S(s)\, \mathrm{d}s \cdot \int_L F_0(\sigma)\, S(\sigma)\, \mathrm{d}\sigma}{-(1/2\pi) \int_L \mathrm{d}s \int_L \mathrm{d}\sigma\, G(s, \sigma)\, S(s)\, S(\sigma)} \tag{20}$$

or

$$A = \frac{\left[\int_L F_0(s)\, S(s)\, \mathrm{d}s\right]^2}{-(1/2\pi) \int_L \mathrm{d}s \int_L \mathrm{d}\sigma\, G(s, \sigma)\, S(s)\, S(\sigma)}. \tag{21}$$

The expression (21) is more than a trivial identity, for it is easy to see that the value of A is stationary for small variations of the function $S(s)$: in formula

$$\delta A = 0. \tag{22}$$

The reduction in torsional rigidity is obtained if we can find a function $S(s)$ which makes the expression (21) stationary. If we assume for $S(s)$ a physically plausible expression $S^*(s)$, which contains a number of unknown constants, the "best" value of A is

$$A = \text{stat.} \frac{[\int_L F_0(s)\, S^*(s)\, \mathrm{d}s]^2}{-(1/2\pi) \int_L \mathrm{d}s \int_L \mathrm{d}\sigma\, G(s,\sigma)\, S^*(\sigma)\, S^*(s)}. \tag{23}$$

The boundary values of $S(s)$ are known. We have $S(s)=0$, if s is on C and $S(a) \sim \frac{1}{\sqrt{|s-a|}}$, if a is an inner endpoint. We always have to take trial functions $S^*(s)$ satisfying the boundary conditions.

We now prove the stationary property. We have

$$\left.\begin{aligned} \delta A \cdot - \frac{1}{2\pi} \int_L \mathrm{d}s \int_L \mathrm{d}\sigma\, G(s,\sigma)\, S(s)\, S(\sigma) = \\ - A \cdot \frac{1}{2\pi} \int_L \mathrm{d}s \int_L \mathrm{d}\sigma\, G(s,\sigma)\, S(\sigma) \cdot \delta S(s) - \\ + A \cdot \frac{1}{2\pi} \int_L \mathrm{d}s \int_L \mathrm{d}\sigma\, G(s,\sigma)\, S(s) \cdot \delta S(\sigma) \\ + \int_L F_0(s)\, \delta S(s)\, \mathrm{d}s \cdot \int_L F_0(\sigma)\, S(\sigma)\, \mathrm{d}\sigma + \\ + \int_L F_0(\sigma)\, \delta S(\sigma)\, \mathrm{d}\sigma \cdot \int_L F_0(s)\, S(s)\, \mathrm{d}s. \end{aligned}\right\} \tag{24}$$

For the right side of (24) we have

$$\left.\begin{aligned} \frac{A}{2\pi} \int_L \mathrm{d}s \cdot \delta S(s) \left\{ \int_L \mathrm{d}\sigma \cdot G(s,\sigma)\, S(\sigma) + F_0(s) \cdot 2\pi \right\} \\ + \frac{A}{2\pi} \int_L \mathrm{d}\sigma \cdot \delta S(\sigma) \left\{ \int_L \mathrm{d}s \cdot G(s,\sigma)\, S(s) + F_0(\sigma) \cdot 2\pi \right\}. \end{aligned}\right\} \tag{25}$$

By virtue of (12) the terms in braces are zero, so $\delta A = 0$.

4. *Example. Circular cross-section with complete radial slit*

(a) exact solution

As an example we solve the problem of the circular cross-section with radial slit.

The conformal mapping of the circle with radius a onto the unit circle $|\omega|<1$ is obtained by

$$\omega = \frac{z}{a}. \tag{26}$$

The representation, in which the point z_0 is carried into the origin, is according to (17)

$$\omega = a \frac{z - z_0}{a^2 - \bar{z}_0 z}, \tag{27}$$

from which Green's function is derived:

$$G(z, z_0) = -\log\left| a\,\frac{z-z_0}{a^2-\bar{z}_0 z}\right|. \tag{28}$$

With

$$z = r\,e^{i\theta},\ z_0 = \varrho e^{i\varphi}, \tag{29}$$

the Green's function becomes

$$G(r,\theta;\,\varrho,\varphi) = \tfrac{1}{2}\log\frac{a^2+\frac{r^2\varrho^2}{a^2}-2r\varrho\cos(\theta-\varphi)}{r^2+\varrho^2-2r\varrho\cos(\theta-\varphi)}. \tag{30}$$

We take the slit with length b along the x-axis. Then, in the integral equation (12) we can put $\theta=\varphi=0$ and we have

$$\int_a^b \log\left|\frac{a\left(1-\frac{r\varrho}{a^2}\right)}{r-\varrho}\right| S(r)\,\mathrm{d}r = -2\pi\cdot\frac{1-\varrho^2}{2}, \qquad (b<\varrho<a). \tag{31}$$

We introduce non-dimensional quantities

$$\bar{r} = r/a,\ \bar{\varrho} = \varrho/a,\ \bar{b} = b/a, \tag{32}$$

and equation (31) becomes (dropping the bars)

$$\int_1^b \log\left|\frac{1-r\varrho}{r-\varrho}\right| S(ar)\,\mathrm{d}r = -\frac{\pi}{a}(1-a^2\varrho^2), \qquad (b<\varrho<1). \tag{33}$$

We proceed by transforming the variables. We introduce x, y, by

$$x = \frac{1-r}{1+r},\ y = \frac{1-\varrho}{1+\varrho},\ r = \frac{1-x}{1+x},\ \varrho = \frac{1-y}{1+y}, \tag{34}$$

and equation (33) becomes after some operations

$$\int_{\frac{1-b}{1+b}}^{0} \log\left|\frac{x+y}{x-y}\right| \frac{S\left(a\frac{1-x}{1+x}\right)}{(1+x)^2}\,\mathrm{d}x = -\frac{\pi}{2a}\left(1-a^2\left(\frac{1-y}{1+y}\right)^2\right), \qquad \left(\frac{1-b}{1+b}<y<0\right). \tag{35}$$

We define the function $T(x)$ by

$$T(x) = \frac{1}{(1+x)^2}\ S\left(a\,\frac{1-x}{1+x}\right) \tag{36}$$

and we differentiate equation (35) to y. We find

$$\int_{\frac{1-b}{1+b}}^{0} T(x)\,\frac{x\,\mathrm{d}x}{y^2-x^2} = \pi a\,\frac{1-y}{(1+y)^3}. \tag{37}$$

If we proceed with the new variables

$$y^2 = t,\ x^2 = s \tag{38}$$

equation (37) becomes

$$\int_0^{\left(\frac{1-b}{1+b}\right)^2} T(\sqrt{s})\,\frac{\mathrm{d}s}{t-s} = -2\pi a\,\frac{1-\sqrt{t}}{(1+\sqrt{t})^3}, \qquad \left(0<t<\left(\frac{1-b}{1+b}\right)^2\right). \tag{39}$$

The equation (39) is a well-known singular integral equation (ref. 9). We look for the solution which remains finite for $s=0$, but becomes infinite for $s=\left(\frac{1-b}{1+b}\right)^2$. This agrees with the requirement that the solution of (33) is finite for $r=a$ and infinite for $r=b$.
The solution of (39) is

$$T(\sqrt{s}) = -\frac{2a}{\pi} \frac{\sqrt{s}}{\sqrt{\left(\frac{1-b}{1+b}\right)^2 - s}} \int_0^{\left(\frac{1-b}{1+b}\right)} \frac{\sqrt{\left(\frac{1-b}{1+b}\right)^2 - t}}{\sqrt{t}} \frac{1-\sqrt{t}}{(1+\sqrt{t})^3} \frac{\mathrm{d}t}{t-s}, \tag{40}$$

or

$$T(s) = -\frac{4a}{\pi} \frac{s}{\sqrt{\left(\frac{1-b}{1+b}\right)^2 - s^2}} \int_0^{\frac{1-b}{1+b}} \frac{1-t}{(1+t)^3} \sqrt{\left(\frac{1-b}{1+b}\right)^2 - t^2} \frac{\mathrm{d}t}{t^2-s^2}. \tag{41}$$

We have evaluated the integral (41) for the case $b=0$, the complete radial slit. The formula becomes

$$T(s) = -\frac{4a}{\pi} \frac{s}{\sqrt{1-s^2}} \int_0^1 \sqrt{1-t^2} \frac{1}{(1+t)^3} \frac{t}{t^2-s^2} \mathrm{d}t. \tag{42}$$

and we find (dimensionally)

$$S(r) = \frac{4a}{\pi} \frac{1}{\sqrt{\bar{r}}} \left[\tfrac{1}{2}\sqrt{\bar{r}} \left(\frac{1}{\bar{r}^3} - \bar{r}\right) \log \frac{1-\sqrt{\bar{r}}}{1+\sqrt{\bar{r}}} + \left(\frac{1}{\bar{r}^2} - \bar{r}\right) : \tfrac{1}{3}\left(\frac{1}{\bar{r}} \quad 1\right) \right]. \tag{43}$$

For the torsional rigidity we find from (13)

$$\left\{ \begin{aligned} D &= D_0 + G \int_0^a F_0(r)\, S(r)\, \mathrm{d}r = \\ &= \frac{\pi}{2} a^4 G + \tfrac{1}{2} a^4 G \int_0^1 (1-\bar{r}^2) \left(\frac{S(\bar{r})}{a}\right) \mathrm{d}\bar{r} \\ &= G\pi a^4 \left(1 - \frac{64}{9\pi^2}\right), \end{aligned} \right. \tag{44}$$

a result found already in another way in ref. (4).
The numerical value of $\pi\left(1-\frac{64}{9\pi^2}\right)$ is 0.8780557.

(b) Comparison with the approximate value found by means of the variational principle

A trial function which has the right boundary value at $r=a$ and the right singularity at $r=0$ is

$$S^*(\bar{r}) = \left(\frac{1}{\sqrt{\bar{r}}} - \bar{r}\right). \tag{45}$$

With this function we compute the reduction factor A from (21).

We have

$$A = -\frac{\pi}{2} a^4 \frac{\left(\int_0^1 (1-x^2) \left(\frac{1}{\sqrt{x}} - x \right) dx \right)^2}{\int_0^1 dx \left(\frac{1}{\sqrt{x}} - x \right) \int_0^1 dy \left(\frac{1}{\sqrt{y}} - y \right) \log \left| \frac{1-xy}{x-y} \right|} \tag{46}$$

We find

$$\int_0^1 (1-x^2) \left(\frac{1}{\sqrt{x}} - x \right) dx = 27/20. \tag{47}$$

$$\int_0^1 \log \left| \frac{1-xy}{x-y} \right| \left(\frac{1}{\sqrt{y}} - y \right) dy = \frac{2}{\sqrt{x}} (1-x) \log \frac{1+\sqrt{x}}{1-\sqrt{x}} - \frac{1}{2} \left(x - \frac{1}{x} \right) + \frac{1}{2} x^{-\frac{1}{2}} \left(1 - \frac{1}{x^2} \right) \log (1-x) - \frac{5}{2} \log x. \tag{48}$$

With (48) the denumerator of (46) is

$$-\frac{2}{3} - \frac{2}{25} - \frac{2}{84} + \int_0^1 \left\{ \frac{(1-t^3)(1-t^8)}{t^4} \log (1-t^2) + \frac{1}{t^2} \right\} dt + 4 \int_0^1 \frac{(1-t^2)(1-t^4)}{t} \log \frac{1-t}{1+t} dt. \tag{49}$$

The integrals of (49) are calculated by means of a series expansion of the integrand. We find

$$\int_0^1 \left\{ \frac{(1-t^3)(1-t^8)}{t^4} \log (1-t^2) + \frac{1}{t^2} \right\} dt = \frac{\pi^2}{12} - \frac{16}{15} \log 2 + \frac{7}{25} - \frac{25}{96}. \tag{50}$$

We also find

$$4 \int_0^1 \frac{(1-t^3)(1-t^2)}{t} \log \frac{1+t}{1-t} dt = \pi^2 - \frac{16}{15} \log 2 - 4 - \frac{2}{15}. \tag{51}$$

From these computations we find

$$A = -\frac{\pi}{2} a^4 \frac{(27/20)^2}{4.3757} = -0.66646\, a^4, \tag{52}$$

from which we derive for the torsional rigidity

$$D = D_0 - 0.67\, Ga = 0.90\, Ga^4. \tag{53}$$

The agreement with (44) is good. A better result can be obtained, if we add to the trial function $S^*(\bar{r})$ as given by (45) a polynomial in $\bar{r}$, containing a number of constants, which are to be determined with the well-known Rayleigh-Ritz technique.

5. *Discussion*

Although we have restricted the paper to the discussion of one simple example, it is obvious that the method which has been developed in sections 2 and 3 can be used for the calculation of the reduction in torsional rigidity for a wide class of cross-sections with slits. There are two difficulties, which arise in a more general case:

(a) it is often rather complicated, if not impossible to find the exact Green's function.

(b) the integrations are very involved.

In many cases of practical interest we can construct an approximate Green's function with the help of (17) from a mapping function, which gives an approximation for the conformal representation onto the unit circle. The theory of this approximation is well developed (ref. 10). For the execution of the integrations numerical methods are preferable. Especially if one has the disposal of an electronic computer, the method given in this paper can be used to obtain rapidly accurate solutions of technically important problems.

REFERENCES

1. Saint–Venant, B. de, De la torsion des prismes, avec des considérations sur leur flexion, Mémoires des savants étrangers, **14** (1855).
2. Filon, L. N. G., On the resistance to torsion of certain forms of shafting, with special reference to the effect of keyways, Phil. Trans. A, **193**, 309–352 (1900).
3. Shepherd, W. M., The torsion and flexure of shafting with keyways or cracks, Proc. Roy. Soc. (London) A, **138**, 607–634 (1932).
4. Wigglesworth, L. A., Flexure and torsion of a circular shaft with two cracks, Proc. Lond. Math. Soc. (2), **47**, 20–37 (1940).
5. Nowacki, W., On certain cases of torsion of bars, Arch. Mech. Stos. **5**, 21–46 (1953).
6. Lord Rayleigh, The theory of sound, MacMillan and Co., London, 88 (1929). Temple, G. and B. G. Bickley: Rayleigh's principle, Dover, New York (1956).
7. Levine, H., and J. Schwinger, On the theory of diffraction by an aperture in an infinite plane screen I, Phys. Rev. **74**, 958–974 (1948).
8. Nehari, Z., Conformal Mapping, MacGraw Hill, New York, 181 (1952).
9. Muskhelishvili, N. I., Singular Integral Equations, P. Noordhoff, Groningen, 351 (1953).
10. Kantorovich, L. V. and V. I. Krylov, Approximate methods of higher analysis, P. Noordhoff, Groningen, 358 (1958).

AUTOFLUORESCENCE AND AGE OF SOME FOSSIL POLLEN AND SPORES

BY

P. VAN GIJZEL [1])

(Communicated by Prof. I. M. VAN DER VLERK at the meeting of October 29, 1960)

ABSTRACT

The term fluorescence palynology is proposed by the author for the application of the phenomenon of autofluorescence of fossil pollen and spores in palynology. Some conclusions can be drawn from measurements of relative fluorescence intensity. Fluorescence palynology concerns firstly the relation between autofluorescence and the taxonomic positions of fossil pollen and spores, and secondly the relation between the spectral ratio of these objects in UV-light and their geological age. This ratio (Q-quotient) in general decreases with increasing geological age. It is calculated from measurements of fluorescence colour which shifts from green or yellow to orange with increasing age. In principle fluorescence palynology has solved the problem of contamination of humic sediments with secondary pollen and spores.

INTRODUCTION

Since HAITINGER and others started to study fluorescence, this phenomenon is often used in biological, medical and others sciences (*c.f.* BRÄUTIGAM & GRABNER, 1949; GOODWIN, 1953 and others).

However, to this date only very little has been published on fluorescence of pollen grains. BERGER (1934) stated this phenomenon of recent pollen in his studies of hay-fever procreators. WETZEL (1959), who studied slides of organic sediments from Germany, was the only one who observed the phenomenon of luminiscence of sporomorphae and other microfossils, but gave no special attention to the fluorescence of pollen and spores.

In this note special attention is given to the use of autofluorescence for different palynological purposes, summarized in the term fluorescence palynology, which is hereby introduced. This phenomenon and its applications in chronostratigraphy will be described in this preliminary note.

Autofluorescence or primary fluorescence of matter is based on the faculty to transpose light with comparitively short wavelengths (unvisible UV light) into visible light with much longer λ, without any activation by means of colouring (which would cause secondary fluorescence). If fossil pollen and spores are observed with UV-light they show splendid

[1]) Department of historical geology and paleontology, Leiden University.

fluorescence colours, varying with age and type. The fluorescence light emitted by pollen and spores is not monochromatic. Their colour is determined by the intensities at different wavelengths. As photo electrical measuring instruments are too inaccurate for measuring these intensities, the subjective fluorescence measuring method ("Methode der subjektiven Fluoreszenz-Messungen") according to RUCH was used. My measurements, carried out in Prof. Ruch's laboratory in Zürich, supported some of my suppositions concerning fluorescence palynology.

By means of this accurate method, measurements are taken of intensities, relative to those of fluorescing uranglass. The values of these intensities (in the figs. signed as $I_{rel.}$) have to be considered as preliminary, because they are dependent on the adjustment of the apparatus. Independent of this adjustment however, is the *spectral ratio Q*, being a proportional number.

The relative intensities are measured at the wavelengths of 500, 530, 560, 600 and 640 mμ. The spectral ratio is obtained by dividing the relative intensity at 500 mμ (green) by the one at 640 mμ (orange). The quotient Q forms an important scale for fluorescence colour. In the following the importance of these values for palynological purposes will be dealt with.

While preparing the pollen preparations, the use of acid liquids which may diminish autofluorescence, must be avoided.

AUTOFLUORESCENCE AND TAXONOMIC POSITION

Some differences in colour appear when fossil pollen and spores are fluorescing. Firstly there is a difference in colour between pollen and spores. While the latter have a characteristic blue colour, the pollen is emitting light of longer wavelengths, colouring the grains from pale green to orange or red. Secondly, differences in colour are seen between various pollen types. The fluorescence colours of some of the most important pollen types from the Quaternary of N.W. Europe are given in table I.

In this table the variation in colour has been given, which is greater for the grains of younger deposits (Holocene) than for older grains (Pleistocene). Besides, with increasing age an important change in colour takes place towards the red part of the spectrum (see next paragraph). This variation within one pollen type is related to different species inside that type. Investigations on fossil pollen compared with recent species under UV-light, are in progress. The relations between autofluorescence of pollen and spores and their taxonomic positions can be summarized as follows:

A pollen type or group of pollen types of a certain age may possess a characteristic fluorescence colour.

Measurements of the relative fluorescence intensity give possibilities for the determination of the fluorescence characteristics of different pollen

types. In fig. 1 diagrams are given of some pollen and spores from Upper Holocene peat. They show that the spectral ratio Q is a useful criterion for an objective determination of fluorescence colours. The measured grains are chosen arbitrarily.

To determine an average value as standard characteristic, it is necessary to observe a large amount of grains of the same type. Q-values of *Pinus silvestris* of Holocene age show a clear variation (see fig. 1). Notable is the little difference in the values of various sediment types of Holocene age.

The cause of autofluorescence of pollen and spores is unknown. Probably the main chemical component of these grains, known as sporonine (ERDTMANN, 1954; AFZELIUS, 1956) or tryphine (ERDTMANN, 1960) or sporopollenine, is responsible for it. Possibly admixtures of other components in minute concentrations may cause the fluorescence. The differ-

TABLE I

Fluorescence-colours of some pollen and spores from Quaternary peats and clays

Type	Fluorescence-colours			
	Upper Holocene		Middle-Pleistocene	
	main-colour	variation in colour	main-colour	variation in colour
Pollen:				
Alnus	yellowish green	yellow	yellow	yellowish orange
Betula	yellowish green	yellow	yellow	yellowish orange
Carpinus	yellow	not observed	yellow	pale yellow
Fagus	yellow	from green to orange	—	—
Picea	yellow	not observed	yellow	yellowish brown
Pinus silvestris	pale green	yellowish green	yellow	from yellowish green to yellowish orange
Quercus	pale green	yellowish orange	yellow	not observed
Corylus	yellow	yellowish green	yellowish orange	yellow
Ericaceae	yellowish green	from pale green to yellow	yellow	not observed
Gramineae	orange	from yellow to red	yellowish brown	not observed
Cyperaceae	orange	yellow	orange red	not observed
Spores:				
Filices	blue	blueish green	from pale blue to green	not observed
Sphagna	blue	blue grey	pale green	not observed

Observations in UV-light with Leitz-filters 2 mm UG 1 and 4 mm UG 1 (filtering visible light).

ences in fluorescence colour between pollen and spores are obvious. This may be caused by a difference in chemical composition. The high resistance of these components, however, makes it very difficult to determine the chemical composition.

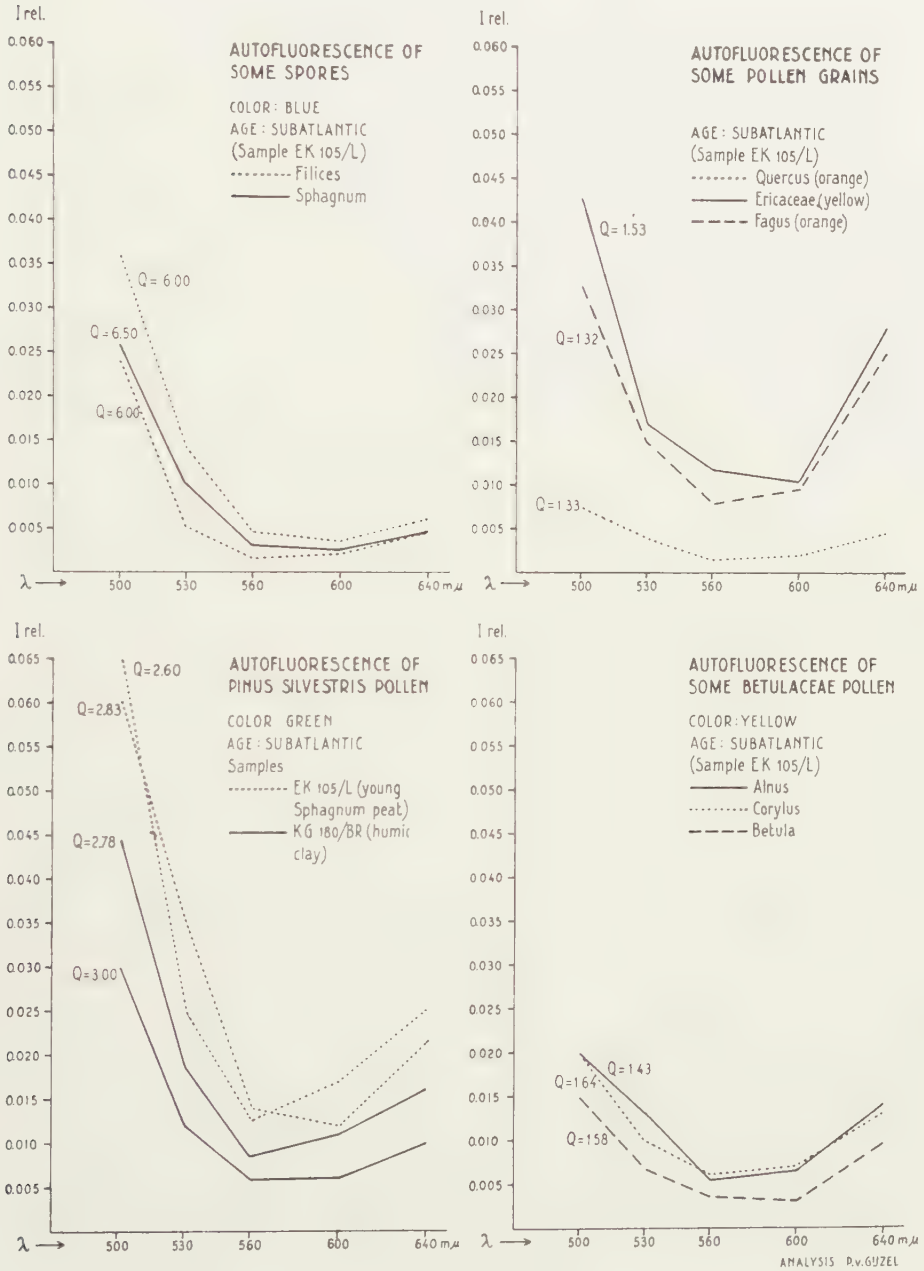

Fig. 1

AUTOFLUORESCENCE AND GEOLOGICAL AGE

Fluorescence palynological investigations of many samples of varying age show a distinct relation between the fluorescence colour and geological age. This may be formulated as follows:

Autofluorescence of fossil pollen and spores show with increasing age a change in colour of short wavelengths towards colours of longer wavelengths, followed by complete invisibility.

This phenomenon is clearly noticeable on pollen of *Pinus silvestris*. In Holocene clays and peats these grains are fluorescing pale green, in similar Pleistocene deposits yellowish green to yellow and in Tertiary clays yellowish orange to red-brown. Other forms as *Picea*, *Alnus*, *Betula* and *Corylus*, from the Holocene and Tertiary show the same tendency. Spores of *Sphagnum* from Tertiary deposits are not fluorescent, those of *Filices* faintly pale blue to green. In the fluorescence of Lower Tertiary pollen yellow and brownish colours are dominating, while green and blue are lacking. Upper Mesozoic pollen and spores are even darker and less yellow. On the other hand, Carboniferous spores show a complete extinction of visible fluorescence light. The fluorescence of pollen from these old deposits is strikingly different from that of Holocene ones showing a brilliant colour-gradation. It is notable that the pollen from Tertiary browncoals show a revival in colour, in comparison with that of the Middle and Lower Pleistocene peats. This may be caused by the process of carbonization of peat into browncoal. This chemical reaction possibly activates the fluorescence of pollen.

Fig. 2 shows the spectral composition of some *Pinus silvestris* grains at different ages. The content of green light gradually decreases in favour of that of orange light. The colours of the grains in this figure are as follows: Upper Holocene pale green (Q = 3.00), Middle Pleistocene pale yellow (Q = 1.75), Lower Pleistocene yellow (Q = 1.44) and Middle Oligocene redbrown (Q = 0.68).

Many measurements have still to be taken to determine the exact relation between fluorescence and age.

APPLICATIONS TO STRATIGRAPHICAL PROBLEMS

1. Fluorescence palynology can be applied when palynological age-determination fails due to contamination of humic sediments with older, secondary pollen. This, for example, is the case with so-called "potklei" (pottery clay) of the N. Netherlands (*c.f.* v. Geel, Overweel & Veenstra, 1959). The method of Iversen (1936) could not be used here. The same problem arises in investigations of the detailed biostratigraphy of that territory, still in progress. In principle the application of fluorescence palynology has solved this problem. Of the majority of the pollen it can be established which grains are secondary or autochthonous. Some time ago I presumed (*c.f.* v. Geel c.s., 1959) the top of this pottery-clay was

deposited during the Saale-glacial, while strong erosion of older sediments resulted in a contamination of this clay with large quantities of Pliocene, Miocene and older pollen and spores. Measurements of *Pinus silvestris*' spectral ratio confirm this supposition. Some of the grains from the clay have a Q-value which corresponds with a Middle Pleistocene age. On the other hand about 80 % of the grains possess a lower spectral ratio, according to that of Tertiary clays. These observations are of importance for biostratigraphical studies of other contaminated sediments. The greater the difference in age of secondary and autochthonous pollen, the clearer is the difference in fluorescence and the easier they may be distinguished from each other.

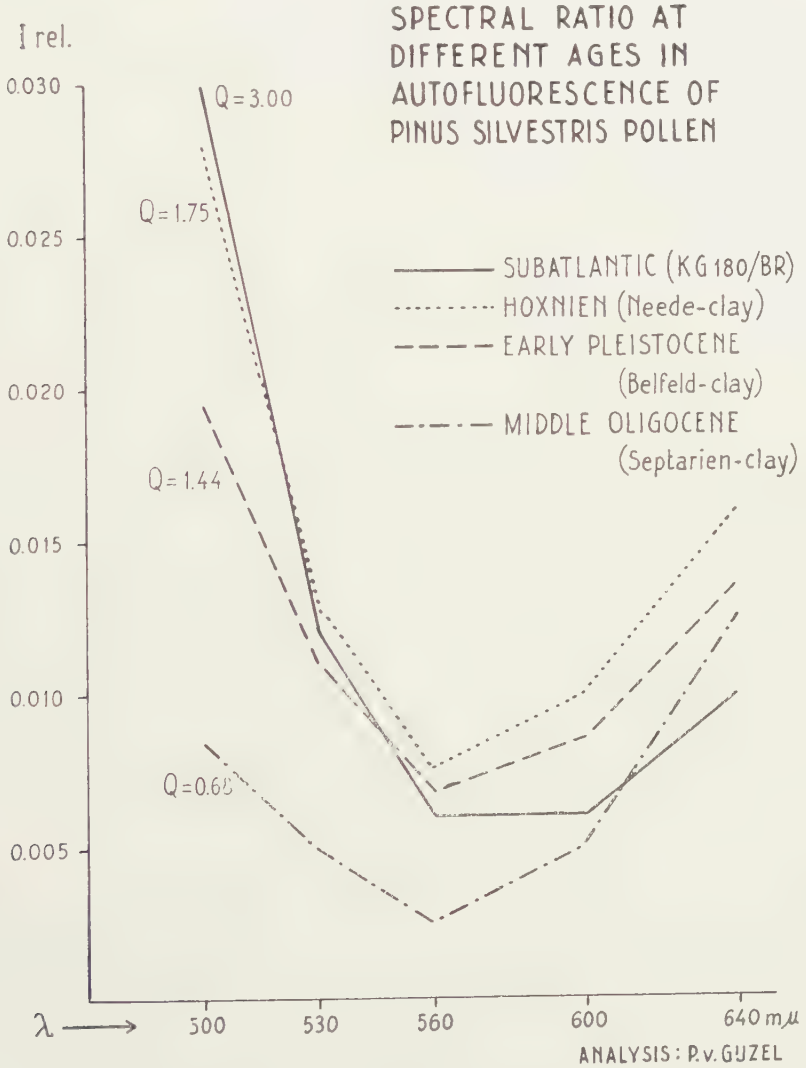

Fig. 2

2. It is well known that dating and correlating of some not contaminated Pleistocene sediments is impossible because of the absence of zonings in pollen-diagrams (WOLDSTEDT, 1950, 1954, 1958). New points of view may be brought forward by the application of fluorescence palynology.

3. Fluorescence palynology may be applied on species determination for biostratigraphical purposes, especially of Tertiary pollen and spores, which are hard to determine. The principle of this question has already been discussed above.

Perhaps there are possibilities to test the relations of extinct and recent living species.

Extensive investigations on principles of fluorescence palynology and on the aforementioned applications are in rapid progress and will be published later. Special attention will then be given to age determination and time correlation.

ACKNOWLEDGEMENTS

First of all I would like to give my thanks to Prof. Dr. F. Ruch (Eidgen. Technische Hochschule in Zürich), who allowed me so kindly to use his fluorescence apparatus to make measurements on palynological objects. Moreover I express my thanks to the Board of the "Molengraaff Fonds" for the financial support of my visit to Zürich.

ZUSAMMENFASSUNG

Der Verfasser hat Fluoreszenz-Mikroskopie auf die Pollenanalyse angewandt. Subjektive Fluoreszenz-Intensitätsmessungen haben folgendes erwiesen:

1. Es besteht ein Zusammenhang zwischen jedem Pollentyp und seiner Fluoreszenzfarbe bei gleichem Alter. Während die Sporen blau bis blaugrün fluoreszieren, haben die Pollenkörner immer Fluoreszenzlicht mit höheren Wellenlängen.

2. Im allgemeinen tritt in das primäre Fluoreszenzlicht der Pollen- und Sporenkörner bei zunehmenden Alter eine Aenderung der Intensität nach höheren Wellenlängen auf. Wahrscheinlich wird das Farbeverhältnis ("spectral ratio") durch das Alter bedingt.

Die Anwendung der Fluoreszenz-Palynologie hat im Prinzip die Lösung für die Frage der sekundär Pollen verunreinigter Sedimente gegeben.

REFERENCES

AFZELIUS, B. M., Electron-microscope investigations into exine stratification; Grana Palynologica, N.S. 1 : 2 (1956).

BERGER, F., Das Verhalten der Heufieber erregender Pollen im filtrierten ultravioletten Licht; Beitr. z. Biol. d. Pflanzen, 22, 1.H. (1934).

BRÄUTIGAM, F. und A. GRABNER, Beitrage zur Fluoreszenzmikroskopie; Verl. G. Fromme & Co., Wien, 131 p. (1949).

ERDTMAN, G., An introduction to pollen analysis; New Ser. Plant Sc. Books, **XII**, 21–23 (1954).

————, Pollen walls and angiosperm phylogeny. On three new genera from the Lower Headon Beds, Berkshire; Botan. Notiser, 113, Fasc. 1, Lund (1960).

Goodwin, R. H., Fluorescent substances in Plants; Ann. Rev. Plant Physiol., 4, Stanford, Calif., USA (1953).

Gijzel, P. van, C. J. Overweel and H. J. Veenstra, Geological investigations on boulder-clay of E. Groningen; L.G.M., 24, 721–759 (1959).

Haitinger, M., Fluoreszenzmikroskopie, Ihre Anwendung in der Histologie und Chemie, Leipzig (1938).

Iversen, J., Sekundäres Pollen als Fehlerquelle. Eine Korrektionsmethode zur Pollenanalyse minerogener Sedimente; Danm. Geol. Unders. IV, R., Bd. 2, Nr. 15, 24 p. (1936).

Wetzel, W., Das lumineszenzmikroskopische Verhalten von Sedimente; N. Jb. Geol. Pal., Abh. 107, 261–277 (1959).

Woldstedt, P., Norddeutschland und angrenzende Gebiete im Eiszeitalter. Stuttgart, 434 p. (1950).

————, Das Eiszeitalter, Grundlinien einer Geologie des Quartärs, I Bd. Die allgemeinen Erscheinungen des Eiszeitalters; 2. Aufl., 374 p. Stuttgart (1954).

————, Ibid., II. Bd.: Europa, Vorderasien und Nordafrika im Eiszeitalter; 2. Aufl., Stuttgart, 438 p. (1958).

SOME EXPERIMENTS ON HEAT TRANSFER AND MAGNETISM BELOW 1° K. I

BY

A. R. MIEDEMA

(Communicated by Prof. C. J. GORTER at the meeting of October 29, 1960)

SYNOPSIS

The experiments which will be reported have been performed at temperatures below 1° K which were attained by the method of adiabatic demagnetization. A short description of the experimental methods will be given in chapter I.

Experiments on a new type of paramagnetic substances, solidified solutions of paramagnetic ions in alcohols, are described in chapter II. At very low temperatures one obtains a glassy substance in which the magnetic ions are regularly distributed. The interactions between the magnetic moments of the ions and the electrical field due to the surrounding alcohol and water molecules appears to be much larger than usually found in paramagnetic crystals. In solutions of low concentration, irreversible processes occur during demagnetization which indicates that long relaxation times exist between magnetic moments and the heat waves.

The problem of heat transfer at very low temperatures is considered in chapter III. Using alcoholic solutions as a cooling substance single crystals have been cooled. The temperature dependence of the heat-flow measured between 0.6 and 0.015° K showed that a boundary resistance was not important. At the lowest temperatures the heat-flow was determined by the limited thermal conductivity of the single crystals. The experimental data are discussed using the theory for heat transfer by phonons and the different methods for indirect cooling, which have been used by several investigators, will be compared. It is suggested that in indirect cooling experiments the best results will be obtained if for the cooling salt a large number of flat plates, cut from a magnetic single crystal, which are glued to copper plates are used. This cooling salt can absorb large amounts of heat in a relatively short time.

The magnetic behaviour of single crystals of $MnNH_4$-, $CoNH_4$-, $CuNH_4$- and CuK-tutton salt is described in chapter IV. The crystals of the first two compounds show a very anisotropic magnetic behaviour which is antiferromagnetic in one direction and apparently ferromagnetic in a direction perpendicular to this. From the two copper tutton salts investigated $CuNH_4$-tutton salt seems to be antiferromagnetic whereas in CuK-tutton salt very high values for the susceptibility have been measured, which suggests the occurrence of ferromagnetism. In the latter salt a remarkable minimum is found in the specific heat at an entropy of $\frac{1}{2} R \ln 2$.

In chapter V the results are compared with a molecular field model, which accounts for both dipolar and exchange interactions. From X-ray investigations one expects each magnetic ion to have exchange interaction with two types of magnetic neighbours. The contributions of the different neighbours are estimated from the magnetic data.

The hyperfine structure interaction in magnetically ordered $CoNH_4$- and $MnNH_4$-tutton salt has been investigated by means of the anisotropic distribution of the γ-radiation emitted by ^{60}Co and ^{54}Mn nuclei (chapter VI). The magnitude of the γ-ray anisotropies and the direction of the nuclear alignment axes differ from the values predicted from the magnetic results.

APPARATUS AND SOME EXPERIMENTAL METHODS

1. *Experimental arrangement*

For the method of adiabatic demagnetization one needs a suitable paramagnetic substance in a cryostat with liquid helium at as low a temperature as possible and mounted in such a way that it can be magnetized in heat contact with the liquid helium (isothermally) and demagnetized under thermal insulation (adiabatically). The equipment used in the Kamerlingh Onnes Laboratory has been described extensively several times, ref. [1], [2] and [3]. A short description will be given here. The cryostat is located between the poles of an 80 kW electromagnet, which gives a field of 22300 oersted in a pole gap of 7.5 cm and which is homogeneous to within 1 % over a region with a diameter of 5 cm.

In order to obtain a low starting temperature for the demagnetization process the liquid helium is evaporated under reduced pressure. By means of a combination of an oil diffusion pump (Booster) and a large capacity mechanical pump the temperature of the liquid helium bath can be reduced to somewhat below 1° K. The heat contact between the salt and the liquid helium bath is made and broken with the help of exchange gas; the sample is mounted in a vacuum space and during isothermal magnetization the space is filled with helium gas at a pressure of about 10^{-3} mm Hg. Thereafter the gas is pumped off with a Hg diffusion pump and then the field is removed. The sample being now thermally isolated from the surrounding helium bath the demagnetization is practically isentropic and the temperature of the salt falls. After demagnetization the sample warms up again slowly. The amount of heat which enters the sample can be reduced to less than 0.1 erg/s, which makes it possible to perform the low temperature measurements nearly isothermally, if the heat capacities of the cooled substances are not too small.

2. *The measuring bridge*

The magnetic properties, such as the static susceptibility χ_0 and the real and imaginary parts of the oscillating susceptibility χ' and χ'', have been determined by means of an induction bridge of the Hartshorn type. It can be used for both ballistic and a.c. measurements. A schematic diagram of the bridge method can be seen in fig. 1.1. M_1 represents the paramagnetic salt surrounded by the primary and secondary windings of a mutual inductance. This is connected in series with a variable inductance M_2, which is a part of the bridge circuit. If the bridge is used for ballistic measurements, the primary circuit is fed from a storage cell;

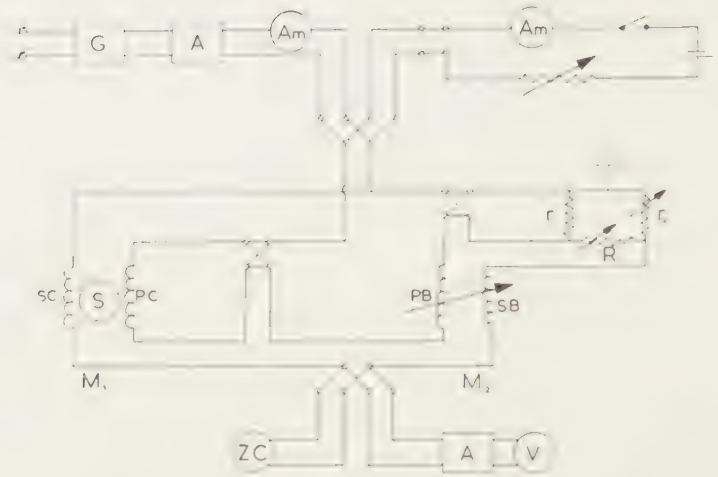

Fig. 1.1 The measuring bridge.

G	generator	PC	primary coil cryostat	SB	secondary bridge
A	amplifier	SC	secondary coils cryostat	ZC	ballistic galvanometer
Am	ammeter	PB	primary bridge	V	vibration galvanometer
S	sample				

for measurements with alternating measuring fields the voltage is taken from a low frequency signal generator (200 Hz), the detecting device being a ballistic galvanometer (Z.C.) or a vibration galvanometer, respectively. The vibration galvanometer is used as a null detector. The secondary voltage of M_1 can be resolved into two components only one of which is in phase with the alternating current and can be compensated by M_2. The other component, which is due to a.c. losses occurring in the sample can be compensated by tapping off a small voltage from a potentiometer (r_1, r_2, R) in the primary circuit. Zero deflection of the vibration galvanometer can only be obtained if both M_2 and R_{eff}, which equals $r_1 r_2/(r_1+r_2+R)$ are set to the correct value. The two components of the susceptibility are found from the experimental values of M_2 and R_{eff} by means of

$$\chi' = (-M_0 + M_2)/q \qquad \text{and} \qquad \chi'' = R_{eff}/\omega q \tag{1.1, 1.2}$$

where $\chi_0 = \chi' - i\chi''$. M_0 is the value of M_2 when compensating the empty mutual inductance M_1. q is the efficiency factor when measuring the variation of M_1 and ω the angular frequency of the measuring field. In our apparatus $r_1 = 1\Omega$, R is a resistance of 10^2, 10^3, 10^4 or $10^5\Omega$ and r_2 is variable from $0-100\Omega$. The values of M_0 and q are found from susceptibility measurements between 4 and 1° K. In this temperature region most of the investigated paramagnetic substances follow the Curie law

$$\chi = C/T \tag{1.3}$$

The Curie constant C equals $NJ(J+1)g^2\mu_B{}^2/3k$ and its value is known if the value of g is known from other experiments, which is usually the case. The temperature values are calculated from the measured vapour pressure of the liquid helium bath, using the tables of Van Dijk and Durieux (T_{55} scale). The differences between the T_{58} temperature scale and the T_{55} scale are of no practical importance; the differences between the two scales are smaller than 0.003° K and the corresponding error in our measurements is less than 0.5 %. From a graph of the relation between M_2 and $1/T$ the values of M_0 and q can be derived easily.

3. *Temperature measurements below* 1° *K*

It is easy to determine the temperatures as long as Curie's law is valid, since then the susceptibility is inversely proportional to the temperature. In general, the quantity C/χ is denoted by T^*, called the magnetic temperature and equal to the real temperature when the energy differences caused by the crystalline interactions are low compared to T and thus Curie's law applies.

The magnitude of a magnetic field inside a magnetized sample differs from the external field due to the demagnetizing field. At high temperatures the deviation from Curie's law caused by the demagnetizing field is described by $\chi = C/(T-\theta)$ with $\theta = -NC'$ (where N is the demagnetizing factor and C' the Curie constant per cm³). A second correction occurs because of the interactions between the magnetic ions. If the magnetic ions have a cubic arrangement the interaction gives a contribution to θ of $(4\pi/3)C'$, if no exchange interaction is taken into account. For a sphere $N = 4\pi/3$ and thus the resulting value of $\theta = 0$.

The T^* and susceptibility values, χ_0, χ' and χ'', given in the following correspond to the values of $\mathrm{d}M/\mathrm{d}h$ for a spherical sample, h being the measuring field. When the investigated magnetic material had not a spherical shape, the experimental values of $\mathrm{d}M/\mathrm{d}h$ were corrected by means of:

$$\chi = \chi_e[1 + (4\pi/3 - N)\chi_v]^{-1} \tag{1.4}$$

where χ_e is the experimental value of the susceptibility and χ_v the susceptibility per cm³.

At the lowest attainable temperatures large deviations from Curie's law may occur. In measuring the absolute temperature it will be essential to use the fundamental definition of temperature introduced by Kelvin:

$$dQ = T\,\mathrm{d}S \tag{1.5}$$

Performing a large number of demagnetizations from various initial conditions it is possible to obtain the relation between entropy, calculated from the initial field and temperature values, and a certain quantity which will be called the thermometric parameter P_t (for instance, T^*).

When a known amount of heat is added to the sample the increase of entropy can be derived from the change of P_t.
During the measurements to be described here, the heat is added by an alternating magnetic field. The heat absorption in the sample is given by:

$$dQ/dt = (1/2)h_0^2\omega\chi'' \tag{1.6}$$

h_0 being the amplitude of the alternating field. The heat may be added continuously or in short periods. In the first case the absolute temperatures follow from:

$$T = (dQ/dt)/(dP_t/dt)(dS/dP_t) \tag{1.7}$$

In the second case the deduced value of T is the averaged value during the heating period being found by means of the formula:

$$T = \int_{t_1}^{t_2} (1/2)h_0^2\omega\ \chi''\ dt/(S_2 - S_1) \tag{1.8}$$

When determining absolute temperatures, it is important to use a heat input which is large compared to the heat leak: at least 10 times larger. A correction for the heat leak cannot be accurate, since it may cause a inhomogeneous distribution of the temperature.

The value of χ'' depends strongly on entropy in most cases and thus the amplitudes of the alternating fields must vary with entropy in order that the required heating be obtained. If the thermometric parameter depends on the amplitude of the measuring field, it may not be convenient to use the first measuring method, an accurate relation between P_t and entropy for each field value not always being available. If quantities independent of h_0 are measurable, as, for instance, χ' and χ'' in the case of alcoholic solutions of paramagnetic ions, the first method is preferable to the second one.

Another way to add heat to a demagnetized sample in a nearly homogeneous way can be found in the absorption of γ-rays. The γ-rays cause a constant heat input, which can be calibrated, measuring the entropy variation at high temperatures, where Curie's law is valid.

It is clear that if the relation between entropy and temperature has been found, any temperature-sensitive property can be used as a secondary thermometer as its variation as a function of entropy can easily be determined. Magnetic thermometers, such as χ' and χ'', have the disadvantage that their measured value depends on the shape of the sample and may vary a little for different samples of the same paramagnetic substance. Relatively large quantities of a salt are needed to get a high measuring accuracy.

In some cases a preferable thermometer may be the anisotropy of gamma rays emitted by oriented radioactive nuclei. The γ-ray intensities emitted in a given direction are dependent on temperature. In several cases the relation between γ-ray anisotropy and temperature has been

thoroughly investigated. A γ-ray thermometer is shape independent in zero field, it does not vary for different samples of the same salt and it can also be used if only small amounts of salt are present. The latter fact means an important advantage for experiments on heat transfer (see chapter III). A γ-ray thermometer can only be used for crystals, not for alcoholic solutions (chapter II) and for many nuclei it is not highly accurate at temperatures above 0.1° K. There are, however, ions which have such large h.f.s. interactions that an anisotropic γ-ray distribution is found even at 1° K for radioactive nuclei (for example ^{166}Ho [4]).

(To be continued)

REFERENCES

1. De Klerk, D., Thesis, Leiden (1948).
2. Steenland, M. J., Thesis, Leiden (1952).
3. Beun, J. A., Thesis, Leiden (1957).
4. Postma, H., A. R. Miedema and Miss M. C. Eversdijk Smulders, Commun. Kamerlingh Onnes Lab., Leiden 316a; Physica 25, 671 (1959).

SOME EXPERIMENTS ON HEAT TRANSFER AND MAGNETISM BELOW 1° K. II

BY

A. R. MIEDEMA

(Communicated by Prof. C. J. GORTER at the meeting of October 29, 1960)

ON SOLIDIFIED SOLUTIONS OF PARAMAGNETIC SALTS

The possibility of investigating solutions of paramagnetic ions below 1° K only exists if solvents are used which do not crystallize. Some liquids are known which can be supercooled if the temperature is lowered below their normal freezing point. These liquids attain a glassy state at very low temperatures instead of crystallizing. Examples of such liquids are ethanol [1], 1-propanol [2] and glycerol [3]. Pure ethanol may crystallize between 110 and 160 K if the cooling has not been fast enough, whereas with propanol it is difficult to obtain the crystalline state. Gibson *e.a.* describe 1-propanol at 125° K as having a jelly-like consistency which contracts at lower temperatures to a hard, transparent glass.

Solutions of copper chloride in ethanol and propanol have been investigated with X-rays at liquid air temperatures. The X-ray patterns showed that no crystals of copper chloride were present. [1])

The solubility of inorganic salts in the three above mentioned liquids is rather high due to the large electrical dipole moment in the liquids. Especially nitrates and chlorides can be dissolved in large amounts; sulphates are less soluble in these alcohols. The maximum obtainable concentrations at room temperature are given in table II.I for a few paramagnetic salts. They are compared with the concentrations of magnetic ions in crystals which have been used frequently for adiabatic demagnetization experiments.

TABLE II, I

Concentrations of paramagnetic ions in some solutions and crystals, used for demagnetization experiments, units mole/cm³

Salt	Solubility in 1-propanol at 300° K	Crystal	Concentration
$FeCl_3 \cdot 6H_2O$	17.5×10^{-4}	$Ce_2Mg_3(NO_3)_{12} \cdot 24H_2O$	28×10^{-4}
$Cr(NO_3)_3 \cdot 9H_2O$	7.5×10^{-4}	$CrK(SO_4)_2 \cdot 12H_2O$	37×10^{-4}
$CuCl_2 \cdot 2H_2O$	8.5×10^{-4}	$CuK_2(SO_4)_2 \cdot 6H_2O$	55×10^{-4}

[1]) I am much indebted to Prof. C. H. MAC GILLAVRY and her coworkers who performed the X-ray analysis.

The apparatus used during the measurements on alcoholic solutions is shown in fig. 2.1. The solutions are put in a glass sphere with a diameter of about 3 cm. This sphere is connected to a piece of CrK-alum, which absorbs the heat coming from the bottom of the apparatus. In preliminary experiments it was found that the thermal contact between the sample and the wall of its surrounding sphere could become very bad, due to the contraction of the solidified alcohol. After reducing the temperature of the helium bath to between 4 and 1° K the temperature of the sample decreased only very slowly, and after a demagnetization it could take a long time to get the sample back to 1° K, even when exchange gas was present between the glass sphere and the wall of the apparatus. In order to improve thermal contact, helium gas was put inside the glass sphere before mounting.

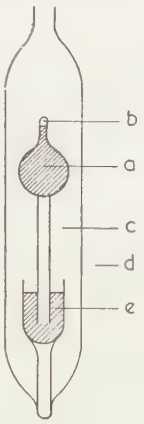

Fig. 2.1
Apparatus used for experiments with solidified solutions.

a alcoholic solution
b filling tube with He gas
c exchange gas
d liquid helium bath
e CrK-alum guard cylinder

1. *$Cr(NO_3)_3 \cdot 9H_2O$ in 1-propanol* (7.5×10^{-4} *mole/cm³*)

Susceptibility measurements were carried out with an a.c. measuring bridge (frequency 225 Hz). In the liquid helium temperature range Curie's law was valid within the experimental accuracy. Demagnetizations were performed starting from a number of fields and an initial temperature of about 1° K. From this the relation between entropy and susceptibility has been derived. The results, which reproduced for several measuring days, are shown in fig. 2.2. The real part of the susceptibility χ' increases rapidly at entropies below $R \ln 2$. The imaginary part χ'' becomes important at entropies below 0.6 R. The entropies are calculated from the initial values of the magnetic fields and temperatures with $g = 2$ and are corrected for the entropy of the lattice heat waves and the entropy change due to the electric contributions to the energy splittings. For the first correction a value of $S_L = 0.05RT^3$ has been derived from demagnetizations from initial temperatures of 1 and 1.5° K. If compared to the values for crystals this correction is rather large, as may be seen from the corresponding value of the Debye constant θ which equals 40° K.

At entropies above $R \ln 2$ the experimental points are in good agreement with Hebb and Purcell's formulae, if for the stark splitting parameter

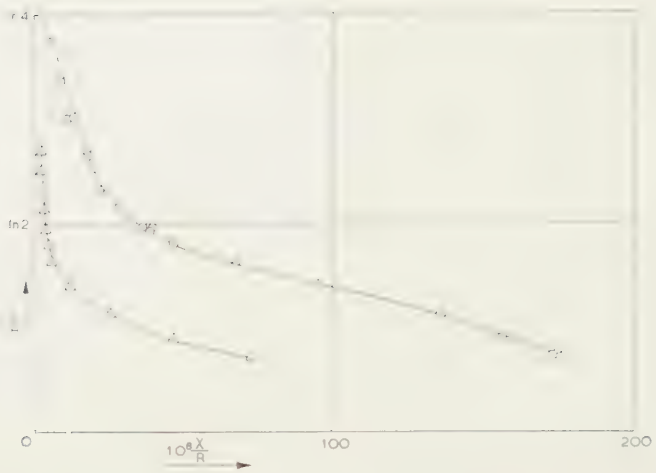

Fig. 2.2 Susceptibility *versus* entropy for a solution of chromic nitrate in propyl alcohol (7.5×10^{-4} mole/cm³). A curve calculated with $\delta/k = 0.30°$ K is given in the high entropy region (dashed line).

○ $10^8 \times \chi'/R$ △ $10^9 \times \chi''/R$

the value $\delta/k = 0.30°$ K is assumed. The calculated relation is given in fig. 2.2 as a dashed line. The value found for δ roughly equals the value obtained with crystalline chromium nitrate, ref. [4] and [5], and it differs only slightly from the values found in the chromium alums [6].

The relatively high values of χ'' below $S = 0.6\ R$ gave us the opportunity to measure the thermodynamic temperature in this entropy region by the a.c. heating method. χ'' proved to be independent of the amplitude of the alternating field for the values between 0.08 and 8 oersted used. The energy was added continuously (10 erg/s) or in periods of 10 seconds (30 erg/s). Fig. 2.3 shows the relation between entropy and absolute

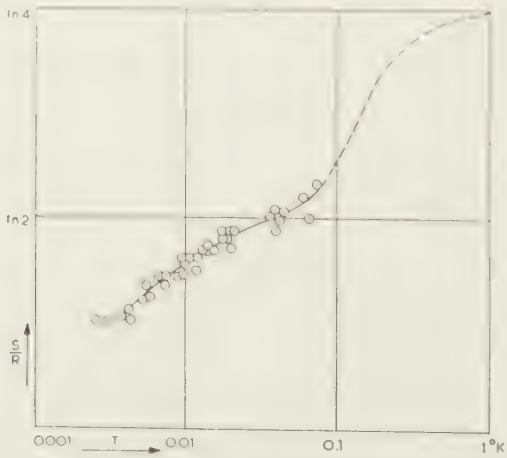

Fig. 2.3 The relation between entropy and absolute temperature of a solution of chromic ions in propyl alcohol (7.5×10^{-4} mole/cm³). The dashed curve is calculated with $\delta/k = 0.30°$ K.

temperature obtained. The lowest temperature attained was 0.003° K. The experimental points measured at entropies below 0.8 R are in agreement with the S *versus* T relation for entropies above $R \ln 2$, calculated with the electrical field splitting concluded from the S *versus* χ' relation (dashed line in fig. 2.3).

In fig. 2.3 the temperatures are plotted on a logarithmic scale, hence the derivatives of the S *versus* T curve are proportional to the specific heat. It can be concluded from the figure that the specific heat has a pronounced minimum between 0.05 and 0.02° K. At lower temperatures it rises roughly in proportion to $1/T$.

2. *$Cr(NO_3)_3 \cdot 9H_2O$ in 1-propanol* (2.5×10^{-4} *mole/cm³*)

The value for the entropy of the heat waves of $S_L = 0.05\ RT^3$ found with the former solution suggested that the lattice entropy was small enough to reach lower temperatures when demagnetizing less concentrated chromium nitrate solutions. Experimentally, however, it was found to be hardly possible to reach temperatures below 0.1° K. Figure 2.4 shows

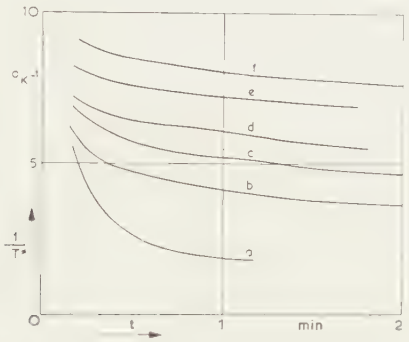

Fig. 2.4 Warming up curves obtained with a $Cr(NO_3)_3 \cdot 9H_2O$ solution (2.5×10^{-4} mole/cm³) after demagnetization from $H = 2 \times 10^4$ Oe, $T = 1°$ K. The sample was kept at $H = 1 \times 10^4$ Oe, $T = 0.5°$ K for a time increasing from curve a to curve f.

a	0 min.	d	6 min.
b	1 min.	e	15 min.
c	3 min.	f	31 min.

a number of warming-up curves obtained after demagnetization from the same initial field and temperature ratio ($H/T = 2 \times 10^4$ Oe/deg). For the curves b–f the magnetic field was reduced to half its initial value at first and after a waiting time, varying from 1 minute for curve b to 31 minutes for curve f, the magnetic field was removed completely. The figure shows that after a longer waiting period the warming-up rate is significantly smaller.

The results indicate that irreversible processes occur during demagnetization, which may be ascribed, for instance, to a temperature difference between heat waves and electron spins. Demagnetizing to 0.5° K at first has the result that a large part of the entropy of the heat waves is removed

before the complete demagnetization takes place. The relatively large difference existing between the curves e and f (waiting times 15 and 31 minutes, respectively, suggests that a relaxation time between the electron spin system and the heat waves at 0.5° K in a field of 10^4 Oe is of the order of 10 minutes, at least.

In earlier experiments with a more diluted chromium nitrate solution (1×10^{-4} mole/cm^3) no temperatures lower than 0.5° K could be reached after demagnetization ($H/T = 2 \cdot 10^4$ Oe deg). The longest time during which the magnetic field was kept at half its initial value was 10 minutes in this case. With more concentrated solutions of chromium nitrate, ferric chloride and copper chloride no indications for the occurrence of irreversible processes have been found in the warming-up curves.

3. *$CrCl_3 \cdot 6H_2O$ in 1-propanol* (10×10^{-4} *mole/cm^3*)

Two, freshly prepared solutions of chromium chloride of the same concentration have been investigated, one solution being prepared at room temperature, the other one being warmed to 70° C when dissolving the chromium salt. Figure 2.5 gives the relation between entropy and the

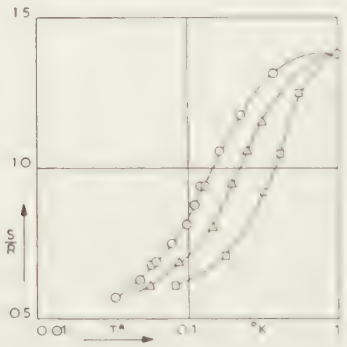

Fig. 2.5 The relation between entropy and magnetic temperature for three solutions of chromic ions in 1-propanol.

○ $Cr(NO_3)_3 \cdot 9H_2O$ conc. 7.5×10^{-4} mole/cm^3, prepared at 20° C
△ $CrCl_3 \cdot 6H_2O$ conc. 10×10^{-4} mole/cm^3, prepared at 70° C
□ $CrCl_3 \cdot 6H_2O$ conc. 10×10^{-4} mole/cm^3, prepared at 20° C

magnetic temperature in the high entropy region for both chromium chloride solutions and for the chromium nitrate solution mentioned before. The curves can be characterized by the value of the Stark splitting parameter δ, which, as a matter of fact, will be an average value for ions in a solution. For the solution prepared at 70° C we derived a value for δ/k of about 0.5° K, for the solution prepared at room temperature the mean value of δ/k is 1.0° K. The S *versus* T^* relation for chromium nitrate is in agreement with $\delta/k = 0.30°$ K.

An explanation for the different δ values can be found in the chemical behaviour of chromic ions. Two complexes of chromic ions occur in

chromium chloride, a violet and a green one, their formulae being $[Cr(H_2O)_6]^{3+}$ and $[Cr(H_2O)_4Cl_2]^{+}$, respectively. According to OLIE [7] the number of each type of ions present in a solution of chromium chloride depends on temperature and concentration. In crystalline chromium chloride only the green modification is present. Upon dissolving the salt $[Cr(H_2O)_4Cl_2]^{+}$ ions will be transformed to $[Cr(H_2O)_6]^{3+}$ ions, the equilibrium time varying from many days at room temperature to several minutes at 70° C.

When preparing a solution at room temperature it may be expected that mainly $[Cr(H_2O)_4Cl_2]^{+}$ ions are present, whereas when preparing a chromium chloride solution at 70° C part of the green modification will be transformed into the violet one. In the chromium nitrate solutions which were always prepared at room temperature, only $[Cr(H_2O)_6]^{3+}$ ions occur. The magnetic measurements with this solution thus represent the magnetic behaviour of chromic ions surrounded by six water molecules and it is not surprising that the derived value for the crystal field splitting ($\delta/k = 0.3°$ K) equals the value found for chromium nitrate crystals.

If the results obtained with the chloride solution prepared at room temperature ($\delta/k = 1°$ K) correspond to the δ value of $[Cr(H_2O)_4Cl_2]^{+}$ ions, one might evaluate from the δ/k value of the warmly prepared solution its composition; $\delta/k = 0.5°$ K corresponds to about 70 % $[Cr(H_2O)_6]^{3+}$ and 30 % $[Cr(H_2O)_4Cl_2]^{+}$ ions.

4. *$FeCl_3 \cdot 6H_2O$ in 1-propanol (17.5×10^{-4} and 3.5×10^{-4} mole/cm³)*

Two solutions of ferric chloride were investigated, the one with the lower concentration being prepared by diluting the concentrated solution a factor 5 with a propanol-water mixture of the same composition as present in the 17.5×10^{-4} mole/cm³ solution.

Susceptibility measurements showed that in the temperature range between 4 and 1° K Curie's law was not obeyed. The χ *versus* $1/T$ plot was not a straight line but the slope of the curve decreased about 15 % between 4 and 1° K.

From measurements performed with the same apparatus on a spherical sample of CrK-alum with the same volume and nearly the same susceptibility per cm³ as the 17.5×10^{-4} mole/cm³ ferric chloride solution, it was derived that at 2° K the χ value of the ferric ions was not more than 66 % of the value calculated from the theoretical Curie constant. This suggests that the electrical crystal field at the position of a ferric ion due to the surrounding water and alcohol molecules, causes splittings of the $S = 5/2$ ground level which are of the order of several degrees Kelvin. These splittings are much larger than those known for hydrated crystals containing ferric ions.

Figure 2.6 shows the relation between both T and T^* and entropy. The T^* values are calculated with the mean slope of the χ *versus* $1/T$ curve between 4 and 1° K and the entropy values, which are calculated from

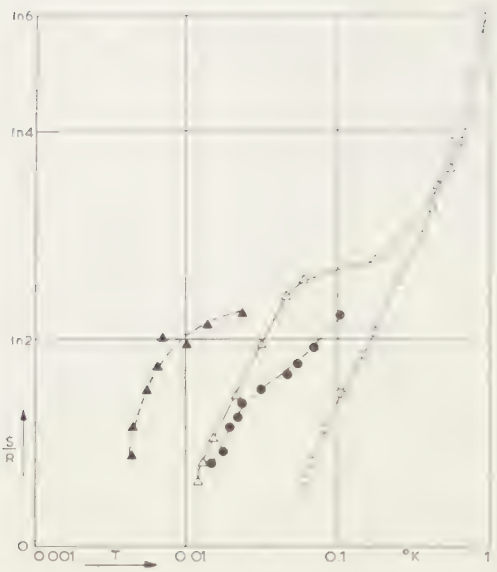

Fig. 2.6 The relation between entropy and T, T^* obtained with solutions of $FeCl_3 \cdot 6H_2O$ in 1-propanol.

○ T^* conc. 17.5×10^{-4} mole/cm³ △ T^* conc. 3.5×10^{-4} mole/cm³
● T conc. 17.5×10^{-4} mole/cm³ ▲ T conc. 3.5×10^{-4} mole/cm³

$S = {}^5/_2$ and $g = 2$, have been corrected for the entropy of the heat waves, as found with solution 1. The T values have been measured with the relaxation heating method. It is clear that the T, T^* and entropy values given in fig. 2.6 have no absolute meaning; they can be used, however, when comparing the two solutions with different iron concentrations. The figure shows that in the low entropy region the values of T and T^* derived for the two solutions differ by practically the same factor as the concentrations do (a factor 5).

The T and T^* values which are reached at entropies smaller than R ln 2 can be expected to be determined by the magnetic dipolar interactions between different magnetic ions. Van Vleck [8] has shown that to a first approximation this interaction is characterized by the so-called internal magnetic field H_i, which can be found from the formula

$$(H_i)^2 = 2\mu^2 \sum_{p \neq q} r_{pq}^{-6} \tag{2.1}$$

μ^2 is the average square of the magnetic moment of one ion, q indicates an arbitrary ion and the summation over p has to be extended over all other ions in the whole crystal (solution). Our experimental results are in agreement with this formula since in a 5 times less concentrated solution the distances r_{pq} are altered by a factor ${}^3\!/5$ and hence H_i decreases a factor 5.

The result differs from the relation between H_i and concentration

measured in crystals diluted by replacing magnetic ions by diamagnetic ions. In this case, (see, for instance, ref. [9] for measurements with cobalt ammonium tutton salt) H_i^2 and not H_i depends linearly on concentration, in agreement with formula (2.1), since now the distances r_{pq} remain unchanged but the number of ions over which the summation should be extended decreases proportionally with the dilution factor.

5. *$CuCl_2 \cdot 2H_2O$ in 1-propanol* (8.5×10^{-4} *mole/cm³*)

In the liquid helium temperature range the susceptibility of a copper chloride solution followed Curie's law within the experimental accuracy. Demagnetizations have been performed from a number of fields and the resulting relation between S and T, T^* can be seen in figure 2.7. The entropy values are calculated from the conditions before demagnetization with $g = 2.2$ and $S = \frac{1}{2}$ and are corrected for the entropy of the heat waves with $S_L = 0.05\ RT^3$.

Fig. 2.7 $CuCl_2 \cdot 2H_2O$ in 1-propanol (8.5×10^{-4} mole/cm³). T and T^* as functions of entropy.

The imaginary component of the susceptibility becomes measurable below $S = 0.5\ R$ and reaches its highest value, $\chi''/\chi' = 0.03$, at the lowest entropy. χ'' proved to be independent of the amplitude of the alternating field between 0.08 and 0.8 oersted. Below $S = 0.45\ R$ the absolute temperature has been measured with the relaxation heating method. The lowest temperature reached is 0.008° K.

Assuming that T equals T^* in the high entropy region, the specific heat can be derived from the slope of the curve in fig. 2.7, the temperature scale being logarithmic. The specific heat at relatively high temperatures

is found to be proportional to $1/T^2$ and can be written as $C_v = 0.0020\, R/T^2$. At lower temperatures the specific heat has a minimum at an entropy of $S = 0.4\, R$ (fig. 2.8).

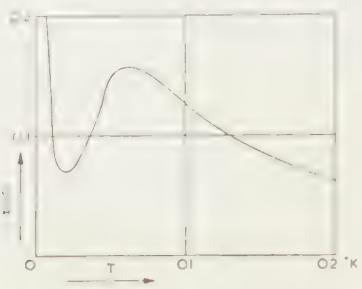

Fig. 2.8 The specific heat of a solution of $CuCl_2 \cdot 2H_2O$ in 1-propanol (8.5×10^{-4} mole/cm^3) as a function of temperature.

Such a minimum in the specific heat may occur if short range order effects are important in the copper solution. The distances between copper ions will vary irregularly while the positions of the neighbouring oxygen atoms will be different for different copper ions. It seems reasonable to suppose that one particular copper ion has only one nearest copper neighbour, being defined as the copper ion to which it has the strongest magnetic interaction. An ordering of copper spins in pairs may cause a minimum in the specific heat if ferromagnetic or both ferromagnetic and antiferromagnetic interactions are present.

A system of 2 spins ($S = \frac{1}{2}$) can be described by 4 basic states. For completely free spins the 4 states have equal energy and the entropy per ion will be $k \ln 2$. The exchange interaction causes a splitting into a singlet and a triplet state. For interactions with the ferromagnetic sign the triplet state has the lowest energy and when going to low temperatures an entropy of $k(\ln 4 - \ln 3)\ 2$ will be removed. For interactions with the antiferromagnetic sign the singlet lies lowest and when decreasing the temperature the total entropy of $k \ln 2$ will be removed.

Strictly, the splitting into a singlet and a triplet state is only true for isotropic g values. In our case the assumption of an isotropic g value will be roughly justified since $g - 2$ is small. The value of g has been found by comparing the magnetization in a field of 2×10^4 Oe with the value of the zero field susceptibility at 1 K. Since we are not able to measure the magnetization directly in such a large field it was derived from the magnetization curve in a longitudinal field after the sample was demagnetized from $H/T = 2 \times 10^4$ Oe/deg. At low temperatures the magnetization is practically saturated in a field of 600 Oe and without much difficulty it was possible to extrapolate the isentropic magnetization curve to $H = 2 \times 10^4$ Oe.

The zero field susceptibility at 1 K is proportional to g^2 whereas the

magnetization in a field of 2×10^4 Oe is roughly proportional to g as it equals

$$M = Ng\mu_B(e^{\alpha} - e^{-\alpha})/2(e^{\alpha} + e^{-\alpha}) \tag{2.2}$$

where $\alpha = g\mu_B H/2kT$. As a result a g value of 2.20 ± 0.10 has been derived which nearly equals the mean value for copper ions in several paramagnetic crystals (chapter IV).

6. *$Ce(NO_3)_3 \cdot 9H_2O$ in ethanol* (25×10^{-4} *mole/cm^3*)

Preliminary measurements have been performed with an alcoholic solution of cerium nitrate. Between 4 and 1° K Curie's law was valid. After demagnetization from $H/T = 2 \times 10^4$ Oe/deg a value for T^* of 0.004° K was measured. In a second experiment with the same sample the magnetic properties were completely different. The slope of the calibration curve was much smaller and no low temperatures were reached after demagnetization. We ascribed this effect to the crystallization of ethanol, when the sample warmed up very slowly between the two measuring days.

7. *The negative result of an attempt to obtain nuclear polarization*

A solution of ferric chloride (5×10^{-4} mole/cm^3) in propanol, containing about 10 μC of both radioactive ^{52}Mn and ^{60}Co has been investigated. Polarizing fields between 100 and 1000 Oe were used but no γ-ray anisotropy larger than 0.5 % was present. The temperatures being low enough, the lack of γ-ray anisotropy may suggest that for cobalt and manganese ions in an alcoholic solution the h.f.s. interaction is very anisotropic. This results in a strong coupling of the nuclear spins to the electrical crystal field, which in a solution will cause nuclear alignment in a direction which varies from ion to ion. For cobalt ions an anisotropic h.f.s. interaction exists in several paramagnetic crystals but for manganese ions it is rather surprising. Apparently it was not possible, even in an external field of 1000 Oe, to magnetize the manganese electron magnetic moments in a direction which differs from their preferential direction, as determined by the crystal field. *(To be continued)*

REFERENCES

1. Kelley, K. K., J. Amer. Chem. Soc. **51**, 779 (1929).
2. Gibson, G. E., G. S. Sparks and W. M. Latimer, J. Amer. Chem. Soc. **42**, 1542 (1920).
3. Simon, F., Ann. Phys. **68**, 241 (1922).
4. Teunissen, P., Thesis, Groningen (1939).
5. Casimir, H. B. G., D. de Klerk and D. Polder, Commun. Kamerlingh Onnes Lab. Leiden **261a**; Physica **7**, 737 (1940).
6. Beun, J. A., A. R. Miedema and M. J. Steenland, Commun. **315a**; Physica **25**, 399 (1959).
7. Olie, J., Z. Anorg. Chem. **51**, 29 (1906).
8. Van Vleck, J. H., J. Chem. Phys. **5**, 320 (1937).
9. Broek, J. van den, L. C. van der Marel and C. J. Gorter, Commun. **314c**; Physica **25**, 371 (1959).

SOME EXPERIMENTS ON HEAT TRANSFER AND MAGNETISM BELOW 1° K. III

BY

A. R. MIEDEMA

(Communicated by Prof. C. J. GORTER at the meeting of October 29, 1960)

ON HEAT TRANSFER

1. *General remarks*

One of the main purposes of demagnetization work is, besides investigating the thermal and magnetic properties of paramagnetic materials, to cool down other substances. In this kind of experiment it is necessary to achieve good thermal contact between a material which can be cooled by the method of adiabatic demagnetization (the cooling salt) and the material under investigation. In such experiments, where heat transfer is essential, the following thermal "resistances" may be important.

a. The inverse heat transmission coefficient between the electron spins of the cooling salt and its heat waves.
b. The inverse thermal conductivity of the cooling salt.
c. The contact resistance at the surface between the cooling salt and the transfer medium.
d. The thermal resistance of the transfer medium, which, in case a certain distance exists between the cooling salt and the substance under investigation, will be called the heat-link.
e. The boundary resistance between the transfer medium and the substance under investigation.
f. The inverse thermal conductivity of the substance itself.

The cooling salt consists of a magnetically concentrated material in which the "resistance" a is expected to be of no importance. For example, according to the data of BÖLGER [1] the energy transfer between the electronic spin system and lattice heat waves in a crystal of CrK alum is in the liquid helium region given by $\dot{Q} = 3 \times 10^6 T^{-0.9}$ erg/s cm^3, the extrapolated value of this heat flow being much higher than the flow permitted by other resistances, as will be shown later.

The thermal conductivity of a lattice is known to be proportional to its specific heat and therefore to T^3 at very low temperatures. In the case of a non superconducting metal, the heat conduction will be mainly due to the free electrons, which results in its proportionality to T. For this reason if a copper wire is used for the heat link, its diameter being chosen not too small, the thermal resistance d will be less important than b at the lowest temperatures.

A number of physicists have performed experiments on thermal contact below 1° K. In order to know the cooling rate of the investigated substance, one must measure its temperature. Thus in the first instance, materials having properties known as functions of temperature, are to be used. These materials will be referred to as the thermometer in the following.

The first metal-to-cooling-salt contact was constructed by Mendoza [2]. Thin copper sheets were soldered to a copper rod. The spaces between the copper sheets were filled with powdered CrK-alum crystals and a binding agent of plastic cement. The sample was pressed under a pressure of 2000 atmospheres. The cooling salt and the thermometer were prepared in the same way, the contact area being 30 cm². Mendoza obtained data on the heat transport between 1 and 0.2° K, the latter temperature being the equilibrium temperature when the cooling salt was demagnetized from $H/T = 12 \times 10^3$ Oe/deg, the thermometer being not demagnetized at all. The results for the heat flow between the two salt pills could be represented by the empirical formula:

$$\dot{Q} = \beta A (T_1^3 - T_2^3) \tag{3.1}$$

A represents the contact area, T_1 is the temperature of the thermometer, T_2 the temperature of the copper and β a constant. The experimental value of β was about 10^2 erg/s cm² deg³. Mendoza's basic idea was developed and modified by several investigators [3], [4]. The copper vanes were replaced by copper wires and the contact area was largely increased. In an unpublished Leiden experiment by Wheatley, 500 wires with a total contact area of 100 cm² were used. In order to cool 10 grms of CrK-alum to 0.06° K with this apparatus a time of three quarters of an hour was needed.

Better results were obtained by Robinson in Oxford [5]. The sample was not compressed at all in his experiments, glycerol being used as a binding agent. With a very large contact area it was possible to cool a pill of cerium magnesium nitrate to 0.025° K within one hour. A cooling salt of this type was used in the experiments on nuclear demagnetization of Kurti *e.a.* [6]. A mixture of CrK-alum, glycerol and water cooled the metal nuclear sample, the total area of contact being 400 cm². In an experiment, where instead of the nuclear sample a CeMg-nitrate mixture was cooled, which was prepared in the same way as the cooling substance, a temperature of 0.011° K was measured 10 minutes after demagnetization, the heat-leak at the place of the thermometer being 1 erg/min. The heat transport between the cerium salt and the CrK-alum mixture could be described by formula (3.1) when β is about 10^3 erg/s cm² deg³.

Experiments on the cooling of single crystals have been reported by Wheatley *e.a.* [7]. Single crystals of ferric ammonium alum were glued to a thermal link of copper or crystalline quartz. The experimental data

for the heat-flow, obtained at temperatures between 0.2 and 0.16° K gave much larger values than that measured in earlier experiments. Also, in this case formula (3.1) was in good agreement with the experiments. β having a value of about 10^4 erg/s cm^2 deg^3.

All authors ascribe the thermal resistance found in the heat flow experiments to a contact resistance at the boundary between different materials.

2. *Recent Leiden experiments*

In 1956 experiments on heat transfer were started, making use of solidified solutions of paramagnetic ions in alcohol as a cooling salt. 1-propanol was chosen for the solvent because of its low freezing point (146° K). The low freezing point is an advantage in experiments on thermal contact, the contact being made at a temperature below the normal freezing point and the shrinking of materials at lower temperatures being of no importance. As stated in the foregoing chapter, ethyl alcohol has the disadvantage that it may crystallize when passing slowly through the liquid-air temperature region. Nearly all nitrates and chlorides can be dissolved in alcohols. High values for the concentration of paramagnetic ions and hence large thermal capacities at low temperatures can be obtained with ferric chloride, chromic chloride and chromic nitrate (Table II, I). A solution of ferric chloride has not been used in the heat transfer experiments because it reacts chemically with copper. With a chromic nitrate solution, in combination with enamelled copper wires, a chemical reaction takes place only after the sample had been cooled down and warmed up again to room-temperature a few times. In principle the reactions might have been avoided if use was made of a copper chloride solution for the cooling salt or of gold wires instead of copper wires.

In a first experiment both the cooling salt and the thermometer consisted of a solidified solution of chromium chloride in propanol. The solutions were contained in glass spheres, their volumes being 11 and 3.5 cm^3, respectively. Thermal contact was attained by means of a string of 1000 copper wires 0.05 mm in diameter. The area of contact between this heat-link and the alcoholic solutions was 30 cm^2 on each side, the average distance between the two samples being 7 cm. Data about the heat transfer between 0.07 and 0.10° K have been obtained.

The other experiments concern heat transport from paramagnetic single crystals to a solution of paramagnetic ions in 1-propanol. Fig. 3.1 shows the apparatus. The cooling agent had a volume of 12 cm^3 and consisted of a solution of chromium nitrate [$Cr(NO_3)_3 \cdot 9H_2O$] in propyl alcohol, the concentration being 7.5×10^{-4} mole/cm^3. Thermal contact between the cooling solution and the copper heat-link was achieved by means of 130 copper wires 0.07 cm in diameter and with a total area of 70 cm^2 in contact with the solution. The wires were soldered in a copper

vase, which was connected to a wire of electrolytically pure copper with a diameter which was varied for several measuring days between 0.02 and 0.09 cm. On the upper end the heat link ended in a circular copper plate 0.02 cm thick and 1.2 cm in diameter. Two sets of experiments with single crystals were performed. In the first one two halves of a spherical single crystal of CrK-alum were glued to each side of the copper plate with Apiezon N grease. The crystals, which had a total volume of 0.75 cm^3, were pressed against the copper plate by two german silver pinches (contact area 2 cm^2). The heat flow from the CrK-alum crystals was measured between 0.6 and 0.04° K. The susceptibilities of the alum and of the cooling solution were used as thermometers.

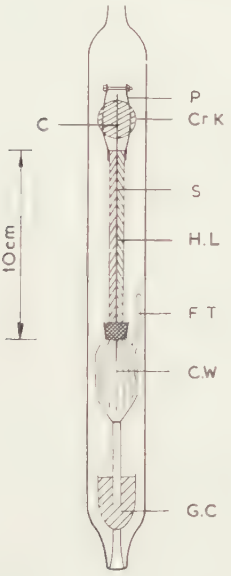

Fig. 3.1
Apparatus used for indirect cooling experiments.

CrK	CrK-alum thermometer
P	pinches
C	copper plate
S	supports
H.L	heat-link
C.W	contact wires
F.T	filling tube
G.C	guard cylinder

In a second set of experiments the CrK-alum was replaced by small CeMg-nitrate crystals containing some radioactive ^{60}Co. The surface area in contact with the copper was about 1 cm^2 and the total volume of the crystals about 0.15 cm^3. In this case the temperature was deduced from the γ-ray anisotropy.

3. *Experimental data and analysis*

During the first experiments on 2 chromium chloride samples a temperature difference was created by demagnetizing the two pills from different fields. The magnetic temperatures of both solutions were measured as functions of time with the a.c. bridge. A typical run which shows that it is possible to perform a temperature measurement, in less than five seconds, can be seen in fig. 3.2. During the first five minutes, when the temperature difference is large, it decreases rapidly, but it takes a long time before thermal equilibrium is reached. The temperatures have been

evaluated from the magnetic temperatures making use of $\delta/k = 0.5°$ K as found for a chromium chloride solution prepared at 70° C.

The 3.5 cm³ sample (thermometer) was demagnetized from the lower field and thus it has the higher temperature in fig. 3.2. During an experimental run it was possible to reverse the sign of the temperature difference by means of a magnetic field of 300 oersted, which was placed at the position of the smaller sample. Upon removing this field after several minutes, the smaller sample reached the lowest temperature, warming up rather quickly afterwards.

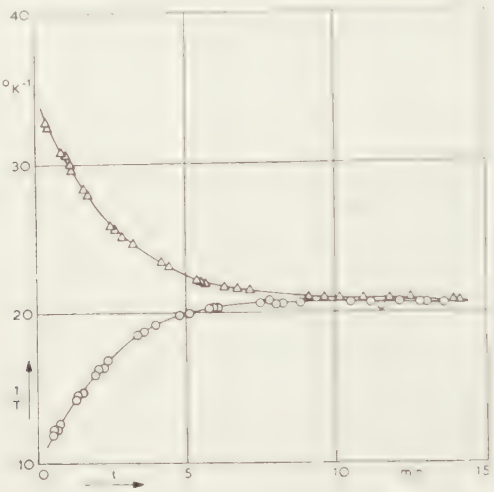

Fig. 3.2 Heat transfer between two alcoholic solutions of chromium chloride.
○ $1/T$ *versus* time 3.5 cm³ sample
△ $1/T$ *versus* time 11 cm³ sample

Values of the heat-flow have been derived at the moments when relatively large temperature differences were present, the higher temperature varying between 0.10 and 0.07° K. Assuming that the heat-flow could be described by:

$$\dot{Q} = B(T_h^n - T_c^n) \tag{3.2}$$

where T_h and T_c are the temperatures of the "hot" and the cold sample, it was not possible to find an accurate value for n from the measurements. Agreement between formula and experiment could be obtained for n values between 2 and 3, the coefficient B being 54×10^2 erg/s deg² in the case where $n = 2$ and 6.5×10^4 erg/s deg³ for $n = 3$.

If the contact resistance between copper wires and paramagnetic solution dominates and if it corresponds to formula (3.2) with n = 3 as suggested by Mendoza, Wheatley *e.a.* and Kurti *e.a.* the value of β equals 0.5×10^4 erg/s cm² deg³ since $B = A\beta^2$ and $A = 30$ cm². In fact, this relatively high value for β will be still larger, because the thermal resistance of the copper heat-link is not negligible in this case. If

alternatively the total thermal resistance found is ascribed to the heat-link, a value for the thermal conductivity of the copper wires at 0.1° K of $K = 0.4\,T$ watt/cm deg is derived. This value is of the order of magnitude of the value estimated from the electrical conductivity of electrolytically pure copper using Wiedemann–Franz law which roughly equals the value for the thermal conductivity of copper reported by several investigators (average value 1.8 T watt/cm deg, ref. [8]). The experiment with two alcoholic samples indicates that the thermal contact between an alcoholic solution and copper wires is good, the values of β being not smaller than the values reported by Wheatley *e.a.* for a single crystal, glued very carefully to a copper plate.

During the experiment in which CrK-alum crystals were used as a thermometer, the crystals were heated up by a 2 MHz oscillating field after demagnetization from fields between 5 and 22 kOe. According to Ambler and Hudson [9] chromium alums have a strong absorption for frequencies of this order of magnitude up to temperatures of about 0.1° K. At higher temperatures the heat will mainly be generated in the copper plate. Starting from 0.01 K° it was found to be possible to reach temperatures between 0.05 and 0.5° K in a few seconds. After each heating period the susceptibilities of the CrK-alum and the cooling solution were measured as functions of time by means of an a.c. measuring bridge. A frequency of 225 Hz and a field amplitude of about 0.1 oersted were used.

From the susceptibilities the temperatures of the "hot" and the "cold" sample (T_h and T_c) were obtained as functions of time. The relation between susceptibility and temperature for CrK-alum has been taken from measurements of Beun *e.a.* [10], a correction for the value of the Curie–Weiss constant θ found in the helium temperature range by Van Dijk and Durieux [11], being applied. Table III, I shows the relation between temperature, entropy and susceptibility. For the chromium solution this relation has been given in the foregoing chapter.

TABLE III, I

Thermal and magnetic properties of CrK-alum

T °K	S/R	$\chi/R \times 10^8$
0.40	1.335	5.23
0.30	1.321	6.87
0.25	1.271	8.10
0.20	1.233	10.0
0.15	1.145	12.8
0.10	1.017	17.1
0.08	0.949	19.3
0.06	0.866	21.1
0.05	0.821	23.9
0.04	0.774	25.9

A typical run is shown in fig. 3.3.

Fig. 3.3 A typical run. Temperatures of CrK-alum crystal and cooling solution as functions of time.

○ T_h temperature upper salt
□ T_c temperature cooling agent

Using the known specific heat of CrK-alum the heat flow can easily be calculated. The heat flow at various values of T_h and T_c is given in table III, II. It varies from 580 erg/s for a $T_h = 0.55°$ K to 0.25 erg/s for $T_h = 0.04°$ K.

TABLE III, II

The heat flow between a CrK-crystal and the cooling agent at several temperatures

T_h °K	T_c °K	$\dot{Q}$ erg/s	Q calculated erg/s	T_h °K	T_c °K	$\dot{Q}$ erg/s	Q calculated erg/s
0.55	0.25	580	600	0.17	0.06	43	46
0.55	0.35	450	440	0.10	0.06	6.7	7.2
0.48	0.26	370	390	0.10	0.06	6.9	7.2
0.40	0.17	320	321	0.10	0.04	10.2	9.0
0.35	0.18	200	206	0.09	0.06^5	2.8	4.4
0.35	0.11	220	252	0.08	0.05^5	2.7	2.9
0.30	0.11^5	230	177	0.08	0.04^5	3.2	3.2
0.30	0.11^5	160	177	0.07	0.04	2.0	1.8
0.29	0.10	165	174	0.06	0.04^9	1.0	1.0
0.26	0.07	126	119	0.06	0.04^4	0.7^5	0.7
0.26	0.07	108	119	0.05^4	0.04	0.4^4	0.49
0.25	0.07	130	127	0.04^6	0.02^5	0.4^4	0.46
0.21	0.07^5	69	80	0.04	0.02	0.2^9	0.28
0.18	0.08	56	50	0.04	0.02	0.2^5	0.28
0.17	0.08^5	34	40				

In principle, in this experiment five thermal "resistances" occur. They are: the thermal resistance of the cooling solution, the contact resistance between the heat-link and alcohol, the resistance of the heat-link, the contact resistance between the crystal and copper and the thermal resistance of the CrK-alum crystal. The first two may be neglected since the contact resistance at the position of the cooling salt is much smaller

than at the position of the single crystals, as can be concluded from the two alcoholic pill experiments and also from an experiment in which the number of contact wires present in the alcohol was decreased by a factor of 20. It is only after absorption of considerable amounts of heat that the thermal resistance of the alcohol may become a limiting factor for the heat flow.

Let us assume that the heat flow through each of the other 3 resistances can be described by a formula like formula (3.2) $\dot{Q} = B(T_h^n - T_c^n)$ in which T_h and T_c are now the temperatures on both sides of the resistance.

On the basis of earlier data on thermal contact experiments one would expect that a resistance with $n = 3$ is the most important. For this reason we analysed our measurements by comparing the values obtained for $\dot{Q}/(T_h^3 - T_c^3)$ at different values of T_h. If a formula with $n = 3$ could describe the heat flow $\dot{Q}/(T_h^3 - T_c^3)$ would be independent of T_h. Figure 3.4 shows that this is not at all the case. $\dot{Q}/(T_h^3 - T_c^3)$ has a maximum for $T_h = 0.2°$ K and thus a thermal resistance with $n > 3$ has to be present

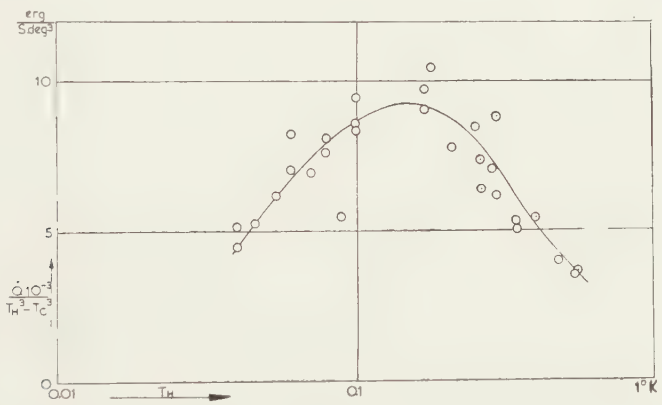

Fig. 3.4 Check of the formula $\dot{Q} = B(T_h^3 - T_c^3)$. If the formula were valid the $\dot{Q}/(T_h^3 - T_c^3)$ *versus* T_h curve should be a horizontal line.

at temperatures lower than 0.2° K and a resistance with a corresponding $n < 3$ is present at temperatures higher than 0.2° K. It was found to be possible to describe the heat flow by a combination of two thermal resistances, with the values $n = 2$ and $n = 4$, respectively. In table III, II the experimental values of $\dot{Q}$ are compared with values calculated by means of:

(3.3) $$\dot{Q} = 12 \times 10^4 (T_h^4 - T_b^4) \text{ erg/s}$$

(3.4) $$\dot{Q} = 26 \times 10^2 (T_b^2 - T_c^2) \text{ erg/s}$$

In these equations T_b represents a temperature between T_h and T_c. Within the experimental accuracy agreement has been obtained. A thermal resistance with $n = 3$ may be present, but its coefficient B has to be larger than 5×10^4 erg/s deg^3, which means that if we ascribe such

a term to a boundary resistance between the alum and the copper $\beta \geqslant 2.5 \times 10^4$ erg/s deg^3 cm^2.

The thermal resistance corresponding to formula (3.4) was obviously due to the heat-link, since its coefficient varies from 40×10^2 to 2.7×10^2 erg/s deg^2 when the diameter of the copper was varied from 0.9 to 0.2 mm. The corresponding values for the thermal conductivity of copper were $K = 0.32\,T$ and $K = 0.64\,T$ watt/cm deg. These relatively low values [8] are not surprising as two solder joints were present in the heat-link.

Mendoza [2], Wheatley *e.a.* [7] and Kurti *e.a.* [6] conclude from their experiments that a boundary resistance is described by $\dot{Q}/A = \beta(T_h^3 - T_c^3)$. If the contact resistance is described by such a formula in our experiments, we must ascribe the resistance with $n = 4$ to the CrK-alum crystals. This agrees with the fact that the coefficient of the thermal resistance with n = 4 was a constant for four successive measuring days, while the crystal-glue-copper contact was renewed before each measuring day.

It is possible to estimate the thermal conductivity of the CrK-alum crystals from equation (3.3). If the thermal conductivity follows a T^3 law, the coefficient λ_1 of $\lambda = \lambda_1 T^3$ will be of the order of 4×10^4 erg/s cm deg^4 (see next section). This value is much smaller than that measured by Garrett [12]: $\lambda_1 = 5.3 \times 10^5$ erg/s cm deg^4.

The value for the thermal conductivity of CrK-alum given by Garrett corresponds to a value for the phonon mean free path l of about 2 mm. whereas our value for λ_1 gives l is about 0.2 mm. This rather small value of the phonon mean free path may be due to the fact that the CrK-alum crystals had been cooled four times from room temperature to very low temperatures before the experimental data were obtained. A similar discrepancy exists between the values of the thermal conductivity measured at higher temperatures by Bijl [13] and by Van den Broek *e.a.* [14]. Van den Broek's values are a factor 10 smaller than those of Bijl, but he also made measurements on a sample which had been cooled from room temperature to helium temperatures many times.

In the experiments with CeMg-nitrate the crystals were heated up immediately after demagnetization in the same way as described for the CrK-alum crystals. The temperatures were derived from the normalized γ-ray intensities, W, measured in the direction of the alignment axis and in the direction perpendicular to it. The relation between the anisotropy ε, defined as $[W(\pi/2) - W(0)]/W(\pi/2)$, and the temperature has been taken from data of Ambler *e.a.* [15]. Figure 3.5 shows the results of two identical runs taken together. After 6 minutes ε reached a value of about 0.08, which corresponds to a temperature of $0.015 \pm 0.002°$ K. In this experiment the contact area between the CeMg-nitrate crystals and the copper plate was about 1 cm^2 and the radioactive heat input was about 0.06 erg/s.

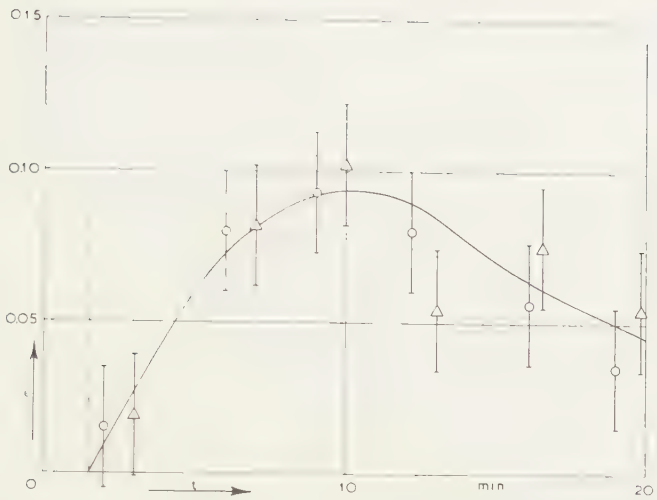

Fig. 3.5 γ-anisotropy of ^{60}Co in CeMg-nitrate as a function of time. The crystals were heated up at $t = 1'30''$. $\varepsilon = 0.08$ corresponds to $T = 0.015°$ K.

4. *Derivation of the value for the thermal conductivity of CrK-alum*

The heat flow differential equation has been solved for the CrK-crystals with the following approximations:

a) The crystal has a cylindrical shape.
b) The specific heat is constant.
c) The thermal conductivity can be written as $\lambda_1 T^3$.
d) The temperature of the cold side of the crystal $T_b = 0$.

In this case the heat flow problem becomes one-dimensional. The equation to be solved is:

$$\frac{\partial^2 T^4}{\partial x^2} = \frac{4C_v}{\lambda_1}\frac{\partial T}{\partial t} \tag{3.5}$$

Assuming $t \geqslant 0$, the solution can be found by the method of separating variables, as the relative temperature distribution will become independent of its actual (unknown) initial conditions. Hence we write T in the form:

$$T(x, t) = f(x)\, g(t) \tag{3.6}$$

$f(x)$ is found by solving numerically the equation:

$$\frac{\partial^2 f^4}{\partial x^2} = \frac{4C_v}{\lambda_1} g'(t)\, f/g^4 \tag{3.7}$$

The relative temperature distribution $f(x)$ is shown by fig. 3.6 in terms of T^4 as a function of x. The solution will also hold for values of $T_b \neq 0$ as long as $T_b{}^4 \leqslant \overline{T}^4$. It is possible to calculate from fig. 3.6 the relation between the heat transport through 1 cm^2 cross-section of the crystal and the average temperature.

$$\dot{Q}/A = 0.85\, \lambda_1 (\overline{T}^4 - T_b{}^4)/L \tag{3.8}$$

In our case approximations b and c will be roughly justified. The specific heat of CrK-alum is nearly constant in the temperature region between 0.1 and 0.04° K where the conductivity of the crystal limits the heat flow in our experiments. The T^3 dependence of the thermal conductivity has been measured by GARRETT [12] and is confirmed by our formula (3.3).

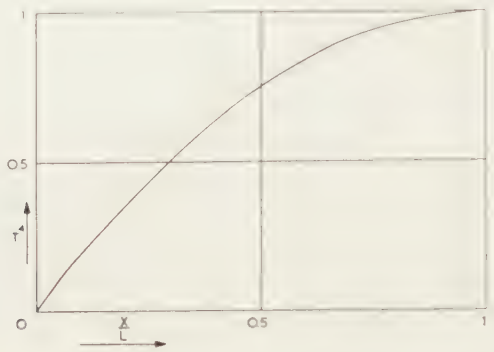

Fig. 3.6 Temperature distribution in a cylindrical CrK-alum crystal of length L, which is cooled at $x = 0$. The heat flow through each cm² cross-section of the crystal is given in arbitrary units by the derivatives of the curve.

When approximating formula (3.8) in the case of the two spherical crystals by taking $L = 0.6$ cm, the result is:

$$\dot{Q} = 2.8\ \lambda_1(\bar{T}^4 - T_b{}^4) \tag{3.9}$$

The coefficient will increase if a correction is applied for the fact that the average susceptibility has been measured instead of the average temperature. The magnitude of this correction depends mainly on the actual value of the temperature of the cold side of the crystal and hence varies throughout the experiments. Assuming (3.9) to be valid, formula (3.3) gives a thermal conductivity of a CrK-alum crystal not higher than $\lambda = 4 \times 10^4 T^3$ erg/s cm deg.

5. *Comparison with theory*

Debye's theory gives the following formulae for the thermal conductivity and lattice specific heat of non-metals at very low temperatures

$$\lambda = (1/3) lcC_v = \lambda_1 T^3 \tag{3.10}$$

$$C_v = 0.4\ k^4 \pi^2 T^3 / \hbar^3 c^3 \tag{3.11}$$

in which

l = phonon mean free path,
C_v = lattice specific heat per unit volume,
c = velocity of sound.

The heat flow through a unit area of a cylindrical crystal with length L is given by:

$$\dot{Q}/A = \lambda_1(T_h^4 - T_c^4)/4L = k^4\pi^2 l(T_h^4 - T_c^4)/30\,\bar{h}^3c^2L \tag{3.12}$$

The maximum possible heat flow at a given value of T_h is obtained with $l = L$ and $T_c \sim 0$.
Thus:

$$\dot{Q}/A \leqslant k^4\pi^2 T_h^4/30\,\bar{h}^3c^2 = 1 \times 10^{17} T_h^4/c^2 \text{ erg/s cm}^2 \tag{3.13}$$

In the case of CeMg-nitrate equation (3.13) gives $\dot{Q}/A \leqslant 2 \times 10^6 T_h^4$ erg/s cm^2 the value of c being deduced from the lattice specific heat at 1° K [16]. In our experiments we approached this maximum value of $\dot{Q}/A$ rather closely. The heat transport of 0.06 erg/s with $T_h = 0.015°$ K corresponds to $\dot{Q}/A$ is about $10^6 T_h^4$ erg/s cm^2.

The question arises why the theoretical value calculated for ideal thermal contact between a crystal and copper should not surpass the experimental value many times, two reflecting surfaces and a glue layer being present at the contact surface. There is a possibility to explain this, discussed hereafter.

It may be expected that in the small CeMg-nitrate crystals the phonon mean free path is of the order of the crystal thickness (1 mm). In this case one may doubt whether it is justified to relate the flow of energy and the temperature, as derived from the observed γ-anisotropy, by means of Debye's theory. The temperature of the system of ^{60}Co nuclei only depends on the frequency distribution in that part of the phonon spectrum with which the cobalt nuclear spins interact and not on that of other frequencies. It cannot be expected that in such small crystals, the thermal vibrations into which the kinetic energy of the emitted β particles is transformed attain a Boltzmann distribution. Since the kinetic energy of the β particles is extremely high if compared to the energy of thermal vibrations, one may expect that a relatively large number of high frequency phonons be generated. If these phonons leave the crystal immediately the energy thus transported adds itself to energy transported in accordance with Debye's theory, in which the temperature of the cobalt nuclear spins and the part of the phonon spectrum that interacts with them, is used. This offers a possibility to explain the fact that the observed energy transport almost equals the value to be expected for ideal thermal contact.

Other data on the heat flow from radioactive crystals come from experiments on the asymmetry of β-rays. In these experiments one uses radioactive layers on a directly demagnetized crystal. In experiments on the β-asymmetry of ^{58}Co and ^{52}Mn nuclei of Postma *e.a.* [17], where the radioactive heat input was of the order of 0.1 erg/s cm^2, the layer warmed up quickly to a temperature which varied between 0.013 and 0.020° K for different experiments, as has been derived from the observed

γ-anisotropies. The energy transport was extremely large if compared to Debye's theory which may suggest that also in these experiments there is no thermal equilibrium in the phonon system.

6. *The thermal resistence of a crystal-glue-copper contact*

It may be expected that apart from the radioactive heat input there is a heat leak in the CeMg-nitrate crystals of the order of 0.01 erg/s. This indicates that the resistance of a crystal-glue-copper contact is rather small. It will be shown in this section that the resistance of a glue layer may not be so important and that it is in principle even possible to have better thermal contact using a glue than in case of perfect mechanical contact without a glue layer.

We shall first neglect the presence of the glue layer and consider the transmission coefficient for phonons at the surface between a crystal and copper. The transmission coefficient Γ_{ik} is determined by the following formula given by RAYLEIGH [18], phonons being in principle acoustical waves of extremely high frequencies.

$$\Gamma_{ik} = 4\varrho_1\varrho_2 c_1 c_2 \cos\theta_1 \cos\theta_2 / (\varrho_1 c_1 \cos\theta_2 + \varrho_2 c_2 \cos\theta_1)^2 \tag{3.14}$$

θ_2 is the angle with the normal on the reflecting surface at which a phonon with an angle of incidence θ_1 will be refracted. The angles θ_1 and θ_2 are related by Snellius' law of acoustic refraction.

In order to know the total amount of refracted energy it will be necessary to integrate over all incident angles θ_1. Calculations have been made by LITTLE [19], who described the thermal resistance at a surface between two different materials by

$$\dot{Q}/A = 5 \times 10^{16} [\Gamma_l / c_l^2 + 2\Gamma_t / c_t^2](T_h^4 - T_c^4) \text{ erg/s cm}^2 \tag{3.15}$$

Γ_l and Γ_t are the transmission coefficients and c_l and c_t the propagation velocities of longitudinal and transverse phonons, respectively. The evaluation of Γ_l and Γ_t is difficult because each wave, whether longitudinal or transverse, in general, breaks up into four waves, reflected transverse and longitudinal waves and refracted transverse and longitudinal waves as has been stated by KOLSKY [20]. Little calculated the transmission coefficients by numerical integration, using an electronic computer. In his paper the results are given in the form of parametric plots, where the values of Γ_l and Γ_t can be derived from the ratios of the densities and the velocities of sound in the two media.

Using the values of ϱ and c as known from measurements at room temperature, Little derived that the reflection of phonons at a contact surface between a crystal (CrK-alum) and copper will correspond to a boundary thermal resistance of the kind given by formula (3.2) with $n = 4$ and $B/A = 0.5 \cdot 10^6$ erg s cm^2 deg^4. The values of ϱ and c of CeMg-nitrate crystals are slightly different from the ones in CrK-alum; the

calculated value of B will be somewhat higher but it remains of the same order of magnitude, 10^6 erg/s cm^2 deg^4.

If a glue layer is present there are two reflecting surfaces between the crystal and the copper plate. The heat flow from a crystal at temperature T_h, of density ϱ_1, and in which the velocity of sound is c_1, through a glue layer of thickness L, density ϱ_2 and velocity of sound c_2 to a metal at temperature zero with quantities ϱ_3 and c_3 will be determined by the following equations:

$$(3.16)\quad (\dot{Q}/A)_{gl} = 1\times 10^{17}(T_h^4 - T_1^4)\Gamma_{12}/c_1^2 = 1\times 10^{17} l(T_1^4 - T_3^4)/c_2^2 L = 1\times 10^{17}\Gamma_{23} T_3^4/c_2^2 \text{ erg/s cm}^2$$

where T_1 and T_3 are the temperatures of the glue at the crystal-glue surface and the glue-copper surface, respectively, and l is the mean free path of the phonons in the glue. By eliminating T_1 and T_3 from the equations the ratio of the heat flow values using glue and without glue can be derived. The result is:

$$(3.17)\qquad \dot{Q}_{gl}/\dot{Q} = [\Gamma_{12}\Gamma_{23}/\Gamma_{13}]\ [\Gamma_{23} + c_2^2(\Gamma_{23} + l/L)\Gamma_{12}/c_1^2(l/L)]^{-1}$$

As an approximation formula (3.14) with $\theta_1 = \theta_2 = \pi/2$, will be used for the calculation of the transmission coefficient. The approximation gives reliable results as can be seen from the comparison of values of the transmission coefficients calculated by Little with the approximate ones. In figs. 3.7 and 3.8 the values of $\dot{Q}_{gl}/\dot{Q}$ are given as a function of the density and the velocity of sound in the glue, using the following values for the other quantities: $\varrho_1 = 2$ g/cm^3, $\varrho_3 = 9$ g/cm^3, $c_1 = 2.3\times 10^5$ cm/s, $c_3 = 3.5\times 10^5$ cm/s. When calculating the curves of fig. 3.7 the thermal resistance of the glue layer has been neglected ($l/L = 1$). Fig. 3.8 is constructed using $l/L = 0.1$. Fig. 3.7 shows that in principle there is a possibility of increasing the transfer of heat when using a glue, if the glue has an acoustical impedance (ϱc) which does not differ much from the acoustical impedance of the crystal, but while it has a much lower velocity of sound. Comparison of the figures 3.7 and 3.8 shows that the thermal resistance of a glue layer ($l/L < 1$) has no large influence if the velocity of sound has a low enough value.

In our experiments with single crystals glued to a copper plate, the Apiezon glue can be expected to have a low c value ($c < 1\times 10^5$ cm/s) which might explain why the thermal resistance of the glue layer is small, even if the mean free path of the phonons in the glue is several times smaller than the thickness of the glue layer (0.05 mm) at a temperature of 0.015° K.

A tentative explanation for the T^3 dependence of the heat flow through a crystal-glue-copper contact, as found at temperatures of about 0.2° K by Wheatley *e.a.* [7], might be given if the mean free path of a phonon in the glue increases with increasing wave length. Such a dependence

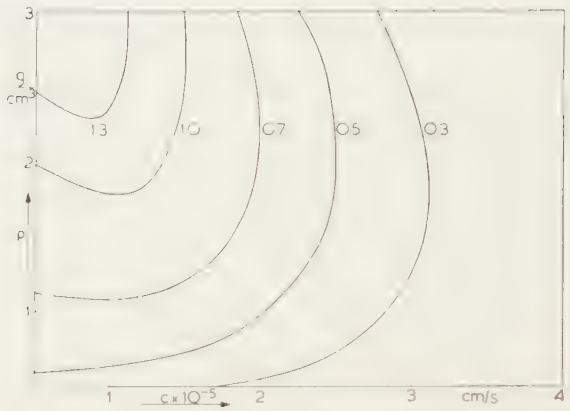

Fig. 3.7 The ratio of the heat flow from a perfect CeMg-nitrate crystal to copper, using a glue and without it, as a function of the density and the velocity of sound in the glue. The thermal resistance of the glue layer itself is neglected ($l/L = 1$).

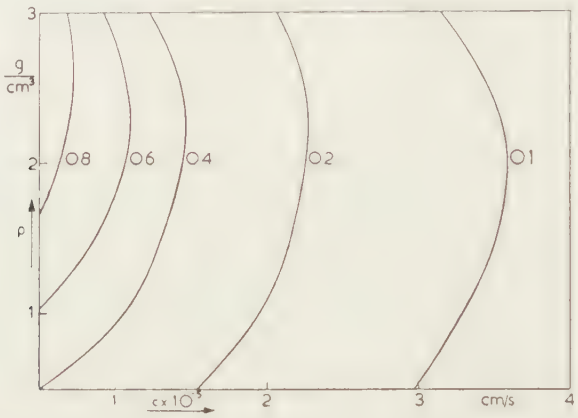

Fig. 3.8 The ratio of the energy transport from a CeMg-nitrate crystal to copper, using a glue and without it, as a function of the properties of the glue. The thermal resistance of the glue layer is described by $l/L = 0.1$.

often has been found experimentally in the attenuation of normal acoustic waves in high polymers [20].

If the thermal resistance measured by Wheatley *e.a.* is only due to the resistance of the glue layer, we obtain $l/L \approx 0.02$ at 0.2° K. ($l \approx 10^{-3}$ mm).

7. *Conclusions and comparison of different indirect cooling methods*

The lowest temperatures obtainable by indirect cooling methods in which conductivity by phonons is essential, are of the order of 0.01° K. Formula (3.13) shows that the heat transportable at 0.01° K through 1 cm² area is of the order of 0.01 erg/s. It would be difficult to reduce the heat leaks below this amount. A temperature of 0.01° K can only be reached in crystals in which the free path of the phonons is not much larger than the smallest dimension of the crystals, thus, only perfect or

very thin crystals can be used. In experiments with radioactive crystals no high activities can be used if α, β^- or β^+ radiation is emitted. For a decay starting with K-capture no restriction is necessary.

In experiments on, for example, two stage demagnetization, nuclear orientation in external magnetic fields or nuclear alignment in antiferromagnetics, where materials with large heat capacities are to be cooled, the time needed to obtain a considerable decrease in temperature will also be an important factor. For the cases where thermal conductivity by phonons is essential, the time factor can be estimated. Fig. 3.9 gives the temperature of a particular crystal as a function of time, the properties of the crystal being assumed as follows: the entropy of the crystal per mole can be written as $10^{-4}R/T^2$, the thickness of the crystal is 1 mm, the molecular weight is 500 and the density is 2. The heat transport is assumed to be described by 10^6T^4 erg/s cm^2. Fig. 3.9 shows that it takes 3 hours in this case to reach a temperature of 0.01° K. For other values of the parameters the corresponding curve can be found easily, the times in fig. 3.9 being plotted on a logarithmic scale and a change of the parameters resulting in a constant shift of the whole curve.

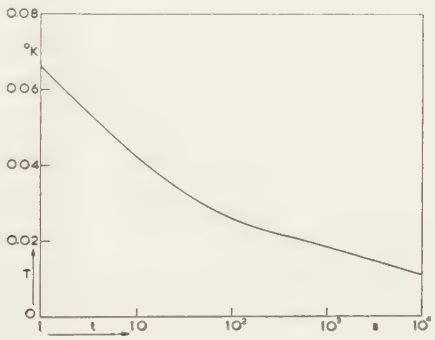

Fig. 3.9 The temperature of a cylindrical crystal as a function of time, the properties of the crystal being assumed as follows.

density = 2 g/cm^3 entropy = $10^{-4}R/T^2$

molar weight = 500 thickness = 1 mm

The cooling rate is given by 10^6T^4 erg/s cm^2

The results obtained when cooling antiferromagnetics (chapter VI) can be compared with this calculation of the cooling time. A crystal of $CoNH_4$-tutton salt of thickness 3 mm could be cooled to about 0.035° K in 1000 s, the entropy of the nuclear spin system being given by $8 \times 10^{-4}\ R/T^2$.

Surface resistances are not necessarily important at the lowest temperatures if crystals are glued to flat plates. The thickness of the glue layer has to be of the order of 0.01 cm. The resistance of a heat-link with electron thermal conductivity can be neglected at the lowest temperatures if the diameter is not too small. With heat-links of crystalline quartz, as are used by Wheatley *e.a.*, 0.01° K cannot be reached. The high

velocity of sound (5×10^5 cm/s) gives a maximum heat flow through a unit area of a quartz heat-link of about $3 \times 10^5 T^4$ erg/s cm^2. In practice this number will be reduced if the heat-link is longer than a few times the phonon mean free path.

The cooling salts which have been used successfully by several investigators can be divided into two groups. One group consists of the kind of cooling substances containing large numbers of copper wires in a paramagnetic salt and a binding agent, the latter being glycerol [6], Apiezon oil [21] or alcohol. The results have shown that the thermal contact using propanol is very good, the freezing point of the alcohol corresponding to a temperature below which the shrinking of materials is not so important. However, not only the thermal contact but also the heat capacity of the cooling salt present in the intimate surroundings of the copper wires should be taken into account. Magnetically more concentrated crystals can be added to an alcoholic solution to increase the heat capacity, but experimentally it turns out that not more than 30 percent crystals (CrK-alum) can be allowed, the heat contact being reduced when using larger amounts of crystals. It appears that, when cooling large thermal capacities, a glycerol and CrK-alum mixture may be preferable to an alcoholic solution for the cooling salt, the heat capacity being larger, the contact resistance being nearly as good and its method of preparation at room temperature being handy.

In other methods for indirect cooling use is made of single crystals. A thermal contact made by means of a glue and a copper plate is preferred above a contact made by single crystals grown around metal wires (ref. [22] and [23]), the copper wires shrinking more than the crystals when cooled below room temperature.

A difficulty encountered in using glued single crystals is the preparation of the crystals and the establishment of a large contact area. The thermal conductivity of crystals can be expected to be much better than that of mixtures, which means that if a large enough contact area can be attained a single crystal cooling salt can give the best results, especially if a large amount of heat must be absorbed by the cooling salt. Such apparatus has been used in the investigations on nuclear alignment (chapter VI), a contact area of about 60 cm^2 being obtained by using 16 flat cylindrical plates 2 cm^2 in cross-section and 3 mm thick cut from a large CrK-alum crystal. All crystal plates were glued to copper on both sides. In fact this cooling salt can be represented by one large cylinder 1.5 mm long with a cross sectional area of 60 cm^2. The heat flow through such a CrK-alum cylinder calculated by means of formula (3.8) and the experimentally derived thermal conductivity is $12 \times 10^6 (T_h^4 - T_c^4)$ erg/s, which consequently indicates that its resistance can be neglected if the substance to be cooled has a contact area of only a few cm^2.

(To be continued)

REFERENCES

1. Bölger, B., Thesis, Leiden (1959).
2. Mendoza, E., Cérémonies Langevin et Perrin, Paris, 62 (1958).
3. Goodman, B. B., Proc. Phys. Soc. (London) **A 66**, 217 (1953).
4. Daunt, J. C., Proc. Int. Conf. Low Temp. Phys. Oxford, 157 (1951).
5. Robinson, F. N. H., Thesis, Oxford (1954).
6. Kurti, N., F. N. H. Robinson, F. Simon and D. A. Spohr, Nature **178**, 450 (1956).
7. Wheatley, J. C., D. T. Griffing and T. L., Estle, Rev. Sci. Instrum. **27**, 1070 (1956).
8. Nicol, J. and T. P. Tseng, Phys. Rev. **92**, 1062 (1953).
9. Ambler, E. and R. P. Hudson, Phys. Rev. **104**, 1500 (1956).
10. Beun, J. A., A. R. Miedema and M. J. Steenland, Commun. Kamerlingh Onnes Lab., Leiden **305**d; Physica **23**, 1 (1957).
11. Dijk, H. van, and M. Durieux, Commun. Suppl. **115**a; Physica **24**, 20 (1958).
12. Garrett, C. G. B., Phil. Mag. **41**, 621 (1950).
13. Bijl, D., Commun. **276**b; Physica **14**, 684 (1948).
14. Broek, J. van den, L. C. van der Marel and C. J. Gorter, to be published Physica.
15. Ambler, E., M. A. Grace, H. Halban, N. Kurti, N. Durand, C. E. Johnson and H. R. Lemmer, Phil. Mag. **44**, 216 (1953).
16. Daniels, J. M. and F. N. H. Robinson, Phil. Mag. **44**, 630 (1953).
17. Postma, H., W. J. Huiskamp, A. R. Miedema, M. J. Steenland, H. A. Tolhoek and C. J. Gorter, Commun. **310**b; Physica **24**, 157 (1958).
18. Lord Rayleigh, Theory of Sound, Mac Millan, London (1894).
19. Little, W. A., Canad. J. Phys. **37**, 334 (1959).
20. Kolsky, H., Stress waves in Solids, Oxford University Press, London (1953).
21. Daniels, J. M. and M. A. R. le Blanc, Canad. J. Phys. **36**, 638 (1958).
22. Dabbs, J. W. T., L. D. Roberts and S. Bernstein, Phys. Rev. **98**, 1512 (1955).
23. Dugdale, J. S., D. K. C. Mac Donald and A. A. M. Croxon, Canad. J. Phys. **35**, 502 (1957).

SOME EXPERIMENTS ON HEAT TRANSFER AND MAGNETISM BELOW 1° K. IV

BY

A. R. MIEDEMA

(Communicated by Prof. C. J. GORTER at the meeting of October 29, 1960)

THE MAGNETIC BEHAVIOUR OF FOUR TUTTON SALTS BELOW 1° K

The investigated tutton salts have the general formula $M^{+}{}_2M^{++}(SO_4)_2 \cdot 6H_2O$ where M^{++} is a divalent ion and M^{+} a monovalent ion. The crystals are monoclinic, their structure having been investigated by HOFFMAN [1]. The angle between the crystalline a and c axes was found to be 106°, the b axis being perpendicular to the ac plane. The dimensions of the unit cell in the directions of the crystalline a, b and c axes are 9.2, 12.4 and 6.2 Å, respectively.

There are two lattice positions for the magnetic ions, [0, 0, 0] and [½, ½, 0], the environment of the one in the ac plane being the mirror image of that of the other. The crystal field acting on the magnetic ions has roughly tetragonal symmetry and has the same character for the two lattice positions. Only the directions in space of the symmetry axes of the crystal field are different. Fig. 4.1 gives the positions of the tetragonal axes (T) and of the principal axes of magnetization (K_1, K_2, K_3). The parameters ψ and α, in the figure shown for the case of $CoNH_4$-tutton salt, are different for different tutton salts as can be seen in table IV. I. The data have been found by paramagnetic resonance methods. For

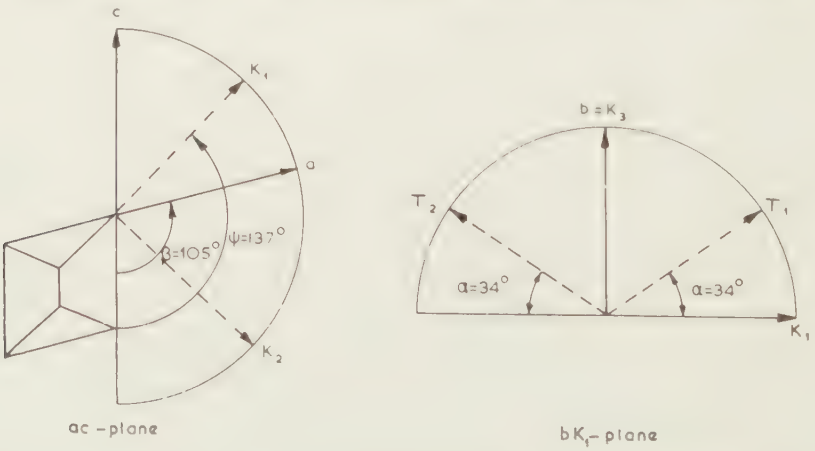

Fig. 4.1 Positions of magnetic susceptibility axes (K) and tetragonal field axes (T) with respect to the crystallographic axes in cobalt ammonium sulphate.

TABLE IV, I

Parameters of the magnetic ions in four tutton salts. The values for Co and Mn ions are obtained on a $ZnNH_4$-tutton salt crystal

Tutton salt	S	ψ	α	$g_{\|\|}$	g_2	$g_\perp$ (K_1K_3)	Ref.
CuK	½	105	42	2.36	2.04	2.14	Bleaney *e.a.* [10]
$CuNH_4$	½	65	39	2.45	2.06	2.12	Bleaney *e.a.* [10]
$CoNH_4$	½	137	34	6.45	3.06	3.06	Van den Broek *e.a.* [11]
$MnNH_4$	5/2	58	32	$D/k = 0.038°$ K		$g = 2$	Bleaney *e.a.* [12]

Co and Mn ions the parameters have been derived from measurements on a crystal which was magnetically diluted with Zn ions. Susceptibility measurements have shown that the parameters are roughly the same for concentrated $CoNH_4$-tutton salt [2], but for the concentrated manganese salt ψ apparently is about 150°, as will be discussed in chap. VI, section 6.

Experiments performed with single crystals of $MnNH_4$-, $CoNH_4$-, $CuNH_4$- and CuK-tutton salt will be reported. The samples were used in the shapes in which they had been grown in order to prevent confusion as to the directions of the axes. The susceptibilities were corrected to the values for a spherical sample, although the investigated crystals did not have an ellipsoidal shape. Though a demagnetizing factor has only a well defined meaning for an ellipsoidally shaped crystal it is assumed that the susceptibilities can be corrected in first approximation by means of an average N value. This N has been determined experimentally by measuring the susceptibility of a piece of Armco iron modelled to the shape of the crystal, as compared with that of an Armco iron sphere (see Huiskamp *e.a.* [3]). The magnetic induction B in such a ferromagnetic sample is inversely proportional to $1/N$ for magnetic fields which are considerably smaller than the saturation value and considerably higher than the coercive field. The estimated N values are given in table IV, II.

TABLE IV, II

Weights and demagnetizing factors (units $4\pi/3$) of the investigated tutton salt crystals

Tutton salt	Weight g	N_1	N_2	N_3
CuK	2.9	0.56	1.79	0.90
$CuNH_4$	3.4	1.02	1.45	0.70
$CoNH_4$	9	1.02	1.20	0.79
$MnNH_4$	11	1.12	0.96	0.83

The ballistically measured susceptibilities have been corrected to the value for a spherical sample by means of:

$$\chi = \chi_e/(1+\varepsilon\chi_e) \tag{4.1}$$

in which χ_e is the experimental value of the susceptibility, $\varepsilon \quad (4\pi/3 \quad N)\varrho/M_0$.

ϱ is the density and M_0 the molecular weight. If strong relaxation effects occur the formula can not be used for susceptibilities measured with an alternating field. In that case the following formulae have been used:

$$\chi'' = \frac{\chi_e''}{1+\varepsilon^2(\chi_e'^2+\chi_e''^2)+2\varepsilon\chi_e'} \tag{4.2}$$

and

$$\chi' = \frac{\chi_e'+\varepsilon(\chi_e'^2+\chi_e''^2)}{1+\varepsilon^2(\chi_e'^2+\chi_e''^2)+2\varepsilon\chi_e'} \tag{4.3}$$

where χ_e' and χ_e'' are the experimental values of the susceptibility per mole.

1. *Manganese ammonium tutton salt*

Previously measurements on powdered crystals of $MnNH_4$-tutton salt have been performed by COOKE [4] and by STEENLAND *e.a.* [5], who found a pronounced maximum in the susceptibility versus entropy curve. Cooke measured the relation between temperature and entropy above the Néel temperature; Steenland *e.a.* did the same below that temperature.

The present experiments were performed with a single crystal, the different magnetic axes being placed in the direction of the vertical measuring field on different measuring days. Fig. 4.2 shows the adiabatic susceptibilities in zero field. The measurements in the K_3 direction were performed ballistically, while for the K_1 and K_2 directions an a.c. bridge was used as the values of χ'' proved to be negligible in these directions. At entropies above ln 4 the susceptibilities are not very different for the three directions, the largest value being found in the K_1 and the lowest value in the K_2 direction. At an entropy of about R ln 4 the K_3 suscepti-

Fig. 4.2 $MnNH_4$-tutton salt. The susceptibility measured in zero field as a function of entropy for the three magnetic axes.
△ K_1 direction □ K_2 direction ○ K_3 direction

bility increases sharply with decreasing entropy to a maximum value which if calculated per cm^3 equals the value $3/4\pi$ within the experimental accuracy of 2 %. At the entropy $S = 1.25\ R$ the K_1 susceptibility passes through a pronounced maximum, whereas the K_2 susceptibility becomes independent of entropy. This entropy of 1.25 R will be considered as the entropy at the Néel temperature (S_N). At the lowest entropy reached ($S = 0.29\ R$), the K_1 susceptibility has decreased to $\chi = 7 \times 10^{-8}\ R$ the K_2 and K_3 susceptibilities being $15 \times 10^{-8}\ R$ and $63 \times 10^{-8}\ R$, respectively.

Relaxation effects only occur in the K_3 direction. The values of χ' and χ'' have been measured as functions of entropy. Both are strongly dependent on the amplitude and the frequency of the measuring field. Fig. 4.3 shows the susceptibilities (χ_0, χ' and χ'') in the K_3 direction measured with an alternating field of 0.05 Oe amplitude at a frequency of 225 Hz. At relatively high entropies, above S_N, χ'' is negligibly small and χ' equals χ_0. Below S_N the value of χ' decreases with decreasing entropy, whereas χ'' reaches a maximum at S is about 0.8 R. The maximum value of χ'' corresponds to $\chi''/\chi_0 = 0.22$. The susceptibilities in fig. 4.3 are corrected for the demagnetizing factor using formulae (4.2) and (4.3).

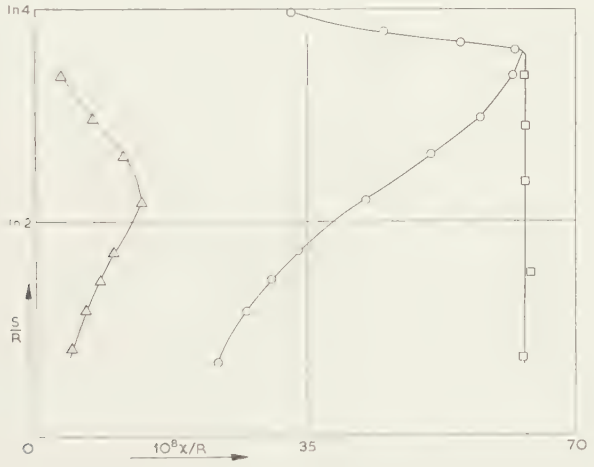

Fig. 4.3 $MnNH_4$-tutton salt. χ_0, χ' and χ'' measured in the direction of the K_3 axis as functions of entropy. The alternating field has an amplitude of 0.05 Oe and a frequency of 225 Hz.

□ χ_0 ○ χ' △ χ''

No remanences have been observed in the three directions in which the susceptibility measurements were performed, using a measuring field of 1 oersted. By means of the relaxation heating method temperature determinations were carried out. As thermometric parameters the values of χ' in the K_3 direction in primary fields of 0.05 and 0.7 Oe were used. The amount of heat supplied was determined from the measured values of χ''. Using the field of 0.7 Oe amplitude for heating the sample, the heat supply was of the order of 1000 erg/s. The amplitude of the field

was chosen large enough that the χ'' *versus* S curve did not show a maximum (see section 3). Thus χ'' decreases with rising temperature which keeps the temperature distribution in the salt more homogeneous. After a heating period of 100 seconds the field was reduced to 0.05 Oe and χ' was measured. Three such heating periods were performed after each demagnetization. The average temperature in one heating period could be calculated using the value of ΔS derived from the 0.05 Oe measurements. From the values of $d\chi'/dt$ measured during a heating period absolute temperatures have also been derived with the aid of the relation $T = (dQ/dt)/(dS/d\chi')\,(d\chi'/dt)$. The results are given in fig. 4.4 and in table IV, III. They can be compared with the relation between entropy and absolute temperature obtained by Cooke, which was obtained using γ-ray heating at entropies above S_N (solid line in fig. 4.4). The agreement is good and connecting our experimental curve with that of Cooke, a value of 0.14° K for T_N is found. Measurements of Steenland *e.a.* gave temperatures of the same order of magnitude but their measurements may have been less accurate, since in powdered crystals the relaxation

TABLE IV, III

Relation between entropy and absolute temperature in $MnNH_4$-tutton salt

S/R	1.1	1.0	0.9	0.8	0.7	0.6	0.5	0.4
T(°K)	0.124	0.117	0.109	0.102	0.093	0.086	0.080	0.074

Fig. 4.4 $MnNH_4$-tutton salt. The relation between absolute temperature and entropy. The solid line in the high entropy region has been derived from measurements of Cooke. The χ' *versus* S relations with two different field amplitudes h_0 are used as a thermometer.

○ $h_0 = 0.05$ Oe △ $h_0 = 0.7$ Oe

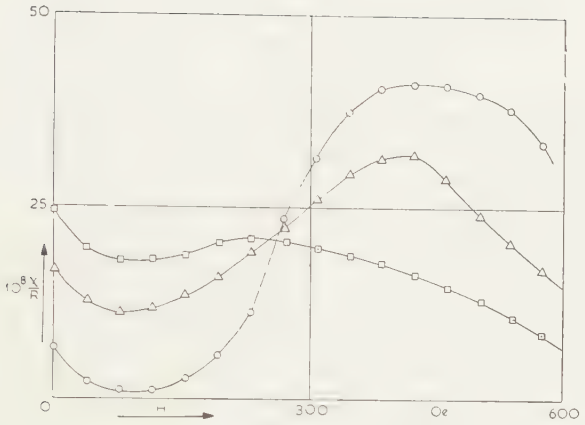

Fig. 4.5 $MnNH_4$-tutton salt. The susceptibility in the K_1 direction as a function of a longitudinal field.

○ $S = 0.29\ R$ △ $S = 0.83\ R$ □ $S = 1.16\ R$

heating is very inhomogeneous due to the different orientations of the K_3 axes of the crystals with respect to the a.c. field.

The susceptibilities in the K_1 and K_3 directions have been measured adiabatically as functions of a longitudinal field and at several values of the entropy below S_N. For the K_1 directions and for three values of the entropy it is seen in fig. 4.5 that the susceptibility, as measured with the a.c. bridge, decreases slightly at first and reaches a minimum in fields of about 100 Oe. Upon increasing the field strength still further, the susceptibility shows a pronounced increase (for $S = 0.29\ R$ it increases by a factor of 40 with respect to the minimum value) and reaches a maximum for field values which vary from 250 Oe for $S = 1.16\ R$ to 460 Oe for $S = 0.29\ R$. The susceptibility curves show an antiferromagnetic character, the strong increase in fields of a few hundred oersted probably being due to the transition from the antiferromagnetic into the paramagnetic state. In the same way as described by GARRETT [2] for $CoNH_4$-tutton salt the changes in temperature produced on isentropic magnetization have been derived for $MnNH_4$-tutton salt. From the $\chi_{\|}$ *versus* H curves the adiabatic magnetization curves were deduced by graphical integration. Using the formula $\Delta T = -{}_0\int^H (\partial M/\partial S)_H \mathrm{d}H$ the temperature during isentropic magnetization has been calculated. The temperature reaches a minimum at a certain field strength and thereafter rises again. It will be assumed here, which may not be strictly correct, that the locus of the minima of the T *versus* H curves (fig. 4.6) corresponds to the boundary of the antiferromagnetic region. The dashed line connects these minima and the extrapolated value at zero temperature gives 540 Oe for the critical field in the K_1 direction. The K_3 susceptibility was measured ballistically. It can be seen in fig. 4.7 that the magnetic behaviour in this direction is very different from that in the K_1 direction. The

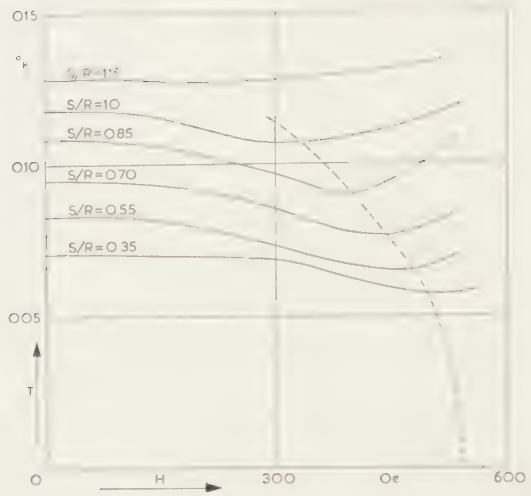

Fig. 4.6 The temperature variation during isentropic magnetization in antiferromagnetic $MnNH_4$-tutton salt. The dashed line represents the boundary of the magnetically ordered region.

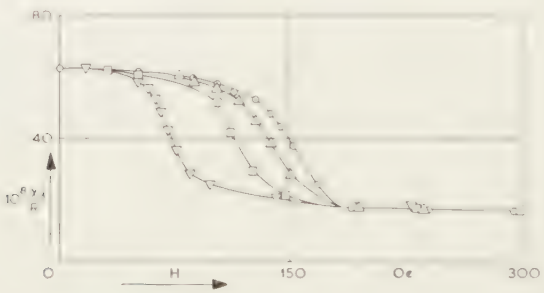

Fig. 4.7 $MnNH_4$-tutton salt. The susceptibility in the K_3 direction as a function of a longitudinal field.

○ $S = 0.29\ R$ □ $S = 0.83\ R$
△ $S = 0.57\ R$ ▽ $S = 1.07\ R$

susceptibility retains the very high value which it had at zero field up to fields which vary from 50 Oe for $S = 1.07\ R$ to about 100 Oe for $S = 0.29\ R$. At higher field values the susceptibility drops to about 30 % of its initial value and becomes nearly independent of the magnetic field.

The χ_3 *versus* H curves show a ferromagnetic character. The values of 3π per cm^3 for the susceptibilities correspond to an infinite value if reduced to an infinitely long cylinder. The susceptibility of 1 N means, in fact, that the χ value of the $MnNH_4$ tutton salt crystal was equal to the susceptibility of the Armco iron sample of the same shape and volume which was used when determining the approximate demagnetizing factor.

In order to derive a value for the ferromagnetic moment from the isentropic magnetization measurements, the experimental M values are

plotted *versus* $H-(4\pi/3)M_v$ in fig. 4.8 (M_v represents the magnetization moment per cm^3). The values of the apparently ferromagnetic saturation moment, M_{fe}, are found at each entropy by extrapolating the linear parts of the magnetization curves to $H-(4\pi/3)M_v=0$. M_{fe} increases with decreasing temperature as can be seen from fig. 4.9. The value of the ferromagnetic saturation moment at complete ordering of the spins is found by extrapolating the curve to $T \ll T_N$. This magnetization is given in table IV, IV together with the values of T_N, S_N and the

TABLE IV, IV

Comparison of the experimental results obtained with single crystals of $CoNH_4$- and $MnNH_4$-tutton salt

	T_N (°K)	$\frac{S_N}{R}$	$\frac{M_{fe}}{R} \times 10^6$	H_{cr} (Oe)	θ_M (degree)
$CoNH_4$	0.084	0.43	85	400	10
$MnNH_4$	0.14	1.25	94	540	16

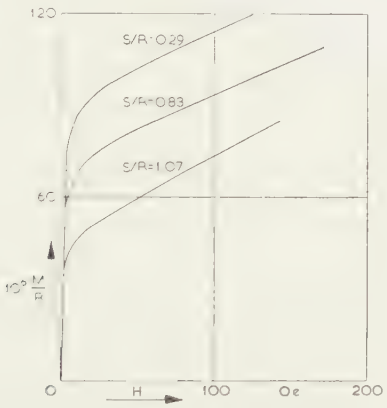

Fig. 4.8 $MnNH_4$-tutton salt. Isentropic magnetization curves for a field in the K_3 direction. The external fields have been corrected with $H = H_e - (4\pi/3)M_v$.

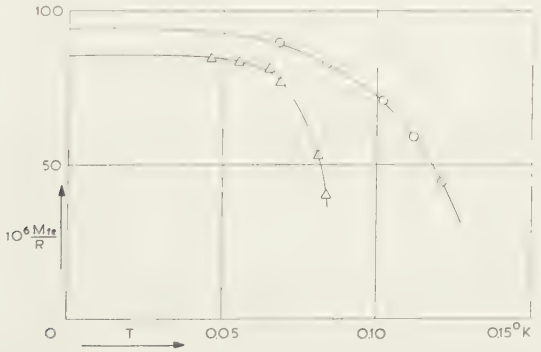

Fig. 4.9 The experimental values of the ferromagnetic saturation moment, M_{fe}, plotted *versus* temperature.

○ $MnNH_4$-tutton salt △ $CoNH_4$-tutton salt

critical field in the K_1 direction. The extrapolated value of M_{fe} equals 31 % of the total saturation moment, the latter being calculated with $S = 5/2$ and $g = 2$.

2. *Cobalt ammonium tutton salt*

A single crystal of $CoNH_4$ tutton salt has been already investigated by GARRETT [2] who measured pronounced anisotropies in the zero field susceptibilities. The K_1 susceptibility, which is the highest in the liquid helium temperature range, shows a pronounced maximum as a function of entropy. At the entropy corresponding to this maximum the K_3 susceptibility increases sharply and reaches a value of about $3/4\pi$ per cm^3. Garrett also determined the relation between entropy and temperature and derived a value of 400 Oe for the critical field in the K_1 direction.

New experiments on a $CoNH_4$-tutton salt crystal were performed in order to make a complete comparison between $CoNH_4$ and $MnNH_4$ tutton salt possible. The ballistic measurements showed a constant susceptibility equal to $3/4\pi$ per cm^3 within the experimental accuracy (2 %) in the K_3 direction at entropies below S_N. The maximum in the χ_3 versus S curve reported by Garrett, apparently is due to the fact that χ_3 was measured with a 40 Hz a.c. field (see section 3).

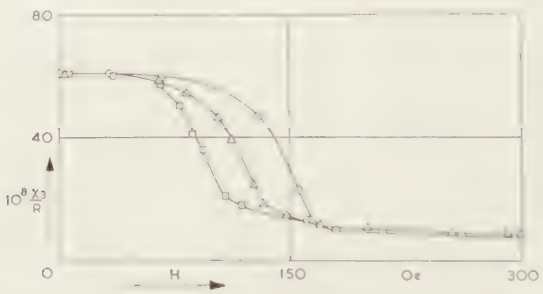

Fig. 4.10 $CoNH_4$-tutton salt. The K_3 susceptibility as a function of a longitudinal field.

○ $S = 0.050\ R$ △ $S = 0.262\ R$ □ $S = 0.365\ R$

Fig. 4.10 shows the susceptibility as a function of a longitudinal field in the K_3 direction. The χ_3 *versus* H curves show the same character as the corresponding curves for the manganese salt. The susceptibility remains nearly constant at its large χ_0 value in small fields and decreases sharply at a field the value of which is largest at the lowest entropy. In fields larger than 150 Oe χ_3 becomes nearly constant again at a value of $10 \times 10^{-8}\ R$. In the same way as described for $MnNH_4$-tutton salt values of the apparently ferromagnetic saturation magnetization have been derived at several entropies. M_{fe} increases with decreasing temperature as may be seen in fig. 4.9. The value of M_{fe} at complete ordering of the spins is given in table IV. IV. It equals 65 % of the saturation magnetization calculated with $g_3 = 4.40$ and $S = 1/2$.

3. *Absorption and dispersion measurements*

The large specific heats of $MnNH_4$- and $CoNH_4$-tutton salt below their Néel temperatures gave the opportunity of observing the relaxation effects occurring in the K_3 direction at nearly constant temperatures. Using a primary field amplitude of 0.05 Oe and frequencies between 3 and 1100 Hz [1]) the relaxation curves were measured at four values of the entropy. Fig. 4.11 shows the results for $MnNH_4$-tutton salt. The scale factor of χ'' is twice that for χ'. The measured χ'' values show a maximum within the range of applied frequencies for three of the entropies. From the shape of the curves, which is not a Debye shape, it may be seen that a well defined single relaxation time does not describe

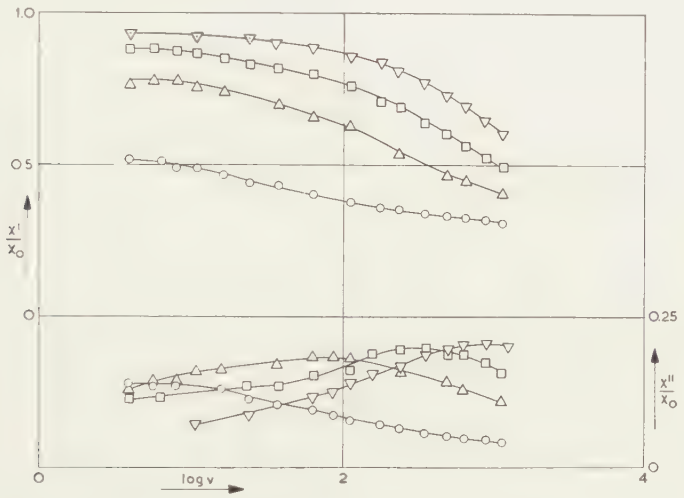

Fig. 4.11 $MnNH_4$-tutton salt. Dispersion and absorption curves measured with a primary field amplitude of 0.05 Oe.

○ $S = 0.29\ R$ □ $S = 0.83\ R$
△ $S = 0.66\ R$ ▽ $S = 0.95\ R$

the phenomena satisfactorily, but an average value, τ_{av}, may be derived. The values of τ_{av} at entropies of 0.95 R, 0.83 R, 0.66 R and 0.29 R are 0.2, 0.5, 2, and about 60 millisecond, respectively. The character of the relations between the entropy and both χ' and χ'' measured for 225 Hz (fig. 4.3) are in agreement with these measurements, as the former may be considered as a dispersion and absorption curve measured at constant frequency with varying relaxation time. The relaxation time values proved to be strongly dependent on the amplitude of the measuring field (fig. 4.12). With increasing amplitude the relaxation time becomes shorter and the maximum in the χ'' *versus* log ν curve becomes higher, which indicates that the distribution of the relaxation times becomes narrower.

[1]) The Hartshorn bridge is the one used by Van der Marel and Van den Broek in paramagnetic relaxation experiments. The cooperation of Mr J. v. d. Broek during these experiments is gratefully acknowledged.

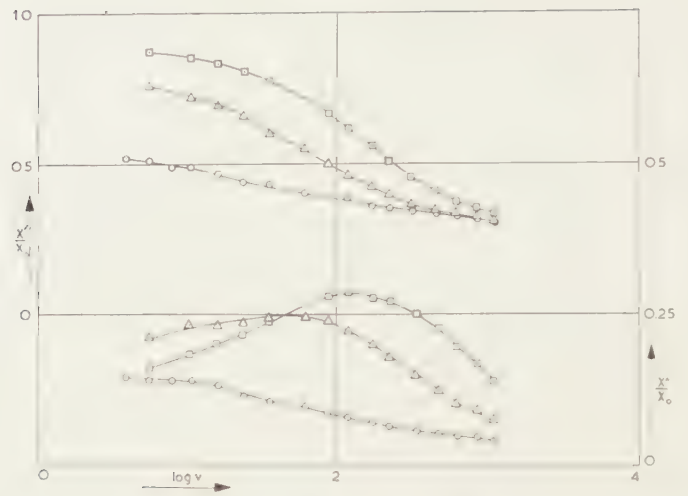

Fig. 4.12 $MnNH_4$-tutton salt. Dispersion and absorption curves measured at $S = 0.29\,R$ with several amplitudes of the primary field.

○ $h_0 = 0.05$ Oe △ $h_0 = 0.125$ Oe □ $h_0 = 0.25$ Oe

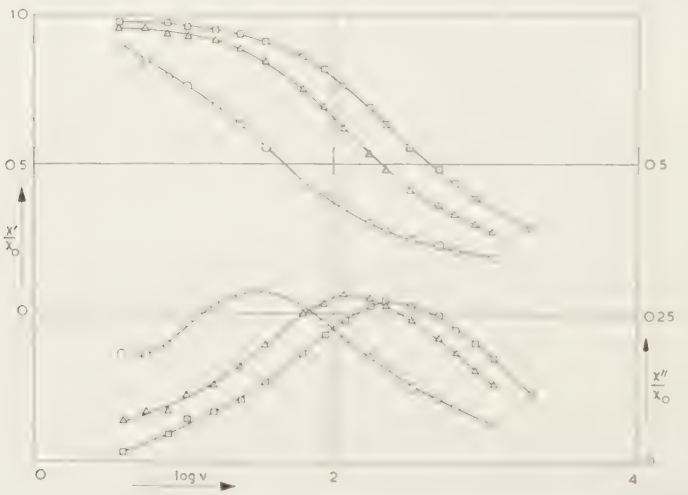

Fig. 4.13 $CoNH_4$-tutton salt. Dispersion and absorption curves measured with a primary field amplitude of 0.05 Oe.

○ $S = 0.01\,R$ △ $S = 0.20\,R$ □ $S = 0.26\,R$

The derived values of τ_{av} at $S = 0.29\,R$ are 60, 4 and 1.2 millisecond for a field amplitude of 0.05, 0.125 and 0.25 Oe, respectively. In fig. 4.12 it may be seen that at the high frequency side χ' approaches a constant value which corresponds to $\chi'/\chi_0 \approx 0.30$.

The absorption and dispersion for $CoNH_4$-tutton salt have been measured at three entropies using a measuring field amplitude of 0.05 Oe. The maxima in the χ'' *versus* log ν curves are more pronounced (fig. 4.13)

than in the case of manganese and the relaxation times are better defined. From fig. 4.13 we derive $\tau_{av} = 4$, 1.3 and 0.6 millisecond for $S = 0.01\ R$, $0.19\ R$ and $0.25\ R$, respectively. At the lowest attainable entropy τ_{av} has been measured for three values of the measuring field amplitude, (0.05 Oe, 0.10 Oe and 0.24 Oe) giving for τ_{av} 4.0, 3.0, and 1.5 millisecond, respectively (fig. 4.14).

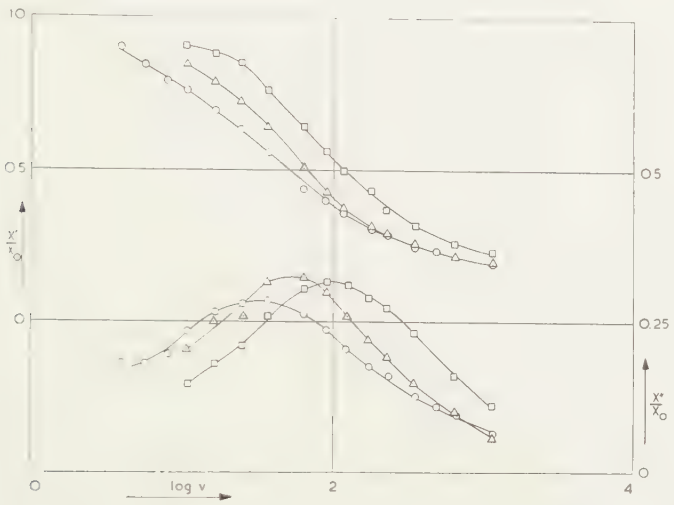

Fig. 4.14 $CoNH_4$-tutton salt. Dispersion and absorption curves measured at $S = 0.01\ R$ with several amplitudes of the primary field.
○ $h_0 = 0.05$ Oe △ $h_0 = 0.10$ Oe □ $h_0 = 0.25$ Oe

From fig. 4.13 and 4.14 it may be seen that χ' tends to approach the same constant value of χ'/χ_0 which is nearly equal to 0.15 for all measured curves at the high frequency side.

At an entropy of $0.19\ R$ the influence of a magnetic field on the value of τ_{av} has been studied. In small fields the values of τ_{av} were independent of the field within the measuring accuracy. At the field value where the ballistic susceptibility (fig. 4.10) drops, the relaxation effects vanish. The absorption and dispersion measurements for $CoNH_4$-tutton salt are satisfactorily described by one rather well defined relaxation time. For the manganese salt the absorption maximum is less pronounced and a broad interval of relaxation times seems to be present. The χ'/χ_0 value does not approach $\chi'/\chi_0 = 1$ at low frequences. Combined with the dependence of the relaxation curves on the amplitude of the alternating field this suggests that some kind of a coercive field may be present. Such a coercive field would be of the order of a few hundredths of an oersted and therefore there is no disagreement with the absence of a remanence, measured ballistically with a measuring field of 1 Oe. Steenland *e.a.* [5] reported a small remanence of 0.10 ± 0.05 gauss cm^3/mole, whereas Kurti [6] measured much higher values on a powdered sample of $MnNH_4$-tutton salt.

The differential susceptibility in a magnetic field, in which the ferromagnetic saturation is reached, and the zero field susceptibility in alternating fields of about 1000 Hz are nearly equal for both salts. This suggests that the susceptibility in a longitudinal field in the K_3 direction can be divided into two parts, a ferromagnetic part where the spin system shows long relaxation times and a quasi-paramagnetic part, where the relaxation effects have disappeared.

4. *Copper ammonium tutton salt*

Copper ammonium sulphate hexahydrate has been investigated at temperatures down to 0.05° K by Cooke *e.a.* [7]. The deviations from Curie's law were measured and found to be described by $\theta = 0.010°$ K.

In the present investigation the adiabatic susceptibility has been measured in the directions of the three magnetic axes as a function of entropy in zero field and as a function of a longitudinal field at several entropies.

The measurements in zero field (fig. 4.15) were performed with an alternating field of 225 Hz and 0.1 Oe, the differences from the ballistically measured susceptibility being negligible. The curves show a maximum for two magnetic axes (K_1, K_3) whereas the K_2 susceptibility tends to approach a constant value at low entropies. The susceptibility maxima occur at entropies of 0.42 R and 0.36 R for the K_1 and the K_3 curve, respectively. The K_1 susceptibility, which is largest at high entropies due to the fact that for this direction the g factor has the largest value, becomes the smallest of the three susceptibilities at low entropies.

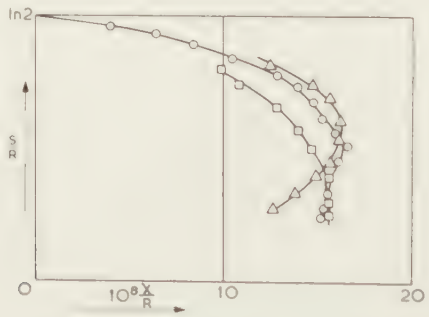

Fig. 4.15 $CuNH_4$-tutton salt. The relation between susceptibility and entropy.
△ K_1 direction □ K_2 direction ○ K_3 direction

χ'' was smaller than $1 \cdot 10^{-9}$ R for all three measuring directions. The dependence of the adiabatically measured susceptibility on a longitudinal field can be seen in fig. 4.16 for the lowest entropy, $S = 0.2$ R. The curves show a pronounced maximum in two cases (K_1, K_3) in fields of about 150 Oe, the increase of the susceptibility being more than a factor two for the K_1 curve. The K_2 curve shows an increase of only 7 % in the

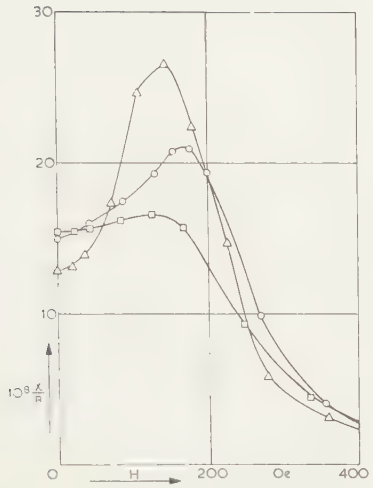

Fig. 4.16 $CuNH_4$-tutton salt. The adiabatic susceptibility as a function of a longitudinal magnetic field at $S = 0.2\ R$.

△ K_1 direction □ K_2 direction ○ K_3 direction

same region. The susceptibility decreases sharply at fields between 150 and 180 Oe for all three directions.

Fig. 4.17 gives the dependence on entropy of the susceptibility in a longitudinal field for the K_1 direction. The maximum in the $\chi_{||}$ *versus* H curve becomes less pronounced at higher entropies but it is still present at an entropy of 0.38 R. The results obtained with $CuNH_4$-tutton salt suggest the occurrence of antiferromagnetism. Maxima in the χ *versus* S

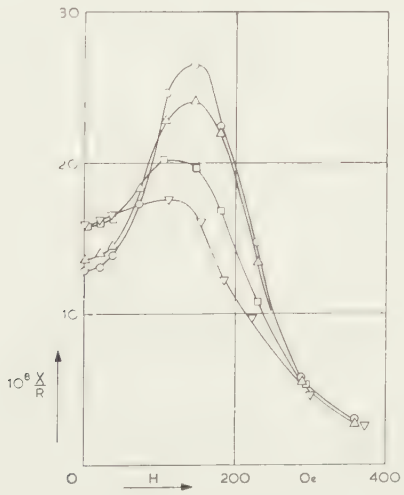

Fig. 4.17 $CuNH_4$-tutton salt. The K_1 susceptibility as a function of a longitudinal field for several entropies.

○ $S = 0.19\ R$ □ $S = 0.32\ R$

△ $S = 0.24\ R$ ▽ $S = 0.38\ R$

and the χ *versus* H curves have been found for two magnetic axes K_1 and K_3. This may be explained if the antiferromagnetic ordering takes place in the K_1K_3 plane, while the alignment direction(s) do not coincide with one of the magnetic axes.

5. *Copper potassium tutton salt*

Previous demagnetization experiments with powdered crystals of copper potassium sulphate hexahydrate were performed by GARRETT [8] and by STEENLAND *e.a.* [9], [5]. The zero field susceptibility showed a maximum as a function of entropy. At entropies above this maximum Garrett derived the absolute temperature *versus* entropy relation from his magnetic data. He gives a value of 0.034° K for the Curie-Weiss constant, the sign being positive. Steenland *e.a.* evaluated the T *versus* S relation in the entropy region below the susceptibility maximum. The temperature of the Curie point was found to be about 0.04° K.

The present investigation of a single crystal has been performed in the directions of the 3 magnetic axes. From fig. 4.18 it can be seen that the zero field susceptibility, measured with an alternating field of 225 Hz and 0.1 Oe, has a maximum for the K_1 and K_3 directions. Its values are much larger than those found for the $CuNH_4$-salt, the χ scale of fig. 4.15 being two times larger. The K_2 susceptibility becomes nearly constant at entropies below 0.4 R at a value which differs not more than 5 % from 3'47 per cm^3. The anisotropy of the susceptibility at low entropies differs completely from the one in the high entropy region where the K_1 susceptibility is largest, corresponding to the large g value in that direction.

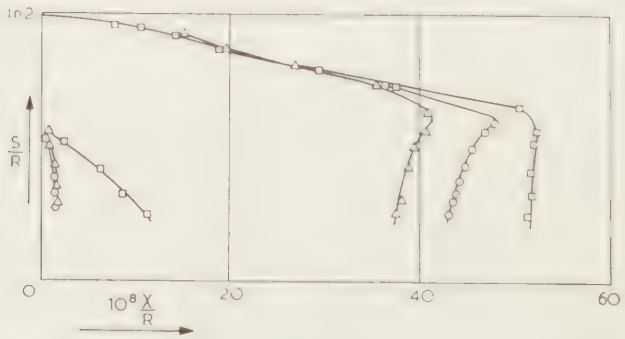

Fig. 4.18 CuK-tutton salt. The relation between susceptibility and entropy.
△ K_1 direction □ K_2 direction ○ K_3 direction

χ'' is measurably large below $S = 0.4$ R. Its values are considerably smaller than those found in the $CoNH_4$ and $MnNH_4$-tutton salts, χ'' being plotted on a tenfold scale in fig. 4.18. The values of χ'' in the K_2 direction are higher than those found in the other two directions. In agreement with the small values of χ'' present in CuK-tutton salt the ballistically measured susceptibility differs only slightly from the χ' values given in fig. 4.18 (≤ 2 %).

In small longitudinal fields the susceptibility keeps its high value but it decreases sharply to a few percent of its initial value in fields of about 100 Oe. The curves obtained at $S = 0.2\ R$ are shown in fig. 4.19. At higher entropies, but below $S = 0.35\ R$, the behaviour remains the same, the steep fall of the susceptibility occurring in lower magnetic fields. The remarkable fact that in small fields the highest susceptibility is reached

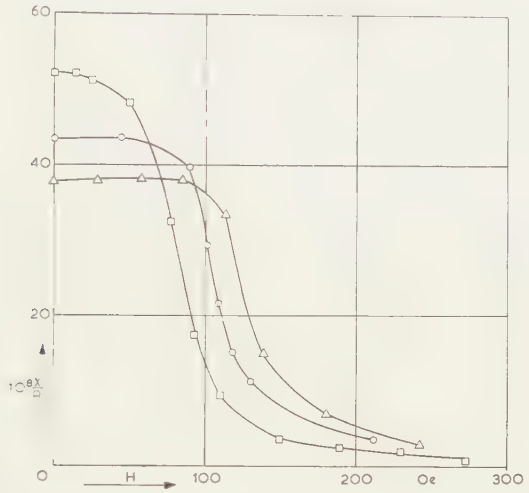

Fig. 4.19 CuK-tutton salt. The susceptibility as a function of a longitudinal field at $S = 0.2\ R$.

△ K_1 direction □ K_2 direction ○ K_3 direction

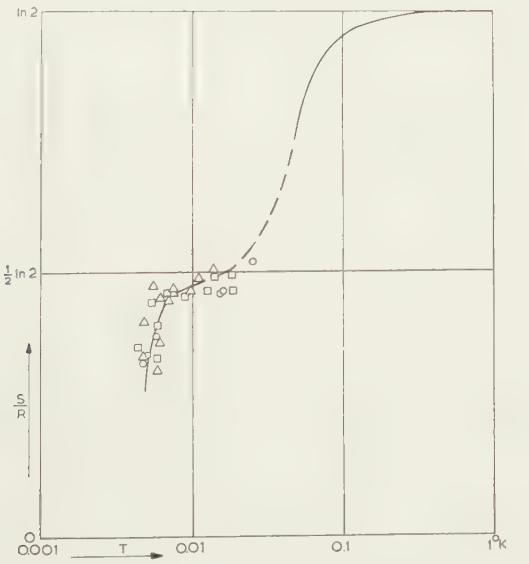

Fig. 4.20 CuK-tutton salt. The relation between absolute temperature and entropy. The solid line, given in the high temperature region, is derived from data of Garrett.

○ Steenland *e.a.* △ χ' thermometer □ χ'' thermometer

in the direction with the smallest g value can be checked easily. It is possible to derive the magnetization as a function of the magnetic field by graphical integration of the curves in fig. 4.19. In agreement with the anisotropy of the g values the magnetization in a field of 250 Oe is largest in the K_1 direction and smallest in the K_2 direction.

Using the χ'' heating method, absolute temperatures have been derived. Both χ' and χ'', measured in the K_3 direction, were used as thermometers. The alternating field had an amplitude of 0.5 Oe which supplied heat to the sample of the order of 10 erg/s. The results can be seen in fig. 4.20, experimental points of Steenland *c.a.* being also given. The solid line drawn in the high temperature region represents data of Garrett. When connecting the two experimental curves a pronounced minimum of the specific heat is found at $S = 0.34\ R$, two maxima for the specific heat occurring near 0.05 and 0.007° K.

The magnetic behaviour of CuK tutton salt seems to be ferromagnetic in the K_2 direction. The value of the ferromagnetic saturation moment obtained by extrapolation to $T = 0$ differs less than 8 % from the total saturation moment, calculated with $g = 2.04$ and $S = {}^1/_2$.

(To be continued)

REFERENCES

1. Hoffmann, W., Z. Kristallogr. **78**, 279 (1931).
2. Garrett, C. G. B., Proc. Roy. Soc. **A 206**, 242 (1951).
3. Huiskamp, W. J., A. N. Diddens, J. C. Severiens, A. R. Miedema and M. J. Steenland, Commun. Kamerlingh Onnes Lab., Leiden 308b; Physica **23**, 605 (1957).
4. Cooke, A. H., Proc. Phys. Soc. (London) **A 62**, 269 (1949).
5. Steenland, M. J., L. C. van der Marel, D. de Klerk and C. J. Gorter, Commun. 279c; Physica **15**, 906 (1949).
6. Kurti, N., Proc. Int. Conf. Low Temp. Phys. M.I.T. 59 (1949).
7. Cooke, A. H., H. Meyer and W. P. Wolf, Proc. Roy. Soc. **A 233**, 536 (1956).
8. Garrett, C. G. B., Proc. Roy. Soc. **A 203**, 375 (1950).
9. Steenland, M. J., D. de Klerk, J. A. Beun and C. J. Gorter, Commun. 284d; Physica **17**, 161 (1951).
10. Bleaney, B., R. P. Penrose and B. I. Plumpton, Proc. Roy. Soc. **A 198**, 406 (1949).
11. Broek, J. van den, L. C. van der Marel and C. J. Gorter, Commun. 314c; Physica **25**, 371 (1959).
12. Bleaney, B. and D. J. E. Ingram, Proc. Roy. Soc. **A 205**, 336 (1951).

THEORY OF RELAXATION PHENOMENA IN A MONATOMIC GAS. I

BY

M. J. OFFERHAUS

(Communicated by Prof. J. DE BOER at the meeting of October 29, 1960)

1. *Introduction and survey* [1])

In this paper we are going to describe some aspects of the development of the state of a gas consisting of identical, spherically symmetric molecules, starting from a completely arbitrary initial state. One can distinguish between the three stages defined by BOGOLUBOV [1]:

I. The stage of *initial mixing*, taking about the time *of* a collision, i.e. the average time during which two colliding molecules are in each other's field of force:

$$t_{\mathrm{I}} \approx \sigma/v \tag{1.1a}$$

(σ = diameter of a molecule; $v = (kT/m)^{\frac{1}{2}} \approx$ mean thermal velocity of the molecules; $\approx$ means: of the order of magnitude of, or: approximately equal to).

II. When stage I has finished, the development of the gas is henceforth described by the velocity-space-distribution function for a single particle, $f(\mathbf{c}; \mathbf{r}, t)$, which, under certain conditions, changes according to the Boltzmann equation (BE). This is called the *kinetic stage*, which is of a duration of the average time *between* successive collisions of the same molecule:

$$t_{\mathrm{II}} \approx l/v \tag{1.1b}$$

(l = mean free path).

III. After stage II, the maximum of information on the gas is contained in the first five moments (*i.e.* $\mathbf{c}$-integrals) of f : ϱ (mass density), $\mathbf{c}_0$("mass-averaged" velocity) and T (temperature), which are functions of $\mathbf{r}$ and t; together we call them $\psi^{[\lambda]}(\mathbf{r}, t)$ ($\lambda = 1, \mathbf{2}, 3$). The changes in t of these ψ are given by the hydrodynamical equations (HDE). These, however, are not self-sufficient, like the BE; in order to solve them,

---

[1]) *Some abbreviations used throughout parts I–IV:*

BE Boltzmann equation; HDE hydrodynamical equations; HD hydrodynamical; MB Maxwell–Boltzmann; ChE Chapman–Enskog; LHS left hand side; RHS right hand side; $\approx$ of the order-of-magnitude of, or: approximately equal to.

Lists of symbols and references are added to part IV.

one has to watch the distribution function f, which by now has become a special solution of the BE closely linked with the moments ψ. This is the *hydrodynamical (HD) stage*, of a duration

$$t_{III} \gtrsim d/v \tag{1.1c}$$

(d = dimension of the vessel). In the absence of external forces, the HD stage ends in the equilibrium distribution of Maxwell-Boltzmann (MB).

In a gas of moderate density, $\sigma \ll l \ll d$: the 3 stages will be well separated.

It is evident that even a schematic description of stage I meets with great difficulties, and it will not concern us here. If, at the beginning of stage II, the BE for the single-particle distribution is valid – we shall not dwell on the arguments and restrictive conditions for its validity – this provides a starting point for a treatment of stages II as well as III. It appears, however, that what is called the kinetic theory of gases mostly concentrates on stage III and on the special solution of the BE, valid in this stage, developed by CHAPMAN and ENSKOG (ChE solution; see, *e.g.* [2], *passim*; [3], chs. 7 and 8; [4]).

Ch. 2: Now this paper will try to give a description of the kinetic stage II, during which many connections between stages II and III will become apparent. This is why we shall first give a survey of some important features of the ChE solution of the BE.

Ch. 3: If, at the beginning of the kinetic stage, the distribution is independent of $\mathbf{r}$: $f = f(\mathbf{c}; t)$, the kinetic process II leads straight to the equilibrium (MB) distribution $f^{(0)}$, and the HD stage III is cut short. This special process, to be numbered IIA, first came up for discussion in connection with Boltzmann's H-theorem. A solution for the *linearized* case, valid when $f(\mathbf{c}; t=0) - f^{(0)}$ is small, was given by WALDMANN ([4], p. 367); the essential features of stage IIA for *arbitrary* initial f were demonstrated by KAC [5], who incidentally used a simplified one-dimensional model of the collision mechanism. We shall present a detailed treatment of this spatially uniform process; the deviation $f - f^{(0)}$ is subject to a decay of exponential type; this is a typical *relaxation* process.

Ch. 4: The special role played by the MB distribution $f^{(0)}$ in the spatially uniform kinetic process is, in a non-uniform gas, taken over by the normal ChE distribution, f^{Ch}; again $f - f^{Ch}$ dies out by relaxation. This process, to which, as far as we know, little reference has been made in literature previously, constitutes the general behaviour of a gas during the kinetic stage II.

The general solutions of the BE for stage II, suggested in chs. 3 and 4, have in common with the normal ChE solution for stage III, that for the distribution function series expansions are given, of which only the first few terms are elaborated, whereas the general character of the left out terms can be made plausible.

Ch. 5: Next the local production of entropy during the kinetic stage

is discussed, for both the uniform and the non-uniform kinetic processes, as well as that of the HD stage. As far as possible, connections have been established with the terminology of the thermodynamics of irreversible processes.

Ch. 6: During stage II, there is a development of the transport quantities (HD pressure tensor and heat current vector) towards the HD values of stage III. Collisions try to break down this transport continually throughout stages II and III. This phenomenon, for which we suggest the term *quasi-relaxation*, was first mentioned, though with an interpretation we do not share, by KOHLER [6].

Ch. 7: The relaxation processes constituting the kinetic stage (chs. 3 and 4), as well as the quasi-relaxation of the transport currents (ch. 6) are characterized by relaxation times which are inverse eigenvalues of the so-called linearized collision operator Ω. WALDMANN ([4], p. 366 sqq.) as well as WANG CHANG and UHLENBECK [7] have given the complete eigenvalue theory of this Ω for the special case of a gas with Maxwellian intermolecular potential (r^{-4}-repulsion), as well as some properties of Ω for a gas with general, spherically symmetric force law. Accordingly, we shall present a qualitative evaluation of the various relaxation processes for the Maxwell gas, followed by an approximative treatment for a non-Maxwell intermolecular potential. The main relaxation times of stage II, which are of the order of the time between collisions, also play the role of coefficients in the standard expression for the ChE distribution function of stage III, thus providing one more link between stages II and III.

Ch. 8: Finally, in order to make the kinetic stage stand out against the following HD stage, we sum up the time scales for the duration of the various HD processes. As stated in (1.1c), the fastest of these takes a time d/v in comparison to the time l/v needed for the kinetic stage.

2. *Velocity distribution in the hydrodynamical stage*

We shall first recall some important features of the ChE method for solving the BE (see ch. 1 for references). This equation, which gives the time derivative of the molecular distribution function $f(\mathbf{c}\,;\,\mathbf{r}, t)$ in a one-component dilute gas, reads as follows:

$$\partial_t f = -\mathbf{c}\cdot\frac{\partial f}{\partial \mathbf{r}} - \mathbf{F}\cdot\frac{\partial f}{\partial \mathbf{c}} + J(ff_1) \equiv \partial_S f + \partial_C f. \tag{2.1}$$

The first two terms of the right hand side (RHS) represent changes in f due to streaming and to the influence of an external force (per mass unit) $\mathbf{F}$:

$$\partial_S f \overset{\text{def}}{=\!=} -\mathbf{c}\cdot\frac{\partial f}{\partial \mathbf{r}} - \mathbf{F}\cdot\frac{\partial f}{\partial \mathbf{c}}; \tag{2.2}$$

the third one accounts for collisions:

$$\partial_C f \overset{\text{def}}{=\!=} J(ff_1) \equiv \int d\varepsilon \int d\chi \sin\chi \int d\mathbf{c}_1 \alpha(|\mathbf{c}-\mathbf{c}_1|, \chi)\cdot\{f(\mathbf{c}')f(\mathbf{c}_1') - f(\mathbf{c})f(\mathbf{c}_1)\}. \tag{2.3}$$

Integrations are over the azimuth ε, over the angle of deflection χ and over the velocity $\mathbf{c}_1$ of a particle colliding with one of velocity $\mathbf{c}$. $\mathbf{c}'$ and $\mathbf{c}_1'$ denote velocities-after-collision of two particles with initial $\mathbf{c}$, $\mathbf{c}_1$; they depend on χ, ε as well as on $\mathbf{c}$, $\mathbf{c}_1$. The differential cross-section α depends on the absolute velocity of relative motion, $g = |\mathbf{c} - \mathbf{c}_1|$ and on χ; the functional relation $\alpha(g, \chi)$ is the point where the intermolecular potential V enters. This is supposed to have spherical symmetry: $V = V(r)$, r being the distance between the centres of two molecules. The α-notation, originally used in the quantum-mechanical theory, equally applies in a classical treatment. Most of our discussions will not distinguish between the two.

There are 5 independent collision-invariant functions of $\mathbf{c}$, characterized by the property

$$\chi(\mathbf{c}) + \chi(\mathbf{c}_1) = \chi(\mathbf{c}') + \chi(\mathbf{c}_1'). \tag{2.4}$$

Obviously (2.4) is satisfied by the following χ, indicated by a superscript $[0\lambda]$:

$$\chi^{[01]} = m\,;\ \boldsymbol{\chi}^{[02]} = m\,\mathbf{c}\,;\ \chi^{[03]} = \tfrac{1}{2}mc^2. \tag{2.5}$$

Integration with f yields the following moments of f :

$$\psi^{[\lambda]} = \int d\,\mathbf{c}\, f \chi^{[0\lambda]}, \tag{2.6}$$

of which $\psi^{[1]}$ represents the zero moment of f; $\boldsymbol{\psi}^{[2]}$ the first moment, and $\psi^{[3]}$, a contraction of the second. They can be expressed in terms of the 5 parameters: ϱ, $\mathbf{c}_0$ and T (see ch. 1), and reversely:

$$\varrho = \psi^{[1]};\quad \mathbf{c}_0 = \frac{\boldsymbol{\psi}^{[2]}}{\psi^{[1]}};\quad \frac{3}{2}\frac{kT}{m} = \frac{\psi^{[3]}}{\psi^{[1]}} - \frac{1}{2}\frac{\boldsymbol{\psi}^{[2]^2}}{\psi^{[1]^2}}. \tag{2.7}$$

$\frac{3}{2}kT/m$ is really the moment $\int d\,\mathbf{c}\, f \cdot \frac{1}{2}C^2$, and its use indicates that moments defined with the "peculiar" or relative velocity $\mathbf{C} = \mathbf{c} - \mathbf{c}_0$ are preferable over those containing $\mathbf{c}$.

In the following, the collective symbol ψ will denote either $\psi^{[\lambda]}$ ($\lambda = 1, \mathbf{2}, 3$) or ϱ, $\mathbf{c}_0$ and T.

Equations for the change of $\psi^{[\lambda]}$ in time are found by integrating $\chi^{[0\lambda]}$ times the BE (2.1) over $\mathbf{c}$:

$$\partial_t \psi^{[\lambda]} = \int d\,\mathbf{c}\, \chi^{[0\lambda]} \partial_S f \tag{2.8}$$

+ a collision term that vanishes:

$$\int d\,\mathbf{c}\, \chi^{[0\lambda]} J(f f_1) = 0 \qquad (\lambda = 1, \mathbf{2}, 3), \tag{2.9}$$

this being a property of the J operator and of the collisional invariants $\chi^{[0\lambda]}$ for all functions $f(\mathbf{c})$. The streaming contribution (2.8) contains an $\boldsymbol{F}$ term (cf. eq. 2.2) which is treated with partial integration; thus we get the hydrodynamical equations (HDE):

$$\partial_t \psi^{[\lambda]} = -V \cdot \boldsymbol{\psi}^{[\lambda]+} + \boldsymbol{F} \cdot \boldsymbol{\psi}^{[\lambda]-}, \qquad (\lambda = 1, \mathbf{2}, 3) \tag{2.10}$$

in which

(2.10a) $$\Psi^{[\lambda]+} \equiv \int d\mathbf{c}\, f \mathbf{c} \chi^{[0\lambda]}$$

and

(2.10b) $$\Psi^{[\lambda]-} \equiv \int d\mathbf{c}\, (\partial f/\partial \mathbf{c})\, \chi^{[0\lambda]}.$$

It appears that the t-derivative of a moment $\psi^{[\lambda]}$ is expressed in terms of the values and $\mathbf{r}$-derivatives of moments higher (Ψ^+) and lower (Ψ^-) than ψ itself. Among all moments $\psi^{[\lambda]\pm}$ we find the 5 $\psi^{[\lambda]}$ themselves, as well as the full second moment of f and a contraction of the third one; as in the case of $\psi^{[3]}$, we prefer a formulation in terms of moments containing $\mathbf{C}$, viz. the pressure tensor P and the heat current vector $\mathbf{q}$, of which the first is "made traceless" by subtracting $\frac{1}{3}\times$ the trace from the diagonal elements, which is indicated by the symbol $^\circ$; the remaining tensor is that of the HD pressure:

(2.11a, b) $$\overset{\circ}{\mathsf{P}} = \mathsf{P} - \frac{1}{3}\operatorname{tr} \mathsf{P} \equiv \int d\mathbf{c}\, fm \mathbf{C}\overset{\circ}{\mathbf{C}};\ \mathbf{q} \equiv \int d\mathbf{c}\, f \tfrac{1}{2} mC^2 \mathbf{C}.$$

The RHS, then, of the 5 eqs. (2.10) contain values and gradients of the ψ themselves and of $\overset{\circ}{\mathsf{P}}$ and $\mathbf{q}$. Both these higher moments enter linearly.

We turn first to the case of a gas without external forces, in which the initial distribution is *spatially uniform*. $f(\mathbf{c}; t)$ now follows from a simplified BE:

(2.12) $$\partial_t f = J(ff_1).$$

The first 5 moments $\psi^{[\lambda]}$ of f are, of course, uniform too; they are, moreover, constant in time, for, on account of (2.9), integration of $\chi^{[0\lambda]}$ times (2.12) simply results in

(2.13) $$\partial_t \psi^{[\lambda]} = 0.$$

Next we introduce the idea, characteristic of the ChE approach, that f shall depend on $\mathbf{r}$ and t through the 5 moments ψ:

(2.14) $$f(\mathbf{c}; \mathbf{r}, t) = f(\mathbf{c}; \psi(\mathbf{r}, t)),$$

meaning that, out of all possible f having the values of the 5 integrals $\psi^{[\lambda]}$ in common, our f is a special one which is known once the ψ are given. Now the ψ do not change in t, and f has to follow the changes in ψ which are none:

(2.15) $$\partial_t f = \sum_\lambda \frac{\partial f}{\partial \psi^{[\lambda]}}\, \partial_t \psi^{[\lambda]} = 0.$$

Thus, the f-ψ-relationship (2.14) necessarily implies equilibrium and f follows from (2.12), which yields:

(2.16) $$J(ff_1) = 0;\ f = f^{(0)},$$

the MB equilibrium distribution, containing the given values of ψ (*i.e.* ϱ, $\mathbf{c}_0$ and T) as parameters.

The *non-uniform* case (f depending on $\mathbf{r}$ as well) is, in the ChE scheme,

based on the wider hypothesis of a distribution function depending on $\boldsymbol{r}$ and t through the moments ψ and their $\boldsymbol{r}$-derivatives of various order, so that $f(\boldsymbol{r})$ is connected with the values of the ψ in a neighbourhood of $\boldsymbol{r}$. One can express this by writing f as a functional of ψ:

$$f^{\mathrm{Ch}}(\boldsymbol{c}; \boldsymbol{r}, t) = f^{\mathrm{Ch}}(\boldsymbol{c}|\psi(\boldsymbol{r}, t)). \tag{2.17}$$

Again, f has to follow the changes of ψ:

$$\partial_t f = \sum_\lambda \frac{\delta f}{\delta \psi^{[\lambda]}} \partial_t \psi^{[\lambda]}. \tag{2.18}$$

Here $\delta f/\delta\psi^{[\lambda]}$ is the functional derivative of f with respect to $\psi^{[\lambda]}$. In our case, one determines it by using the requirement that f has to be a function of the independent variables $\psi^{[\lambda]}$, $\partial\psi/\partial x$, ..., $\partial^2\psi/\partial x^2$, ..., for which we will use the collective symbol $\mathrm{D}_\alpha\psi^{[\lambda]}$ (D for differentiation, α a variable index); so

$$\partial_t f = \sum_\lambda \sum_\alpha \frac{\partial f}{\partial(\mathrm{D}_\alpha \psi^{[\lambda]})} \partial_t(\mathrm{D}_\alpha \psi^{[\lambda]}), \tag{2.19}$$

in which ∂_t and the $\boldsymbol{r}$-differentiation D_α may change place:

$$\partial_t f = \sum_\lambda \sum_\alpha \frac{\partial f}{\partial(\mathrm{D}_\alpha \psi^{[\lambda]})} \mathrm{D}_\alpha(\partial_t \psi^{[\lambda]}), \tag{2.20}$$

so that the functional derivative has the form of a differential operator in $\boldsymbol{r}$-space:

$$\frac{\delta f}{\delta \psi^{[\lambda]}} = \sum_\alpha \frac{\partial f}{\partial(\mathrm{D}_\alpha \psi^{[\lambda]})} \mathrm{D}_\alpha. \tag{2.21}$$

The second idea underlying the ChE theory is that of a series development of f:

$$f^{\mathrm{Ch}} = f^{(0)} + f^{(1)} + \ldots + f^{(n)}(1 + \phi^{(1)} + \phi^{(2)} + \ldots) + f^{(n)}(1 + \phi). \tag{2.22}$$

with terms $f^{(r)}$ normalized in such a way that, no matter where the series $\sum_r f^{(r)}$ is cut off, one obtaines the correct values $\psi(\boldsymbol{r})$ on which the method is based:

$$\psi^{[\lambda]\,(0)} = \psi^{[\lambda]}; \; \psi^{[\lambda]\,(1)} = \ldots = 0 \qquad (\psi^{[\lambda]\,(r)} \equiv \int d\boldsymbol{c} f^{(r)} \chi^{[0\lambda]}). \tag{2.23}$$

Unlike these ψ, higher moments do contain contributions from $f^{(r)}$ other than $f^{(0)}$; in fact, because $f^{(0)}$ will appear to be a local MB distribution, $\boldsymbol{q}$ and $\overset{\circ}{\mathsf{P}}$ are 0 when calculated on the base of $f^{(0)}$, the main contributions coming from $f^{(1)}$:

$$\boldsymbol{q}^{(0)} = 0; \; \overset{\circ}{\mathsf{P}}{}^{(0)} = 0. \tag{2.24}$$

Now let us see how the RHS of the HDE (2:8 or 10) for $\partial_t\psi$ read if we substitute the terms of the f series (2.22) one by one. We start with $f^{(0)}$; if the distribution did not consist of more than a local MB $f^{(0)}$, $\psi^{[\lambda]}$ would vary (cf. 2.8) according to:

$$\partial_t{}^{(0)}\psi^{[\lambda]} = \int d\boldsymbol{c} \chi^{[0\lambda]} \partial_{\mathrm{S}} f^{(0)}. \tag{2.25a}$$

The elaborated form of this RHS (see 2.10) would show the moments ψ, $\overset{\circ}{\mathsf{P}}$ and $\boldsymbol{q}$ based on $f^{(0)}$ alone, i.e., the exact $\psi^{[0]} = \psi$ but $\overset{\circ}{\mathsf{P}} = \boldsymbol{q} = 0$ (cf. 2:23, 24) (Euler equations). Now add $f^{(1)}$: the RHS of (2.8) are increased by

$$\partial_t{}^{(1)}\psi^{[\lambda]} = \int d\boldsymbol{c}\chi^{[0\lambda]}\partial_S f^{(1)}; \tag{2.25b}$$

in the formulation of (2.10), terms with $\overset{\circ}{\mathsf{P}}{}^{(1)}$ and $\boldsymbol{q}^{(1)}$ are added on the RHS (Navier-Stokes equations), and so on. Each new term $f^{(r)}$ gives an additive correction

$$\partial_t{}^{(r)}\psi^{[\lambda]} = \int d\boldsymbol{c}\chi^{[0\lambda]}\partial_S f^{(r)} \tag{2.25c}$$

on the Euler values $\partial_t{}^{(0)}\psi^{[\lambda]}$; in all,

$$\partial_t{}^{\mathrm{Ch}}\psi^{[\lambda]} = \sum_{s=0}^{\sim} \partial_t{}^{(s)}\psi^{[\lambda]} \tag{2.26}$$

and, consequently,

$$\partial_t f^{(r)} = \sum_{\lambda} \frac{\delta f^{(r)}}{\delta\psi^{[\lambda]}} \sum_{s} \partial_t{}^{(s)}\psi^{[\lambda]} = \sum_{s} \partial_t{}^{(s)} f^{(r)}, \tag{2.27}$$

if we define

$$\partial_t{}^{(s)}\, u(\boldsymbol{c}|\psi) \overset{\text{def}}{=} \sum_{\lambda} \frac{\delta u}{\delta\psi^{[\lambda]}} \partial_t{}^{(s)}\psi^{[\lambda]}. \tag{2.28}$$

Thus the series development (2.22) of a distribution function chosen to be a functional of ψ (2.17) leads to an analogous development (2.26) of the time derivative. Insert both series (2:22, 26) into the BE (2.1):

$$\sum_{r=0}^{\infty}\sum_{s=0}^{\infty} \partial_t{}^{(s)} f^{(r)} = \partial_S \sum_{r=0}^{\infty} f^{(r)} + \sum_{r=0}^{\infty}\sum_{s=0}^{\infty} J(f^{(r)} f_1{}^{(s)}). \tag{2.29}$$

This expression is divided into equations for separate determination of $f^{(0)}, f^{(1)}, \ldots$ by introducing a parameter θ as follows:

$$\sum_{r} f^{(r)} \to (1/\theta) f^{(0)} + f^{(1)} + \theta f^{(2)} + \ldots \tag{2.30a}$$

$$\sum_{s} \partial_t{}^{(s)} \to \partial_t{}^{(0)} + \theta\partial_t{}^{(1)} + \theta^2\partial_t{}^{(2)} + \ldots \tag{2.30b}$$

Introducing these series into (2.29) and putting terms containing equal powers of θ separately $= 0$, we get:

$$\begin{cases} [1/\theta^2] & 0 = J(f^{(0)} f_1{}^{(0)}) \\ [1/\theta] & \partial_t{}^{(0)} f^{(0)} = \partial_S f^{(1)} + J(f^{(0)} f_1{}^{(1)}) + J(f^{(1)} f_1{}^{(0)}) \\ [\theta^0] & \partial_t{}^{(0)} f^{(1)} + \partial_t{}^{(1)} f^{(0)} = \\ & \quad = \partial_S f^{(1)} - J(f^{(0)} f_1{}^{(2)}) - J(f^{(1)} f_1{}^{(1)}) - J(f^{(2)} f_1{}^{(0)}), \text{ etc.} \end{cases} \tag{2.31}$$

Of course, θ really $= 1$ and the θ-expansion does not in itself imply a development of f in a series of decreasing terms. Still, one would like the treatment to converge rapidly, because the $[\theta^0]$-equation is already very cumbersome. This means that the local MB $f^{(0)}$, which dutifully emerges

as "zero" approximation from the $[1/\theta^2]$-equation, should be the main contribution to f. In fact, if the next term satisfies $f^{(1)} \ll f^{(0)}$, the total collision term $J(ff_1)$ is effectively approximated by

$$(2.32)\quad \left.\begin{aligned} & J(f^{(0)}f_1^{(1)}) + J(f^{(1)}f_1^{(0)}) \\ &= f^{(0)}(\mathbf{c}) \cdot \int d\varepsilon \int d\chi \sin\chi \int d\mathbf{c}_1 f^{(0)}(\mathbf{c}_1)\{\phi^{(1)}(\mathbf{c}') + \phi^{(1)}(\mathbf{c}_1') - \phi^{(1)}(\mathbf{c}) - \phi^{(1)}(\mathbf{c}_1)\} \\ &\overset{\text{def}}{=} f^{(0)}\Omega\phi^{(1)}. \end{aligned}\right\}$$

which serves as a definition of the "linearized collision operator" Ω acting on any function of $\mathbf{c}$ instead of $\phi^{(1)}$. Using this Ω, the $[1/\theta]$-equation can be written as

$$(2.33a)\quad \boxed{F^{(1)} = \Omega\phi^{(1)}},$$

in which

$$(2.34a)\quad F^{(1)} \equiv (1/f^{(0)})\ (\partial_S f^{(0)} - \partial_t^{(0)} f^{(0)})$$

can be determined from $f^{(0)}$ alone. Similarly the general $[\theta^{r-2}]$-equation from (2.31) takes the form

$$(2.33b)\quad \boxed{F^{(r)} = \Omega\phi^{(r)}},$$

in which

$$(2.34b)\quad F^{(r)} \equiv (1/f^{(0)})\{\partial_S f^{(r-1)} - \sum_{\varrho=0}^{r-1} \partial_t^{(r-1-\varrho)} f^{(\varrho)} + \sum_{\varrho=1}^{r-1} J(f^{(\varrho)} f_1^{(r-\varrho)})\}$$

contains $f^{(0)}, f^{(1)}, \ldots, f^{(r-1)}$.

The linear operator Ω defined by (2.32) if of the greatest importance, for the ChE theory as well as for the extensions we are going to suggest. For the moment, we need the following properties of Ω, which we state without proof:

a) A scalar product of functions of $\mathbf{c}$ be defined by

$$(2.35a)\quad (F, G) = (G, F) \overset{\text{def}}{=} \int d\mathbf{c}\, f^{(0)} FG$$

[If F and G are, instead of scalars, vector or tensor functions, we define correspondingly:

$$(2.35b)\quad (\mathbf{F}, \mathbf{G}) = \sum_\alpha (F_\alpha, G_\alpha);\ (\mathsf{F}, \mathsf{G}) = \sum_\alpha \sum_\beta (F_{\alpha\beta}, G_{\alpha\beta}).]$$

Then

$$(2.36a)\quad (F, \Omega G) = (G, \Omega F)$$

or, introducing "square bracket" notation: $[F, G] \overset{\text{def}}{=} (F, \Omega G)$:

$$(2.36b)\quad [F, G] = [G, F]:$$

Ω is a symmetric operator.

[It is necessary to mention the following discrepancy between our square brackets and those used by Chapman and Cowling:

$$(2.37)\quad \underset{\text{(our notation)}}{(F, \Omega G) \equiv [F, G]} \ = \ \underset{\text{(Ch. and C.)}}{n^2 [F, G]_1} \qquad (n = \varrho/m).]$$

b) Ω is a "non-negative" operator:

$$(F, \Omega F) \equiv [F, F] \geqslant 0. \tag{2.38}$$

c) The eigenvalue equation:

$$\Omega\chi^{[\omega\lambda]} = \omega\chi^{[\omega\lambda]} \tag{2.39}$$

has a discrete spectrum of real eigenvalues ω, each with eigenfunctions $\chi^{[\omega\lambda]}$ numbered by λ; on account of the symmetry of Ω (see (a)),

$$(\chi^{[\omega\lambda]}, \chi^{[\omega'\lambda']}) = 0 \quad \text{if} \quad \omega \neq \omega', \tag{2.40}$$

whereas different eigenfunctions with the same ω can of course be made orthogonal. These χ, which we also suppose to be normalized:

$$(\chi^{[\omega\lambda]}, \chi^{[\omega\lambda]}) = 1, \tag{2.41}$$

form a complete set of functions in c-space.

d) On account of (b), Ω has non-negative eigenvalues only:

$$\omega \geqslant 0; \tag{2.42}$$

as in (2.38), the $=-$sign holds only if the corresponding eigenfunction is a linear combination of the 5 collisional invariants $\chi^{[0\lambda]}$. In fact, it is clear that Ω as defined by (2.32) annihilates the functions χ characterized by (2.4):

$$\Omega\chi^{[0\lambda]} = 0, \tag{2.43}$$

and it is equally possible to prove (2.4) for any χ satisfying (2.43). This explains the notation $\chi^{[0\lambda]}$ used for the collision-invariant functions from the beginning. [For use in the following theory, $\chi^{[0\lambda]}$ as defined by (2.5) have of course still to be normalized and made mutually orthogonal:

$$\chi'^{[01]} = \frac{1}{\sqrt{n}}\,; \mathsf{\chi}'^{[02]} = \sqrt{\frac{2}{3n}}\,\mathsf{C}^*\,; \chi'^{[03]} = \sqrt{\frac{2}{3n}}\left(C^{*2} - \frac{3}{2}\right), \tag{2.44}$$

in which

$$\mathsf{C}^* \overset{\text{def}}{=} \sqrt{\frac{m}{2kT}}\,\mathsf{C}.] \tag{2.45}$$

We now return to the set of equations (2.33). If we formally develop the LHS, $F^{(r)}$, in a series of eigenfunctions of Ω:

$$F^{(r)} = \sum_{\omega}\sum_{\lambda} f^{(r)[\omega\lambda]}\chi^{[\omega\lambda]} \quad \text{with} \quad f^{(r)[\omega\lambda]} = (F^{(r)}, \chi^{[\omega\lambda]}), \tag{2.46}$$

the solution $\phi^{(r)}$ can, again formally, be written down:

$$\phi^{(r)} = \sum_{\omega}\sum_{\lambda} \varphi^{(r)[\omega\lambda]}\chi^{[\omega\lambda]} \quad \text{with} \quad \varphi^{(r)[\omega\lambda]} = \frac{1}{\omega} f^{(r)[\omega\lambda]}. \tag{2.47}$$

In both (2.46) and (2.47), $\omega = 0$ is excluded from the summation: $\sum_{\omega>0}$, for $F^{(r)}$ as well as $\phi^{(r)}$ are orthogonal to all collisional invariants:

$$(F^{(r)}, \chi^{[0\lambda]}) = 0; \tag{2.48}$$

$$(\phi^{(r)}, \chi^{[0\lambda]}) = 0. \tag{2.49}$$

Here (2.49) is just the normalization of $\phi^{(r)}$ introduced in eq. (2.23). Eq. (2.48) is a solubility condition for eqs. (2.33), for if it did not hold, Ω applied to $\phi^{(r)}$ as of (2.47) could never yield $F^{(r)}$. The proof that this condition is actually satisfied, runs as follows: substitute the definition of $F^{(r)}$, (2.43b):

$$(2.50)\quad \begin{aligned}(F^{(r)}, \chi^{[0\lambda]}) &\equiv \int d\mathbf{c}\, \chi^{[0\lambda]} f^{(0)} F^{(r)} = \int d\mathbf{c}\, \chi^{[0\lambda]} \partial_S f^{(r-1)} - \\ &- \sum_{\varrho=0}^{r-1} \int d\mathbf{c}\, \chi^{[0\lambda]} \partial_t^{(r-1-\varrho)} f^{(\varrho)} + \sum_{\varrho=1}^{r-1} \int d\mathbf{c}\, \chi^{[0\lambda]} J(f^{(\varrho}\, f_1^{(r-\varrho)}).\end{aligned}$$

The last sum is a collision contribution which vanishes separately, because of (2.9) and the more general property

$$(2.51)\qquad \int d\mathbf{c}\, \chi^{[0\lambda]} \{J(fg_1) + J(gf_1)\} = 0, \qquad (\lambda = 1, \mathbf{2}, 3)$$

which again holds for all functions f, g. The other terms in the RHS of (2.50) cancel, as is proved as follows: using (2.28),

$$(2.52)\quad -\sum_{\varrho=0}^{r-1} \int d\mathbf{c}\, \chi^{[0\lambda]} \partial_t^{(r-1-\varrho)} f^{(\varrho)} = -\sum_{\varrho=0}^{r-1} \sum_{\lambda'} \partial_t^{(r-1-\varrho)} \psi^{[\lambda']} \frac{\delta}{\delta \psi^{[\lambda']}} \int d\mathbf{c}\, \chi^{[0\lambda]} f^{(\varrho)},$$

in which the remaining integral $= \psi^{[\lambda]} \delta_{\varrho 0}$ because of (2.23), and the functional derivation (2.21) means simply:

$$(2.53)\qquad \frac{\delta}{\delta \psi^{[\lambda']}} (\psi^{[\lambda]} \delta_{\varrho 0}) = \delta_{\lambda' \lambda} \delta_{\varrho 0};$$

so (2.50) becomes

$$(2.54)\qquad (F^{(r)}, \chi^{[0\lambda]}) = \int d\mathbf{c}\, \chi^{[0\lambda]} \partial_S f^{(r-1)} - \partial_t^{(r-1)} \psi^{[\lambda]} = 0,$$

for this vanishes according to (2.25c).

(2.48) and (2.49) are apparently connected, for the normalization (2:23, 49) of $f^{(0)}, \ldots, f^{(r-1)}$ is essential for the step (2.53) in the proof of (2.49), i.e., for the solubility of the equation determining $f^{(r)}$.

Two steps in the actual computation of the complete distribution f^{Ch} are very difficult:

a) successive computation of the $F^{(r)}$ (cf. 2.34b). Only $F^{(1)}$ is well known; from $r = 2$ onwards, cumbersome collision terms like $J(f^{(1)} f_1^{(1)})$ occur.

b) solving the eigenvalue problem of the Ω operator, in order to develop all $F^{(r)}$ in series of $\chi^{[\ldots]}$ (eq. 2.46). This has only been accomplished for a Maxwellian intermolecular potential, $V(r) = +\text{const.}/r^4$. For some details, we refer to ch. 7.

About the convergence of the basic series (2.22) something will be said in ch. 8. Essentially, we have a development in powers of l [illegible] mean free path [illegible] gradient, which implies that convergence is ensured if the gradients of the moments (and gradients *of* these gradients, etc.) cause little relative change in ψ over a distance l.

(To be continued)

THEORY OF RELAXATION PHENOMENA IN A MONATOMIC GAS. II

BY

M. J. OFFERHAUS

(Communicated by Prof. J. DE BOER at the meeting of October 29, 1960)

3. *Velocity distribution in the kinetic stage: uniform case*

We are now going to outline the general solution to the BE for a spatially uniform gas. References to existing literature dealing with this case were already given in ch. 1.

Consider a uniform distribution f independent of $\boldsymbol{r}$ which, at $t=0$, has the completely arbitrary shape

$$f(0) \stackrel{\text{def}}{=} f(\boldsymbol{c}; t=0). \tag{3.1}$$

Eqs. (2.12), (2.13) give the simplified forms of the BE for f and of the HDE for the moments ψ of f:

$$\partial_t f = J(ff_1); \quad \partial_t \psi^{[\lambda]} = 0.$$

We now introduce a MB distribution $f^{(0)}(\boldsymbol{c}; \psi)$ based, at each t, on the moments ψ of the real f. This is a mathematical concept and its t-derivative is, of course, not given by a BE but by eq. (2.15):

$$\partial_t f^{(0)} = \sum_\lambda \frac{\delta f^{(0)}}{\delta \psi^{[\lambda]}} \partial_t \psi^{[\lambda]} = 0. \tag{3.2}$$

So we have a real distribution f changing in t, with constant moments ψ, and a time-independent $f^{(0)}$, equally with moments ψ; the difference

$$f - f^{(0)} = \tilde{f}(\boldsymbol{c}; t) = f^{(0)}(\boldsymbol{c})\tilde{\phi}(\boldsymbol{c}; t) \tag{3.3}$$

is a function of $\boldsymbol{c}$ and t with, as its first 5 moments,

$$\tilde{\psi}^{[\lambda]} = \int d\boldsymbol{c}\, \tilde{f} \chi^{[0\lambda]} = (\tilde{\phi}, \chi^{[0\lambda]}) = 0 \tag{3.4}$$

and an initial value:

$$f^{(0)}\tilde{\phi}(0) \stackrel{\text{def}}{=} \tilde{f}(\boldsymbol{c}; t=0) = f(0) - f^{(0)}. \tag{3.5}$$

$\partial_t \tilde{f}$ is found by substituting (3.3) into the BE (2.12):

$$\partial_t(f^{(0)} + \tilde{f}) = J(f^{(0)} + \tilde{f}, f_1^{(0)} + \tilde{f}_1) \tag{3.6}$$

or, with (2.16) and (3.2),

$$\partial_t \tilde{f} = J(f^{(0)} f_1^{(0)}) + J(\tilde{f} f_1^{(0)}) + J(f^{(0)} \tilde{f}_1) + J(\tilde{f}\tilde{f}_1). \tag{3.7}$$

We now proceed to solve this equation, in close analogy to the ChE method. Again, the total f is developed in a series of terms, of which $f^{(0)}$ is the first:

$$f = f^{(0)} + \tilde{f} = f^{(0)} + \tilde{f}^{(1)} + \tilde{f}^{(2)} + \ldots = f^{(0)}(1 + \tilde{\phi}^{(1)} + \tilde{\phi}^{(2)} + \ldots) = f^{(0)}(1 + \tilde{\phi}), \tag{3.8}$$

with the normalization:

$$\psi^{[\lambda](0)} = \psi^{[\lambda]}; \tilde{\psi}^{[\lambda](1)} = \ldots = 0 \qquad (\tilde{\psi}^{[\lambda](r)} \equiv \int d\boldsymbol{c}\, \tilde{f}^{(r)} \chi^{[0\lambda]}), \tag{3.9}$$

in accordance with (3.4). Introduce the expansion (3.8) into (3.7):

$$\sum_{r=1}^{\infty} \partial_t \tilde{f}^{(r)} = \sum_{r=0,1,\ldots}^{\infty} \sum_{s=0,1,\ldots}^{\infty} J(\tilde{f}^{(r)} \tilde{f}_1^{(s)}) \quad (\tilde{f}^{(0)} \equiv f^{(0)}) \tag{3.10}$$

and insert a constant $\theta = 1$ as follows:

$$\sum_{r=0}^{\infty} \tilde{f}^{(r)} \to (1/\theta)\tilde{f}^{(0)} + \tilde{f}^{(1)} + \theta \tilde{f}^{(2)} + \ldots; \tag{3.11a}$$

$$\sum_{r=1}^{\infty} \partial_t \tilde{f}^{(r)} \to (1/\theta)\, \partial_t \tilde{f}^{(1)} + \partial_t \tilde{f}^{(2)} + \theta \partial_t \tilde{f}^{(3)} + \ldots \tag{3.11b}$$

or, using (3.2):

$$\sum_{r=1}^{\infty} \partial_t \tilde{\phi}^{(r)} \to \partial_t \tilde{\phi}^{(1)} + \theta \partial_t \tilde{\phi}^{(2)} + \theta^2 \partial_t \tilde{\phi}^{(3)} + \ldots. \tag{3.11c}$$

Putting these series in (3.10) and separating terms according to powers of θ, we find:

$$\begin{cases} [1/\theta^2] & 0 = J(f^{(0)} f_1^{(0)}) \\ [1/\theta] & \partial_t \tilde{f}^{(1)} = f^{(0)} \partial_t \tilde{\phi}^{(1)} = J(f^{(0)} \tilde{f}_1^{(1)}) + J(\tilde{f}^{(1)} f_1^{(0)}) \\ [\theta^0] & \partial_t \tilde{f}^{(2)} = f^{(0)} \partial_t \tilde{\phi}^{(2)} = J(f^{(0)} \tilde{f}^{(2)}) + J(\tilde{f}^{(1)} \tilde{f}_1^{(1)}) + J(\tilde{f}^{(2)} f_1^{(0)}), \text{ etc.} \end{cases} \tag{3.12}$$

The choice of the θ-developments (3.11) is such that the $[1/\theta^2]$-equation yields $f^{(0)}$, as required; using the definition of Ω (2.32), we write the $[1/\theta]$-equation for $\tilde{f}^{(1)}$ as follows:

$$\boxed{\partial_t \tilde{\phi}^{(1)} = -\Omega \tilde{\phi}^{(1)}}. \tag{3.13a}$$

The $[\theta^{r-2}]$-equation expresses $\tilde{f}^{(r)}$ in terms of $f^{(0)}$, $\tilde{f}^{(1)}$, ..., $\tilde{f}^{(r-1)}$:

$$\boxed{\partial_t \tilde{\phi}^{(r)} = \tilde{F}^{(r)} - \Omega \tilde{\phi}^{(r)}}, \qquad (r > 2) \tag{3.13b}$$

in which

$$\tilde{F}^{(r)} \equiv (1/f^{(0)})\{J(\tilde{f}^{(1)} \tilde{f}_1^{(r-1)}) + J(\tilde{f}^{(2)} \tilde{f}_1^{(r-2)}) + \ldots + J(\tilde{f}^{(r-1)} \tilde{f}_1^{(1)})\}. \tag{3.14}$$

Eqs. (3.13) form a hierarchy of equations for successive terms of the general distribution f in our special, $\boldsymbol{r}$-independent case, just like eqs. (2.33) did for a special f in the general, $\boldsymbol{r}$-dependent case, This time, t enters explicitly and accordingly we have to take the initial condition (3.5) into account. The initial deviation $\tilde{\phi}(0)$ can be spread at will over

the terms $\tilde{\phi}^{(r)}$; it is logical, and will certainly promote rapid convergence, to assign all of it to $\tilde{\phi}^{(1)}$:

$$\tilde{\phi}^{(1)}(\mathbf{c}; t=0) = \tilde{\phi}(0); \quad \tilde{\phi}^{(2)}(\mathbf{c}; t=0) = \ldots = 0. \tag{3.15}$$

Solution of eqs. (3.13) again involves developments of $\tilde{F}$ and $\tilde{\phi}$ in terms of $\chi^{[\omega\lambda]}$, from which $\chi^{[0\lambda]}$ will be absent:

$$\left.\begin{aligned} (\tilde{F}^{(r)}, \chi^{[0\lambda]}) &= 0; \quad (3.16)\\ (\tilde{\phi}^{(r)}, \chi^{[0\lambda]}) &= 0; \quad (3.17)\\ (\tilde{\phi}(0), \chi^{[0\lambda]}) &= 0. \quad (3.18) \end{aligned}\right\} \quad \lambda = 1, \mathbf{2}, 3.$$

(3.16) is a solubility condition which, like (2.48), is easily proved to be satisfied with the use of (2.9) and (2.51); (3.17) is the normalizing condition put in (3.9), and (3.18) is simply (3.4) at $t=0$.

As in the ChE case, two difficulties bar the way towards a complete solution of the hierarchy of equations (3.13): solution of the Ω-eigenvalue problem and successive computation of $\tilde{F}^{(r)}$ from (3.14). We can, however, give a formal treatment, from which the time-dependence of the complete $\tilde{\phi}$ becomes clear.

The first equation (3.13a) for $r=1$ is formally solved by developing $\tilde{\phi}^{(1)}(t)$, as well as $\tilde{\phi}^{(1)}(t=0) = \tilde{\phi}(0)$, in eigenfunctions of Ω:

$$\tilde{\phi}^{(1)}(\mathbf{c}; t) = \sum_{\omega} \sum_{\lambda} \tilde{\varphi}^{(1)[\omega\lambda]}(t)\, \chi^{[\omega\lambda]}(\mathbf{c}) \tag{3.19}$$

and

$$\tilde{\phi}^{(1)}(\mathbf{c}; t=0) = \tilde{\phi}(0) = \sum_{\omega} \sum_{\lambda} \tilde{\varphi}^{[\omega\lambda]}\, \chi^{[\omega\lambda]}(\mathbf{c}) \text{ with } \tilde{\varphi}^{[\omega\lambda]} = (\tilde{\phi}(0), \chi^{[\omega\lambda]}). \tag{3.20}$$

$\tilde{\varphi}^{[\omega\lambda]}$ is the initial value of $\tilde{\varphi}^{(1)[\omega\lambda]}$:

$$\tilde{\varphi}^{(1)[\omega\lambda]}(t=0) = \tilde{\varphi}^{[\omega\lambda]}. \tag{3.21}$$

Substituting (3.19) into (3.13a), we have for each $\omega\lambda$:

$$(\partial_t + \omega)\, \tilde{\varphi}^{(1)[\omega\lambda]}(t) = 0, \tag{3.22}$$

with the initial condition (3.21); the solution reads:

$$\tilde{\varphi}^{(1)[\omega\lambda]}(t) = \tilde{\varphi}^{[\omega\lambda]}\, e^{-\omega t} \tag{3.23}$$

and the full $\tilde{\phi}^{(1)}$ (3.19) is correspondingly given by

$$\tilde{\phi}^{(1)}(\mathbf{c}; t) = \sum_{\omega} \sum_{\lambda} \tilde{\varphi}^{[\omega\lambda]}\, e^{-\omega t}\, \chi^{[\omega\lambda]}(\mathbf{c}) \equiv \sum_{\omega} \sum_{\lambda} \Psi^{(1)[\omega]}(\mathbf{c})\, e^{-\omega t}, \tag{3.24}$$

in which the Ψ-notation is used in order to group the terms of $\tilde{\phi}^{(1)}$ according to their $\exp(-\omega t)$-factors. This simply means that each $\omega\lambda$-mode of the initial $\tilde{\phi}(0)$ decays with $1/\omega$ as its relaxation time.

Next we will determine $\tilde{\phi}^{(2)}$. Substitute $\tilde{f}^{(1)} \quad f^{(0)}\tilde{\phi}^{(1)}$, as given by (3.24),

back into the definition of $\tilde{F}^{(2)}$ (3.14, $r=2$); we find:

$$\tilde{F}^{(2)} = \frac{1}{f^{(0)}} J(\tilde{f}^{(1)} \tilde{f}_1^{(1)}) = \sum_{\bar{\omega}>0} G^{(2)[\bar{\omega}]} e^{-\bar{\omega}t}, \tag{3.25}$$

in which the sums of any two ω occurring in (3.24), which are of course all >0, have been arranged in order of increasing size and called $\bar{\omega}$. Now write out eq. (3.13b) for $r=2$:

$$(\partial_t + \Omega)\tilde{\phi}^{(2)} - \sum_{\bar{\omega}} G^{(2)[\bar{\omega}]} e^{-\bar{\omega}t} = 0. \tag{3.26}$$

Develop both $\tilde{\phi}^{(2)}$ and $G^{(2)[\bar{\omega}]}$ in χ-series:

$$G^{(2)[\bar{\omega}]}(\mathbf{c}) = \sum_{\omega} \sum_{\lambda} g^{(2)[\bar{\omega}\omega\lambda]} \chi^{[\omega\lambda]}(\mathbf{c}) \tag{3.27}$$

and

$$\tilde{\phi}^{(2)}(\mathbf{c}; t) = \sum_{\omega} \sum_{\lambda} \tilde{\varphi}^{(2)[\omega\lambda]}(t) \chi^{[\omega\lambda]}(\mathbf{c}); \tag{3.28}$$

initially (cf. 3.15):

$$\tilde{\varphi}^{(2)[\omega\lambda]}(t=0) = 0. \tag{3.29}$$

Substitute (3: 27, 28) into (3.26); for each $\omega\lambda$,

$$(\partial_t + \omega)\tilde{\varphi}^{(2)[\omega\lambda]}(t) - g^{(2)[\omega\omega\lambda]} e^{-\omega t} - \sum_{\bar{\omega}\neq\omega}{}' g^{(2)[\bar{\omega}\omega\lambda]} e^{-\omega t} = 0. \tag{3.30}$$

Here we have supposed that the eigenvalue ω is found again among the sums-of-eigenvalues $\bar{\omega}$ occurring in the development (3.25) of $\tilde{F}^{(2)}$. Of course, if this is not true, we simply omit $g^{(2)[\omega\omega\lambda]}$. The solution of (3.30) is easily seen to have the form:

$$\tilde{\varphi}^{(2)[\omega\lambda]}(t) = (\psi^{(2)[\omega\lambda]} + \psi'^{(2)[\omega\lambda]} t) e^{-\omega t} + \sum_{\bar{\omega}\neq\omega}{}' \psi^{(2)[\bar{\omega}\omega\lambda]} e^{-\bar{\omega}t}. \tag{3.31}$$

In order to determine the coefficients ψ, we substitute this back into (3.30) and put coefficients of each $\exp(-\bar{\omega}t)$ separately $=0$:

$$\psi'^{(2)[\omega\lambda]} - g^{(2)[\omega\omega\lambda]} = 0; \tag{3.32a}$$

$$(\omega - \bar{\omega})\psi^{(2)[\bar{\omega}\omega\lambda]} - g^{(2)[\bar{\omega}\omega\lambda]} = 0, \tag{3.32b}$$

while the initial condition (3.29) serves to fix the one remaining coefficient:

$$\psi^{(2)[\omega\lambda]} + \sum_{\bar{\omega}\neq\omega}{}' \psi^{(2)[\bar{\omega}\omega\lambda]} = 0, \tag{3.32c}$$

or, using (3.32b),

$$\psi^{(2)[\omega\lambda]} = -\sum_{\bar{\omega}\neq\omega}{}' \frac{g^{(2)[\bar{\omega}\omega\lambda]}}{\bar{\omega}-\omega}. \tag{3.32d}$$

Putting (3.32a, b, d) in (3.31) and going back to (3.28), we find:

$$(3.33)\quad \begin{cases} \tilde{\phi}^{(2)}(\mathbf{c};t) = \sum_{\omega}\sum_{\lambda}\chi^{[\omega\lambda]}(\mathbf{c})\left(g^{(2)[\omega\omega\lambda]}te^{-\omega t} + \sum_{\bar{\omega}\neq\omega}{}' g^{(2)[\bar{\omega}\omega\lambda]}\frac{e^{-\omega t}-e^{-\bar{\omega}t}}{\bar{\omega}-\omega}\right) \\ \qquad = \sum_{\omega}\sum_{\lambda}\chi^{[\omega\lambda]}(\mathbf{c})\sum_{\bar{\omega}}{}' g^{(2)[\bar{\omega}\omega\lambda]}E^{[\bar{\omega}\omega]}(t), \end{cases}$$

in which we have introduced:

$$(3.34)\quad \begin{cases} (\bar{\omega}\neq\omega) \qquad E^{[\bar{\omega}\omega]}(t) = E^{[\omega\bar{\omega}]}(t) \overset{\text{def}}{=} \frac{e^{-\omega t}-e^{-\bar{\omega}t}}{\bar{\omega}-\omega}\,; \\ \qquad\qquad E^{[\omega\omega]}(t) = \lim_{\bar{\omega}\to\omega} E^{[\bar{\omega}\omega]}(t) = te^{-\omega t}. \end{cases}$$

As for the time-dependent factors of the various modes, $t\exp(-\omega t)$ starts from 0 at $t=0$ at a rate 1, to reach its maximum value $1/\omega e$ at $t=1/\omega$; from that time, it decreases rapidly. $E^{[\bar{\omega}\omega]}(t)$ behaves very much like $t\exp(-\omega t)$: it also starts from 0 at a rate 1; it stays in between $t\exp(-\omega t)$ and $t\exp(-\bar{\omega}t)$, reaching a maximum in between those of $t\exp(-\omega t)$ and $t\exp(-\bar{\omega}t)$ at a time between $1/\omega$ and $1/\bar{\omega}$. This is how all modes behave.

Finally, we rewrite (3.33) in a notation arranging the terms of $\tilde{\phi}^{(2)}$ according to their t-dependent factors $\exp(-\bar{\omega}t)$ and $t\exp(-\bar{\omega}t)$:

$$(3.35)\qquad \tilde{\phi}^{(2)}(\mathbf{c};t) = \sum_{\bar{\omega}}{}'(\Psi^{(2)[\bar{\omega}]}(\mathbf{c}) + \Psi'^{(2)[\bar{\omega}]}(\mathbf{c})t)\,e^{-\bar{\omega}t}.$$

Having dealt with $\tilde{\phi}^{(2)}$ in such detail, we can be short in discussing higher terms. Next comes

$$(3.36)\quad \begin{cases} \tilde{F}^{(3)}(\mathbf{c};t) \equiv (1/f^{(0)})\{J(\tilde{f}^{(1)}\tilde{f}_1^{(2)}) + J(\tilde{f}^{(2)}\tilde{f}_1^{(1)})\} = \\ \qquad\qquad = \sum_{\bar{\omega}}{}'(G^{(3)[\bar{\omega}]} + G'^{(3)[\bar{\omega}]}t)\,e^{-\bar{\omega}t}. \end{cases}$$

as follows on substituting $\tilde{f}^{(1)}$ and $\tilde{f}^{(2)}$, as given by (3: 24, 35), into (3.14, $r=3$); this time $\bar{\omega}$ represents triple sums of eigenvalues ω. The solution $\tilde{\phi}^{(3)}$ of eq. (3.13b) for $r=3$ will read:

$$(3.37)\qquad \tilde{\phi}^{(3)}(\mathbf{c};t) = \sum_{\bar{\omega}}{}'(\Psi^{(3)[\bar{\omega}]}(\mathbf{c}) + \Psi'^{(3)[\bar{\omega}]}(\mathbf{c})t + \Psi''^{(3)[\bar{\omega}]}(\mathbf{c})t^2)\,e^{-\bar{\omega}t}.$$

Continuing in this way, one finds that the general $\tilde{F}^{(r)}$ ($\tilde{\phi}^{(r)}$) consist of terms: $\exp(-\bar{\omega}t)$ times a polynomial in t of maximal degree $r-2$ $(r-1)$. Of course, whether these degrees are actually reached, depends on the recurrence of the eigenvalues ω among the $\bar{\omega}$, which are r-fold sums of ω values.

Thus, $\tilde{\phi}$ goes to zero for $t\to\infty$, because all terms in the developments of $\tilde{\phi}^{(1)}$, $\tilde{\phi}^{(2)}$ etc. contain decreasing powers $\exp(-\bar{\omega}t)$, where the $\bar{\omega}$ are those ω which occur in the χ-development (3.20) of the initial $\tilde{\phi}^{(0)}$, and sums $\bar{\omega}$ of these ω. The smallest of all possible $\bar{\omega}$ is ω_1, the first positive

eigenvalue of Ω, and its inverse is the longest of the decay times of the terms in $\tilde{\phi}$, which is the characteristic relaxation time τ for the kinetic stage:

$$\tau = 1/\omega_1. \tag{3.38}$$

Of course, the effective relaxation time is somewhat smaller if one or more of the lowest ω are missing from (3.20). A discussion of the time scale τ will be given in ch. 7.

Finally, we should say something on the convergence of the series (3.8). The general character of the terms $\tilde{\phi}^{(1)}, \tilde{\phi}^{(2)}, \ldots$ is such that $\tilde{\phi}^{(1)}(\mathbf{c}; t)$ initially equals $\tilde{\phi}(0)$ and then decays, for all $\mathbf{c}$, with a relaxation time $\approx \tau$; $\tilde{\phi}^{(2)}$ and higher terms start at 0 for all $\mathbf{c}$; in a time of order τ, they build up some maximal value (as functions of t, for all $\mathbf{c}$) and then they decay exponentially like $\tilde{\phi}^{(1)}$ does. Now in order to compare the terms $f^{(0)}, \tilde{f}^{(1)}, \tilde{f}^{(2)}, \ldots$, which are functions of $\mathbf{c}$ and t, we consider in particular a time $t \approx \tau$ (because, if $t \gg \tau$, all terms following $f^{(0)}$ vanish anyway) and a velocity $\mathbf{c} \approx \mathbf{c}_0$ (because, in calculating physical properties like entropy production and heat or momentum transport, one or two factors $\tilde{\phi}$ are put in a scalar product, i.e., integrated after multiplication by $\exp\{-m(\mathbf{c}-\mathbf{c}_0)^2/2kT\}$). First, we substitute these values in the series expansion of $\tilde{\phi}^{(1)}$ (3.24); supposing this does contain the first positive eigenvalue ω_1, and neglecting higher modes $\omega_2, \ldots$ on account of the accompanying factors $\exp(-\omega_2 t), \ldots$, we get:

$$\tilde{\phi}^{(1)}(\mathbf{c}_0; \tau) \approx (1/e)\tilde{\varphi}^{[\omega_1\lambda]}\chi^{[\omega_1\lambda]}(\mathbf{c}_0) \approx (1/e)\tilde{\phi}(\mathbf{c}_0; t=0) = \tilde{\varphi}. \tag{3.39a}$$

Likewise, it appears that

$$\tilde{\phi}^{(2)}(\mathbf{c}_0; \tau) \approx \tilde{\varphi}^2 \tag{3.39b}$$

etc.: $1/e$ times the initial value of the deviation $\tilde{\phi}$ at $\mathbf{c} = \mathbf{c}_0$ serves as a parameter setting the pace for the convergence of the $\tilde{\phi}$ series.

4. *Velocity distribution in the kinetic stage: non-uniform case*

After the special (ChE) solution of the $\mathbf{r}$-dependent case (ch. 2) and the general solution of the spatially uniform case (ch. 3), we shall now determine the general non-uniform velocity-space distribution $f(\mathbf{c}; \mathbf{r}, t)$ from the BE, which reads (2.1):

$$\partial_t f(\mathbf{c}; \mathbf{r}, t) = \partial_S f + J(ff_1). \tag{4.1}$$

Many steps in this solution find their parallels in ch. 2, in ch. 3, or in both.

In the ChE method, the solution f had the special characteristic of being a functional of the $\psi^{[\lambda]}$; this, together with (4.1), proved sufficient to determine f. Without such restriction, we are free to impose an initial condition:

$$f(\mathbf{c}; \mathbf{r}; t=0) = f(0). \tag{4.2}$$

Let the solution $f(\mathbf{c}; \mathbf{r}, t)$ have $\psi^{[\lambda]}(\mathbf{r}, t)$ for its first 5 moments. On the base of these ψ, one can determine a complete ChE distribution f^{Ch}, from which f differs by an amount

$$f - f^{\mathrm{Ch}} = \tilde{f}(\mathbf{c}; \mathbf{r}, t) = f^{(0)}\tilde{\phi}, \tag{4.3}$$

$f^{(0)}$ denoting the MB distribution based, like f^{Ch}, on ψ (in fact, this is the first term in the series which constitutes f^{Ch}). We do not require the difference $\tilde{f}$ to be small. At $t=0$, it has a given value

$$\tilde{f}(\mathbf{c}; \mathbf{r}; t=0) = f^{(0)} - f^{\mathrm{Ch}}(0) = f^{(0)}(0)\tilde{\phi}(0). \tag{4.4}$$

Both f and f^{Ch} have $\psi^{[\lambda]}$ for their first 5 moments, so that those of $\tilde{f}$ vanish:

$$\tilde{\psi}^{[\lambda]}(\mathbf{r}, t) \equiv \int d\mathbf{c}\, \tilde{f}\chi^{[0\lambda]} = (\tilde{\phi}, \chi^{[0\lambda]}) = 0; \tag{4.5}$$

in particular,

$$\tilde{\psi}^{[\lambda]}(\mathbf{r}; t=0) = (\tilde{\phi}(0), \chi^{[0\lambda]}) = 0. \tag{4.6}$$

It is this $\tilde{\phi}$ (or $\tilde{f}$) for which we are going to draw up an equation. Because of the definition (4.3), this implies that we should know how f and f^{Ch} change in time. f obeys to the BE (4.1); $\partial_t f^{\mathrm{Ch}}$ does not follow from a BE, because it is not a real distribution but an implicite function of $\mathbf{r}$ and t through the ψ, so that we should start from the HDE for ψ (see 2.10). The RHS of these equations contain the 5 moments $\psi^{[\lambda]}$ themselves, as well as the higher moments $\overset{\circ}{\mathsf{P}}$ and $\boldsymbol{q}$, the latter ones linearly. Now we first determine $\partial_t \psi$ computing these moments $\psi, \overset{\circ}{\mathsf{P}}, \boldsymbol{q}$ on the base of f^{Ch} only: this means inserting the exact ψ but ChE values $\overset{\circ}{\mathsf{P}}^{\mathrm{Ch}}$, $\boldsymbol{q}^{\mathrm{Ch}}$. Then we only have to add terms with $\overset{\circ}{\tilde{\mathsf{P}}}$ and $\tilde{\boldsymbol{q}}$ arising from the correction $\tilde{f}$, because $\tilde{f}$ does not change the ψ values (see 4.5). In all, this gives

$$\partial_t \psi^{[\lambda]} = \int d\mathbf{c}\, \chi^{[0\lambda]} \partial_{\mathrm{S}}(f^{\mathrm{Ch}} + \tilde{f}) = \partial_t{}^{\mathrm{Ch}} \psi^{[\lambda]} + \tilde{\partial}_t \psi^{[\lambda]}, \tag{4.7}$$

in which the second equality, holding term by term, serves to define the "partial" t-derivatives $\partial_t{}^{\mathrm{Ch}}$ and $\tilde{\partial}_t$ of the $\psi^{[\lambda]}$. The change in f^{Ch}, a functional of the ψ, can likewise be divided into two parts:

$$\partial_t f^{\mathrm{Ch}} = \sum_{\lambda} \frac{\delta f^{\mathrm{Ch}}}{\delta \psi^{[\lambda]}} \partial_t \psi^{[\lambda]} = \partial_t{}^{\mathrm{Ch}} f^{\mathrm{Ch}} + \tilde{\partial}_t f^{\mathrm{Ch}}, \tag{4.8}$$

if the obvious definitions hold:

$$\partial_t{}^{\mathrm{Ch}}\, u(\mathbf{c}|\psi^{[\lambda]}(\mathbf{r}, t)) = \sum_{\lambda} \frac{\delta u}{\delta \psi^{[\lambda]}} \partial_t{}^{\mathrm{Ch}}\, \psi^{[\lambda]}; \tag{4.9a}$$

$$\tilde{\partial}_t\, u(\mathbf{c}|\psi^{[\lambda]}(\mathbf{r}, t)) = \sum_{\lambda} \frac{\delta u}{\delta \psi^{[\lambda]}} \tilde{\partial}_t\, \psi^{[\lambda]}. \tag{4.9b}$$

Eq. (4.8) gives a comparison between the actual time derivative of f^{Ch} and the one we would find if the distribution were really f^{Ch} and no

more. The latter follows from the BE as it reads in the ChE case:

$$\partial_t{}^{\mathrm{Ch}} f^{\mathrm{Ch}} = \partial_S f^{\mathrm{Ch}} + J(f^{\mathrm{Ch}} f_1{}^{\mathrm{Ch}}), \tag{4.10}$$

whereas, for the full distribution f, we have the BE (4.1) which reads, introducing $\tilde{f}$ by means of (4.3):

$$\partial_t (f^{\mathrm{Ch}} + \tilde{f}) = \partial_S (f^{\mathrm{Ch}} + \tilde{f}) + J(f^{\mathrm{Ch}} + \tilde{f}, f_1{}^{\mathrm{Ch}} + \tilde{f}_1). \tag{4.11}$$

Combination of eqs. (4: 8, 10, 11) gives the equation for $\partial_t \tilde{f}$ and, consequently, that for $\partial_t \tilde{\phi}$:

$$\partial_t \tilde{f} = f^{(0)} \partial_t \tilde{\phi} + \tilde{\phi} \partial_t{}^{\mathrm{Ch}} f^{(0)} + \tilde{\phi} \tilde{\partial}_t f^{(0)} = \partial_S \tilde{f} + J(f^{\mathrm{Ch}} \tilde{f}_1) + J(\tilde{f} f_1{}^{\mathrm{Ch}}) + J(\tilde{f} \tilde{f}_1). \tag{4.12}$$

The next two steps are, of course, series development of the various quantities and insertion of powers of $\theta = 1$, in order to get a hierarchy of equations to be solved in succession. This time, we might as well combine these two steps and write immediately:

$$f^{\mathrm{Ch}} = (1/\theta) f^{(0)} + f^{(1)} + \ldots = (1/\theta) f^{(0)} (1 + \theta \phi^{(1)} + \ldots); \tag{4.13a}$$

$$\tilde{f} = \tilde{f}^{(1)} + \theta \tilde{f}^{(2)} + \ldots = (1/\theta) f^{(0)} (\theta \tilde{\phi}^{(1)} + \theta^2 \tilde{\phi}^{(2)} + \ldots), \tag{4.13b}$$

with the normalization:

$$\psi^{[\lambda](r)} \equiv \int d\mathbf{c}\, f^{(r)} \chi^{[0\lambda]} = \psi^{[\lambda]} \delta_{r0}; \tag{4.14a}$$

$$\tilde{\psi}^{[\lambda](r)} \equiv \int d\mathbf{c}\, \tilde{f}^{(r)} \chi^{[0\lambda]} = 0 \qquad (r \geqslant 1). \tag{4.14b}$$

Higher moments of f, like P and $\boldsymbol{q}$, also consist of contributions from the terms of (4.13a, b), and so do the RHS of the HDE:

$$\partial_t{}^{\mathrm{Ch}} \psi^{[\lambda]} = \int d\mathbf{c}\, \chi^{[0\lambda]} \partial_S (f^{(0)} + f^{(1)} + \ldots) = (\partial_t{}^{(0)} + \theta \partial_t{}^{(1)} + \ldots) \psi^{[\lambda]}; \tag{4.13c}$$

$$\tilde{\partial}_t \psi^{[\lambda]} = \int d\mathbf{c}\, \chi^{[0\lambda]} \partial_S (\tilde{f}^{(1)} + \tilde{f}^{(2)} + \ldots) = (\theta \tilde{\partial}_t{}^{(1)} + \theta^2 \tilde{\partial}_t{}^{(2)} + \ldots) \psi^{[\lambda]}, \tag{4.13d}$$

as well as the "partial" t-derivatives of any functional u of ψ:

$$\partial_t{}^{\mathrm{Ch}} u = (\partial_t{}^{(0)} + \theta \partial_t{}^{(1)} + \ldots) u; \tag{4.13e}$$

$$\tilde{\partial}_t u = (\theta \tilde{\partial}_t{}^{(1)} + \theta^2 \tilde{\partial}_t{}^{(2)} + \ldots) u, \tag{4.13f}$$

if, like in (4.9), we define:

$$\partial_t{}^{(s)} u(\mathbf{c}|\psi) = \sum_\lambda \frac{\delta u}{\delta \psi^{[\lambda]}} \partial_t{}^{(s)} \psi^{[\lambda]}; \tag{4.15a}$$

$$\tilde{\partial}_t{}^{(s)} u(\mathbf{c}|\psi) = \sum_\lambda \frac{\delta u}{\delta \psi^{[\lambda]}} \tilde{\partial}_t{}^{(s)} \psi^{[\lambda]}. \tag{4.15b}$$

As regards $\partial_t \tilde{f} \quad \partial_t (f^{(0)} \tilde{\phi})$, because $f^{(0)}$ is t-dependent (unlike the *uniform* $f^{(0)}$), we must assign the factor θ^r either to $\partial_t \tilde{f}^{(r+1)}$ or to $\partial_t \tilde{\phi}^{(r)}$. The latter choice seems preferable:

$$\partial_t \tilde{\phi} = \partial_t \tilde{\phi}^{(1)} + \theta \partial_t \tilde{\phi}^{(2)} + \ldots. \tag{4.13g}$$

Substitute (4.13a, b, e, f, g) into (4.12) and put coefficients of each power θ^r separately $=0$; for the J terms, we use an obvious shorthand notation:

$$
(4.16)\quad \left\{\begin{array}{l}
[1\ 0] \quad f^{(0)}\partial_t\tilde{\phi}^{(1)} \quad J(f^{(0)}\tilde{f}_1^{(1)}) \quad J(\tilde{f}^{(1)}f_1^{(0)}) \quad J(01;\tilde{1}0)\\
[\theta^0] \quad \tilde{\partial}_t^{(1)}f^{(0)}+f^{(0)}\partial_t\tilde{\phi}^{(2)}+\tilde{\phi}^{(1)}\partial_t^{(0)}f^{(0)}=\partial_S\tilde{f}^{(1)}+J(0\tilde{2};1\tilde{1};\tilde{1}1;\tilde{2}0;\tilde{1}\tilde{1})\\
[\theta^2] \quad \tilde{\partial}_t^{(1)}\tilde{f}^{(1)} \quad \tilde{\partial}_t^{(2)}f^{(0)} \quad f^{(0)}\partial_t\tilde{\phi}^{(3)} \quad \tilde{\phi}^{(1)}\partial_t^{(1)}f^{(0)} \quad \tilde{\phi}^{(2)}\partial_t^{(0)}f^{(0)}+\\
\quad +\tilde{\phi}^{(1)}\tilde{\partial}_t^{(1)}f^{(0)}=\partial_S\tilde{f}^{(2)}+J(0\tilde{3};1\tilde{2};2\tilde{1};\tilde{1}2;\tilde{2}1;\tilde{3}0;\tilde{1}\tilde{2};\tilde{2}\tilde{1}),\ \text{etc.}
\end{array}\right.
$$

There is a complete analogy to the comparable equations in the uniform case (3.12) in that operations on the unknown $\tilde{\phi}^{(r)}$ include the linearized collision operator in $\mathbf{c}$ space and differentiation ∂_t. This leads to an abbreviated notation identical with (3.13a, b):

$$
\boxed{\begin{array}{ll}
(4.17a) & \partial_t\tilde{\phi}^{(1)}=-\Omega\tilde{\phi}^{(1)};\\
(4.17b) & \partial_t\tilde{\phi}^{(r)}=\tilde{F}^{(r)}-\Omega\tilde{\phi}^{(r)}
\end{array}},\quad (r\geq 2)
$$

in which, this time, both $\tilde{F}^{(r)}$, which has the new meaning:

$$
(4.18)\quad \left\{\begin{array}{l}
\tilde{F}^{(r)}=(1/f^{(0)})\{\partial_S\tilde{f}^{(r-1)}-\sum\limits_{\varrho=0}^{r-2}\tilde{\partial}_t^{(r-1-\varrho)}f^{(\varrho)}-\sum\limits_{\varrho=1}^{r-1}\tilde{\phi}^{(\varrho)}\partial_t^{(r-1-\varrho)}f^{(0)}-\\
\quad -\sum\limits_{\varrho=1}^{r-2}\tilde{\phi}^{(\varrho)}\tilde{\partial}_t^{(r-1-\varrho)}f^{(0)}+\sum\limits_{\varrho=1}^{r-1}J(\varrho,\widetilde{r-\varrho};\tilde{\varrho},r-\varrho;\tilde{\varrho},\widetilde{r-\varrho})\}
\end{array}\right.
$$

and $\tilde{\phi}^{(r)}$ depend parametrically on $\mathbf{r}$. The initial condition (4.4) can again be imposed on $\tilde{\phi}^{(1)}$ alone:

$$
(4.19)\qquad \tilde{\phi}^{(r)}(\mathbf{c};\mathbf{r};t=0)=\tilde{\phi}(0)\delta_{r0}.
$$

Normalization of $\phi^{(r)}$ must take place according to (4.14b):

$$
(4.20)\qquad (\tilde{\phi}^{(r)},\chi^{[0\lambda]})=0.
$$

If we now develop all functions occurring in the general eq. (4.17b) in eigenfunctions $\chi^{[\omega\lambda]}$ of Ω, $\partial_t\tilde{\phi}^{(r)}$ will not contain collisional invariants $\chi^{[0\lambda]}$ because, by (4.20), $\tilde{\phi}^{(r)}$ does not at any time, and $\Omega\tilde{\phi}^{(r)}$ is of course orthogonal to $\chi^{[0\lambda]}$, so that again

$$
(4.21)\qquad (\tilde{F}^{(r)},\chi^{[0\lambda]})=0
$$

is a condition of solubility. As in the ChE case, (4.21) for a given r is proved by the aid of (4.20) for $1, 2, \ldots, r-1$, as follows:

$$
(4.22)\quad \left\{\begin{array}{l}
(\tilde{F}^{(r)},\chi^{[0\lambda]})=\int d\mathbf{c}\,\chi^{[0\lambda]}\partial_S\tilde{f}^{(r-1)}-\sum\limits_{\varrho=0}^{r-2}\int d\mathbf{c}\,\chi^{[0\lambda]}\tilde{\partial}_t^{(r-1-\varrho)}f^{(\varrho)}-\\
\quad -\sum\limits_{\varrho=1}^{r-1}\int d\mathbf{c}\,\chi^{[0\lambda]}\tilde{\phi}^{(\varrho)}\partial_t^{(r-1-\varrho)}f^{(0)}-\sum\limits_{\varrho=1}^{r-2}\int d\mathbf{c}\,\chi^{[0\lambda]}\tilde{\phi}^{(\varrho)}\tilde{\partial}_t^{(r-1-\varrho)}f^{(0)}+\\
\quad +\sum\limits_{\varrho=1}^{r-1}\int d\mathbf{c}\,\chi^{[0\lambda]}\cdot J(\varrho,\widetilde{r-\varrho};\tilde{\varrho},r-\varrho;\tilde{\varrho},\widetilde{r-\varrho})=\\
\quad =(\mathrm{I})+(\mathrm{II})+(\mathrm{III})+(\mathrm{IV})+(\mathrm{V}),
\end{array}\right.
$$

in which we work out the single terms as follows:

$$
\left.\begin{aligned}
&\text{(I)} \quad = \tilde{\partial}_t{}^{(r-1)}\psi^{[\lambda]} \qquad \text{by (4.13d)};\\
&\text{(II)} \quad = -\sum_{\varrho=0}^{r-2}\sum_{\lambda'} \tilde{\partial}_t{}^{(r-1-\varrho)}\psi^{[\lambda']}\frac{\partial}{\partial\psi^{[\lambda']}}\int d\mathbf{c}\;\chi^{[0\lambda]}f^{(\varrho)} \qquad \text{by (4.15b)}\\
&\qquad\quad = -\tilde{\partial}_t{}^{(r-1)}\psi^{[\lambda]} \qquad \text{(see 2: 52, 53)};\\
&\text{(III)} = -\sum_{\varrho=1}^{r-1}\sum_{\lambda'} \partial_t{}^{(r-1-\varrho)}\psi^{[\lambda']}\frac{\partial}{\partial\psi^{[\lambda']}}\int d\mathbf{c}\;\tilde{\phi}^{(\varrho)}\chi^{[0\lambda]}f^{(0)} \qquad \text{by (4.13c)}\\
&\qquad\quad = 0 \text{ by (4.14b)};\\
&\text{(IV)} = -\sum_{\varrho=1}^{r-2}\sum_{\lambda'} \tilde{\partial}_t{}^{(r-1-\varrho)}\psi^{[\lambda']}\frac{\partial}{\partial\psi^{[\lambda']}}\int d\mathbf{c}\;\tilde{\phi}^{(\varrho)}\chi^{[0\lambda]}f^{(0)} \qquad \text{by (4.13d)}\\
&\qquad\quad = 0, \text{ again by (4.14b)};\\
&\text{(V)} \quad = 0, \text{ by (2: 9, 51)}.
\end{aligned}\right\} \tag{4.23}
$$

So finally (I) + (II) = 0, which proves (4.21).

We conclude that the equations (4.17), with the normalization (4.20), the solubility conditions (4.21) and the initial condition (4.19) – normalized by (4.6) – have exactly the same character as the corresponding expressions for the $\boldsymbol{r}$-independent case (3: 13, 17, 16, 15, 18), the only differences being (a) that all functions depend parametrically on $\boldsymbol{r}$, and (b) that $\widetilde{F}^{(r)}$ in the present case (4.18) is still more cumbersome to compute than the spatially uniform $\widetilde{F}^{(r)}$ defined in (3.14). In fact, $\widetilde{F}^{(r)}$ as determined from $f^{(0)}, f^{(1)}, \ldots, \tilde{f}^{(r-1)}$ now contains terms linear in the $\tilde{f}^{(\varrho)}$ as well as quadratic, so that already the expansion of $\widetilde{F}^{(2)}$ in decreasing e-powers (3.25):

$$\widetilde{F}^{(2)} = \sum_{\bar{\omega}} G^{(2)[\bar{\omega}]}\, e^{-\bar{\omega}t}$$

will contain $\bar{\omega}$-values which are simple eigenvalues ω, as well as binary sums of these ω. However, the occurrence of simple ω values among the sums $\bar{\omega}$ has already been taken into account in the treatment of ch. 3, so that the results obtained there fully apply to the present, $\boldsymbol{r}$-dependent case.

The terms of the deviation of f from a normal distribution of ChE type: $\tilde{f} = f - f^{\mathrm{Ch}}$, thus decay according to equations like:

(3.24) for $\tilde{\phi}^{(1)}$;
(3: 28, 33, 35) for $\tilde{\phi}^{(2)}$;
(3.37) for $\tilde{\phi}^{(3)}$, etc.

Like in the spatially uniform case (cf. eq. 3.39a), the first-order deviation in $\boldsymbol{r}$ at $t = \tau$; $\mathbf{c} = \mathbf{c}_0$ is of the order-of-magnitude of the initial ($t = 0$) deviation in $\boldsymbol{r}$ at $\mathbf{c} = \mathbf{c}_0$:

$$\tilde{\phi}^{(1)}(\boldsymbol{r}; \mathbf{c}_0; \tau) \approx (1/e)\,\tilde{\phi}(\boldsymbol{r}; \mathbf{c}_0; t = 0) = \tilde{\varphi}(\boldsymbol{r}). \tag{4.24}$$

This time, analogous equations (like 3.39b) for $\tilde{\phi}^{(2)}$ etc. only hold if the terms of each "partial BE" (4.16) are of the same order-of-magnitude,

so that the "θ-procedure" (eqs. 4.13) is not merely formal. Only then the local $\tilde{\varphi}(\boldsymbol{r})$-value serves again as a convergence parameter. This requirement is met if not only the initial $\tilde{\phi}(\boldsymbol{r})$ is comparable to the local Chapman $\phi(\boldsymbol{r})$, but also similar relations hold between successive gradients $(\partial/\partial \boldsymbol{r})$ of $\tilde{\phi}$ and ϕ. This of course limits the range of initial values $\tilde{\phi}(\boldsymbol{r};\ t=0)$, for which the given procedure results in a quickly converging expansion of the distribution function at later times. Physically, this means that, even if the initial $\tilde{\phi}$ is $\ll 1$ everywhere, a smooth approach to the ChE distribution for all $\boldsymbol{r}$ is only guaranteed if restrictions are applied to the gradients of $\tilde{\phi}$ $(t=0)$, whereas, in other cases, local disturbances may travel through the gas before they are eventually damped out. Such processes, though formally covered by our treatment, will be treated with better hope of quick convergence by choosing a different "θ-grouping" method.

As a conclusion to this treatment of the general non-uniform kinetic process, we may say that this theory provides an argument in favour of statements like that of Chapman and Cowling ([2], p. 117), who said that the velocity distribution in a gas, starting at an arbitrary initial value, moves towards a normal value; and that, on physical grounds, this normal distribution has to be the one of ChE, which is fully determined once one knows the five moments $\psi^{[\lambda]}$ as functions of $\boldsymbol{r}$.

(To be continued)

THEORY OF RELAXATION PHENOMENA IN A MONATOMIC GAS. III

BY

M. J. OFFERHAUS

(Communicated by Prof. J. DE BOER at the meeting of October 29, 1960)

5. *Entropy production*

In order to discuss the entropy density and its development in time, we start from the following definitions:

a) *H-function*: as usual in statistical mechanics, we instead of $\mathbf{c}$ take the momentum

$$\mathbf{p} = m\mathbf{c} \tag{5.1}$$

as a variable. In a space of momentum $\mathbf{p}$ and position $\mathbf{r}$, we consider a dimensionless distribution $\bar{f}$, defined by

$$\bar{f}(\mathbf{p}; \mathbf{r}, t)\, d\mathbf{p} \overset{\text{def}}{=} h^3 f(\mathbf{c}; \mathbf{r}, t)\, d\mathbf{c}, \quad \text{or} \quad \bar{f}(\mathbf{p}) \equiv (h/m)^3 f(\mathbf{c}) \tag{5.2}$$

(h = Planck's constant); in terms of this $\bar{f}$, we define the H-function, following PRIGOGINE [8], by

$$H(\mathbf{r}) = -h^{-3} \int d\mathbf{p}\, \bar{f}(1 - \ln \bar{f}), \tag{5.3}$$

or, back in velocity space:

$$H(\mathbf{r}) = -\int d\mathbf{c}\, f\{1 + 3 \ln (m/h) - \ln f\}. \tag{5.4}$$

The integral $\int d\mathbf{r} H$ is dimensionless, so H can be looked upon as the local density of a dimensionless probability function.

b) *S-density*: the entropy per unit volume is defined as

$$s(\mathbf{r}) = -kH(\mathbf{r}) = k \int d\mathbf{c}\, f\{1 + 3 \ln (m/h) - \ln f\}. \tag{5.5}$$

This definition differs from the usual one (with $-f \ln f$ in the integrand) by the addition of $1 + 3 \ln (m/h)$ to $-\ln f$. This choice has the advantage of leading back, in the case of equilibrium, to the Sackur Tetrode formula for the entropy content of an ideal gas in a volume V, as derived by statistical mechanics:

$$S = s^{(0)} V = knV \ln \left\{ (1/n) \left(\frac{2\pi mkT}{h^2} \right)^{3/2} e^{5/2} \right\}. \tag{5.6}$$

We now take a non-equilibrium distribution

$$f(\mathbf{c};\,\mathbf{r},\,t)=f^{(0)}\,(\mathbf{c})\,(1+\phi(\mathbf{c};\,\mathbf{r},\,t)); \tag{5.7}$$

for the time being, ϕ will denote an arbitrary deviation (of ChE type or not) from a local MB distribution. With

$$\ln f^{(0)}=\ln\{n(m/2\pi kT)^{3/2}\}-C^{*2}\equiv\gamma-C^{*2} \tag{5.8}$$

and the expansion

$$\ln(1+\phi)=\phi-\tfrac{1}{2}\phi^2+-\ldots, \tag{5.9}$$

we get the following expression for $s(\mathbf{r})$, in which the integrand has been arranged according to powers of ϕ:

$$\left\{\begin{aligned} s=k\int d\mathbf{c}\,f^{(0)}[\{1+3\ln(m/h)-\gamma+C^{*2}\}+\\ +\phi\{3\ln(m/h)-\gamma+C^{*2}\}-\tfrac{1}{2}\phi^2\pm\ldots]. \end{aligned}\right. \tag{5.10}$$

Now because f and $f^{(0)}$ must have the same first 5 moments $\psi^{[\lambda]}$, ϕ is normalized by

$$\int d\mathbf{c}\,f^{(0)}\phi=\int d\mathbf{c}\,f^{(0)}\phi C^{*2}=0, \tag{5.11}$$

so that the contribution linear in ϕ is zero:

$$\left\{\begin{aligned} s=k\int d\mathbf{c}\,f^{(0)}[\{1+3\ln(m/h)-\gamma+C^{*2}\}-\tfrac{1}{2}\phi^2\pm\ldots]\equiv\\ \equiv s^{(0)}+s^{(2)}+s^{(3)}+\ldots\,. \end{aligned}\right. \tag{5.12}$$

Here, $s^{(0)}$ represents s as found by using only the MB term $f^{(0)}$ of f; $s^{(2)}$ forms a first, essentially non-positive correction. It is easily seen that the insertion of a development for ϕ, like

$$f=f^{(0)}(1+\phi^{(1)}+\phi^{(2)}+\ldots) \tag{5.13}$$

of terms decreasing in order of magnitude leads to the analogous result:

$$s=s^{(0)}-\tfrac{1}{2}\,k\int d\mathbf{c}\,f^{(0)}\phi^{(1)^2}\qquad+\text{higher terms}, \tag{5.14}$$

the contributions of $\phi^{(2)}$, $\phi^{(3)}$ etc. being confined to these higher terms.

The time derivative of s reads:

$$\partial_t s=k\int d\mathbf{c}\,\partial_t f\{3\ln(m/h)-\ln f\}. \tag{5.15}$$

By inserting the BE:

$$\partial_t f=\partial_S f+\partial_C f\qquad(\partial_S f\equiv-\mathbf{c}\cdot\frac{\partial f}{\partial\mathbf{r}}-\mathbf{F}\cdot\frac{\partial f}{\partial\mathbf{c}};\ \partial_C f\equiv J(ff_1)) \tag{5.16}$$

we divide $\partial_t s$ into a *streaming* part:

$$\partial_S s=k\int d\mathbf{c}\,\partial_S f\{3\ln(m/h)-\ln f\}, \tag{5.17}$$

which can have either sign, and a *collision* part:

$$\partial_c s = k \int d\mathbf{c}\, J(ff_1)\{3 \ln (m/h) - \ln f\}; \tag{5.18}$$

the constant $3 \ln (m/h)$ can be omitted on account of (2.9):

$$\partial_c s = -k \int d\mathbf{c}\, J(ff_1) \ln f. \tag{5.19}$$

In the usual proof of the H-theorem (see, *e.g.* [2], p. 69), it is shown that this integral is essentially $\leqslant 0$, so that

$$\partial_c s \geqslant 0. \tag{5.20}$$

We shall now write $\partial_c s$, as given by (5.20), in terms of ϕ, like we did to s itself in (5.10). Again by (2.9), we diminish $\ln f$ by $\ln f^{(0)}$, which is a collisional invariant (cf. 5.8); $J(f^{(0)}f_1^{(0)})$ is of course zero; develop $\ln (1+\phi)$ in a power series and introduce Ω (cf. 2.32):

$$\partial_c s = k \int d\mathbf{c}\{f^{(0)}\Omega\phi - J(f^{(0)}\phi, f_1^{(0)}\phi_1)\}(\phi - \tfrac{1}{2}\phi^2 + \tfrac{1}{3}\phi^3 - + \ldots). \tag{5.21}$$

For small ϕ,

$$\boxed{\partial_c s \approx k(\phi, \Omega\phi) \quad k(\phi, \phi)} \tag{5.22}$$

(bracket notation introduced in (2.37)), which is $\geqslant 0$, just like the exact $\partial_c s$. In these formulae, ϕ always represents the relative difference between the actual, arbitrarily chosen f and the corresponding local MB distribution (see 5.7). This quantity we called ϕ in the ChE case (ch. 2); $\tilde{\phi}$ in the general uniform case (ch. 3) and $\phi + \tilde{\phi}$ in the general non-uniform case (ch. 4). For each of these cases, numbered III, IIA, II according to the classification of ch. 1, we shall now derive approximative expressions showing how changes of s by streaming and by collisions (5: 17, 18) influence the terms of the series (5.12). To this end, we write down each time:

a) the full time derivatives of the first 2 terms of (5.12), $s^{(0)}$ and $s^{(2)}$;

b) the s- and c-parts of the t-derivative of the full s.

Of course,

$$\partial_t(s^{(0)} + s^{(2)} + s^{(3)} + \ldots) = \partial_s s + \partial_c s \tag{5.23}$$

and we want to compare the separate terms on both sides. For shortness, we will use the abbreviation

$$3 \ln (m/h) - \ln f^{(0)} \equiv K(C). \tag{5.24}$$

K is a dimensionless function of the length C of the vector of relative velocity $\mathbf{C}$, of order-of-magnitude 1, reaching a maximum of about 10 for $C=0$ in a typical case (H_2 at NTP); K is a linear combination of collisional invariants $\chi^{[0\lambda]}$.

III ChE distribution: $f^{(0)}(1+\phi)$

(5.25)

(1) term	(2) explicit expression	(3) approximate value	(4) approximations used	(5) remarks
$\partial_t s^{(0)}$	$k\int d\mathbf{c}\,\partial_t f^{(0)}\cdot K$	$\approx k\int d\mathbf{c}\,\partial_t^{(0)} f^{(0)}(K-\phi)$	$\partial_t f^{(0)} \approx \partial_t^{(0)} f^{(0)}$	$\int d\mathbf{c}\begin{Bmatrix}\partial_t^{(0)} f^{(0)}\\ \partial_t f^{(0)}\end{Bmatrix}\phi=0$, $\{\}$ being collisional invariants
$\partial_t s^{(2)}$	$= -k\int d\mathbf{c}(\frac{1}{2}\partial_t f^{(0)}\phi^2+f^{(0)}\phi\partial_t\phi)$	≈ 0	$\phi \cdot K$ $f^{(0)}\partial_t\phi \cdot\cdot \partial_t f^{(0)}$	$\partial_t s^{(0)}$: (both terms in $\partial_t s^{(2)}$) $=1$: ϕ^2 (order of magn.)
$\partial_S s$	$k\int d\mathbf{c}\,\partial_S\{K-\ln(1+\phi)\}$	$\approx k\int d\mathbf{c}\,\partial_S f^{(0)}(K-\phi)$	$\partial_S f \approx \partial_S f^{(0)}$ $\ln(1-\phi)\approx\phi$	although $\phi \ll 1$, we retain ϕ in $K-\phi$
$\partial_C s$	$= k\int d\mathbf{c}J(ff_1)\{K-\ln(1+\phi)\}$	$\approx k\int d\mathbf{c}(-f^{(0)}\Omega\phi)(K-\phi)$	$J(ff_1)\approx -f^{(0)}\Omega\phi$	although $\int d\mathbf{c}\,Kf^{(0)}\Omega\phi \quad [K,\phi]=0$, we retain K in $K-\phi$.

As to the first remark in column 5,

$$\partial_t f^{(0)} = \sum_\lambda \frac{\partial f^{(0)}}{\partial \psi^{[\lambda]}} \partial_t \psi^{[\lambda]}; \quad \partial_t^{(0)} f^{(0)} = \sum_\lambda \frac{\partial f^{(0)}}{\partial \psi^{[\lambda]}} \partial_t^{(0)} \psi^{[\lambda]}, \tag{5.26}$$

and all 5 $\partial f^{(0)}/\partial \psi^{[\lambda]}$ are some collisional invariant $\chi^{[0\lambda']}$ times $f^{(0)}$. All approximations in column 4 are properties of the ChE correction ϕ, valid in particular if the terms of

$$f^{\mathrm{Ch}} = f^{(0)}(1+\phi) = f^{(0)}(1+\phi^{(1)}+\phi^{(2)}+\ldots) \tag{5.27}$$

converge rapidly. If this is actually the case, we may also suppose ϕ to approximately satisfy the equation for $\phi^{(1)}$, (2.33a):

$$\partial_t^{(0)} f^{(0)} \approx \partial_S f^{(0)} - f^{(0)} \Omega \phi. \tag{5.28}$$

Now it is evident from column 3 that the approximations given in (5.25) for the terms of (5.23) balance. In fact, we conclude:

$$\partial_t s^{(0)} \approx \partial_S s + \partial_C s; \tag{5.29a}$$

$$\partial_t s^{(2)} \approx \partial_t s^{(3)} \ldots \approx 0, \tag{5.29b}$$

with, in particular,

$$\partial_C s \approx k[\phi, \phi]: \tag{5.29c}$$

at all times, $s^{(0)}$ exceeds $s^{(2)}$ by two orders-of-magnitude; changes in s both by streaming and by collision are mainly used to adapt $s^{(0)}$ to the changes in $f^{(0)}$ during the HD development.

As we already stated, the sign of $\partial_S s$ depends on the case considered. In a typical transport experiment, during which a gradient is maintained, it will even be negative, because streaming has to make up for the constant increase of s by collisions (5.29c). As an example, in the case of heat transport $\boldsymbol{q}$ down a constant temperature gradient ∇T, the values of column 3 read:

$$\partial_t s^{(0)} = \partial_t s^{(2)} = 0; \quad \partial_S s = -T^{-1} \boldsymbol{q} \cdot \nabla T = -\lambda (\nabla \ln T)^2; \quad \partial_C s = +\lambda (\nabla \ln T)^2 \tag{5.30}$$

(λ = coefficient of heat conductivity).

For a detailed discussion of the entropy production in the ChE case, and of the restrictions on the validity of the approximative result (5.29a), see Prigogine [8].

II A. General uniform distribution: $f^{(0)}(1+\tilde{\phi})$

(5.31)

(1) term	(2) explicit expression		(3) approximate or exact value	(4) approximations used	(5) remark
$\partial_t s^{(0)}$	$= k \int d\boldsymbol{c}\, \partial_t f^{(0)} \cdot K$	$=$	0	—	$\partial_t f^{(0)} = 0$
$\partial_t s^{(2)}$	$= k \int d\boldsymbol{c} (\frac{1}{2} \partial_t f^{(0)} \cdot \tilde{\phi}^2 - f^{(0)} \tilde{\phi} \partial_t \tilde{\phi})$	$=$	$k \int d\boldsymbol{c}\, f^{(0)} \tilde{\phi} \partial_t \tilde{\phi}$		$\partial_t f^{(0)} = 0$
$\partial_S s$	$= k \int d\boldsymbol{c}\, \partial_S f \{K - \ln(1+\tilde{\phi})\}$	$=$	0	—	$\partial_S f = 0$
$\partial_C s$	$= k \int d\boldsymbol{c}\, J(ff_1) \{K - \ln(1+\tilde{\phi})\}$	$\approx$	$k \int d\boldsymbol{c}\, f^{(0)} \tilde{\phi} \cdot \Omega \tilde{\phi}$	$J(ff_1) \approx f^{(0)} \Omega \tilde{\phi}$ by (2.9). $\ln(1+\tilde{\phi}) \approx \tilde{\phi}$	$\int d\boldsymbol{c} J(ff_1) K$

The approximations in column 4 rest on $\tilde{\phi} \ll 1$ only. Again, if $\tilde{\phi}$ is expanded in a convergent series:

$$\tilde{\phi} = \tilde{\phi}^{(1)} + \tilde{\phi}^{(2)} + \ldots, \tag{5.32}$$

$\tilde{\phi}$ will approximately satisfy the equation for its first term $\tilde{\phi}^{(1)}$ (3.13a):

$$\partial_t \tilde{\phi} \approx -\Omega\tilde{\phi}, \tag{5.33}$$

so that the balance (5.23) now reads, in detail:

$$\partial_t s^{(0)} = 0;\ \partial_S s = 0;\ \partial_t s^{(2)} \approx \partial_C s, \tag{5.34}$$

with

$$\partial_C s \approx k[\tilde{\phi}, \tilde{\phi}].$$

This time s does not change by streaming. Collisions, however, cause changes in s: not in $s^{(0)}$ which is tied to the constant $f^{(0)}$, but in $s^{(2)}$ which, containing $\tilde{\phi}^{(2)}$, vanishes as $\tilde{\phi}$ dies out by relaxation. (Of course, the same holds for $s^{(3)}$ etc., which contain higher powers of $\tilde{\phi}$). $s^{(2)}$ dies out twice as fast as $\tilde{\phi}$: if the longest-living mode of $\tilde{\phi}$ is (cf. 3.24)

$$\tilde{\phi}^{(1)} \simeq \Psi^{(1)[\omega]}(\mathbf{c}) e^{-\omega t}, \tag{5.35a}$$

then

$$s^{(2)} \simeq \sigma^{(2)[\omega]}(\mathbf{c}) e^{-2\omega t}, \tag{5.35b}$$

in which

$$\sigma^{(2)[\omega]} = -\tfrac{1}{2} k(\Psi^{(1)[\omega]}, \Psi^{(1)[\omega]}). \tag{5.35c}$$

($\simeq$ means: asymptotically equal to).

The formulae of this section may serve to illustrate the usual proofs of the H-theorem (like in [2], p. 69), by giving the behaviour of $\tilde{\phi}$, H and s in detail, for the case of small initial $\tilde{\phi}$.

II. General non-uniform distribution: $f^{(0)}(1+\phi+\tilde{\phi})$

(5.36) (see following page)

This time, the approximations in column 3 satisfy the balance (5.23) if both ϕ and $\tilde{\phi}$ approximately fit the equations for their first terms (5: 28, 33), which is the case if the series developments (5: 27, 32) for f^{Ch} and $\tilde{f}$ both converge reasonably .In detail, we thus find:

(5.37)

$$\begin{cases} \partial_t s^{(0)} \approx \partial_S s + k[\phi, \phi+\tilde{\phi}] \\ \partial_t s^{(2)} \approx k[\tilde{\phi}, \phi \quad \tilde{\phi}] \\ \partial_t s^{(3)} \approx \ldots \approx 0, \\ \partial_C s \approx k[\phi+\tilde{\phi}, \phi+\tilde{\phi}]. \end{cases}$$

with (d)

Conclusions, in this approximation, are: $s^{(0)}$ changes in t owing to both streaming and collisions; $s^{(2)}$ is only influenced by collisions (changes in $s^{(3)}$ and higher terms, although of course present, are not noticeable on

(5.36)

(1) term	(2) explicit expression	(3) approximate value	(4) approximations used	(5) remarks
$\partial_t s^{(0)}$	$= k \int d\mathbf{c}\, \partial_t f^{(0)} \cdot K$	$\approx k \int d\mathbf{c}\, \partial_t^{(0)} f^{(0)} (K - \phi - \tilde{\phi})$	$\partial_t f^{(0)} \approx \partial_t^{(0)} f^{(0)}$	see eqs. (5.25)
$\partial_t s^{(2)}$	$= \begin{matrix} -k \int d\mathbf{c} \{ \frac{1}{2} \partial_t f^{(0)} (\phi + \tilde{\phi})^2 + \\ + f^{(0)} (\phi + \tilde{\phi})\, \partial_t (\phi + \tilde{\phi}) \} \end{matrix}$	$\approx -k \int d\mathbf{c}\, f^{(0)} (\phi + \tilde{\phi})\, \partial_t \phi$	$\phi + \tilde{\phi} \ll K$ $f^{(0)} \partial_t \phi \ll \partial_t f^{(0)}$	
$\partial_s s$	$= k \int d\mathbf{c}\, \partial_s f \{ K - \ln (1 + \phi + \tilde{\phi}) \}$	$\approx k \int d\mathbf{c}\, \partial_s f^{(0)} (K - \phi - \tilde{\phi})$	$\partial_s f \approx \partial_s f^{(0)}$	$\phi + \tilde{\phi}$ retained beside K
			$\ln (1 + \phi + \tilde{\phi}) \approx \phi + \tilde{\phi}$	
$\partial_{ss} s$	$= k \int d\mathbf{c}\, J(f f_1) \{ K - \ln (1 - \phi - \tilde{\phi}) \}$	$\approx \begin{matrix} k \int d\mathbf{c} (-f^{(0)} \Omega \phi)(K - \phi - \tilde{\phi}) \\ + k \int d\mathbf{c} (-f^{(0)} \Omega \tilde{\phi})(-\phi - \tilde{\phi}) \end{matrix}$	$J(f f_1) \approx -f^{(0)} \Omega (\phi + \tilde{\phi})$	one K retained, one K left out (neither K contributes)

the present scale). When $\tilde{\phi}$ has eventually died out, as described in ch. 4, the ordinary ChE balance (5.29) remains.

Comparing the three cases: III, ϕ; IIA, $\tilde{\phi}$; II, $\phi+\tilde{\phi}$, we conclude:

1) In the cases of $s^{(0)}$ changing in time (III, II), $\partial_t s^{(0)}$ contains a "streaming" contribution $\partial_S s$ which can have either sign.

2) The collisional contribution $\partial_C s$, which is essentially positive, finds expression in:

a) an increase $k[\phi, \phi]>0$ in $s^{(0)}$ if $\phi \neq 0$;

b) an increase $k[\tilde{\phi}, \tilde{\phi}]>0$ in $s^{(2)}$ if $\tilde{\phi}\neq 0$, to which should be added

c) equal changes $k[\phi, \tilde{\phi}]=k[\tilde{\phi}, \phi]$ (cf. 2.36b) in both $s^{(0)}$ and $s^{(2)}$, if $\phi \neq 0$ as well as $\tilde{\phi}\neq 0$.

We shall next look at the irreversible entropy production $\partial_S s$ from the viewpoint of the thermodynamics of irreversible processes.

III. ChE distribution $f^{(0)}(1+\phi)$: we introduce transport "forces" X and corresponding "currents" J as follows: for the viscosity,

$$\mathsf{X}_\mu = -\overline{\overline{\nabla \mathbf{c}_0}}^{\circ} \text{ and } \mathsf{J}_\mu = \overset{\circ}{\mathsf{P}} \text{ (tensor of HD pressure)} \tag{5.38}$$

(the symbol $\overline{\overline{\ }}$ serves to symmetrize a tensor: $\overline{\overline{T}}_{\alpha\beta}=\frac{1}{2}(T_{\alpha\beta}+T_{\beta\alpha})$) and for the heat conductivity,

$$\boldsymbol{X}_\lambda = -\nabla \ln T \text{ and } \boldsymbol{J}_\lambda = \boldsymbol{q} \text{ (vector of heat transport).} \tag{5.39}$$

These forces occur in the LHS of the integral equation (2.33a) for $\phi^{(1)}$:

$$(\tfrac{5}{2}-C^{*2})\mathbf{C}\cdot\nabla \ln T - 2\mathbf{C}^*\overset{\circ}{\mathbf{C}}^* : \overline{\overline{\nabla \mathbf{c}_0}}^{\circ} = \Omega\phi^{(1)} \tag{5.40}$$

and, consequently, in the solution

$$\phi^{(1)} = \mathbf{A}\cdot\nabla \ln T + \mathsf{B} : \overline{\overline{\nabla \mathbf{c}_0}}^{\circ}; \tag{5.41}$$

equalizing coefficients of each separate gradient, we have:

$$(\tfrac{5}{2}-C^{*2})\mathbf{C} = \Omega\mathbf{A}; \quad -2\mathbf{C}^*\overset{\circ}{\mathbf{C}}^* = \Omega\mathsf{B}. \tag{5.42}$$

The LHS functions in these integral equations happen to return in the definitions of the currents J; therefore

$$\mathsf{J}_\mu = \overset{\circ}{\mathsf{P}} = -kT(\phi, -2\mathbf{C}^*\overset{\circ}{\mathbf{C}}^*) = -kT[\phi, \mathsf{B}]; \tag{5.43a}$$

$$\boldsymbol{J}_\lambda = \boldsymbol{q} = -kT(\phi, (\tfrac{5}{2}-C^{*2})\mathbf{C}) = -kT[\phi, \mathbf{A}]. \tag{5.43b}$$

Multiply each equation by $1/T$ times the corresponding X and add the results, supposing the $\phi^{(1)}$-equation (5.41) to approximately hold for ϕ:

$$T^{-1}(\mathsf{J}_\mu : \mathsf{X}_\mu + \boldsymbol{J}_\lambda\cdot\boldsymbol{X}_\lambda) \approx k[\phi, \phi] \approx \partial_C s. \tag{5.44}$$

Here the first $\approx$ sign comes in because of the approximation $\phi \approx \phi^{(1)}$; the second one is introduced by the linearization of the collision operator,

which presupposes $\phi \ll 1$. These neglections are both allowed if the series (5.27) is duly convergent.

The irreversible s-production has thus been written as a sum of products of streams and corresponding forces. The balance (5.29) can accordingly also be formulated as:

$$\begin{cases} \partial_t s^{(0)} \approx \partial_S s + T^{-1} \sum JX \\ \partial_t s^{(2)} \approx \ldots \approx 0. \end{cases} \tag{5.45}$$

Using the phenomenological relations, which connect the currents J to the forces by means of the transport coefficients (μ of viscosity, λ of heat conductivity):

$$\begin{cases} \mathsf{J}_\mu = 2\mu \mathsf{X}_\mu = L_{\mu\mu} \mathsf{X}_\mu ; \\ \boldsymbol{J}_\lambda = \lambda T \boldsymbol{X}_\lambda = L_{\lambda\lambda} \boldsymbol{X}_\lambda . \end{cases} \tag{5.46}$$

one can also write $\partial_C s$ in terms of the phenomenological coefficients L:

$$\partial_C s \approx T^{-1} (L_{\mu\mu} \mathsf{X}_\mu^2 + L_{\lambda\lambda} \boldsymbol{X}_\lambda^2). \tag{5.47}$$

II. General $\mathbf{r}$*-dependent distribution* $f^{(0)}(1+\phi+\tilde{\phi})$: As in the ChE case (III), we consider the sum (5.44)

$$T^{-1} (\mathsf{J}_\mu \cdot \mathsf{X}_\mu + \boldsymbol{J}_\lambda \cdot \boldsymbol{X}_\lambda),$$

in which the transport currents now read:

$$\begin{cases} \mathsf{J}_\mu = \mathsf{P} = kT(\phi + \tilde{\phi}, (\tfrac{2}{3} C^* \cdot \mathsf{C}^*)) = kT[\phi + \tilde{\phi}, \mathsf{B}] \\ \boldsymbol{J}_\lambda = \boldsymbol{q} = -kT(\phi + \tilde{\phi}, (\tfrac{5}{2} - C^{*2})\boldsymbol{C}) = -kT[\phi + \tilde{\phi}, \boldsymbol{A}]. \end{cases} \tag{5.48}$$

which leads to

$$T^{-1} \sum JX \approx k[\phi + \tilde{\phi}, \phi] \tag{5.49}$$

instead of (5.44). Comparing this result with the balance (5.37), we see that, like in the ChE case (5.45), $T^{-1} \sum JX$ renders the contribution of collisions to the change in $s^{(0)}$:

$$\partial_t s^{(0)} \approx \partial_S s + T^{-1} \sum JX. \tag{5.50}$$

This latter contribution can now have either sign; together with the collisional change in $s^{(2)}$, of course, it forms $\partial_C s$ which is always positive.

Finally, we point out the following difference between the ChE (ϕ) case and the general ($\phi + \tilde{\phi}$) one: in the ϕ case (5 : 44, 47),

$$\partial_C s = T^{-1} \sum JX = T^{-1} \sum LXX ; \tag{5.51}$$

in the $\phi + \tilde{\phi}$ case, however, these three quantities all differ: (5 : 37d, 49):

$$\partial_C s = k[\phi + \tilde{\phi}, \phi + \tilde{\phi}] \tag{5.52a}$$

$$T^{-1} \sum JX = k[\phi + \tilde{\phi}, \phi] \tag{5.52b}$$

$$T^{-1} \sum LXX = k[\phi, \phi], \tag{5.52c}$$

(c) holding because the relation between the ChE-ϕ and the gradients is the one (5.41) valid in the case of ϕ alone. Looking at eqs. (5.52a, b, c), one is tempted to suggest that $\partial_C s$ could be identified with $T^{-1} \sum L^{-1} JJ$ (L^{-1} being the inverse of the L matrix), but this is not correct.

6. *Transport currents; quasi-relaxation*

We shall now describe the behaviour of the transport currents $\mathsf{J}_\mu = \mathsf{P}$ and $\boldsymbol{J}_\lambda = \boldsymbol{q}$ during the kinetic stage, like we did for the entropy density in the preceding chapter. The treatment will correspond to section II of ch. 5, for we shall immediately consider the general non-uniform distribution $f^{(0)}(1+\phi+\tilde{\phi})$, of which the ϕ- and $\tilde{\phi}$-distributions are, of course, special cases.

We introduce functions G and H as follows:

$$-2\boldsymbol{C}^* \mathring{\boldsymbol{C}}^* = \mathsf{G}_\mu ; \ (\tfrac{5}{2} - C^{*2})\boldsymbol{C} = \boldsymbol{G}_\lambda \tag{6.1}$$

$$\mathsf{H}_\mu = -kT\mathsf{G}_\mu = -m\boldsymbol{C}\mathring{\boldsymbol{C}}; \ \boldsymbol{H}_\lambda = -kT\boldsymbol{G}_\lambda = (\tfrac{1}{2}mC^2 - \tfrac{5}{2}kT)\boldsymbol{C}. \tag{6.2}$$

Using these H, we can write the transport currents J as follows (cf. 5.48):

$$\begin{cases} \mathring{\mathsf{P}} = \mathsf{J}_\mu = \int d\boldsymbol{c}\, f\mathsf{H}_\mu = (\mathsf{H}_\mu, \phi + \tilde{\phi}) \\ \boldsymbol{q} = \boldsymbol{J}_\lambda = \int d\boldsymbol{c}\, f\boldsymbol{H}_\lambda = (\boldsymbol{H}_\lambda, \phi + \tilde{\phi}), \end{cases} \tag{6.3}$$

in which we have omitted terms

$$(\mathsf{H}_\mu, 1) = 0; \qquad (\boldsymbol{H}_\lambda, 1) = 0 \tag{6.4}$$

which vanish because the MB term $f^{(0)}$ does not contribute to $\mathring{\mathsf{P}}$ and $\boldsymbol{q}$ (cf. 2.24).

Apparently, both currents J consist of the ChE contribution (H, ϕ) + a deviation $(H, \tilde{\phi})$ which, like $\tilde{\phi}$ itself, dies out during the kinetic stage. A formal expression for the t-dependence of J will be given later (see 6.14a).

Next, we make a division of the derivative $\partial_t J$, in the way we did for $\partial_t s$ in (5: 17, 18):

$$\partial_t J = \partial_t \int d\boldsymbol{c}\, fH = \int d\boldsymbol{c}\, (\partial_S f + \partial_C f)H + \int d\boldsymbol{c}\, f\, \partial_t H = \partial_S J + \partial_C J + \partial_H J ; \tag{6.5}$$

here $\partial_S J$ derives from changes in f by streaming; $\partial_C J$ from changes in f by collisions; $\partial_H J$ comes in because H_μ and $\boldsymbol{H}_\lambda$ are functions of $\boldsymbol{c}$ depending parametrically on the moments ψ (from (6.2) it is seen that H_μ contains $\boldsymbol{c}_0$, $\boldsymbol{H}_\lambda$ contains both $\boldsymbol{c}_0$ and T); hence:

$$\partial_t H(\boldsymbol{c}; \psi^{[\lambda]}) = \sum_\lambda \frac{\partial H}{\partial \psi^{[\lambda]}} \partial_t \psi^{[\lambda]}. \tag{6.6}$$

We now make approximations for the terms of (6.5), just like we did for $\partial_t s$ in (5.36):

(6.7)

(1) term	(2) explicit expression	(3) approximate value	(4) approximations used
$\partial_t J$	$= \int d\mathbf{c}\, \partial_t (fH) \approx \int d\mathbf{c}\, f^{(0)} H \partial_t \tilde{\phi}$		$\phi + \tilde{\phi} \ll 1$; $f^{(0)} \partial_t \phi \ll \partial_t f^{(0)}$; $\partial_t \begin{Bmatrix} f^{(0)} \\ H \end{Bmatrix} \approx \partial_t^{(0)}$
$\partial_S J$	$= \int d\mathbf{c}\, \partial_S f \cdot H \approx f \int d\mathbf{c}\, \partial_S f^{(0)} \cdot H$		$\partial_S f \approx \partial_S f^{(0)}$
$\partial_C J$	$= \int d\mathbf{c} J(ff_1) H \approx \int d\mathbf{c}\, \{-f^{(0)} \Omega(\phi + \tilde{\phi})\} H$		$J(ff_1) \approx -f^{(0)} \Omega(\phi + \tilde{\phi})$
$\partial_H J$	$= \int d\mathbf{c}\, f\, \partial_t H \approx \int d\mathbf{c}\, f^{(0)}\, \partial_t^{(0)} H$		$\phi + \tilde{\phi} \ll 1$; $\partial_t H \approx \partial_t^{(0)} H$.

Here $\partial_t^{(0)}$ applied to a function $u(\mathbf{c}; \psi)$ has the meaning given in (2.28), where $\partial_t^{(s)}$ applied to a functional $u(\mathbf{c}|\psi)$ was defined; in this simple case,

$$\partial_t^{(0)} u(\mathbf{c}; \psi) = \sum_\lambda \frac{\partial u}{\partial \psi^{[\lambda]}} \partial_t^{(0)} \psi^{[\lambda]}. \tag{6.8}$$

If $\phi + \tilde{\phi} \ll 1$ as supposed, the differences $\partial_t \psi - \partial_t^{(0)} \psi$ and $\partial_t u - \partial_t^{(0)} u$ are relatively small for any u. This and the other approximations of column 4 lead to the result for $\partial_t J$ given in column 3 of (6.7) in the following way:

$$\begin{aligned} \partial_t J &\approx \int d\mathbf{c} [H\{(1-\phi-\tilde{\phi})\partial_t f^{(0)} - f^{(0)} \partial_t \phi - f^{(0)} \partial_t \tilde{\phi}\} - f^{(0)}(1-\phi-\tilde{\phi}) \partial_t H] \\ &\approx \int d\mathbf{c} \{\partial_t^{(0)}(f^{(0)} H) + f^{(0)} H \partial_t \tilde{\phi}\} = \partial_t^{(0)}(H, 1) + (H, \partial_t \tilde{\phi}), \end{aligned} \tag{6.9}$$

of which the first term vanishes by (6.4).

Resuming (6.7) and combining the ∂_S and ∂_H contributions, which are both, in a sense, streaming effects, we find:

$$\begin{aligned} (\partial_S + \partial_H) J &\approx \int d\mathbf{c}\, H(\partial_S f^{(0)} - \partial_t^{(0)} f^{(0)}) = (H, F^{(1)}) \\ \partial_C J &\approx -(H, \Omega[\phi + \tilde{\phi}]) \\ \hline \partial_t J &\approx (H, \partial_t \tilde{\phi}). \end{aligned} \tag{6.10}$$

Here $F^{(1)}$ is the LHS (2.34a) of the integral equation (2.33a) for $\phi^{(1)}$; like the $\partial_t s$-balance (5.36), the present one is in order on condition that ϕ approximately satisfies the $\phi^{(1)}$-equation and $\tilde{\phi}$ the one for $\tilde{\phi}^{(1)}$ (eqs. 5 : 28, 33), i.e. on condition that the series developments of ϕ and $\tilde{\phi}$ are both reasonably convergent. This leads to the following survey, listing the terms of (6.10) for each of the 3 distributions treated in chs. 2, 3, 4:

(6.11)

stage	II A	II	III
distr.	$\tilde{\phi}$	$\phi + \tilde{\phi}$	ϕ
$(\partial_S + \partial_H) J$	0	$[H, \phi]$	
$\partial_C J$	$-[H, \tilde{\phi}]$	$-[H, \phi + \tilde{\phi}]$	$-[H, \phi]$
$\partial_t J$	$[H, \tilde{\phi}]$		0

We draw the following conclusions with regard to the development of $J=(H, \phi+\tilde{\phi})$ in time (stages indicated by roman numerals as in chs. 1 and 5):

II A. Kinetic stage in a spatially uniform gas, $\tilde{\phi}$ only: J is not changed by streaming, but collisions cause a change in J to the amount

$$\partial_t (H, \tilde{\phi}) \approx -[H, \tilde{\phi}] \ . \tag{6.12a}$$

This equation indicates that J dies out due to a relaxation process, to which we shall return presently.

II. Kinetic process in a non-uniform gas, $\phi+\tilde{\phi}$: streaming changes tend to build up J during the kinetic stage at a constant rate depending on the existing ψ gradients:

$$(\partial_S+\partial_H) J \approx (H, F^{(1)}) \approx [H, \phi] \tag{6.11a}$$

but collisions try to annihilate J at a rate increasing together with the value of J itself:

$$\boxed{\partial_C (H, \phi \quad \tilde{\phi}) \approx \quad [H, \phi \cdot \tilde{\phi}].} \tag{6.12b}$$

Together,

$$\partial_t J \approx -[H, \tilde{\phi}]. \tag{6.11b}$$

ϕ does not change but $\tilde{\phi}$ dies out rapidly.

III. As the kinetic stage comes to an end and the next (HD) stage sets in,

$$\partial_C J \approx -[H, \phi] \approx -(\partial_S+\partial_H) J: \tag{6.12c}$$

streaming and collision contributions cancel. As f reaches the ChE value, the transport J reaches the HD value (H, ϕ).

In each of these 3 cases, the collisional derivatives of J are related to J itself by equations of the same type (6.12a, b, c). Only in case II A collisions are not counteracted by streaming; in case II there is such a counteraction, in case III there is even a balance. We would like therefore to indicate the phenomenon of (6.12) as *quasi-relaxation*.

The implications of eq. (6.12b) will become clearer if, using the approximations $\phi \approx \phi^{(1)}$ and $\tilde{\phi} \approx \tilde{\phi}^{(1)}$ also in J itself, we develop $\phi^{(1)}$, $\tilde{\phi}^{(1)}$ and H in Ω-eigenfunctions χ. As for H,

$$H(\mathbf{c}) = \sum_{\omega} \sum_{\lambda} h^{[\omega\lambda]} \chi^{[\omega\lambda]} \text{ with } h^{[\omega\lambda]} = (H, \chi^{[\omega\lambda]}), \tag{6.13}$$

in which, as usual, $\omega > 0$, because all H are orthogonal to the collision-invariant functions $\chi^{[0\lambda]}$ of (2.44). The developments of $\phi^{(1)}$ and $\tilde{\phi}^{(1)}$ are given in (2.47) and (3.24):

$$\phi^{(1)} = \sum_{\omega} \sum_{\lambda} (1/\omega) f^{(1)[\omega\lambda]} \chi^{[\omega\lambda]}; \ \tilde{\phi}^{(1)} = \sum_{\omega} \sum_{\lambda} \tilde{\phi}^{[\omega\lambda]} e^{-\omega t} \chi^{[\omega\lambda]};$$

they contain the χ-series coefficients of $F^{(1)}$ and of $\tilde{\phi}(t=0)$. Substitution of these series into (6.3) and (6.12b) gives:

$$J \approx \sum_{\omega}\sum_{\lambda}\{(1/\omega)\, f^{(1)[\omega\lambda]} + \tilde{q}^{[\omega\lambda]} e^{-\omega t}\}\, h^{[\omega\lambda]} \equiv \sum_{\omega}\sum_{\lambda} J^{[\omega\lambda]}; \tag{6.14a}$$

$$\partial_C J \approx -\sum_{\omega}\sum_{\lambda}(f^{(1)[\omega\lambda]} + \tilde{q}^{[\omega\lambda]}\omega e^{-\omega t})h^{[\omega\lambda]} \equiv \sum_{\omega}\sum_{\lambda}(\partial_C J)^{[\omega\lambda]}; \tag{6.14b}$$

here, J and $\partial_C J$ have been written as sums of „modes", of which the one numbered $\omega\lambda$ decays according to the relaxation equation

$$(\partial_C J)^{[\omega\lambda]} = -\omega J^{[\omega\lambda]}. \tag{6.15}$$

Again, $1/\omega$ assumes the role of a relaxation time for the $\omega\lambda$ mode. In the next chapter we will give one-term approximations to the developments (6.13) of both H_μ and $\boldsymbol{H}_\lambda$, which of course greatly simplify matters, leaving us with two quasi-relaxation times $1/\omega$ only, one for $\mathring{\mathsf{P}}$ and one for $\boldsymbol{q}$ (τ_μ and τ_λ).

Mention of something like this quasi-relaxation was first made by Kohler [6], who dealt with the change-by-collisions of the 3 quantities

$$\theta_\alpha = (m/k)\int d\mathbf{c}\, f(C_\alpha^2 - \tfrac{1}{3}C^2) \qquad (\alpha = x, y, z) \tag{6.16}$$

which he characterized as $T_\alpha - T$, the excess of the "temperature" T_α of the α-component of heat motion over $T = \frac{1}{3}\sum_\alpha T_\alpha$, during the HD stage. Clearly

$$k(T - T_\alpha) = \mathring{P}_{\alpha\alpha}, \tag{6.17}$$

the diagonal element of the HD pressure; therefore Kohler's result is contained in the present treatment. From his formula, reading in our notation:

$$\partial_C \theta_\alpha = -\theta_\alpha/\tau_\mu \tag{6.18}$$

Kohler concludes:

a) τ_μ measures the speed of mutual exchange of energy between the degrees of freedom α;

b) the viscosity μ arises as a consequence of the finite time of establishment of the "one-direction-temperatures" θ_α.

Instead, we would prefer the following statements:

a) The quasi-relaxation phenomenon involving the *second*-degree moment $\mathring{\mathsf{P}}$ has to do with the transport of a *first*-degree function of $\mathbf{C}$, i.e. with the transport of momentum. τ_λ measures the speed of the exchange of momentum in one direction α between colliding molecules, like τ_μ measures the transport of kinetic energy;

b) the viscosity μ results from the equilibrium between increase (by streaming) and breakdown (by collisions) of the pressure tensor P.

Incidentally, Kohler complicates his argument unnecessarily by the use of so-called main axes (a system in which the $\mathbf{c}_0$ tensor is diagonal).

(To be continued)

THEORY OF RELAXATION PHENOMENA IN A MONATOMIC GAS. IV

BY

M. J. OFFERHAUS

(Communicated by Prof. J. DE BOER at the meeting of October 29, 1960)

7. *Collision operator; time scale of the kinetic stage*

Numerical description of the relaxation processes discussed in the preceding chapters requires solving the eigenvalue problem of the Ω operator (2.39). The results will largely depend on the nature of the (spherically symmetric) intermolecular potential field, $V(r)$, and, for general V, no complete solutions are known. There is one property of this general solution, however, which follows from the invariance of Ω with respect to rotations in $\mathbf{c}$ space about the point $\mathbf{c}_0$. It is easier to consider Ω as an integral operator in $\mathbf{C}$ space, invariant under rotations about the origin. Choosing polar coordinates C, θ, φ, it is easy to prove the following statements:

1) The matrix of Ω in a representation in spherical harmonics $Y_{lm}(\theta\varphi)$:

$$\int \sin\theta d\theta \int d\varphi Y^*_{l'm'}(\theta\varphi)\Omega Y_{lm}(\theta\varphi) \tag{7.1}$$

is diagonal with respect to l; the diagonal elements, $\Omega^{(l)}$, which are integral operators in one-dimensional C space, do not depend on m.

2) If $\Omega^{(l)}$ has eigenfunctions $\xi^{(lr)}$ with corresponding eigenvalues $\omega^{(lr)}$:

$$\Omega^{(l)}\xi^{(lr)} = \omega^{(lr)}\xi^{(lr)}, \tag{7.2}$$

Ω has these $\omega^{(lr)}$ as its eigenvalues with, as corresponding eigenfunctions, the products ξY:

$$\Omega[\xi^{(lr)}(C)Y_{lm}(\theta\varphi)] = \omega^{(lr)}\xi^{(lr)}(C)Y_{lm}(\theta\varphi) \quad (m=-l, -l+1, \ldots, +l). \tag{7.3}$$

Thus the Ω eigenvalue problem in $\mathbf{C}$ space is reduced to the $\Omega^{(l)}$-problem in C space, which does not make things easier; more important, the angle-dependent part of each eigenfunction χ appears to be a spherical harmonic. Each $\omega^{(lr)}$ is $(2l+1)$-fold degenerate, to begin with; further degeneration is still possible, because ω with different (lr) may coincide.

This is illustrated by the one case in which the Ω-problem has been solved: that of a *Maxwellian gas* (subscript M), in which the molecules repel each other according to

$$V_{\mathrm{M}}(r) = \varkappa/r^4. \tag{7.4}$$

The solution for the Maxwell case, which was first indicated by MAXWELL himself, has been elaborated, using different methods, by WALDMANN ([4], p. 370) and WANG CHANG & UHLENBECK [7]. The general eigenfunction of $\Omega_M^{(l)}$ reads:

$$\xi_M^{(lr)} = C^{*l} S_{l+\frac{1}{2}}^{(r)}(C^{*2}) \tag{7.5}$$

(the $S(x)$ are Sonine polynoms, a special choice of associated Laguerre polynoms). We quote the lowest 3 eigenvalues, with the corresponding eigenfunctions, in the following table (neither Y nor $\chi = \xi Y$ are normalized):

TABLE 1

ω_M	lr	$\xi_M^{(lr)}$	Y_{lm}	degeneracy ν
$\omega_0 = 0$	00	1	Y_{00}	$\nu_0 = 5$
	01	$\frac{3}{2} - C^{*2}$	Y_{00}	
	10	1	$Y_{11,10,1-1}$	
$\omega_{1M} = 1.374\, n\sqrt{2\varkappa/m}$	02	$\frac{15}{8} - \frac{5}{2}C^{*2} + \frac{1}{2}C^{*4}$	Y_{00}	$\nu_1 = 4$
	11	$C^*\left(\frac{5}{2} - C^{*2}\right)$	$Y_{11,10,1-1}$	
$\omega_{2M} = 2.062\, n\sqrt{2\varkappa/m}$ $= \frac{3}{2}\omega_{1M}$	03	$\frac{35}{16} - \frac{35}{8}C^{*2} + \frac{7}{4}C^{*4} - \frac{1}{6}C^{*6}$	Y_{00}	$\nu_2 = 9$
	12	$C^*\left(\frac{35}{8} - \frac{7}{2}C^{*2} + \frac{1}{2}C^{*4}\right)$	$Y_{11,10,1-1}$	
	20	C^{*2}	$Y_{22,21,20,2-1,2-2}$	

The $\omega_0 = 0$ entry with $\nu_0 = 5$ is, of course, common to all potentials $V(r)$. The degeneracies of the next two eigenvalues ω_{1M} and ω_{2M}: $\nu_1 = 4$ and $\nu_2 = 9$, probably are special characteristics of the Maxwell gas. We find, in particular, that the 3 components of the $\mathbf{G}_\lambda$ or $\mathbf{H}_\lambda$ vectors (see 6: 1, 2) are linear combinations of the 3 functions $\xi_M^{(11)} Y_{1m}$, whereas the 9 components of the G_μ or H_μ tensors (see again 6: 1, 2), of which 5 are independent, are all combinations of the 5 functions $\xi_M^{(20)} Y_{2m}$. Thus:

$$\Omega_M \mathbf{G}_\lambda = \omega_{1M} \mathbf{G}_\lambda;\ \Omega_M G_\mu = \omega_{2M} G_\mu. \tag{7.6}$$

Owing to these properties of the Maxwell gas, many expressions given on the preceding pages become especially simple and elegant; *e.g.*,

1) the integral equations (5.42)

$$\mathbf{G}_\lambda = \Omega_M \mathbf{A};\ G_\mu = \Omega_M B$$

are satisfied by

$$\mathbf{A} = (1/\omega_{1M})\mathbf{G}_\lambda;\ B = (1/\omega_{2M}) G_\mu; \tag{7.7}$$

hence, the ChE *distribution*, first approximation (5.41) reads:

$$\phi^{(1)} = (1/\omega_{1M})\mathbf{G}_\lambda \cdot \nabla \ln T + (1/\omega_{2M}) G_\mu : \overline{\overline{\nabla \mathbf{c}_0}}. \tag{7.8}$$

2) The *transport* currents in the HD stage read (5.43):

$$\left\{\begin{aligned} &\boldsymbol{q}^{(1)} = \boldsymbol{J}_\lambda^{(1)} = (\boldsymbol{H}_\lambda, \phi^{(1)}) = -\frac{kT}{\omega_{1\mathrm{M}}}(\boldsymbol{G}_\lambda, \boldsymbol{G}_\lambda \cdot \nabla \ln T) = \\ &\qquad -\frac{kT}{3\omega_{1\mathrm{M}}}\nabla \ln T(\boldsymbol{G}_\lambda, \boldsymbol{G}_\lambda) = -\frac{5}{2}\frac{nk^2T}{m\omega_{1\mathrm{M}}}\nabla T = -\lambda \nabla T; \\ &\overset{\circ}{\mathsf{P}}{}^{(1)} = \mathsf{J}_\mu^{(1)} = (\mathsf{H}_\mu, \phi^{(1)}) = -\frac{kT}{\omega_{2\mathrm{M}}}(\mathsf{G}_\mu, \mathsf{G}_\mu : \overset{\circ}{\overline{\overline{\nabla \boldsymbol{c}_0}}}) = \\ &\qquad = -\frac{kT}{5\omega_{2\mathrm{M}}}\overset{\circ}{\overline{\overline{\nabla \boldsymbol{c}_0}}}(\mathsf{G}_\mu, \mathsf{G}_\mu) = -2\frac{nkT}{\omega_{2\mathrm{M}}}\overset{\circ}{\overline{\overline{\nabla \boldsymbol{c}_0}}} = -2\mu\overset{\circ}{\overline{\overline{\nabla \boldsymbol{c}_0}}}; \end{aligned}\right. \tag{7.9a}$$

apparently, the coefficients of heat conductivity and viscosity are expressed in terms of the eigenvalues ω_{M} by

$$\lambda = \frac{5}{2}\frac{nk^2T}{m\omega_{1\mathrm{M}}}; \qquad \mu = \frac{nkT}{\omega_{2\mathrm{M}}}. \tag{7.10}$$

In (7.9), use has been made of the following values of scalar products:

$$(\boldsymbol{G}_\lambda, \boldsymbol{G}_\lambda) = \frac{15}{2}\frac{nkT}{m}; \qquad (\mathsf{G}_\mu, \mathsf{G}_\mu) = 10\, n. \tag{7.11}$$

3) Each component of both $\boldsymbol{H}_\lambda$ and H_μ, being an eigenfunction of Ω_{M}, has a χ-development (6.13) consisting of one term only; the same is true for the developments (6.14a, b) of J and $\partial_{\mathrm{C}}J$. Consequently the *quasi-relaxation* of $\boldsymbol{J}_\lambda$ and J_μ due to collisions is described by equations of the type (6.15):

$$\partial_{\mathrm{C}}\boldsymbol{J}_\lambda = -\omega_{\mathrm{M}}\boldsymbol{J}_\lambda; \quad \partial_{\mathrm{C}}\mathsf{J}_\mu = -\omega_{2\mathrm{M}}\mathsf{J}_\mu. \tag{7.12}$$

So we can interpret $1/\omega_{1\mathrm{M}}$ and $1/\omega_{2\mathrm{M}}$ as the relaxation times connected with the transport of heat and that of momentum:

$$1/\omega_{1\mathrm{M}} = \tau_\lambda; \quad 1/\omega_{2\mathrm{M}} = \tau_\mu (= \tfrac{2}{3}\tau_\lambda). \tag{7.13}$$

Using these relaxation times τ as well as the transport forces X (see 5 : 38, 39), we can write eq. (5.40) and its solution (7.8) as follows:

$$-\boldsymbol{G}_\lambda \cdot \boldsymbol{X}_\lambda - \mathsf{G}_\mu : \mathsf{X}_\mu = \Omega_{\mathrm{M}}\phi^{(1)}; \tag{7.14}$$

$$\phi^{(1)} = -\tau_\lambda \boldsymbol{G}_\lambda \cdot \boldsymbol{X}_\lambda - \tau_\mu \mathsf{G}_\mu : \mathsf{X}_\mu. \tag{7.15}$$

Finally we introduce τ_λ and τ_μ in the transport coefficients (7.10):

$$\lambda = \frac{5}{2}\frac{nk^2T}{m} \cdot \tau_\lambda; \quad \mu = nkT \cdot \tau_\mu. \tag{7.16}$$

4) As we have remarked at the end of ch. 3, the inverse of the lowest positive eigenvalue ω_1 has the meaning of a *relaxation* time for the decay of ϕ during the kinetic stage. In a Maxwell gas,

$$\tau = \frac{1}{\omega_{1\mathrm{M}}} = \frac{1}{1.374\, n}\sqrt{\frac{m}{2\varkappa}} = \tau_\lambda. \tag{7.17}$$

This time $\tau \approx$ the mean time between successive collisions. To recognize this, consider a pair of molecules moving towards each other: relative distance $= r$; reduced mass governing relative motion $= \frac{1}{2}m$; initially ($r = \infty$), kinetic energy of relative motion $= \varepsilon$ and velocity of this motion: $v = (4\varepsilon/m)^{\frac{1}{2}}$. They can get as near as $r = \sigma = (\varkappa/\varepsilon)^{\frac{1}{2}}$ (see 7.4). Apparently for particles with thermal velocity (for pairs or single particles) $\approx v$, the potential field acts as if they were hard spheres of diameter σ, for which, as is well known, the mean free path $l \approx 1/n\sigma^2$. The mean time between successive collisions is estimated by

$$\tau_C \approx \frac{l}{v} \approx \frac{1}{n\sigma^2}\sqrt{\frac{m}{4\varepsilon}} = \frac{1}{n}\sqrt{\frac{m}{4\varkappa}}. \tag{7.17a}$$

which is of the same order-of-magnitude as τ (7.17). Incidentally, τ_C does not depend on ε: for a Maxwell gas, both τ and τ_C are independent of temperature.

We now return to the Ω problem for the non-Maxwellian *general intermolecular potential*. Several properties of Ω, of its eigenvalues ω and -functions χ have already been mentioned in ch. 2 (eqs. 2: 35–45) and at the beginning of the present chapter (eqs. 7: 1–3). We do not know ω and χ but we do have at our disposal some scalar products

$$(\chi_M^{[\omega\lambda]}, \Omega\chi_M^{[\omega'\lambda']}) \equiv [\chi_M^{[\omega\lambda]}, \chi_M^{[\omega'\lambda']}],$$

matrix elements of the general Ω in a representation of functions χ_M, the eigenfunctions of the Maxwellian Ω (see e.g. [2], p. 161; [3], p. 511), which have been calculated for use in the determination of the transport coefficients. The number of available elements, however, is far too small to make possible a diagonalization of the Ω matrix. Of course, this matrix has a first row and a first column ($\omega = 0$; $\omega' = 0$) consisting of zero elements; among the first non-zero elements are the following two:

$$\begin{cases} (\mathsf{G}_\lambda, \Omega\mathsf{G}_\lambda) \equiv [\mathsf{G}_\lambda, \mathsf{G}_\lambda] = \sqrt{\frac{kT}{m}}\, \Omega^{(1,1)} \\ (\mathsf{G}_\mu, \Omega\mathsf{G}_\mu) \equiv [\mathsf{G}_\mu, \mathsf{G}_\mu] = 16\, n^2\, \Omega^{(2,2)}. \end{cases} \tag{7.18}$$

Here $\Omega^{(2,2)}$ is a temperature-dependent average "cross-section", according to the definition of $\Omega^{(r,s)}$ in [2], p. 157 ($\Omega^{(r)}(s)$ in the notation of this reference; for a discrepancy between definitions of square bracket expressions, see (2.37)), of dimension r^3/t; the matrix elements of the normalized functions are, of course (cf. 7.11):

$$\omega_\lambda \equiv \frac{[\mathsf{G}_\lambda, \mathsf{G}_\lambda]}{(\mathsf{G}_\lambda, \mathsf{G}_\lambda)} = \frac{16}{15} n\Omega^{(2,2)}; \omega_\mu \equiv \frac{[\mathsf{G}_\mu, \mathsf{G}_\mu]}{(\mathsf{G}_\mu, \mathsf{G}_\mu)} = \frac{8}{5} n\Omega^{(2,2)} = \frac{3}{2}\omega_\lambda. \tag{7.19}$$

The matrix elements ω_λ and ω_μ, of dimension $1/t$, are entitled to take the places held by ω_{1M} and ω_{2M} in the Maxwellian gas, as is seen from the following remarks, which we have arranged in 4 groups, like the analogous discussion for the Maxwell case.

1) The integral equations (5.42) for the coefficients found in $\phi^{(1)}$:

$$\boldsymbol{G}_\lambda = \Omega \boldsymbol{A};\ \mathsf{G}_\mu = \Omega \mathsf{B}, \tag{7.20}$$

are usually solved by the Enskog method of successive approximation to $\boldsymbol{A}$ and B. We shall discuss the first approximation only, which reads:

$$\boldsymbol{A} \approx a\boldsymbol{G}_\lambda;\ \mathsf{B} \approx b\mathsf{G}_\mu \tag{7.21}$$

with a and b constant; with (7.20),

$$\boldsymbol{G}_\lambda - \Omega(a\boldsymbol{G}_\lambda) \approx 0;\ \mathsf{G}_\mu - \Omega(b\mathsf{G}_\mu) \approx 0. \tag{7.22}$$

a and b are now fixed by requiring that the first of the LHS in (7.22) shall be $\perp \boldsymbol{G}_\lambda$, the second $\perp \mathsf{G}_\mu$:

$$(\boldsymbol{G}_\lambda,\ \boldsymbol{G}_\lambda - \Omega[a\boldsymbol{G}_\lambda]) = 0;\ (\mathsf{G}_\mu,\ \mathsf{G}_\mu - \Omega[b\mathsf{G}_\mu]) = 0, \tag{7.23}$$

or, using (7.19):

$$a = 1/\omega_\lambda;\ b = 1/\omega_\mu. \tag{7.24}$$

So the *distribution* $\phi^{(1)}$ reads, in first Enskog approximation:

$$[\phi^{(1)}]_1 = (1/\omega_\lambda)\boldsymbol{G}_\lambda \cdot \nabla \ln T + (1/\omega_\mu)\mathsf{G}_\mu : \nabla \boldsymbol{c}_0. \tag{7.25}$$

2) From the formulae (5.43) for the *transport* currents in a ChE distribution $\phi^{(1)}$:

$$\begin{cases} \boldsymbol{q}^{(1)} = \boldsymbol{J}_\lambda{}^{(1)} = -kT(\boldsymbol{G}\ ,\ \phi^{(1)}) = -\tfrac{1}{3}k(\boldsymbol{G}_\lambda,\ \boldsymbol{A})\nabla T \\ \overset{\circ}{\mathsf{P}}{}^{(1)} = \mathsf{J}_\mu{}^{(1)} = -kT(\mathsf{G}_\mu,\ \phi^{(1)}) = -\tfrac{1}{5}kT(\mathsf{G}_\mu,\ \mathsf{B})\overline{\overline{\nabla \boldsymbol{c}_0}}, \end{cases} \tag{7.26}$$

we derive the following expressions for the coefficients of transport, which are linear in $\boldsymbol{A}$ and B:

$$\lambda = \tfrac{1}{3}k(\boldsymbol{G}_\lambda,\ \boldsymbol{A});\ \mu = \tfrac{1}{10}kT(\mathsf{G}_\mu,\ \mathsf{B}). \tag{7.27}$$

Using the integral equations (7.20), we find alternative expressions quadratic in $\boldsymbol{A}$ and B:

$$\lambda = \tfrac{1}{3}k[\boldsymbol{A},\ \boldsymbol{A}];\ \mu = \tfrac{1}{10}kT[\mathsf{B},\ \mathsf{B}]. \tag{7.28}$$

These formulae are still exact. Now we substitute (7.21) in order to determine the first Enskog approximations to λ and μ; clearly the requirement (7.23) ensures that (7.27) and (7.28) lead to the same result, viz.

$$\begin{cases} [\lambda]_1 = \tfrac{1}{3}k\ a(\boldsymbol{G}_\lambda,\ \boldsymbol{G}_\lambda) = \tfrac{5}{2}\dfrac{nk^2T}{m\omega_\lambda} \\ [\mu]_1 = \tfrac{1}{10}kT\ b(\mathsf{G}_\mu,\ \mathsf{G}_\mu) = \dfrac{nkT}{\omega_\mu}. \end{cases} \tag{7.29}$$

3) The collisional time derivative of the currents J is given by the approximative formula (6.12b), which we modify using the symmetry of Ω:

$$\partial_C J = \partial_C(H,\ \phi + \tilde{\phi}) \approx -[H,\ \phi + \tilde{\phi}] = -[\phi + \tilde{\phi},\ H] \equiv -(\phi + \tilde{\phi},\ \Omega H). \tag{7.30}$$

First Enskog approximations to ΩH follow from eqs. (7.22) which, of course, hold for H as well as for G:

$$\boldsymbol{H}_\lambda \approx \Omega(a\boldsymbol{H}_\lambda);\ \mathsf{H}_\mu \approx \Omega(b\mathsf{H}_\mu). \tag{7.31}$$

Substituting this into (7.30), we get the following equations for *quasi-relaxation*:

$$\begin{cases} \partial_C \boldsymbol{J}_\lambda \approx -(1/a)\boldsymbol{J}_\lambda = -\omega_\lambda \boldsymbol{J}_\lambda \\ \partial_C \mathsf{J}_\mu \approx -(1/b)\mathsf{J}_\mu = -\omega_\lambda \mathsf{J}_\mu. \end{cases} \tag{7.32}$$

Apparently,

$$1/\omega_\lambda = a = \frac{15}{16 n\Omega^{(2,2)}} = \tau_\lambda \text{ and } 1/\omega_\mu = b = \frac{5}{8 n\Omega^{(2,2)}} = \tau_\mu \tag{7.33}$$

are the relaxation times pertinent to the quasi-relaxation of heat transport and of momentum transport, respectively. Formulae (7: 14, 15) giving the integral equation for $\phi^{(1)}$ and its solution in terms of X and τ, and (7.16) expressing λ and μ by means of these τ_λ and τ_μ all remain valid (approximately of course) in the non-Maxwell case.

4) To give an approximate value for the lowest positive eigenvalue ω_1, we try a variation method, using, as trial functions, three of the eigenfunctions χ_M of Ω_M belonging to the lowest Maxwell eigenvalue ω_{1M}, viz. $\boldsymbol{G}_\lambda$:

$$\omega_1 \approx \frac{(\boldsymbol{G}_j, \Omega\boldsymbol{G}_j)}{(\boldsymbol{G}_j, \boldsymbol{G}_j)} = \omega_j = \tfrac{16}{15} n\Omega^{(2,2)}. \tag{7.34}$$

Again,

$$1/\omega_j = \tau_j = \boxed{\frac{15}{16 n\Omega^{(2,2)}} \tau}\ . \tag{7.35}$$

which approximately gives the *relaxation* time of $\tilde{\phi}$, i.e. the time scale of the kinetic stage. The following argument will show that this τ is once more $\approx$ the average time between collisions. We apply Ω (see definition, eq. 2.32) to $\boldsymbol{G}_\lambda$; over all values of $\boldsymbol{c}, \boldsymbol{c}_1, \varepsilon$ and χ, $(\boldsymbol{G}_\lambda + \boldsymbol{G}_\lambda' - \boldsymbol{G}_{\lambda 1} - \boldsymbol{G}_{\lambda 1}')$ and α, the differential cross-section, will have average values $\bar{\boldsymbol{G}}$ and $\bar{\alpha}$, and, looking at orders-of-magnitude:

$$\Omega\boldsymbol{G}_\lambda \approx n\bar{\alpha}\boldsymbol{G};\ \tau \approx \frac{(\boldsymbol{G}_\lambda, \boldsymbol{G}_\lambda)}{(\boldsymbol{G}_\lambda, \Omega\boldsymbol{G}_\lambda)} \approx \frac{n\bar{\boldsymbol{G}}^2}{n^2\bar{\alpha}\bar{\boldsymbol{G}}^2} = \frac{1}{n\bar{\alpha}}. \tag{7.36}$$

An estimate for $\bar{\alpha}$ is provided by $v\sigma^2$, v being the mean thermal velocity and σ^2 the cross-section of the molecules. So

$$\tau = \frac{1}{vn\sigma^2} \approx \frac{l}{v} = \tau_C \tag{7.37}$$

(l = mean free path), in which τ_C is some average time between successive collisions.

8. *Time scale of the hydrodynamical stage*

The development in time of the basic moments $\psi\,(=\varrho, \boldsymbol{c}_0, T)$, in the absence of external forces, is determined by the HDE (2.10), which we

quote in their usual form:

$$\text{(8.1)}\qquad \begin{cases} \partial_t \varrho = -\mathbf{c}_0 \cdot \nabla\varrho - \varrho \nabla \cdot \mathbf{c}_0 \\ \partial_t \mathbf{c}_0 = -(\mathbf{c}_0 \cdot \nabla)\mathbf{c}_0 - (1/\varrho)\nabla \cdot \mathsf{P} \\ \partial_t T = -\mathbf{c}_0 \cdot \nabla T - \dfrac{2m}{3k\varrho}(\mathsf{P} : \nabla \mathbf{c}_0 + \nabla \cdot \mathbf{q}). \end{cases}$$

They follow from the BE by integration and are therefore valid during both the kinetic and the HD stage. During the kinetic stage, the rapid changes which the distribution function f undergoes will also be reflected in the t-derivatives of its moments ψ; when f has reached its normal ChE value f^{Ch} and the HD stage has set in, further changes of the moments ψ will be much slower, as we shall now demonstrate.

The ChE distribution f^{Ch} has the form of a "Hilbert expansion" (2.22):

$$\text{(8.2)}\qquad f^{\mathrm{Ch}} = f^{(0)}(1 + \phi^{(1)} + \phi^{(2)} + \ldots),$$

with successive terms of decreasing size; in fact, introducing a small positive number φ, we may suppose that

$$\text{(8.3)}\qquad \phi^{(1)} \approx \varphi;\ \phi^{(2)} \approx \varphi^2;\ \ldots \qquad (0 < \varphi \ll 1)$$

If we restrict ourselves to the first correction, $\phi^{(1)}$, the transport quantities P and $\boldsymbol{q}$ in (8.1) are given by the phenomenological equations:

$$\text{(8.4)}\qquad \mathsf{P} = p\mathsf{U} - 2\mu\overline{\overline{\nabla \mathbf{c}_0}}^{\circ} \text{ and } \boldsymbol{q} = -\lambda \nabla T,$$

with

$$\text{(8.5)}\qquad p = k\varrho T/m$$

and

$$\text{(8.6)}\qquad \lambda = \frac{5}{2} \cdot \frac{3k}{2m} \cdot \mu.$$

We substitute (8: 4, 5, 6) into (8.1), with the result:

$$\text{(8.7)}\qquad \begin{cases} \partial_t \varrho = & -\mathbf{c}_0 \cdot \nabla\varrho & -\varrho \nabla \cdot \mathbf{c}_0 & \\ \partial_t \mathbf{c}_0 = & (-\mathbf{c}_0 \cdot \nabla)\mathbf{c}_0 & -(1/\varrho)\nabla p & +2(\mu/\varrho)\nabla \cdot (\overline{\overline{\nabla \mathbf{c}_0}}^{\circ}) \\ & & & = (\mu/\varrho)\{\Delta \mathbf{c} + \tfrac{1}{3}\nabla \cdot (\nabla \mathbf{c}_0)\} \\ \partial_t T = & -\mathbf{c}_0 \cdot \nabla T & -\frac{2}{3} T \nabla \cdot \mathbf{c}_0 & +4m\mu\,(3k\varrho)^{-1}(\overline{\overline{\nabla \mathbf{c}_0}}^{\circ})^2 \quad \cdot \frac{5}{2}(\mu/\varrho)\nabla T. \end{cases}$$

(1) (2) (3a) (3b)

(The grouping of the RHS terms will be discussed in connection with eqs. (8.13)).

The magnitude of the gradients of T and $\mathbf{c}_0$ occurring in (8.7) is restricted by the estimates (8.3). To begin with, the estimate for $\phi^{(1)}$

determines the magnitude of the first-order gradients; for, using (7.15), we have

$$\phi^{(1)} \approx \tau_\lambda(\tfrac{5}{2}-C^{*2})\mathbf{C}\cdot\nabla \ln T - 2\tau_\mu \mathbf{C}^*\overset{\circ}{\mathbf{C}}^*:\overline{\overline{\nabla \mathbf{c}_1}} = \phi_\lambda^{(1)} + \phi_\mu^{(1)} \approx \varphi. \tag{8.8}$$

τ_λ = the kinetic relaxation time τ; $\tau_\mu = \frac{2}{3}\tau$; $\frac{5}{2}-C^{*2}$ and $\mathbf{C}^*\mathbf{C}^*$ are of order unity (in the velocity range of interest) and $\mathbf{C}$ is comparable to the mean thermal velocity $v=(kT/m)^{\frac{1}{2}}$. Hence,

$$\phi_\lambda^{(1)} \approx \tau v(\nabla T/T) \approx \varphi \ll 1; \tag{8.9a}$$

$$\phi_\mu^{(1)} \approx \tau \nabla \mathbf{c}_0 \approx \varphi \ll 1. \tag{8.9b}$$

$\tau v = l$ is a length $\approx$ the mean free path; so (8.9a) illustrates the fact that, in a development of $f/f^{(0)}$ in powers of $l\nabla$, $\phi^{(1)}$ is the linear term, which is small if the relative change over a distance l of the moments ψ (e.g., T) is $\ll 1$. Likewise, (8.9b) restricts the change along l of $\mathbf{c}_0$ to an amount small compared to $l/\tau = v$. Apparently the thermal velocity v serves as the proper velocity of reference for $\mathbf{c}_0$.

Although $\phi^{(1)}$ does not contain a $\nabla\varrho$-term comparable to the ∇T- and $\overline{\overline{\nabla \mathbf{c}_0}}$-terms, it stands to reason that a condition similar to (8.9a, b) is imposed on $\nabla\varrho$:

$$l(\nabla\varrho/\varrho) \approx \varphi \ll 1. \tag{8.9c}$$

For the gradient of the hydrostatic pressure $p = \varrho v^2$, (8.9a, c) imply a restriction

$$(l/\varrho v^2)\nabla p \approx \varphi \ll 1. \tag{8.10}$$

In a similar way, we use the estimate of $\phi^{(2)}$ in (8.3) in order to determine the magnitude of the second-order gradients of T and $\mathbf{c}_0$ occurring in (8.7). This second correction consists of terms reading $l^2\nabla\nabla$; $\nabla\nabla$ symbolizes products of first gradients $\left(\frac{1}{\psi}\nabla\psi\cdot\frac{1}{\psi}\nabla\psi\right)$ as well as second-order gradients (like $\Delta\psi/\psi$). By virtue of (8.3), all these terms will be $\approx \varphi^2$; *e.g.*,

$$\phi_{\lambda\lambda}^{(2)} \approx (l^2/T)\,\Delta T \approx \varphi^2; \tag{8.11a}$$

$$\phi_{\mu\mu}^{(2)} \approx (l^2/v)\,\nabla\cdot(\overline{\overline{\nabla \mathbf{c}_0}}) \approx \varphi^2. \tag{8.11b}$$

Finally, the magnitude of the viscosity coefficient μ can be inferred from the connection (7.35) between $\Omega^{(2,2)}$ and the kinetic relaxation time τ:

$$\mu \approx [\mu]_1 = \frac{5kT}{8\Omega^{(2,2)}} \approx \frac{mv^2}{1.07\tau} \approx \varrho v l. \tag{8.12}$$

We are now in a position to replace each term in the RHS of the

HDE (8.7) by its order-of-magnitude; using the estimates (8: 9, 10, 11, 12), we get:

(8.13)
$$\left.\begin{aligned} \frac{\partial_t \varrho}{\varrho} &\approx \frac{1}{\tau}\Big(\frac{c_0}{c}\varphi \Big) \\ \frac{\partial_t \mathfrak{c}_0}{c} &\approx \frac{1}{\tau}\Big(\frac{c_0}{c}\varphi \Big) \\ \frac{\partial_t T}{T} &\approx \frac{1}{\tau}\Big(\frac{c_0}{c}\varphi \Big) \end{aligned}\right\} \quad \begin{matrix} (1) \\ \\ \\ \end{matrix} \quad \left.\begin{aligned} &\varphi \Big) \\ &\varphi \\ &\varphi \end{aligned}\right\} \quad \begin{matrix} (2) \\ \\ \\ \end{matrix} \quad \left.\begin{aligned} &\varphi^2 \Big) \\ &\varphi^2 \end{aligned}\right\} \quad \begin{matrix} (3a) \\ \\ \end{matrix} \quad \left.\begin{aligned} &\varphi^2 \Big) \end{aligned}\right\} \quad \begin{matrix} (3b) \\ \\ \\ \end{matrix}$$

All terms inside the brackets at the RHS are $\ll 1$, as we may safely assume c_0 not to exceed v. Each term corresponds to a contribution $\tau\partial_t\psi/\psi$, and therefore they indicate the local changes in ϱ, $\mathfrak{c}_0$, T relative to ϱ, v, T in a time τ which it has previously taken the gas to pass through the kinetic stage. Apparently these changes are all $\ll 1$, so that the HD development is certainly slow in comparison to the kinetic process.

The grouping of terms in eqs. (8.7) and (8.13) has been made in order to distinguish between HD processes of a different nature; for each process we quote a characteristic time, viz. the time after which, according to (8.13), the process would have caused a relative change in ψ or order unity:

1) local changes in all three ψ due to bulk movement with velocity $\mathfrak{c}_0$:

(8.14a)
$$t_{\mathrm{III},1} = \tau v/c_0\varphi.$$

2) remaining first order effects (decrease of ϱ and T if $\mathfrak{c}_0$ is locally divergent; acceleration of the gas down a hydrostatic pressure gradient):

(8.14b)
$$t_{\mathrm{III},2} = \tau/\varphi.$$

3a) second degree, first order process (dissipation of kinetic energy of bulk movement by friction), and

3b) second order processes (local yield of transport of momentum and heat); for both (a) and (b),

(8.14c)
$$t_{\mathrm{III},3} = \tau/\varphi^2.$$

Estimates of the ψ-gradients more specific than those in terms of the development parameter φ are provided by the following suppositions:

a) the local gradient $\nabla\psi$, if continued along the vessel dimension d, would correspond to a relative ψ difference between the extremities of d of order 1:

(8.15a)
$$l(\nabla\psi/\psi) \approx l/d;$$

b) in analogy, the gradient *of* $\nabla\psi$ is restricted by

(8.15b)
$$(l/\psi)\,\nabla(\nabla\psi) \approx l/d^2.$$

Using these estimates instead of (8: 9, 10, 11), we obtain the following HD times for the various processes mentioned:

$$t_{\mathrm{III},1} = d/c_0;\ t_{\mathrm{III},2} = d/v;\ t_{\mathrm{III},3} = d^2/lv. \tag{8.16}$$

All these times are $\gg \tau$. Which of the corresponding processes predominates, depends on which is the shortest. In general $c_0 < v$, so the first order processes (2) will in general prevail. In their absence, streaming (1) and 2nd order or 2nd degree processes (3) can act. Which of these is first, depends on the ratio:

$$\frac{t_2}{t_1} = \frac{c_0 l}{vl} = \mathrm{Re}. \tag{8.17}$$

This appears to be Reynolds's number, and we can distinguish between the following 3 cases:

a) $\mathrm{Re} \ll 1$, laminar flow: $t_1 \gg t_3$: processes of 2nd order and 2nd degree are preponderant.

b) $\mathrm{Re} \approx 1$, flow still laminar: $t_1 \approx t_3$: both groups of terms contribute to the HD development.

c) $\mathrm{Re} > 1000$, turbulent flow: first order terms dominate.

Acknowledgement

This work forms part of the research program of the Foundation for Fundamental Research of Matter (F.O.M.), which is financially supported by the Organization for Pure Scientific Research (Z.W.O.).

REFERENCES

1. Bogolubov, N., as quoted by G. E. Uhlenbeck, lecture notes, Leiden (1955) (unedited).
2. Chapman, S. and T. G. Cowling, The mathematical theory of non-uniform gases. Cambridge (1939, 1952).
3. Hirschfelder, J. O., C. F. Curtiss and R. B. Bird, Molecular theory of gases and liquids. New York (1954).
4. Waldmann, L., Handb. d. Phys. 12, 295 514 (1958).
5. Kac, M., colloquium notes Magnolia Petr. Company, Dallas, 98 100 (1956).
6. Kohler, M., Z. f. Phys. 125, 715 (1949).
7. Wang Chang, C. S. and G. E. Uhlenbeck, report M 999, Eng. Res. Inst., Univ. of Michigan (1952).
8. Prigogine, I., Physica 15, 272 (1949).

List of symbols

(Missing symbols are explained near to the place where they are used. Superscripts and subscripts are mentioned separately at the bottom. In the equations quoted, the symbol is defined, first mentioned, or best elucidated.)

(5.41)	$\left\{ \begin{matrix} \boldsymbol{A} \\ B \end{matrix} \right\}$	coefficients in $\phi^{(1)}$
	$\boldsymbol{c}$	velocity of a molecule
(2.7)	$\boldsymbol{c}_0$	local average velocity
	$\boldsymbol{C}$	$\boldsymbol{c} - \boldsymbol{c}_0$
(2.45)	$\boldsymbol{C}^*$	reduced value of $\boldsymbol{C}$
(2: 33, 34; 3: 13, 14; 4: 17, 18)	$\left\{ F \right\}$	LHS of integral equations
	f	velocity-space distribution
(6: 1, 2)	G, H	functions of $\boldsymbol{C}$
(5.3)	H	H-function (used in ch. 5 only)
(2.3)	$J(ff_1)$	collision operator
(5: 38, 39)	$\mathsf{J}_\mu, \boldsymbol{J}_\lambda$	transport currents
	k	Boltzmann's constant
	l	mean free path
	m	mass of a molecule
	n	local number density
(5.43)	$\left\{ \mathsf{P} \right.$	pressure tensor
	$\left. \boldsymbol{q} \right\}$	heat current
(5.5)	s	local entropy density
	T	temperature
(1.1)	$t_{\mathrm{I,II,III}}$	characteristic times of stages I, II, III
	v	mean thermal velocity $(kT/m)^{\frac{1}{2}}$
(5: 38, 39)	$\mathsf{X}_\mu, \boldsymbol{X}_\lambda$	transport "forces"
(2.30; 3.11; 4.13)	θ	series development parameter $(=1)$
(7.9)	$\left\{ \lambda \right.$	coefficient of viscosity
	$\left. \lambda' \right\}$	coefficient of heat conductivity
(2.7)	ϱ	mass density
(7.37)	τ	kinetic relaxation time
(2.22; 3.8; 4.3)	ϕ	deviation of f relative to $f^{(0)}$ or f^{Ch}
(8.3; 3.39)	φ	series development parameter
(2.39; 2.5)	$\chi^{[\omega\lambda]}$	eigenfunction of Ω
(2.6)	$\psi^{[\lambda]}$	moment of $\chi^{[0\lambda]}$
(2.32)	Ω	linearized collision operator
(2.39)	ω	eigenvalue of Ω
(3.25, etc.)	$\bar{\omega}$	sum of ω values
	∂_t	partial derivative with respect to t
(2.2; 5.17; 6.7)	∂_{S}	contribution to ∂_t by "streaming"
(2.3; 5.18; 6.7)	∂_{C}	contribution to ∂_t by collisions
(6.7)	∂_H	contribution to ∂_t by change of H
(2: 22, 23, 26, etc.)	$(r), (s)$	e.g., $f^{(r)}$, $\psi^{[\lambda](r)}$, $\partial_t{}^{(s)}$, $\mathsf{P}^{(1)}$: term index in series of Hilbert type
	Ch	e.g., f^{Ch}: ChE value
(3.3; 4.3)	$\sim$	e.g., $\tilde{f}, \tilde{\phi}, \tilde{F}$: deviation from MB value (ch. 3) or from ChE value (ch. 4)

(2: 39, 46, etc.)	$[\omega\lambda]$	e.g., $\chi^{[\omega\lambda]}$, $\varphi^{[\omega\lambda]}$: indices of Ω-eigenfunctions χ and of χ-development coefficients φ; λ counts degenerate levels
(3.25, etc.)	$[\bar{\omega}]$	e.g., $\Psi^{[\omega]}$: index of development coefficients in $e^{-\omega t}$-series
(5: 38, 39; 7.33)	λ, μ	e.g., τ_λ, τ_μ: quantities connected with transport of heat/momentum
	$=$ / $\circ$ \	e.g., $\overset{\circ}{\overline{\overline{C}}}_0$: $\overline{\overline{T}}_{\alpha\beta} = \frac{1}{2}(T_{\alpha\beta} + T_{\beta\alpha})$ / $\overset{\circ}{T}_{\alpha\beta} = T_{\alpha\beta} - \frac{1}{3}\sum_\alpha T_{\alpha\alpha}$
(2.35)	$(\ )$	e.g., (ϕ, χ): scalar product
(2.37)	$[\ ]$	e.g., $[\boldsymbol{A}, \boldsymbol{A}]$: matrix element of Ω

DISSOCIATION CONSTANTS OF ALKYL-SUBSTITUTED CYCLOHEXANECARBOXYLIC ACIDS AND CYCLOHEXANEACETIC ACIDS

(preliminary communication)

BY

H. VAN BEKKUM [1]), P. E. VERKADE, AND B. M. WEPSTER

(Communicated at the meeting of November 26, 1960)

During the realization of a research program concerning synthesis, configuration, and conformation of cyclohexane derivatives a fairly large number of pure alkyl-substituted cyclohexanecarboxylic acids and cyclohexaneacetic acids became available. The apparent dissociation constants of these acids in 50 vol.% ethanol-water at 25° were determined potentiometrically. Considering the present-day interest in cyclohexane derivatives, and in particular also in the acids in question, it would seem desirable to us to record these data in a preliminary communication. For additional information reference is made to the thesis of one of us (v. B.) shortly to appear and to papers to be published elsewhere at a later date.

The *cis*- or *trans*-configuration of nearly all the 4-alkylcyclohexanecarboxylic acids involved in the present work has been established by us, as was that of the 2- and 3-methylcyclohexanecarboxylic acids by others, by a chemical method, *viz.* by correlating these compounds with the corresponding cyclohexanedicarboxylic acids, the configuration of which had been put beyond doubt. The assignment of the configuration to the other alkyl-substituted cyclohexanecarboxylic acids took place on the basis of the method of preparation and the stability of these compounds, while making use, wherever necessary and possible, of data in the literature of other nature. Finally the alkyl-substituted cyclohexaneacetic acids were correlated chemically with the corresponding alkyl-substituted cyclohexanecarboxylic acids. We feel sure that the configuration of the acids thus deduced by us is the correct one.

For the determination of the apparent dissociation constants we used a Beckman Model G pH-meter with a glass electrode and a calomel reference electrode. Each compound was examined in three separate solutions at $^1/_3$, $^1/_2$, and $^2/_3$ neutralization. The mean of the three values for the pK_a thus found, which were invariably in excellent agreement, is given in the Tables below.

---

[1]) Present address: Koninklijke/Shell-Laboratorium, Badhuisweg, Amsterdam-N.

In addition the melting points of the acids in question, as found by us, are listed in the Tables. Finally — invariably assuming the cyclohexane ring to have the rigid chair form, which is undoubtedly reasonable — for all the compounds examined the predominating conformation of the substituents has been indicated with the aid of the letters *e* (for equatorial)

Alkyl-substituted cyclohexanecarboxylic acids

alkyl group(s)	*cis*-isomer [a] m.p.	conf.	pK_a	*trans*-isomer [a] m.p.	conf.	pK_a
H				30–31°	*e*	6.30
4-methyl	30.5–31.5°	*ae*	6.53	110.5–111.5°	*ee*	6.26
4-ethyl	22.5–23.5°	*ae*	6.57	49.5–50°	*ee*	6.28
4-isopropyl	40–41°	*ae*	6.66	94–94.5°	*ee*	6.26
4-tert.butyl	118–118.5°	*ae*	6.78	175–176°	*ee*	6.28
4-neopentyl	64–64.5°	*ae*	6.57	120.5–121°	*ee*	6.28
3-methyl	[b]	*ee*	6.31			
3-isopropyl	[c]	*ee*	6.41			
3-tert.butyl	94.5–95.5°	*ee*	6.42	119–119.5°	*ae*	6.95
2-methyl	20–21°	*ae*	6.52	53.5–54.5°	*ee*	6.24
2-ethyl	37.5–38°	*ae*	6.67	75–76°	*ee*	6.38
2-isopropyl	35.5–36.5°	*ae*	7.16	46.5–47.5°	*ee*	6.47
2-tert.butyl	64–65°	*ae*	7.45	58.5–59.5°	*ee*	6.65
2,6-dimethyl	87–88°	*aee*	7.21	103–104°	*eee*	6.34
2,4,6-trimethyl	105.5–106°	*aeee*	7.30	96–96.5°	*eeee*	6.33
3,5-dimethyl	69–69.5°	*eee*	6.35			
3,5-di-tert.butyl	192.5–193.5°	*eee*	6.56			
1-methyl	37.5–38.5°	*ae*	6.79			

[a] In the acids with two or three alkyl groups examined by us these groups all occupy the same position relative to the ring; the acids in question are *meso*-acids. *Cis* and *trans* here indicate the position of the carboxyl group relative to the alkyl groups.

[b] Liquid; n_D^{25} 1.4548.

[c] Liquid; n_D^{25} 1.4648.

Alkyl-substituted cyclohexaneacetic acids

alkyl group(s)	*cis*-isomer m.p.	conf.	pK_a	*trans*-isomer m.p.	conf.	pK_a
H				30–31°	*e*	6.18
4-methyl	43–44°	*ea*	6.24	73–73.5°	*ee*	6.20
4-isopropyl	40–41°	*ae*	6.26	78–78.5°	*ee*	6.21
4-tert.butyl	98–99°	*ae*	6.32	96.5–97°	*ee*	6.23
3-tert.butyl	34–35°	*ee*	6.27			
2-tert.butyl	111–112°	*ae*	6.44			
3,5-di-tert.butyl	149–150°	*eee*	6.38			

and *a* (for axial); the letter coming first refers to the conformation of the carboxyl group.

In the following paragraphs we shall confine ourselves to a few brief remarks with reference to the pK_a values listed in the Tables. For a fuller discussion of these numerical data reference may be made to the thesis of one of us (v. B.) shortly to appear and to papers to be published elsewhere at a later date.

(1) Applying the basic idea of the work of WINSTEIN and HOLNESS [2]) to certain compounds examined by us, we assume that the dissociation constants found for *cis*- and *trans*-4-tert.butylcyclohexanecarboxylic acids are those of the conformationally pure compounds (*ae* and *ee* respectively). On the basis of these two dissociation constants and of that found for cyclohexanecarboxylic acid, it is then possible to calculate, in the way introduced for reaction rates by the investigators just mentioned and applied by STOLOW [3]) and by TICHÝ, JONÁŠ, and SICHER [4]) to dissociation constants, the free-energy difference between the two conformations of cyclohexanecarboxylic acid and of cyclohexane carboxylate ion, with the substituent in the axial and the equatorial position respectively; this calculation yields the following results: $\Delta\Delta F_{COOH} = 1.6$ kcal/mole and $\Delta\Delta F_{COO^-} = 2.3$ kcal/mole.

(2) Considering the very small difference between the dissociation constants of *trans*-4-tert.butylcyclohexanecarboxylic acid and cyclohexanecarboxylic acid, it is no doubt more advisable to base the calculation of the two above-mentioned as well as any further $\Delta\Delta F$-values on the generally accepted free-energy difference between the two conformations of methylcyclohexane, $\Delta\Delta F_{CH_3} = 1.8$ kcal/mole [5]). We then follow the procedure applied by STOLOW [3]) and by TICHÝ, JONÁŠ and SICHER [4]). On the basis of the dissociation constants of *cis*- and *trans*-4-tert.butylcyclohexanecarboxylic acids, of those of the other *cis*-4-alkylcyclohexanecarboxylic acids examined by us, and of the said value of $\Delta\Delta F_{CH_3}$, the following free-energy differences have been calculated:

$$\begin{aligned} \Delta\Delta F_{COOH} &= 1.5 \text{ kcal/mole} \\ \Delta\Delta F_{COO^-} &= 2.1 \quad \text{..} \\ \Delta\Delta F_{Et} &= 2.0 \\ \Delta\Delta F_{iPr} &= 2.5 \quad \text{..} \\ \Delta\Delta F_{Neop} &= 2.0 \quad \text{..} \end{aligned}$$

(3) The *cis*-3-alkyl- and *cis*-3,5-dialkylcyclohexanecarboxylic acids examined by us, with practically complete equatorial position of all the

---

[2]) S. WINSTEIN and N. J. HOLNESS, J. Am. Chem. Soc. **77**, 5562 (1955).

[3]) R. D. STOLOW, J. Am. Chem. Soc. **81**, 5806 (1959).

[4]) M. TICHÝ, J. JONÁŠ, and J. SICHER, Collection Czechosl. Chem. Commun. **24**, 3434 (1959).

[5]) C. W. BECKETT, K. S. PITZER, and R. SPITZER, J. Am. Chem. Soc. **69**, 2488 (1947).

substituents, have a higher pK_a value than cyclohexanecarboxylic acid; thus in these cases a small but marked acidity-weakening effect of the alkyl group(s) is unexpectedly found to occur.

(4) In the 2-alkyl- and 2,6-dialkyl-substituted cyclohexanecarboxylic acids steric hindrance of the carboxyl group and the carboxylate ion by the alkyl group(s) can no doubt play an important role. In the *cis*-isomers in question, with the carboxyl group largely in axial position, in addition conformational hindrance by the axial hydrogen atoms in positions 3 and 5 will occur. It is no doubt partly due to this that in these cases the difference between the dissociation constant of a *cis*-isomer and that of the corresponding *trans*-isomer increases considerably with increasing size of the alkyl group or with increasing number of these groups. The *cis*-acids of the type under consideration include remarkably weak acids.

(5) In the alkyl-substituted cyclohexaneacetic acids axial or equatorial position of the $-CH_2.COOH$ group is found to give rise to only small differences of acidity. This was to be expected.

For some of the acids examined by us, the dissociation constant had already been determined by other workers, though in other media [3][4][6][7][8].

Laboratory of Organic Chemistry,
Technical University,
Delft, Netherlands

[6] N. Zelinsky and N. Izgaryschew, J. Russ. Phys. Chem. Soc. **40**, 1379 (1908); Chem. Zentralbl. **I**, 531 (1909).

[7] J. F. J. Dippy, S. R. C. Hughes and J. W. Laxton, J. Chem. Soc. **4102** (1954).

[8] P. F. Sommer, V. P. Arya, and W. Simon, Tetrahedron Letters **20**, 18 (1960).

SYNTHESIS OF UNSATURATED HYDROCARBONS BY THE WITTIG REACTION

(PRELIMINARY COMMUNICATION)

BY

H. HEITMAN, J. H. SPERNA WEILAND AND H. O. HUISMAN

(Communicated by Prof. J. F. ARENS at the meeting of September 24, 1960)

A recent publication by McDONALD and CAMPBELL [1] in which the attempted preparation of 1,6-diphenyl–1, 3,5-hexatriene (VI) was described by means of a WITTIG reaction with 1,4-bis(triphenylphosphonium)-2-butene dichloride and benzaldehyde, prompt us to communicate our own results in the same field at an early stage.

1,4-bis(triphenylphosphonium)-2-butene dibromide (V) was prepared by selective partial hydrogenation of 2-butyn–1,4-diol (I) to 2-butene–1,4-diol (II) followed by treatment with dry hydrogen bromide and conversion of the so formed 1,4-dibromo–2-butene (III) into the corresponding bistriphenylphosphonium compound (V) by a modification of the method used by FRIEDRICH and HENNING [2] for the preparation of 1,3-bis(triphenylphosphonium)propane dibromide using dimethylformamide as the solvent.

$$\underset{\text{I}}{HOCH_2C{\equiv}CCH_2OH} \xrightarrow[H_2]{\text{Lindlar}} \underset{\text{II}}{HOCH_2CH{=}CHCH_2OH} \xrightarrow[h\nu]{HBr} \underset{\substack{\text{III trans}\\ \text{(m.p. 55.5–56°)}}}{BrCH_2CH{=}CHCH_2Br}$$

$$\underset{\text{III}}{BrCH_2CH{=}CHCH_2Br} + \underset{\text{IV}}{(C_6H_5)_3P} \xrightarrow{DMF} \underset{\substack{\text{V}\\ \text{(m.p. 254–256°)}}}{(C_6H_5)_3P^{+}Br^{-}-CH_2CH{=}CHCH_2-P^{+}Br^{-}(C_6H_5)_3}$$

Contrary to the results of McDONALD and CAMPBELL [1] the compound VI could be obtained in good yield by a WITTIG reaction carried out in alcoholic solution and with a lithiumalkoxide as the base.

$$\underset{\text{V}}{(C_6H_5)_3P^{+}Br^{-}-CH_2CH{=}CHCH_2-P^{+}Br^{-}(C_6H_5)_3} + 2\,C_6H_5CHO \xrightarrow{\text{base}} \underset{\substack{\text{VI}\\ \text{(m.p. 200.5–201.5°)}}}{\text{ 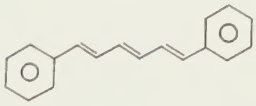 }}$$

λ_{max}: 335, 351 and 370 mμ (ethanol)

The reaction was carried out also with anisic aldehyde (VII), cinnamic aldehyde (VIII), β-ionylidene acetaldehyde (IX) and furfural (X), all leading to the corresponding unsaturated hydrocarbons (XI–XIV).

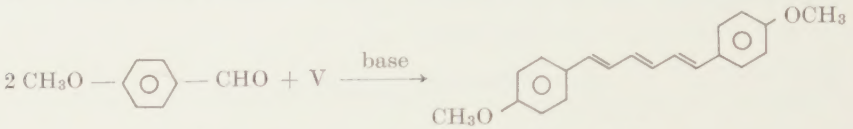

VII

XI
(m.p. 250–251°)
λ_{max}: 346, 362 and 380 mμ (ethanol)

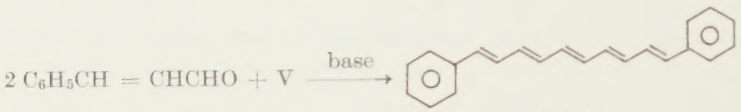

VIII

XII
(m.p. 252–254°)
λ_{max}: 380, 402 and 426 mμ (benzene)

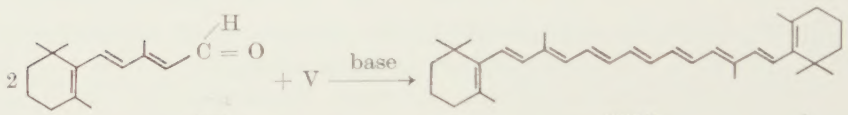

IX

XIII
(m.p. 160–161°)
λ_{max}: 412 mμ (cyclohexane)

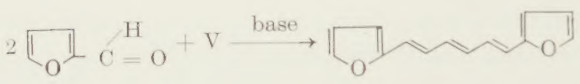

X

XIV
(m.p. 154–155°)
λ_{max}: 348, 366 and 388 mμ (cyclohexane)

When the reaction was carried out with ketones we were unable to obtain the hydrocarbons to any substantial amount, although there were indications that traces of the desired compounds were formed.

By taking a trialkylphosphine instead of triphenylphosphine (IV) the reaction took place much faster and the yields were considerably better.

More detailed studies about the influence of the substituent in the aromatic nucleus of the aldehyde on the yield of the reaction are in progress.

There are some indications leading to the assumption that in the cases described above one of the steps of the WITTIG reaction might proceed by a free radical mechanism.

Full details of this work will be published in the thesis of Mr H. HEITMAN as well as in forthcoming papers.

Laboratory for Organic Chemistry
of the University of Amsterdam

REFERENCES

1. McDONALD, R. N. and T. W. CAMPBELL, J. Org. Chem. 24, 1969 (1959).
2. FRIEDRICH, K. and H. G. HENNING, Chem. Ber. 92, 2756 (1959).

CONTENTS

Biochemistry

BUNGENBERG DE JONG, H. G. and J. TH. HOOGEVEEN: Silicon tetrachloride treated paper in the paper chromatography of phosphatides. IVA, p. 1.

BUNGENBERG DE JONG, H. G. and J. TH. HOOGEVEEN: Silicon tetrachloride treated paper in the paper chromatography of phosphatides. IVB, p. 18.

Chemistry, Organic

BEKKUM, H. VAN, P. E. VERKADE and B. M. WEPSTER: Dissociation constants of alkyl-substituted cyclohexanecarboxylic acids and cyclohexaneacetic acids, p. 161.

HEITMAN, H., J. H. SPERNA WEILAND and H. O. HUISMAN: Synthesis of unsaturated hydrocarbons by the Wittig reaction. (Communicated by Prof. J. F. ARENS), p. 165.

Chemistry, Physical

BOER, J. H. DE and A. B. C. VAN DOORN: Graphitic oxide. VI, p. 34.

Mechanics

ALBLAS, J. B.: On the torsion of a cylindrical bar with slits. (Communicated by Prof. C. J. BOUWKAMP), p. 47.

Paleontology

GIJZEL, P. VAN: Autofluorescence and age of some fossil pollen and spores. (Communicated by Prof. I. M. VAN DER VLERK), p. 56.

LOOSE, H.: Dicerorhinus hemitoechus Falc. in the Netherlands, (Communicated by Prof. I. M. VAN DER VLERK), p. 41.

Physics

MIEDEMA, A. R.: Some experiments on heat transfer and magnetism below 1° K. I. (Communicated by Prof. C. J. GORTER), p. 64.

MIEDEMA, A. R.: Some experiments on heat transfer and magnetism below 1° K. II. (Communicated by Prof. C. J. GORTER), p. 70.

MIEDEMA, A. R.: Some experiments on heat transfer and magnetism below 1° K. III. (Communicated by Prof. C. J. GORTER), p. 80.

MIEDEMA, A. R.: Some experiments on heat transfer and magnetism below 1° K. IV. (Communicated by Prof. C. J. GORTER), p. 98.

OFFERHAUS, M. J.: Theory of relaxation phenomena in a monatomic gas. I. (Communicated by Prof. J. DE BOER), p. 115.

OFFERHAUS, M. J.: Theory of relaxation phenomena in a monatomic gas. II. (Communicated by Prof. J. DE BOER), p. 125.

OFFERHAUS, M. J.: Theory of relaxation phenomena in a monatomic gas. III. (Communicated by Prof. J. DE BOER), p. 136.

OFFERHAUS, M. J.: Theory of relaxation phenomena in a monatomic gas. IV. (Communicated by Prof. J. DE BOER), p. 149.

PRINTED IN THE NETHERLANDS
DRUKKERIJ HOLLAND N.V., AMSTERDAM